A University of Sussex DPhil thesis

Available online via Sussex Research Online:

http://sro.sussex.ac.uk/

This thesis is protected by copyright which belongs to the author.

This thesis cannot be reproduced or quoted extensively from without first obtaining permission in writing from the Author

The content must not be changed in any way or sold commercially in any format or medium without the formal permission of the Author

When referring to this work, full bibliographic details including the author, title, awarding institution and date of the thesis must be given

Please visit Sussex Research Online for more information and further details

Study of film thickness in elastohydrodynamic contacts by electrical capacitance

By

Karolina Jabłonka

Submitted for the degree of Doctor of Philosophy

University of Sussex

School of Engineering and Informatics

Department of Engineering and Design

January 2015

Declaration

I hereby declare that this thesis has not been and will not be, submitted in whole or in part to another University for the award of any other degree.

……..

Karolina Jablonka

Abstract

The current work, sponsored by the SKF Engineering and Research Centre in the Netherlands, is focused on studying aspects of lubrication relevant to rolling element bearings using electrical capacitance. This includes comparative film thickness measurements in glass-on-steel and steel-on-steel contacts, interaction of polar components with surfaces, as well as grease lubrication. It has been proven that the capacitive method can be successfully applied to very thin films, even down to around 10 nm thickness.

The main part of the experimental work has been conducted on a test rig that simulates a contact between a ball and a raceway in a ball bearing. In this apparatus an EHD contact is formed between a steel ball and either a glass, or steel disc. For the first time it has been possible to perform parallel measurements of film thickness with an optical method, and electrical capacitance of an EHD contact, which allowed establishing an alternative approach to extracting quantitative film thickness values from the measured capacitance.

This procedure has been further applied to a modified rolling element bearing in which all but one of the steel balls were replaced with non-conductive ceramic balls. By simplifying the experimental setup and focusing on a contact between a single ball and raceways it was possible to eliminate some of the system variables, such as unloaded region capacitance, thus giving a much clearer picture of the film thickness in a rolling bearing.

The current study shows a high potential of the method giving further insight into the behaviour of lubricants in high-pressure contacts. The information obtained from measured capacitance can be treated as complementary to the output of other available techniques (optical interferometry, surface force apparatus, resistance, and ultrasound) providing a better understanding of the phenomena observed.

Selected presentations and published work

Peer reviewed publications

Jablonka K, Glovnea R, Bongaerts J. Evaluation of EHD films by electrical capacitance. Journal of Physics D: Applied Physics 2012;45:385301.

Jablonka K, Glovnea R, Bongaerts J, Morales-Espejel G. The effect of the polarity of the lubricant upon capacitance measurements of EHD contacts. Tribology International 2013;61:95–101.

Extended abstracts in conference proceedings

Jablonka K, Glovnea R, Bongaerts J. Evaluation of film thickness in elastohydrodynamic contacts by electrical capacitance, ITC Hiroshima 2011 – International Tribology Conference 2011, 31.10 – 03.11.2011, Hiroshima, Japan

Jablonka K, Glovnea R, Bongaerts J, Morales-Espejel G. The effect of the polarity of the lubricant upon capacitance measurements of EHD contacts, 9th Annual Tribo-UK Conference in Tribology, 14 – 15.03.2012, University of Southampton, UK

Jablonka K, Glovnea R, Bongaerts J, Morales-Espejel G. Comparative Measurements of EHD Film Thickness in Ball-on-Flat Rig and Rolling Element Bearing, STLE 2012 Annual Meeting, 6 – 10.05.2012 St Louis, USA

Jablonka K, Glovnea R, Bongaerts J, Morales-Espejel G The effect of the polarity of the lubricant upon capacitance measurements of EHD contacts, 39th Leeds-Lyon Symposium on Tribology, 4 – 7.09.2012 Leeds, UK

Jablonka K, Glovnea R, Bongaerts J. Study on the behaviour of polar additives in EHD contacts by electrical capacitance. World Tribology Congress, 8 – 13.09.2013 Torino, Italy

I dedicate this thesis to my mum

Tę pracę dedykuję mojej mamie

Contents

List of Figures

List of Figures

List of Tables

List of symbols

a	semimajor contact axis
A	contact area
b	semiminor contact axis
c	speed of sound in the lubricant layer
C	capacitance
$C_{flooded}$	capacitance of the flooded region
C_{cav}	capacitance of the cavitated region
$C_{outside}$	outside of contact capacitance
C_{total}	total measured capacitance
$C_{contact}$	Hertzian contact capacitance
$C_{steel\ ball}$	capacitance of the contacts between steel ball and the raceways
C_{inner}, C_{outer}	inner-ring and outer-ring contacts capacitance
C_Z	coefficient for Z calculation
C_1, C_2, C_3, C_4	constants for density-pressure dependence
D_Z	coefficient for Z calculation
d	separation between the plates of a capacitor
D_1, D_2	constants in the density-pressure relation
E'	reduced Young's modulus
E_A	Young's modulus of body A
E_B	Young's modulus of body B
f	resonant frequency
$\bar{G}$	dimensionless material parameter
G_0	coefficient for variation of dynamic viscosity with temperature
h	film thickness
$\bar{h}$	film thickness where a pressure gradient is zero in a line contact
h_l	thickness of the reduced mobility layer
$\widetilde{H}_c$	isothermal dimensionless central film thickness
$\widetilde{H}_{min}$	isothermal dimensionless minimum film thickness
h_{gap}	gap between the ball and the disc
$\bar{I}$	relative intensity of oil film
$\overline{I_0}$	relative intensity of zero film
k	ellipticity parameter

k_1, k_2	constants for contact dimensions calculation
K_f	thermal conductivity
L	the full contact length
n	refractive index
n_p	high-pressure refractive index
M	molecular weight
N_A	Avogadro number
p	pressure
p_{max}	maximum contact pressure
R	reflection coefficient
R'	reduced radius of curvature
R_x	reduced radius of curvature in the x-direction
R_x	reduced radius of curvature in the y-direction
R_{ax}	reduced radius of curvature of body A in the x-direction
$\mathrm{R_{ay}}$	reduced radius of curvature of body A in the y-direction
R_{bx}	reduced radius of curvature of body B in the x-direction
R_{by}	reduced radius of curvature of body B in the y-direction
S_f	minimum inlet distance
S	slide-to-roll ratio
S_0	coefficient for variation of dynamic viscosity with temperature
T	temperature
u, U	entrainment speed
$\bar{U}$	dimensionless speed parameter
u_a	velocity of the upper surface in the x-direction
u_b	velocity of the upper surface in the y-direction
$\tilde{u}$	entraining velocity in the x-direction
v_a	velocity of the lower surface in the x-direction
v_b	velocity of the lower surface in the y-direction
$\tilde{v}$	entraining velocity in the y-direction
V_0	atmospheric pressure volume
ΔV	volume change
w_a	velocity of the upper surface in the z-direction

w_b	velocity of the lower surface in the z-direction
W	contact load
$\bar{W}$	dimensionless load parameter
z'	acoustic impedance of the contacting material
Z	dimensionless constant
α	pressure-viscosity coefficient
α^*	Roelands' pressure-viscosity coefficient
α_d	molecular polarizability
ε	thermal expansion coefficient
ε_r	dielectric constant
ε_r', ε_r''	real and imaginary parts of the dielectric constant
ε_0	vacuum permittivity
ε_l	dielectric constant of the reduced mobility layer
ε_{oil}	dielectric constant of the lubricant
ρ	density
ν	kinematic viscosity
λ	Wavelength of the monochromatic light
η	dynamic viscosity
υ_A	Poisson's ratio of body A
υ_B	Poisson's ratio of body B
τ	shear stress
Φ_T	thermal reduction factor
ρ_0	atmospheric pressure viscosity

Chapter 1: Introduction

1.1 Background

Energy efficiency is of primary importance for all machine components nowadays. Reduction of frictional losses in lubricated contacts is a major way of achieving this goal. This usually leads to a film thickness reduction, and therefore more robust components and effective lubricants to provide surface protection are essential. Optimisation of both, the machine element design and lubricant composition, requires verification by experimental evaluation.

The application of an electrical capacitance method in lubricant film thickness measurements has been around since early experimental works on elastohydrodynamic (EHD) lubrication in the 1950s; however, the method lost its importance when the improvements of optical interferometry made the latter the preferred technique.

Optical interferometry, even though it allows accurate measurements down to very thin films, requires one of the contacting bodies to be made of a material transparent for visual light, and as a consequence it cannot be used where steel on steel contact occurs.

For the purpose of monitoring lubrication conditions in real machine components, such as rolling element bearings, the advantage of the capacitance method therefore still remains unquestionable. An inverse relationship between capacitance and film thickness makes the method very suitable for studying thin-film region. There are currently no alternatives to the capacitive method in this range, as both the ultrasound and resistance measurement can only provide useful information at higher separations.

The majority of experimental work in elastohydrodynamic lubrication, including film thickness measurements, is nowadays carried out in a ball-on-flat arrangement, which is used to simulate conditions found in rolling bearings. However, due to a different geometry and material pair used (glass disc if optical interferometry is applied) it is not possible to replicate the exact condition of an operating bearing and therefore the lubricant behaviour found in such contacts.

1.2 Aims of the study

The current work, sponsored by SKF, is focused on studying aspects of lubrication relevant to rolling element bearings, using the electrical capacitance method.

The main aim of the study was to establish an experimental approach to film thickness evaluation from capacitance measurements in a ball-on-flat arrangement, including steel-on-steel contacts.

During the course of the work it was also intended to:

- examine how a lubricant's polarity affects the capacitance measurements and film thickness evaluation in EHD contacts,
- study the behaviour of blends of polar and nonpolar base oils,
- evaluate the effect of additives, such as organic friction modifiers,
- investigate grease lubrication with the electrical capacitance method.

Additionally, due to very promising results in ball-on-flat experimental test rig, the study has been extended to cover film thickness measurements in a modified rolling element bearing.

1.3 Layout of the thesis

This thesis consists of 9 main chapters, which are summarised below:

Chapter 1: Introduction: introduces the main research subject and discusses why it is considered necessary.

Chapter 2: Lubrication fundamentals: describes the fundamental principles of lubricant film formation, including Hertzian theory, Reynolds' equation and elastohydrodynamic film thickness formulas.

Chapter 3: Lubricants: provides basic information on lubricants' chemistry, functions and properties.

Chapter 4: Experimental methods for studying EHD films: reviews the existing literature focused on experimental studies with electrical and optical methods.

Chapter 5: Lubrication of rolling element bearings: reviews the findings and a current understanding of grease lubrication mechanism in rolling element bearings.

Chapter 6: Properties of lubricants: focuses on high-pressure and dielectric properties relevant to the current study.

Chapter 7: Experimental methodology: describes techniques and methodology used in this thesis, focusing on film thickness evaluation and capacitance measurements.

Chapter 8: Results and discussion: contains the results of experiments performed also discussing their practical implications to capacitance method application.

Chapter 9: Conclusions: the final chapter contains a summary of all the findings and conclusions of this thesis, together with suggestions for future work on the subjects.

Chapter 2: Lubrication fundamentals

It has been recognized early that an introduction of a lubricating film between two surfaces in relative motion results in a reduction of friction and an increase of the durability of contacting surfaces, thus lubrication is applied in various forms to machine elements, mechanisms, machines and in general in systems where contact between solid surfaces needs to be avoided.

Lubrication mechanism and contact conditions are determined by the conformity of the surfaces. For conforming surfaces, such as those found in journal bearings (Figure 2.1) the load carrying area is relatively large in comparison to the bearing dimensions and therefore contact pressures are low (usually less than 5 MPa). In the case of nonconforming surfaces the contact area is small which results in high contact pressures. Examples of nonconforming contacts include rolling bearings, gears and cam-follower mechanisms.

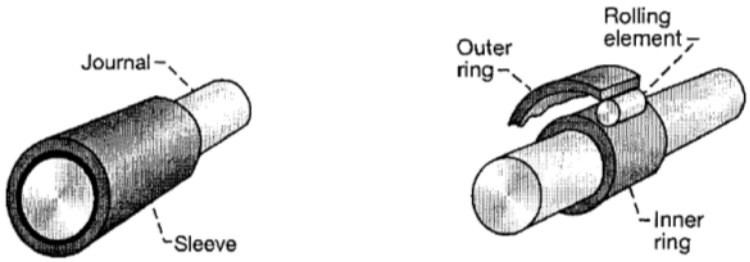

Figure 2.1: Conformal and non-conformal contacts (Hamrock et al., 2004)

The majority of contacts, found in machine components, are lubricated without external pumping and the lubricant is entrained into the contact purely by the motion of either one or both surfaces. This mechanism is called hydrodynamic lubrication, as opposed to hydrostatic lubrication found in externally pressurised bearings.

2.1 Lubrication regimes

Lubrication regimes can be defined based on the nature of the lubricant used (solid lubrication, fluid film lubrication, etc.), the mechanisms of the film formation (e.g. hydrodynamic, elastohydrodynamic, hydrostatic and boundary), or the proportion of the load carried by solid-solid interaction or fluid film (e.g. boundary, full-film or mixed). A graphical illustration of the friction generated in various lubrication regimes is given by the so-called Stribeck curve, which shows variation of friction coefficient as a function of a product of speed, lubricant viscosity and load. An example is displayed in Figure 2.2, while the separation of the surfaces in different regimes is schematically shown in Figure 2.3.

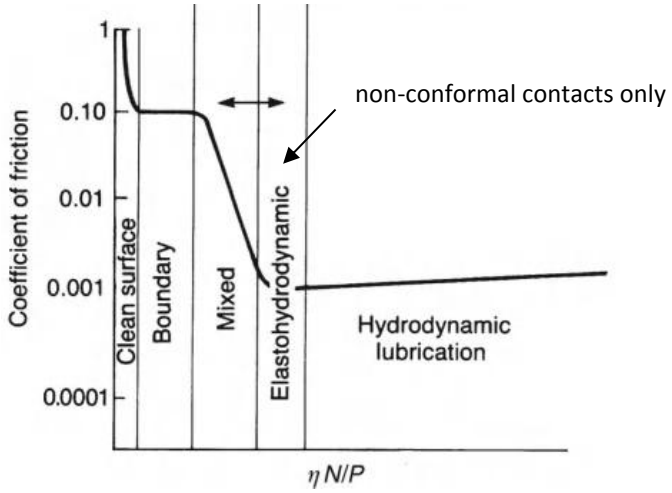

Figure 2.2: Stribeck curve (Bhushan, 2013)

Hydrodynamic (HD) lubrication

This mechanism of lubrication is found in conformal contacts, but can also exist in nonconformal contacts at very low load, when elastic deformation of the surfaces does not take place. Typical examples of machine components working in this regime include journal and thrust bearings.

During the conditions of high speeds, low loads or with high-viscosity lubricants, a thick (typically 5–500 μm) lubricating film, which fully separates the contacting surfaces, is

formed. Here, the load carrying capacity of the lubricant film is a result of pressure generated within this film.

The coefficient of friction is low and the only source of frictional resistance to motion is shearing of the fluid. Slight increase of the coefficient of friction with speed is caused by viscous drag. Lubricant film thickness can be determined from the Reynolds' equation (section 2.2.2).

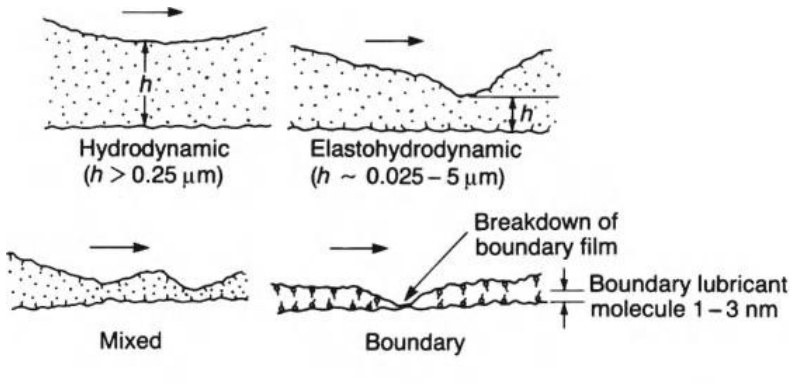

Figure 2.3: Separation of surfaces in different regimes (Bhushan, 2013)

Boundary lubrication

On the other extreme, where speeds are low, loads are high or low-viscosity fluids are used, a regime exists where the surfaces are separated by a layer formed as a result of chemical or physical interaction of lubricant molecules with the solid surfaces. Here, frequent contact between asperities of the opposing surfaces occurs and therefore the load is almost entirely carried by the asperities, which results in high friction. Boundary film thickness is in the range of few nanometres depending on the molecular size of the species. Even though friction in the boundary regime is much higher than in hydrodynamic lubrication, it is still much lower than for unlubricated surfaces.

Elastohydrodynamic (EHD) lubrication

Similarly as in HD regime, surfaces are fully separated, however, the contacting bodies have nonconforming geometry. This results in relatively small contact areas, which in turn leads to high contact pressures, up to few gigapascals. There are two important implications of high contact pressures found in EHD contacts. First is an elastic

deformation of surfaces, and the other is a nearly exponential increase of a lubricant's viscosity with pressure. Lubricant film formation in EHD regime is thus due to a combination of these three mechanisms: lubricant entrainment in a converging wedge, elastic deformation of the surfaces and variation of the lubricant's viscosity with pressure.
Rolling element bearings, gears and contacts between cams and tappets operate in this regime, with films ranging from nanometres to few micrometres thickness.

Mixed lubrication
This lubrication regime can be treated as a transition between boundary and full-film conditions (elastohydrodynamic or hydrodynamic), and as the name suggests it shows features of both. The surfaces are separated by a lubricant film; however, occasional metal-metal contact occurs. The load is carried partially by the lubricating film and partially by asperities. As the speed or viscosity decreases, or the load increases, more direct contact between surfaces takes place, therefore increasing coefficient of friction.

Machine components are generally designed to work under either hydrodynamic or elastohydrodynamic conditions as those offer low friction and wear. In some cases, however, as for example during start/stop or at high operating temperature they will experience mixed or even boundary lubrication.

2.2 Elastohydrodynamic lubrication theory

Within the EHD regime, researchers distinguish two types of lubrication depending on the elastic properties of the materials, namely Soft- and Hard-EHD. Hard-EHD exists with materials of high elastic modulus, such as metals; while low elastic modulus

solids, such as rubbers, fall into the Soft-EHD category. Maximum pressure in Soft-EHD is much lower, with values reaching only few MPa.

As the main interest of the current research is on lubrication of contacts between rolling elements and raceways in rolling bearings, only hard-EHD is concerned and this regime will be referred to from now on simply as EHD.

2.2.1 Hertzian theory of smooth contact surfaces

It is known from contact mechanics that when an elastic solid body is subjected to a load, reversible elastic deformation takes place. However, if the stresses within the material exceed its yield stress value, plastic flow occurs, leading to permanent plastic deformation.

Two solids can come into contact at zero load at either a point or a line. When the load is applied these expand forming an ellipse or a rectangle, respectively. The size and shape of the contact area depends on the geometry of the bodies, their elastic properties and the magnitude of load applied.

The theory of elastic contact for smooth surfaces was developed by Hertz (1881) in 1881. In his work, Hertz considered two contacting bodies with convex surfaces, as seen in Figure 2.4.
The following assumptions were introduced by Hertz (Hamrock et al., 2004; Stachowiak and Batchelor, 2001):

- the two contacting bodies are homogenous and the yield stress of the material is not exceeded,
- there are no tangential forces acting between the solids,
- the contact area is very small compared to dimensions of the solids,
- the contacting surfaces are at rest and in equilibrium.

According to Hertz, the contact between two simple nonconforming surfaces can be approximated with an equivalent nonconforming surface in contact with a plane. This allows a reduced radius of curvature to be calculated:

$$\frac{1}{R'} = \frac{1}{R_x} + \frac{1}{R_y} = \frac{1}{R_{ax}} + \frac{1}{R_{bx}} + \frac{1}{R_{ay}} + \frac{1}{R_{by}} \quad (1)$$

Where:

R_x is the reduced radius of curvature in the x-direction

R_x is the reduced radius of curvature in the y-direction

R_{ax} is the reduced radius of curvature of body A in the x-direction

$\mathrm{R_{ay}}$ is the reduced radius of curvature of body A in the y-direction

R_{bx} is the reduced radius of curvature of body B in the x-direction

R_{by} is the reduced radius of curvature of body B in the y-direction

As seen in Figure 2.5.

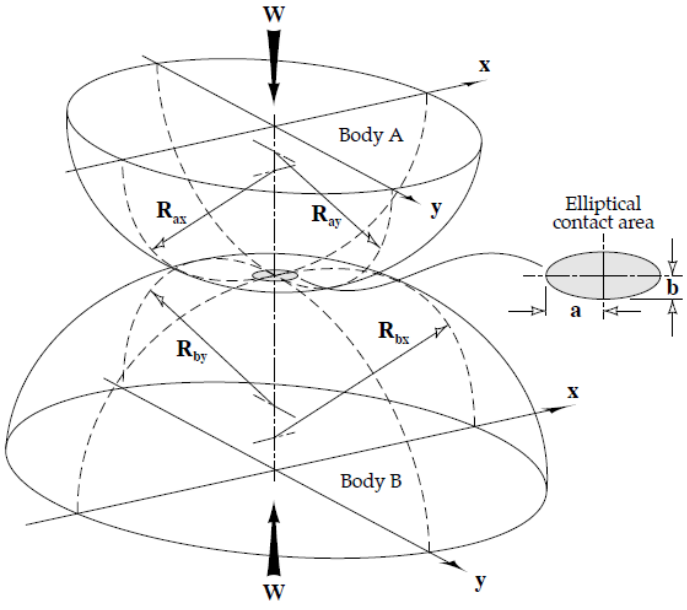

Figure 2.4: Geometry of two contacting bodies having convex surfaces

(Stachowiak and Batchelor, 2001)

It is important to note that “positive” (convex surface) or “negative” (concave surface) curvature has to be included in calculation of reduced radius.

Based on the Hertzian theory it is possible to calculate not only the dimensions of the contact and the maximum contact pressure, but also the maximum deflection in the centre of the contact as well as the position of the maximum shear stress below the surface.

For a general elliptical contact case, as found between two solids of different radii of curvature, the contact dimensions, a and b, are given by:

$$a = k_1 \left(\frac{3WR'}{E'}\right)^{1/3} \qquad b = k_2 \left(\frac{3WR'}{E'}\right)^{1/3} \tag{2}$$

where a is a semimajor axis and b is the semiminor axis, W is the normal load, and E' is the reduced Young's modulus defined as:

$$\frac{1}{E'} = \frac{1}{2}\left[\frac{1-\upsilon_A^2}{E_A} + \frac{1-\upsilon_B^2}{E_B}\right] \tag{3}$$

Where: υ_A and E_A are Poisson's ratio and Young's modulus of body A, while υ_B and E_B are elastic properties of body B.

Maximum contact pressure, p_{max}, is given by the formula:

$$p_{max} = \frac{3W}{2\pi ab} \tag{4}$$

2.2.2 Reynolds' equations

A hydrodynamic film is formed between two converging surfaces in relative motion as a result of viscous entrainment of lubricant into a gap between them. As the lubricant passes through the gap it is compressed and a pressure field is generated resulting in a load carrying capacity. This principle is schematically shown in Figure 2.5.

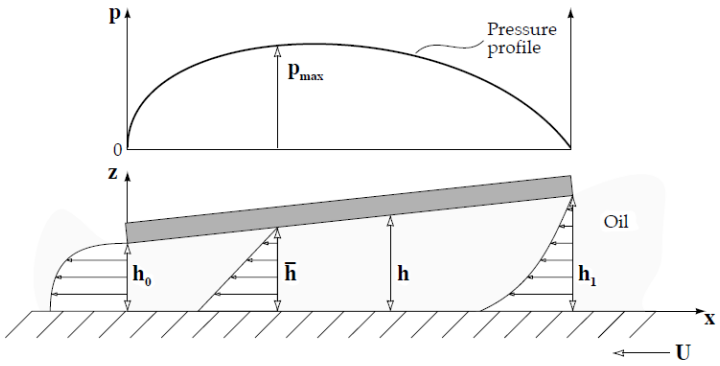

Figure 2.5: Generation of hydrodynamic pressure within the lubricant film (Stachowiak and Batchelor, 2001)

Towards the end of 19th century a British engineer and scientist, Osborne Reynolds (1886), following pioneering experimental work by B. Tower, developed the fundamental equation governing the pressure distribution in fluid film lubrication. Reynolds' equation can be derived from either the Navier-Stokes equations with consideration of continuity equation, or from the laws of viscous flow and conservation of mass principle. In his analysis, Reynolds considered only incompressible fluids and smooth surfaces and he included a series of assumptions applicable to the case of slow viscous motion where pressure and viscous terms are dominant.

These assumptions are: (1) the lubricant behaves in a Newtonian manner and the flow is laminar; (2) both inertia and body forces are negligible; (3) surface tension effects are not considered, (4) the fluid film thickness is much smaller in comparison to other bearing dimensions; (5) the pressure, density and viscosity of the fluid are constant across the film, and (6) there is no slip at the boundaries.

The general Reynolds equation can be written according to Hamrock et al. (2004):

$$0 = \frac{\partial}{\partial x}\left(-\frac{\rho h^3}{12\eta}\frac{\partial p}{\partial x}\right) + \frac{\partial}{\partial y}\left(-\frac{\rho h^3}{12\eta}\frac{\partial p}{\partial y}\right) + \frac{\partial}{\partial x}\left(\frac{\rho h(u_a+u_b)}{2}\right)$$

$$+ \frac{\partial}{\partial y}\left(\frac{\rho h(v_a+v_b)}{2}\right) + \rho(w_a + w_b) - \rho u_a \frac{\partial h}{\partial x} - \rho v_a \frac{\partial h}{\partial y} + h\frac{\partial \rho}{\partial t} \qquad (5)$$

From this, more specific equations for special cases can be derived. For instance, if only tangential motion under steady state is considered, $\partial h/\partial t = 0$, $w_b = 0$ and $w_a = u_a\,\partial h/\partial x + v_a\,\partial h/\partial y$, the Reynolds equation can be written as (after Bhushan, 2013):

$$\frac{\partial}{\partial x}\left(\frac{\rho h^3}{\eta}\frac{\partial p}{\partial x}\right) + \frac{\partial}{\partial y}\left(\frac{\rho h^3}{\eta}\frac{\partial p}{\partial y}\right) = 12\tilde{u}\frac{\partial(\rho h)}{\partial x} + 12\tilde{v}\frac{\partial(\rho h)}{\partial y} \tag{6}$$

Where:

$\tilde{u} = \frac{u_a+u_b}{2} = constant$ and $\tilde{v} = \frac{v_a+v_b}{2} = constant$

This equation is applicable to elastohydrodynamic lubrication.

If the lubricant flow in y-direction, due to side leakage is neglected, the equation is reduced to:

$$\frac{\partial}{\partial x}\left(\frac{\rho h^3}{\eta}\frac{\partial p}{\partial x}\right) = 12\tilde{u}\frac{\partial(\rho h)}{\partial x} \tag{7}$$

2.2.3 Film thickness calculation

Several attempts to predict lubricant film thickness in highly-loaded nonconforming contacts have been carried out during the first half of the 20th century. It was not until pioneering work by Ertel, published by Grubin (Spikes, 2006; Lugt and Morales, 2011), who combined hydrodynamic action with both elastic deformation of surfaces and exponential increase of viscosity with pressure, when realistic film thickness values were obtained.

Ertel's equation for film thickness where a pressure gradient is zero in a line contact, $\bar{h}$, can be written as follows (Stachowiak and Batchelor, 2001):

$$\left(\frac{\bar{h}}{R'}\right) = 1.657\left(\frac{U\eta_0\alpha}{R'}\right)^{0.7273}\left(\frac{W}{LE'R'}\right)^{-0.0909} \tag{8}$$

Where U is the entrainment velocity, W is the contact load, L is the full contact length and α is a pressure-viscosity coefficient. While R' and E' are defined as earlier.

Based on his analysis Ertel also predicted a reduction of film thickness and an accompanying pressure spike near the contact outlet, as shown schematically in Figure 2.6. This has been confirmed 10 years later by Dowson and Higginson (1959).

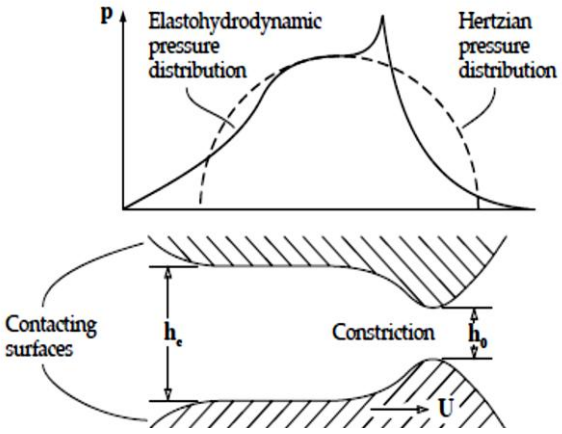

Figure 2.6: EHD film thickness and pressure (Stachowiak and Batchelor, 2001)

In 1976 Hamrock and Dowson published a series of papers (Hamrock and Dowson 1976; Hamrock and Dowson 1976; Hamrock and Dowson 1977), including more general formulas allowing calculating isothermal dimensionless central (h_c/R') and minimum (h_{min}/R') film thickness in both line and elliptical contacts:

$$\widetilde{H}_{min} = 3.63\bar{U}^{0.68}\bar{G}^{0.49}\bar{W}^{-0.073}(1 - e^{-0.68k}) \quad (9)$$

$$\widetilde{H}_c = 2.69\bar{U}^{0.67}\bar{G}^{0.53}\bar{W}^{-0.067}(1 - 0.61e^{-0.73k}) \quad (10)$$

Given the ellipticity parameter, k, equal to $1.03\left(\frac{R_y}{R_x}\right)^{0.64}$, and $\bar{U}$, $\bar{G}$ and $\bar{W}$ are the dimensionless speed, material and load parameters defined as:

$$\bar{U} = \frac{u\eta_0}{E'R'} \qquad \bar{G} = \alpha E' \qquad \bar{W} = \frac{W}{E'R'^2} \quad (11)$$

Where u is the entrainment speed ($u = \frac{u_a + u_b}{2}$).

Chapter 3: Lubricants

Lubricants are used practically everywhere where relative motion of surfaces occurs. From an application point of view, lubricants can be divided into two groups: automotive and industrial, both having roughly the same market share. Majority of automotive lubricants are engine oils, with some proportion of transmission fluids. Industrial lubricants cover a wide range of fluids including hydraulic fluids, gear oils, metalworking fluids, greases, solid lubricants and other industrial oils.

Since lubricants are found in a range of machine components, they are exposed to various operating conditions, as seen in Figure 3.1. It is clear that such a complexity of requirements cannot be met by one simple fluid and therefore a number of chemistries are used nowadays.

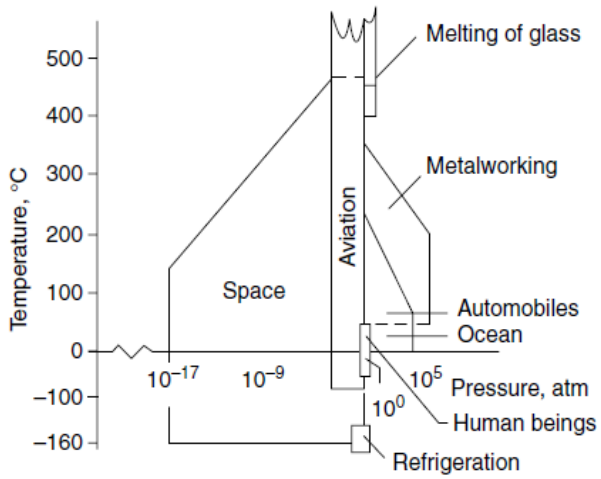

Figure 3.1: Operation temperature and pressure range for lubricants in various applications (Rudnick, 2006)

A general trend towards miniaturization results in higher contact loads and puts more stress on modern lubricants. Additionally, they are required to operate for extended periods of time with no significant deterioration of performance. These factors push the formulators to seek innovative solutions that would be able to meet more and more stringent requirements.

3.1 Functions and properties

The fundamental function of all lubricants is preventing direct contact between the surfaces and thus reducing wear and friction. Lower friction also gives a benefit of lower operating temperatures which in turn extends the service life of lubricants and machine components. Depending on the application, lubricants may also act as sealants, such as greases in rolling element bearings, or provide cleaning function by removing wear particles and deposits, such as for example engine oils. Lubricating oils also act as coolants by helping removing the heat from tribological contacts.

One basic property of all liquid lubricants, which can be directly correlated to the ability to form a separating film between moving surfaces (Chapter 2), regardless of the origin and chemical structure, is viscosity. Viscosity is a measure of internal friction within the lubricating film and can be expressed as either *dynamic* (η) or *kinematic* viscosity (ν). The two are connected via density (ρ), according to the equation:

$$\nu = \frac{\eta}{\rho} \tag{12}$$

Viscosity is also used to assign the oils into different grades in official lubricants classifications, such as ISO 3448 for industrial oils (International Organization for Standardization, 1992), SAE J306 for automotive gear oils (SAE International, 2005) and SAE J300 for automotive engine oils (SAE International, 2013).

As already mentioned, most of the machine components will be required to operate under a range of temperatures; therefore it is necessary to ensure that the lubricant chosen is able to fulfil its function at all times. For that reason it is essential to know how viscosity of the oil changes with temperature. One way of describing this dependence, commonly used in the industry, is with the aid of a property known as viscosity index (VI), where the higher viscosity index means lower decrease of viscosity with temperature.

While viscosity index is mostly used to describe high-temperature characteristics, a different property, called pour point, gives an indication of low-temperature fluidity of oils. At temperatures below the pour point the oil no longer flows and therefore cannot be entrained between the contacting bodies to provide surface separation.

3.2 Chemistry

3.2.1 Lubricating oils

Around 90% of the total lubricants consumption can be attributed to lubricating oils. These in turn consist of a base oil and an additive package. The amount of additives in the formulation depends on the application and requirements and it can vary from below 1% (e.g. hydraulic fluids and compressor lubricants) up to even 30% (e.g. metalworking fluids, greases and gear oils) (Mang and Wilfried, 2007).

Base oils can be simply divided depending on their origin into two types: petroleum based and non-petroleum based fluids. The majority of base oils used in modern lubricants are mineral-oil derived.

More systematically, base oils can be assigned into one of five groups according to a well-known API (American Petroleum Institute) classification (American Petroleum Institute, 2012). Groups I to III are produced by crude oil refining and Groups IV and V are chemically synthesized. Petroleum based oils fall into an appropriate category based on their unsaturation level, sulphur content and viscosity index, as can be seen in Table 1.

Table 1: Classification of base oil according to API (American Petroleum Institute, 2012)

Base oil category	Sulphur, %		Saturates, %	Viscosity index
Group I	>0.03	and/or	<90	80 to 120
Group II	<0.03	and	>90	80 to 120
Group III	<0.03	and	>90	>120
Group IV	Polyalphaolefins (PAOs)			
Group V	All other base oils			

Additionally, within Group II and III unofficial higher-quality subcategories are recognized to differentiate the base stocks having properties in the upper range of the limits. Thus Group II+ base stocks have viscosity indexes between 110 and 120, while Group III+ oils will cover those with VI above 140 (Mortier et al., 2010).

Group I, the least processed base oils, are classified as mineral oils and are characterised by the highest unsaturation level and heteroatoms (such as sulphur) content. They are obtained by mild refining using solvents, which removes most of the impurities and therefore are called solvent neutral – SN.

Group II base oils are further refined by hydrogen treatment (hydrofinishing) which helps removing the majority of heteroatoms and also improves thermo-oxidative stability of the stock by saturating the prone to oxidation double bonds.

Group III base stocks are produced using deep refining processes described as unconventional (hydrocracking and hydroizomerization), during which a change of the molecular structure occurs. These processes significantly improve the viscosity index of Group III base oils.

API group IV is reserved for polyalphaolefines (PAOs), which are oligomers of α-decene, or other α-olefin. PAOs are free from heteroatoms and are fully saturated. Thanks to that they offer high thermo-oxidative stability and very high viscosity indexes.

The last group in API classification (V), covers all the remaining synthetic chemistries. Esters, polyalkylene glycols, polysiloxanes and other specialised types are included here.

The choice of base oil for certain application is dictated by requirements that oil has to meet to fulfil its function. Economic aspects and availability are also very important and not always the best quality oil in the market will be chosen. The price of base oils increases from Group I to Group V, which is related to the production cost.

The quality of base stock chosen will also depend on the assumed life of lubricant. In some cases, where it is difficult, or even impossible to replenish or replace the lubricant, higher quality base stock which provides longer service life would be preferred. In some cases additional, special requirements may have to be taken into account, such as low toxicity (lubricants used in food and drugs processing) and biodegradability (environmentally sensitive areas).

3.2.2 Additives

As a result of ever-increasing demands for machine elements' performance, lubricants get more complex as they are now required to provide a long life of components in much more harsh and sometimes even extreme operating conditions. To be able to cope with that, a number of additives are added to the base oil. Their purpose is to either enhance the existing properties or to introduce new ones.

Two types of additives, namely viscosity index improvers (VIIs), also called viscosity modifiers, and pour point depressants (PPDs) act to modify existing properties of the base oil. Both types are widely used nowadays as they allow modifying high temperature viscometrics of a formulation (VII) and fluidity of the oil at low temperatures (PPD).

Even the best quality base stocks when exposed to high temperatures in the presence of oxygen (from the air) and under catalytic influence of metals will eventually start degrading. Therefore all modern lubricants contain oxidation inhibitors which help in delaying that process.

One of the main functions of a lubricant is preventing wear of the contacting surfaces. This can be achieved by adding compounds, anti-wear (AW) and extreme pressure (EP) additives, which can react with the surfaces forming a protective layer.

As the surfaces wear, they become more prone to corrosion; therefore anti-rust additives (corrosion inhibitors) are also often included in the formulation.

Another important function of lubricants is lowering friction. Some base oils on their own show higher benefits than others, while the addition of effective friction modifiers can provide further improvement.

Deposit control additives, including detergents and dispersants are crucial for engine oils application as they act to neutralize acidic species in the oil originating from either combustion by-products or oxidation of the oil itself, and help keeping the surfaces clean.

Some additives can perform multiple functions. Viscosity modifiers can also improve low-temperature fluidity of oils, while anti-wear additives, such as zinc dialkyldithiophosphates (ZDDPs) also act as antioxidants.

3.2.3 Greases

Due to their consistency greases are advantageous over liquid lubricants in applications where oils would normally leak out while a grease is able to stay in contact. Additionally, they provide a sealing function which would not be achieved with the use of an oil.

Greases are classified based on their consistency, determined by worked penetration, into nine grades created by the National Lubricating Grease Institute (NLGI). The higher the NLGI number the more “solid” grease’s consistency.

Grease contains between 70 and 95% of a base oil, thickener accounts for 5–25% and additives contribute to another 0.5–10% (Rudnick, 2010). Relative proportions of these three ingredients vary with the type of grease and application.

In general all types of base oils can be used for production of greases, and some will be preferred over the other depending on the requirements. The viscosity range of the base oils is between 15 to 1500 cSt at 40^{o}C (Rudnick, 2006).

Greases owe their consistency to thickener's dispersion in the base oil, which creates a fibrous framework embedding the base oil. Most commonly used thickening agents are metal soaps produced by reacting metal hydroxide (e.g. lithium, calcium, sodium or aluminium) with fatty acids.

Apart from simple soaps, consisting of a soap of single fatty acid, complex soaps produced by the addition of a complexing agent (soap of short chain carboxylic acid) are often found.

Polyureas (diurea and tetraurea) and inorganic thickeners, such as silica, polytetrafluoroethylene (PTFE) and chemically modified clays are also produced.

The thickener type strongly affects the maximum temperature at which certain grease can be used (Table 2). The important parameter is here a dropping point, which refers to a temperature at which a grease becomes fluid.

As can be clearly seen complex greases have much higher dropping points than simple greases and therefore are more suitable for high-temperature conditions. Their maximum operation temperature is as high as polyurea and organoclay greases.

Table 2: Influence of a thickener on temperature properties of greases (based on Rudnick (2010))

Thickener	**Dropping point, ^{o}C***	**Maximum Usable Service Temperature, ^{o}C***
Aluminum soap	110	79
Calcium soap	132-143	121
Sodium soap	171-177	121
Lithium soap	199	135
Calcium complex	>260	177
Lithium complex	>260	177
Aluminum complex	>260	163
Polyurea (nonsoap)	>232	177
Organoclay (nonsoap)	>260	177

* values recalculated from ^{o}F

There are a few types of additives that are usually included in the greases' formulation to enhance their performance in some areas. As the main function of grease, similarly to liquid lubricant, is protection of surfaces against wear, AW and EP agents are often added. Apart from the same chemistries as used for oils, solid lubricants based on graphite or molybdenum compounds can also be included in the additive package. Another two important additives for greases are antioxidants and corrosion inhibitors.

Rheology of greases is rather complex, as they show viscoelastic behaviour and their properties depend on the shear rate. If a critical value of shear rate, known as the yield point, is exceeded, grease starts flowing and behaving in a Newtonian manner.

Chapter 4: Experimental methods for studying EHD films

4.1 Electrical methods

4.1.1 Capacitance

Pioneering work by Crook (1958) in the late 1950s provided the first experimental evidence proving the validity of Elastohydrodynamic Lubrication theory for line contacts. Crook evaluated lubricant film thickness from the measurements of electrical capacitance in an oil-lubricated twin-disc machine. In his calculations he considered that the inlet is fully-filled with oil and at the exit side layers of oil adhere to each of the discs.

Apart from measuring capacitance between the discs, he also measured capacitance of the oil layers after going through the contact, by taking readings between rotating discs and stationary unloaded pads sliding on those layers. He found that the two values are proportional up to the load at which elastic deformation starts taking place, indicating the offset of elastic deformation.

His experiment with an interrupted oil-supply (Figure 4.1) shows that when the oil supply to the contact is stopped, a gradual decrease of film thickness is observed, which is accompanied by a gradual increase of disc temperature. When the oil supply is resumed the film thickness does not return to its initial value instantly, but again gradually, following the change of disc temperature and its return to the initial level.

Crook also estimated the temperature of the oil passing through the contact based on resistivity measurements in rolling and rolling-sliding conditions. He concluded that lubricant film thickness is determined by the viscosity of the oil in the inlet conjunction, not inside the EHD contact.

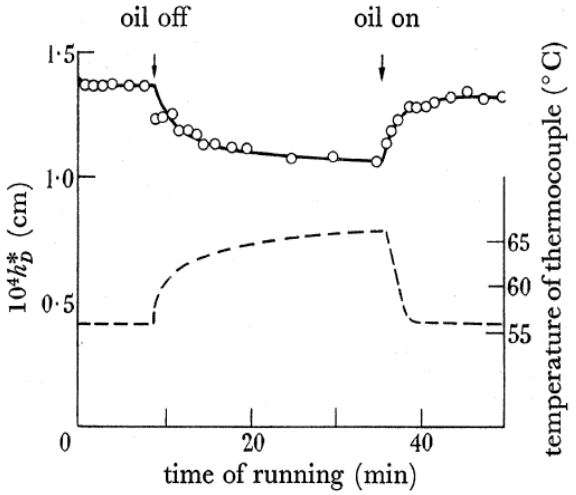

Figure 4.1: Experiment with intermitted oil supply (Crook, 1958)

These observations were also confirmed by Archard and Kirk (1961) for a more severe case of a point contact. The authors tested a conjunction between two crossed rotating cylinders with the same mineral turbine oil, as used earlier by Crook (1958). Qualitative information about the presence of a lubricating film over a wide range of operating conditions was deduced from resistance measurements. Electrical capacitance, on the other hand, was used to obtain quantitative data regarding film thickness. Even though no elastohydrodynamic theory for a point contact existed at the time, the authors were able to prove that the same principles will be valid as for the line contact.

A decade later a twin-disc machine was used again by Dyson and co-workers (Dyson et al., 1965a) who measured film thickness with electrical capacitance for a range of fluids in pure rolling and rolling-sliding conditions. Disc temperatures were continuously monitored with thermocouples embedded under the surface (as those trailing on disc surfaces showed temperatures up to 10^{o}C too low) and controlled by adjusting the temperature of test oil. In some conditions it was not possible to maintain stable disc temperature (i.e. high viscosity oils, low temperatures, high speeds or sliding) and in these cases capacitance was correlated to corresponding temperatures. During experiments with sliding, the temperature of the discs varied by up to 5^{o}C despite individual oil supply for each disc.

To establish the relationship between the discs capacitance and lubricant film thickness the shape of the disc was assumed to be according to Hertz theory for dry contact, but with additional separation equal to lubricant film thickness. The authors considered the same lubricant distribution around the contact as Crook (1958) (Figure 4.2).

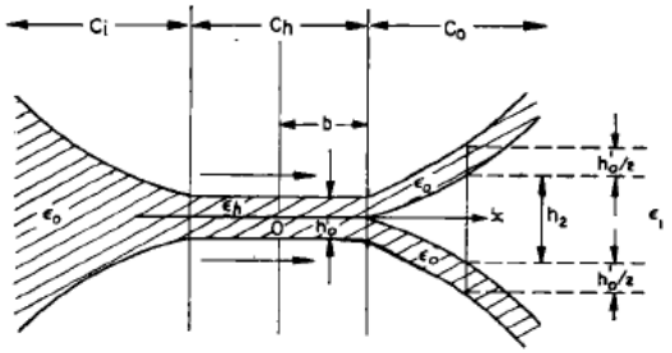

Figure 4.2: Assumptions of oil distribution for capacitance calculations (Dyson et al., 1965a)

The results show in general a good agreement with Dowson and Higginson predictions over a range of 0.025-1 μm for six out of eight fluids studied. Figure 4.3 shows an example of film thickness measurements results. It is important to note that the authors observed a gradual fall of measured film thickness away from theoretical values in higher film thickness region for all fluids. This behaviour is more pronounced when sliding is present; therefore the authors suggest that it is not a result of compression of the lubricant in the inlet region, but rather a consequence of inlet shear heating. The curves of two of the fluids tested (silicone fluid and polymer solution) are shifted relative to Dowson and Higginson theoretical values, giving significantly lower results. The authors state that the reason for this is non-Newtonian behaviour of these fluids under testing conditions. A more detailed study on this subject is presented in the accompanying paper (Dyson et al., 1965b).

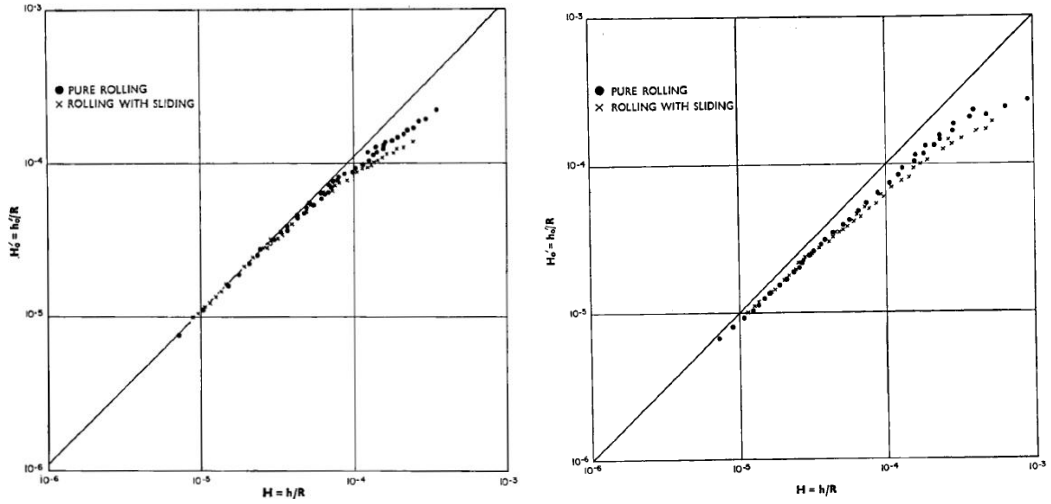

Figure 4.3: Comparison of measured and theoretical non-dimensional film thickness from twin-disc machine (Oil A and F) (Dyson et al., 1965b)

Additionally some of the fluids show slightly higher measured film thicknesses than theoretical values in the thin-film region. Some possible explanations are given, including errors in interpretation of capacitance results; however, the cause of this does not seem to be clear.

As the twin disc machine is used to simulate conditions found in rolling element bearings, a natural next step was extending the study to grease films (Dyson and Wilson, 1969). A range of greases and their base oils were investigated in pure rolling conditions at a fixed speed and controlled temperature of 60^{o}C. The authors distinguished two extreme cases of a “full inlet” and an “empty inlet” (considered the same as exit side) assuming that lubricant film thickness will lie in between the two. Comparing oil and grease films it was found, that contrary to most of the oils showing a more or less stable film thickness over the whole duration of an experiment, grease films showed significantly decreasing thickness. The initial film thickness of greases at the beginning of the tests exceeded that of their base oils. With time, however, gradually they became thinner, falling below values measured for base oils and reaching a stable value of around 40% of the initial thickness.

This finding was further confirmed in Wilson's work on rolling element bearings (Wilson, 1979). Based on capacitance measurements it was concluded that greases in fully-flooded conditions form films reaching values which would normally correspond to oil with a viscosity higher by 30-35% than the base oil viscosity.

In his study Wilson used two types of bearing: a double-row spherical roller bearing (22312; two sets of fourteen rollers) and a single-row cylindrical roller bearing (2312; one set of twelve rollers), with brass and steel cages, respectively. A schematic of a radially loaded bearing is shown in Figure 4.4. Wilson in his calculations considered separate contribution from loaded and unloaded sectors, as well as capacitance due to a metallic cage. The relationship between bearing capacitance and lubricant film thickness was first established for each bearing using a calibration oil. Film thickness was calculated using a minimum film thickness formula and assuming a mean value between inner and outer ring. Temperature of both rings was measured with thermocouples. Lubricant film thickness included the inlet shear heating correction and was calculated for viscosity corresponding to mean temperature of inner and outer ring.

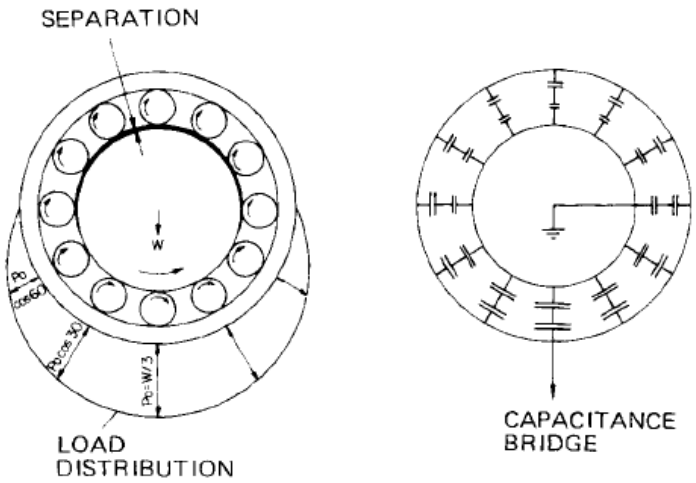

Figure 4.4: Load distribution and corresponding electrical circuit of a radially loaded roller bearing (Wilson, 1979)

In 1982 the development of an instrument capable of monitoring the lubrication condition in rolling element bearings, called Lubcheck, was described by Heemskerk and co-workers (Heemskerk et al., 1982). In this study 6204 standard deep-groove ball bearings (DGBB) were lubricated with mineral oil and grease and tested under purely radial load at room temperature. In order to quantify lubrication condition the authors used metallic contact time fraction (PCT, %) and "lift-off" speed (minimum speed at which PCT goes down to 10%). PCT allows differentiating continuous metallic contact, intermittent contact and complete separation between the surfaces, based on assumed reference voltage level. Figure 4.5 shows an example of an output signal for a bearing run over a range of speeds. As the speed and film thickness increases, the frequency of metallic contact decreases, until the film thickness is sufficient to prevent even occasional metallic contact.

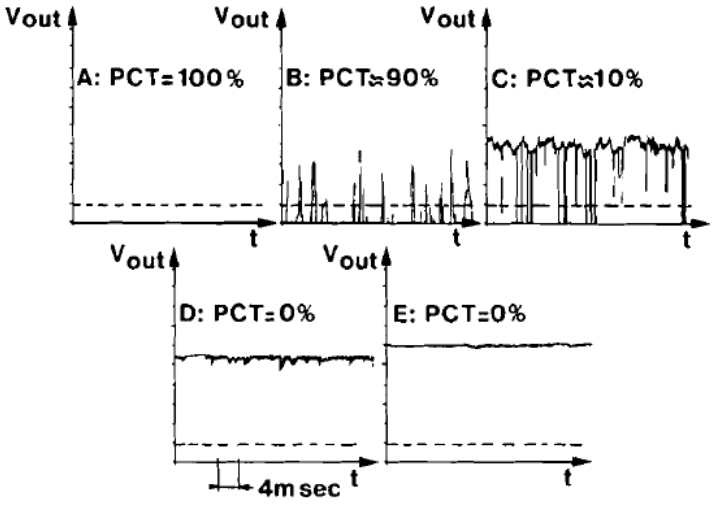

Figure 4.5: Metallic contact fraction (PCT, %) measured for DGBB at few speeds (Heemskerk et al., 1982)

The instrument was later used by Leenders and Houpert (1987) for determination of film thickness in 6309 deep-groove ball bearings and spherical roller bearings (22220 with 2 rows of 19 rollers each). The bearings were lubricated with circulating oil, with continuous measurement of oil inlet and outlet temperature. Inner and outer

ring temperatures were also monitored. All tests were performed under pure radial loads, up to 26 kN for DGBB and up to 140 kN for spherical roller bearings.

In this work a calibration curve was constructed based on calculated bearing capacitance and Hamrock and Dowson central film thickness with a thermal correction factor. It was found that even under so-called marginal lubrication (for thin film or high surface roughness) film thickness results were surprisingly in agreement with EHD theory developed for smooth surfaces (Figure 4.6). The authors concluded that the reason is the elastic conformity or flattening of asperities with rough surfaces, as no indication of insulating chemical film was found on the bearing surfaces.

They also observed running-in by measuring capacitance and the percentage of contact time. Significant changes of capacitance and "lift-off" were observed with time.

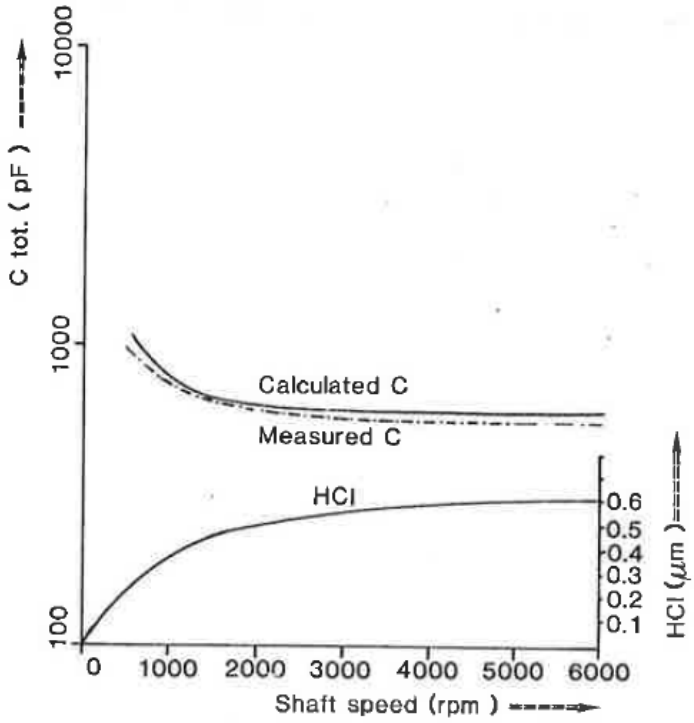

Figure 4.6: Comparison of measured and calculated bearing capacitance and corresponding film thickness at the highest load position in a DGBB test (Leenders and Houpert, 1987)

In another paper (Wikström and Jacobson, 1997) the Lubcheck instrument was used to study lubricant losses in oil lubricated, radially loaded spherical roller bearings (22310 with two rows of 14 rollers). Tests were performed on a modified bearing life test rig, placed in a climate chamber, where two bearings can be tested simultaneously. During the experiments the temperature of the outer ring in the loaded sector was continuously monitored.

Since the bearings were lubricated once (0.5 ml of oil), the authors, by determining the time of lubricant film breakthrough examined the influence of factors such as temperature, viscosity, lubricant type and speed.

The film breakthrough is deduced from Lubcheck signal (V_{cap} exceeding 0.8V) and temperature measurements (increase of 10^{o}C).

Their findings are in agreement with lubricant replenishment theory and they show that lubricant film breakthrough, reflecting contact starvation, will occur quicker in the conditions of high speeds if high viscosity lubricant is used, where lubricant replenishment is reduced. The authors also present an extensive discussion on the balance between lubricant feed and loss in rolling element bearings lubricated with greases, which in more detail, is discussed in Chapter 5.

The Lubcheck instrument was also later used to evaluate the effect of surface roughness on lift-off speed by Masen et al. (2002). The measurements were performed using a two-disc rig, where one of the discs was very smooth, while the other rough. Experiments were run in pure rolling conditions with enough lubricant supplied to provide a fully-flooded inlet. The lift-off speed, similarly as in the paper by Heemskerk et al. (1982), is used here to differentiate the surfaces in terms of their film-forming capability. Figure 4.7 shows data for four ground surfaces with different roughness.

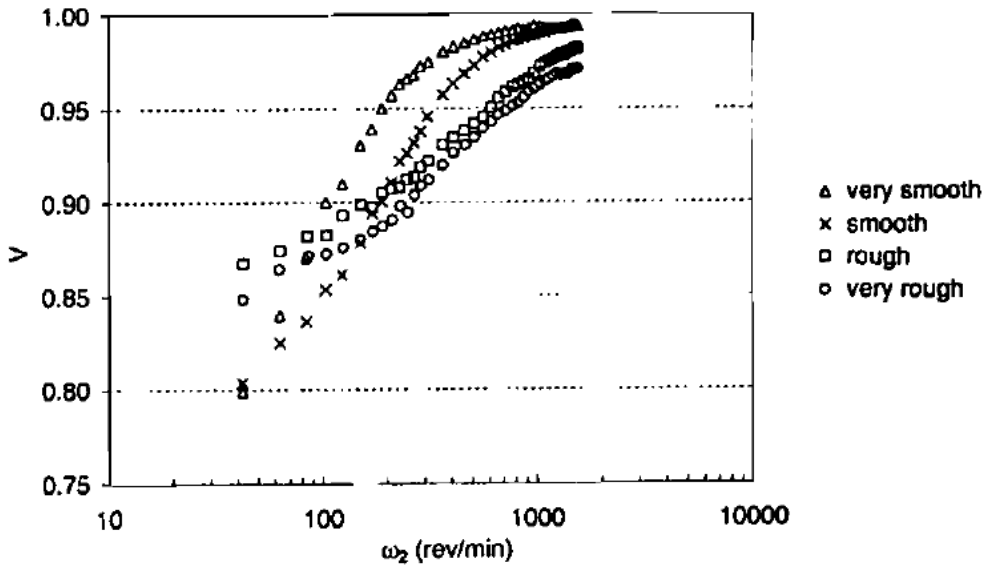

Figure 4.7: Measured lift-off curves for ground surface (V normalized to value at 1600 rpm where full separation occurs) (Masen et al., 2002)

Measurements were performed to verify a theoretical model that allows a prediction of the probability of contact based on deformed micro-geometry. A comparison between model and measurements shows promising agreement; however, a few issues still need to be addressed.

Franke and Poll (1999) presented the development of a system allowing film thickness measurements in high-speed axially loaded ball bearings. Two 7008 angular contact ball bearings are lubricated with grease and tested simultaneously at a 24000 rpm speed and a load of 160N. An electrical breakdown detector is included in the system to prevent errors due to short circuits on metallic contacts of surface roughness. In this work the minimum thermal film thickness is extracted from measured bearing capacitance. As the bearing is under pure axial load, the load is shared equally by all rolling elements, which simplifies calculations and limits the number of assumptions needed.

Grease was applied only at the beginning of the test and experiments were run until either the outer ring temperature exceeded 100^{o}C, or friction torque for both bearings was higher than 400 Nmm. These conditions define the end of service life.

Film thickness and temperature measurement for lithium soap grease, displayed in Figure 4.8, shows comparison between measured and theoretical film thickness.

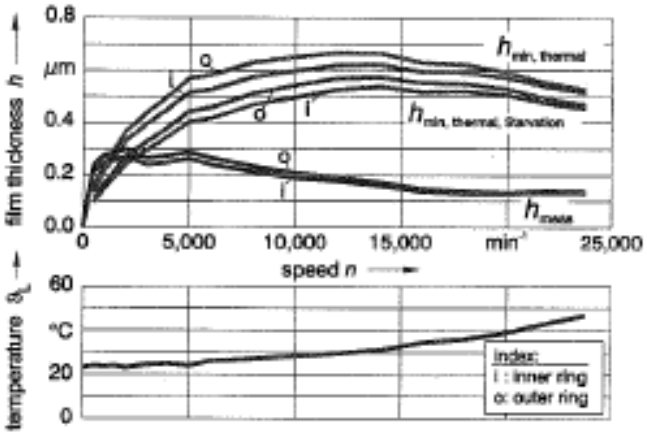

Figure 4.8: Film thickness and bearing temperature for Li-soap test (Franke and Poll, 1999)

The fact that the measured values are significantly lowered than calculated suggests that lubricant starvation may begin at speeds as low as 2000 rpm. Another possibility suggested by the authors is an overestimation of theoretical film thickness due to neglecting spin at the inner race and underestimation of contact temperature.

This experimental setup and film thickness estimation approach was also used in several other publications from the same research group. The paper by Baly et al. (2006) combines grease film thickness and friction measurements in ball-on-flat setup and full-scale bearing measurements. Another study by Gatzen et al. (2009) is focused on the effect of polymer additives on the performance of grease lubricated angular contact ball bearings. Additional ToF-SIMS (time of flight secondary ion mass spectroscopy) measurements are presented in the next paper from the same group (Gatzen et al., 2010).

Recently a new work on application of electrical capacitance for film thickness measurements in ball-on-flat configuration was published by Chua and Stachowiak (2010). The experimental setup, described as Contact Impedance Tribometer (CIT)

allows additionally measuring coefficient of friction and monitoring wear track development on the rotating disc sliding against a stationary ball. Since the focus of this work was on boundary films, for the purpose of calculations the effect of surface roughness was included by considering separate capacitance of "in-contact" (initial Hertzian) and "non-contact" areas, within the apparent contact area (measured from the wear scar).

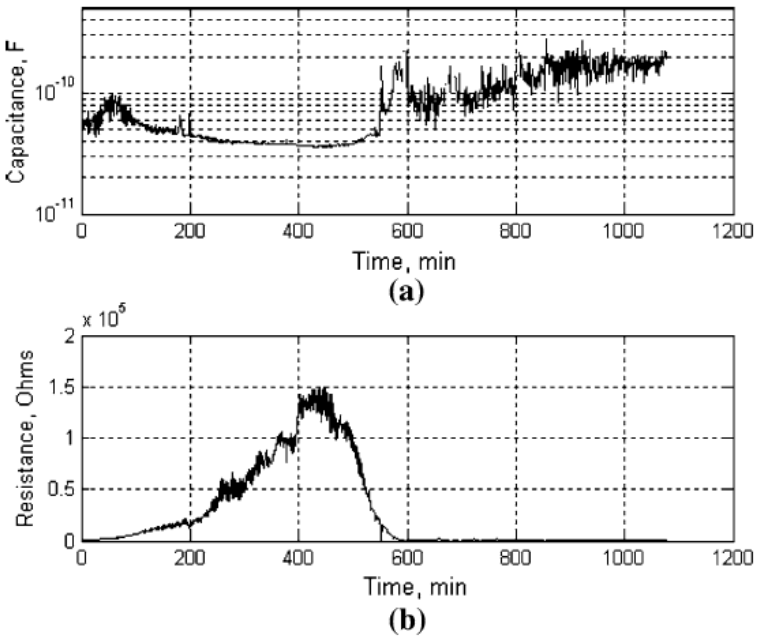

Figure 4.9: Capacitance and resistance measured during a test with sunflower oil (Chua and Stachowiak, 2010)

The authors evaluated the behaviour of sunflower oil and observed a significant decrease of capacitance (Figure 4.9) indicating the development of a boundary-film after approximately one hour from the beginning of the test. This hypothesis was also confirmed by friction and electrical resistance measurements. This film seems to collapse after around 560 minutes; however the reason for this is not clear. Nevertheless, when comparing simultaneous recordings of capacitance and resistance it can be concluded that the former provides more valuable information about the contact condition.

The most recent work involving electrical capacitance applied to EHD contacts is due to Cen et al. (2014). Experiments in a 6306 deep-groove ball bearing were performed to verify the findings from ball/roller-on-disc film thickness measurements which showed a transition speed differentiating film thickness vs speed behaviour for grease lubricated contacts. The measuring technique was based on (Heemskerk et al., 1982), while the experimental setup was similar to that described in section 7.3 of this thesis. Also here all but one steel balls were replaced with ceramic balls and only capacitance between the remaining steel ball and the raceways was evaluated. For simplification both, inner and outer ring film thickness were considered equal. Grease film thickness estimation was based on calibration made with a TT100 mineral oil.

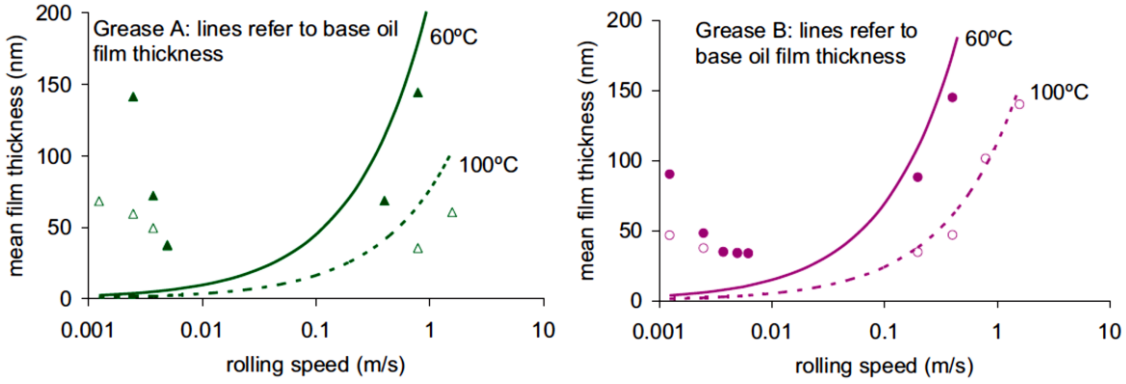

Figure 4.10: Film thickness measured with electrical capacitance for two greases, compared with a base oil (Cen et al., 2014)

As it can be seen in Figure 4.10, bearing measurements confirm observations from a ball-on-flat rig. Grease film thickness indeed initially decreases with increasing speed, showing the role of the thickener in low-speed region, but after the transition speed it approached the values calculated for base oil. Slightly lower film thickness values in comparison to base oil, the authors explain by a possibly higher oil temperature in the contact inlet, than the measured temperature of the outer ring.

The results were then extended and used by the same group in an accompanying paper (Morales-Espejel et al., 2014) to develop a new empirical model designed to calculate the effective viscosity and therefore film thickness for greases.

4.1.2 Resistance

Apart from electrical capacitance, contact resistance is another electrical property which can be used to study the lubrication of EHD contacts. Electrical resistance can provide useful qualitative information about the progress of the running-in process and smothering of surfaces, and also allows monitoring development of reacted and adsorbed insulating layers on the surfaces preventing direct metal-metal contact.

Measurements of electrical resistance can be applied to virtually any experimental setup and contact geometry. Earlier studies included a ball-on-cylinder setup (Furey, 1961), ball-on-disc (Yamaguchi et al., 1998), and also reciprocating pin-on-flat (Georges et al., 1979). Additionally use in a twin-disc machine (Lugt et al., 2001) and a customised rig simulating transient loading conditions which rolling element experiences while entering and leaving loaded zone in a rolling element bearing (Fowell et al., 2014) have been reported.

One of the first studies of steel-on-steel EHD contact through electrical resistance measurements is by Furey (1961), who performed experiments in pure sliding conditions using a ball-on-cylinder setup. The author measured instantaneous and average resistance and evaluated the percentage of metallic contact time for the variation of speed, load, oil viscosity and additives present. A strong effect of some EP and antiwear additives on the amount of metallic contact was observed (Figure 4.11). Formation of a tribofilm and subsequent reduction of metal-on-metal contact in comparison to base oil is clear. The additives studied vary in their activity, with some beginning to work instantly, others more gradually and some showing only minor effect or slightly delayed action.

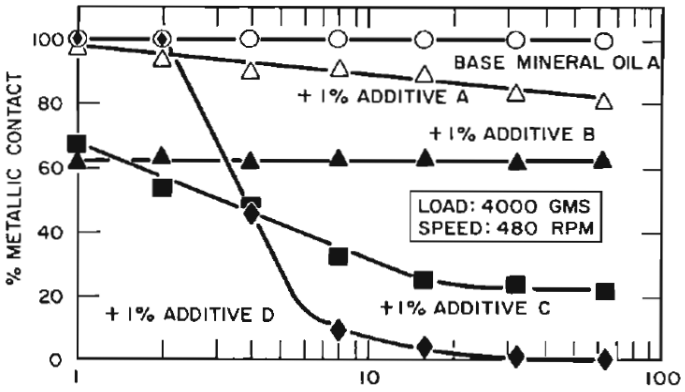

Figure 4.11: Effect of additives on the amount of metallic contact (Furey, 1961)

Georges et al. (1979) focused their work on ZDDPs (Zinc Dialkyltihiophosphates), the most commonly used AW/EP additives at the time. The experimental work covered two tribometers, namely reciprocating (hemispherical) pin-on-flat setup and rotating plane-on-plane arrangement. During both types of tests electrical contact resistance was continuously recorded. Figure 4.12 shows an example of electrical contact resistance recorded during pin-on-flat experiments for different temperatures. It can be clearly seen that at temperatures below thermal degradation of ZDDP (160^{o}C) tribofilm formation is triggered after the same number of cycles, while from 160^{o}C increasing test temperature helps to investigate the tribolayer build-up.

Measurements of electrical contact resistance have been usually used in a qualitative way. First attempts to correlate time-resolved resistance to experimentally measured lubricant film thickness and friction coefficient in a rough ball-on-flat contact are due to Guangteng et al. (1999). In this study the authors first accurately measured lubricant film thickness distribution with a Spacer Layer Imaging Method (section 4.2) and subsequently contact resistance by replacing the spacer layer disc with a glass disc having chromium layer of thickness between 10 and 20 nm. By comparing the percentage of film thickness within the contact below a certain threshold value and the percentage of in-contact time (ECR), the authors concluded that for the surfaces with a composite roughness of 60 nm (out of contact), electrical contact between the asperities may occur if the film thickness is below around 70 nm.

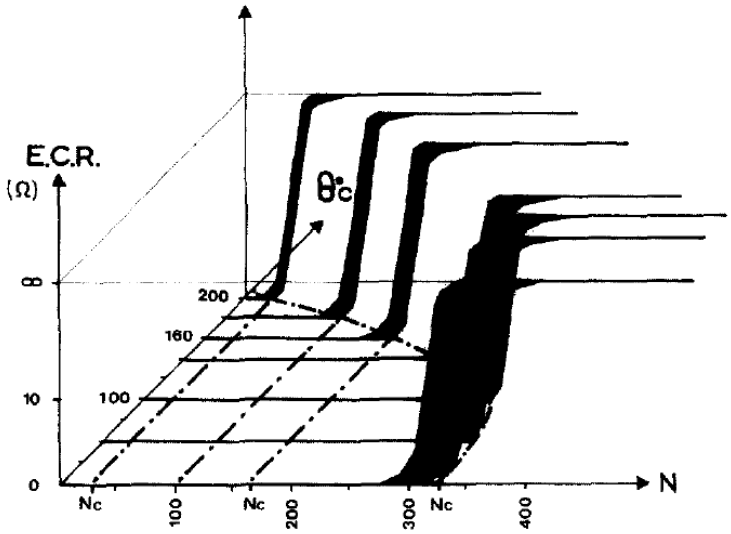

Figure 4.12: ECR as a function of number of reciprocating cycles in a pin-on-flat test (Georges et al., 1979)

ECR was also applied to investigate interaction between ZDDP and other additives found in automotive lubricants formulations, having film-forming ability. Yamaguchi et al. (1998) studied ZDDP and overbased detergents mixtures, and later with an additional dispersant (Yamaguchi et al., 2002). Greenall et al. (2012) focused their work on a combination of ZDDP with an organic anti-wear additive and an overbased detergent. First two studies were performed in a ball-on-disc configuration, while in the third work a hemispherical pin was sliding against a stationary plate with a high frequency.

Yamaguchi et al. (1998) found that oils containing both, an overbased detergent and ZDDP, showed longer induction periods than each of these additives in a single-component solution. Similar antagonistic effect was found for a three-component mixture (Yamaguchi et al., 2002), where not only delay of tribofilm formation was observed, but also a lower durability.

Experiments performed by Greenall et al. (2012), on the other hand, show quite a different picture. Results displayed in Figure 4.13 show contact potential (expressing contact resistance, where 0 is a short circuit, and 0.05 mV is a complete separation) recorded during a test. ZDDP, overbased detergent and organic anti-war additive are marked as Z, C and N, respectively. Their combinations in a base oil are also shown for

comparison. It is clear that all multi-component mixtures formed stable tribofilms instantly. When comparing this study to earlier work by Yamaguchi et al. (2002) it should be remembered that the chemical structure of these additives is most likely different, and also that contact conditions in Greenall's work are more severe. Nevertheless, these results prove the usefulness of ECR for monitoring tribofilm development.

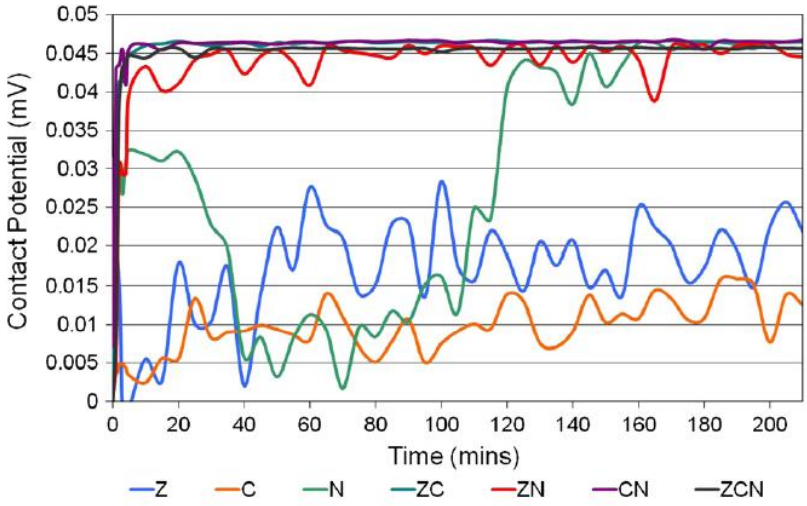

Figure 4.13: Contact potential measured during the tribotests for additive mixtures (Greenall et al., 2012)

Lord and Larsson (2008) in their relatively recent paper investigated film forming capacity of fully formulated mineral gear oil and its base oil in a contact formed between a smooth ball and a rough disc. Both specimens were made of steel and tests were run in rolling, as well as sliding conditions with a fully-flooded inlet. Contact resistance measurements allowed observing run-in behaviour of surfaces with several different surface finishing methods and also studying tribofilm development.

To compensate for varying conditions during the disc rotation due to a specific direction of the roughness lay, the data was recorded only during around 8^{o} of rotation. Apart from the mean value of resistance, also the percentage of time below a threshold limit was also recorded.

Based on the tests with fully-formulated oil it can be concluded that the run-in of the surfaces was significantly faster in sliding conditions in comparison with pure rolling tests, however no topography changes were detected after the tests.

Two surfaces (ground and deburred) were additionally tested with base oil. The results, displayed in Figure 4.14, clearly show their different behaviour. Tribofilm formation, only on the ground surface, can be deduced from these measurements. The authors conclude that chemically deburred surfaces are either passive towards the additives in fully-formulated oil or the contact conditions in their case are too mild to trigger tribofilm formation.

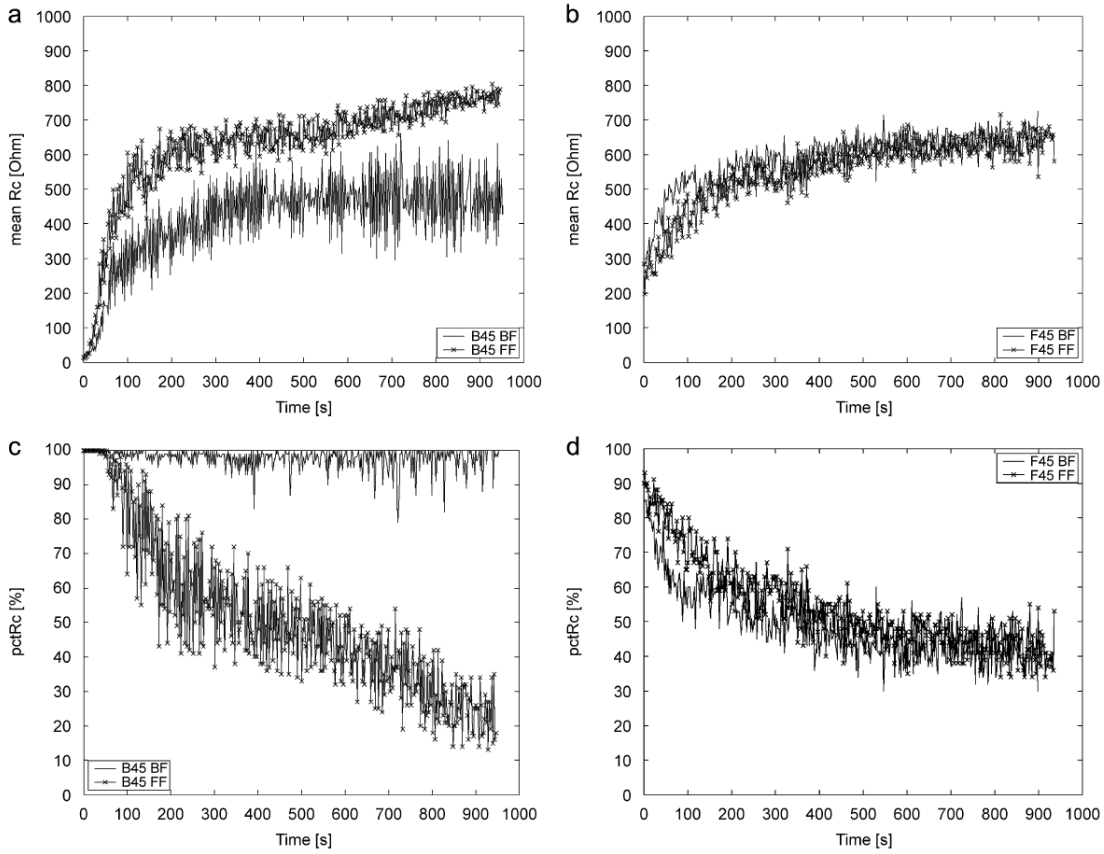

Figure 4.14: Mean contact resistance and percent contact time measured for ground (a, c) and deburred (b, d) surface with base oil and fully-formulated oil (0.4 sliding) (Lord and Larsson 2008)

4.2 Optical interferometry

First attempts to measure film thickness in elastohydrodynamic contacts were carried out by Kirk (1962), who studied lubricant films between two transparent crossed-cylinders made of 'Perspex' – poly(methyl)methacrylate. Due to the properties of the material, mean contact pressure was limited to 48 MPa; nevertheless it was possible to observe film thickness distribution within the contact area based on white light interference (Figure 4.15).

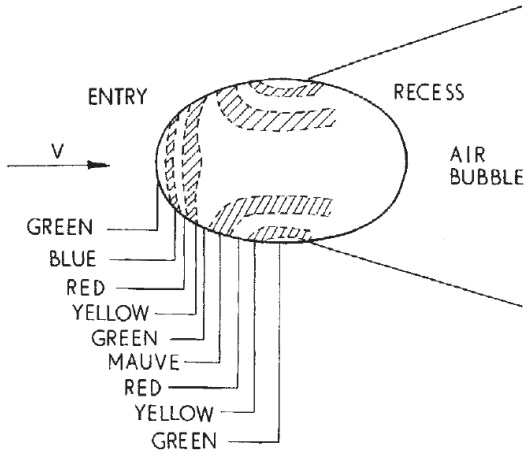

Figure 4.15: Distribution of white light fringes inside a contact between two crossed cylinders (Kirk, 1962)

The load limitation was overcome a year later by Gohar and Cameron (1963), who, using a special Pilkington glass with a high refractive index (n=1.93), were able to measure oil film thickness of a point contact between a steel ball and a glass plate. Film thickness profiles evaluated based on white light fringes are shown in Figure 4.16.

A couple of years later the same authors presented an extended study covering more contact conditions and lubricants (Cameron and Gohar, 1966). In order to allow detailed analysis of film thickness distribution within the contact (Figure 4.17), a microscope was used.

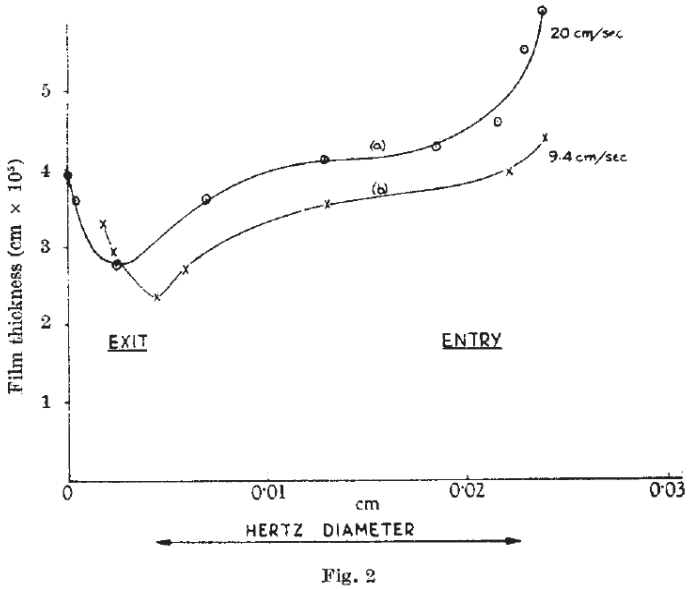

Fig. 2

Figure 4.16: Film thickness profiles along the rolling direction (Gohar and Cameron, 1963)

The authors were also able to performed detailed mapping of film thickness within an EHD contact which clearly shows a typical horse-shoe shape of the film. An example showing film thickness distribution is seen in Figure 4.17, where numbers in brackets correspond to film thickness in 10^{-5} cm.

The accompanying paper by the same authors (Gohar and Cameron, 1967) presents an extended study using the same technique. This time, a variation of contact materials, allowing higher contact pressures, and geometry was included. Apart from a glass plate, also diamond and white synthetic sapphire were used in ball-on-flat configuration, and additional tests with a rotating roller were performed.

The results show that for a point contact the side lobes and constriction at the exit become more pronounced as the load increases and minimum film thickness position shifts towards the centre of the contact as the speed increases.

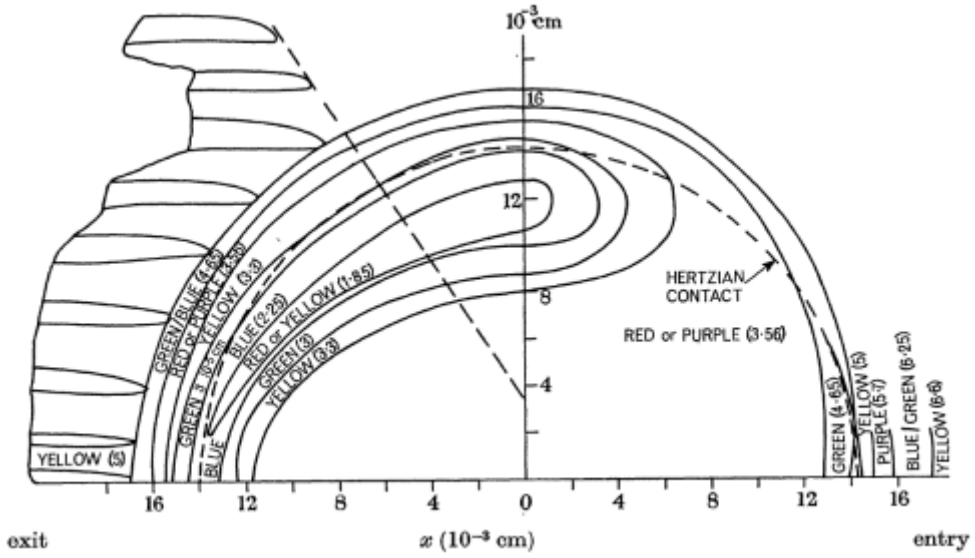

Figure 4.17: Contour maps of film thickness distribution within the contact (Cameron and Gohar, 1966)

Foord et al. (1968) managed to overcome the problem of similarity of refractive indexes of glass and lubricant by introducing a semi-reflective chromium layer on the contacting side of the disc (around 10 nm thickness). Thanks to that they were able to perform experiments with loads up to around 0.6 GPa.

The results show that load has a much stronger effect on minimum film thickness at the side lobes, than in has on central film thickness. Additionally the authors calculated pressure-viscosity coefficients for the fluids tested based on the comparison of film thickness slopes with reference oil. Based on the results they concluded that, apart from silicones and oils containing polymers, the fluid structure does not seem to have any effect on film thickness.

In the next paper Foord et al. (1969) extended the range of loads and speeds tested and also performed experiments in pure sliding and with axis of rotation at an angle, giving 16 percent sliding.

The authors show that in pure rolling the position of minimum film thickness depends on the conditions of speed. It was found that if the load is kept constant, the minimum film thickness will shift from the side lobes to the back as the speed is increased.

The effect of viscous heating of the lubricant in the inlet on film thickness in sliding experiments was observed by the authors, where film thickness was lower for sliding tests in comparison with pure rolling.

The idea of lowering the minimum measurable film thickness limit by the addition of a spacer layer with similar optical properties as lubricant was proposed by Westlake and Cameron (1967) in 1967 but it was not until 1991 when this concept was fully applied.
Johnston et al. (1991) introduced a combination of fixed-thickness silica spacer layer and the use of spectrometer. To distinguish from conventional interferometric technique, the new variant was called Ultra-Thin Film Interferometry (UTFI). The addition of a spectrometer strongly improves the resolution of the method, while the presence of a spacer layer makes it possible to measure very thin films, down to 5 nm. By using a spectrometer accurate separation can be determined between the surfaces (lubricant film + spacer layer) in the central region of the contact by finding the wavelength at which maximum constructive interference occurs.
Experiments were performed with a range of lubricants and included two thicknesses of silica layer. It was found that the thickness of the silica layer should be higher than visible the light wavelength. According to these results some fluids show slightly different EHL speed exponents than the theory predicts in the thickness range between 5 and 15 nm. The authors also show a possibility of calculating pressure-viscosity coefficient based on film thickness behaviour if oil with a known coefficient is tested in the same conditions.
The ability of measuring film thickness which is below roughness level (11 nm composite surface roughness) the authors attribute to elastic flattening of the asperities inside an EHD contact.

Another significant contribution to the optical interferometry technique is due to Gustafsson et al. (1994) who for the first time digitized colour interferometric images and video recordings of a lubricated EHD contact. Absolute film thickness values were determined based on HSI (Hue-Saturation-Intensity) values earlier calibrated versus a known distance between stationary undeformed surfaces. The method is applicable to

films in the range between 95 and 700 nm and allows obtaining film thickness distribution within the contact area.

A couple of years later Cann et al. (1996) combined the application of silica spacer layer with digital analysis of contact images. In their Spacer Layer Imaging Method (SLIM), similarly as in (Gustafsson et al., 1994), colour coordinates, this time RGB values (red, green and blue), are extracted from the images captured, and subsequently converted to HSI values. The improvement over the UTFI was the ability to evaluate the film thickness over the whole contact area, thus obtaining film thickness maps. In this method a calibration curve representing Hue value as a function of silica film thickness was obtained by comparing interferometric images of the contact with film thickness measured with UTFI in static conditions, for a variable spacer layer disc.

The results shown in Figure 4.18 are presented as film thickness profiles transverse or parallel to the rolling direction. Development of side lobes can be clearly seen as the speed, and film thickness increases. Film thickness fluctuations within the contact area, seen in this figure, are attributed to steel ball roughness.

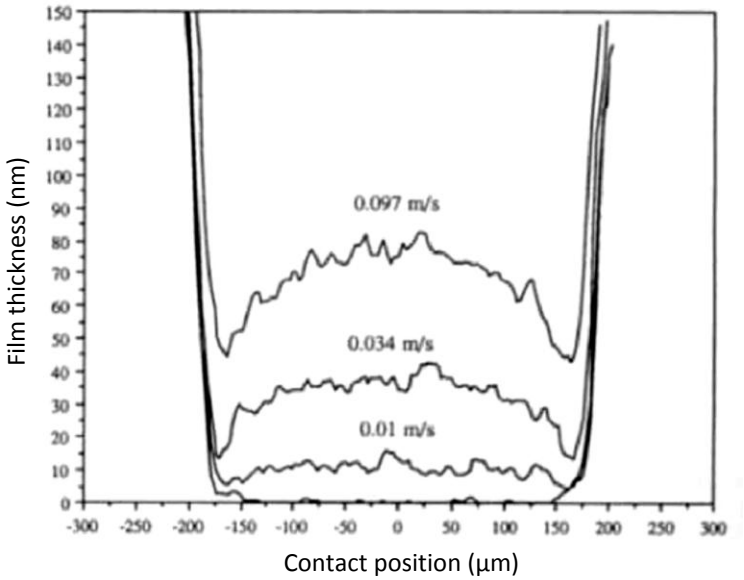

Figure 4.18: Film thickness profiles transverse to the rolling direction (Cann et al., 1996)

Film thickness measured with the SLIM method is also compared with Dowson and Higginson predictions for smooth surfaces, and the results for central and minimum film thickness, shown in Figure 4.19, suggest good agreement for the films down to below 30 nm. It is suggested that the generally lower than the theory minimum film thickness measurements are due to the application of smooth surfaces theory for calculation of film thickness.

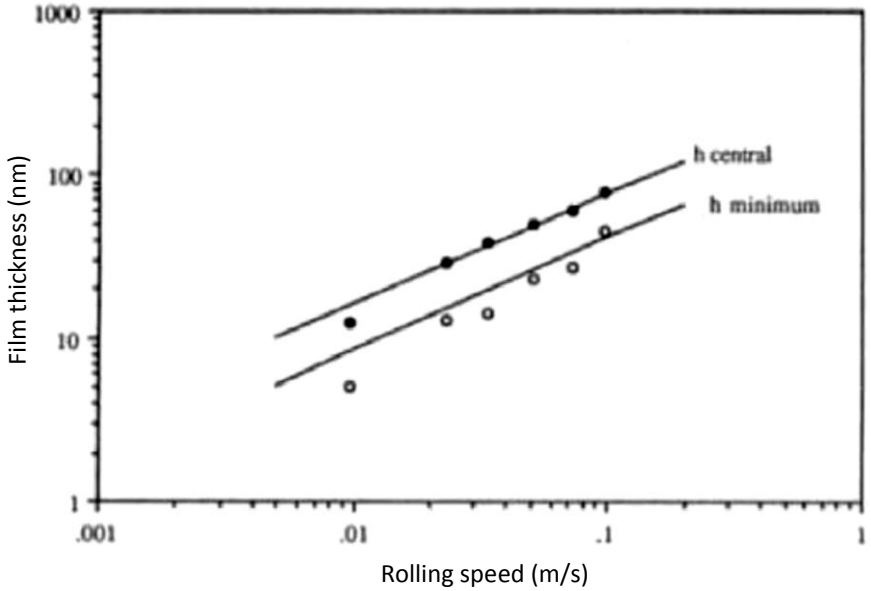

Figure 4.19: Comparison of measured and theoretical central and minimum film thickness (Cann et al., 1996)

The authors claim that lower method resolution (10 nm in comparison to 1 nm for ultra-thin film technique) is mainly due to the calibration step. The method has been subsequently improved by the authors (Spikes and Cann, 2001), by making use of all three of the triplet of colour information (RGB). Calibration is performed with the aid of a reference lubricant for which central film thickness is measured with ultra-thin interferometry. RGB values extracted from interferometric images captured with a high-speed CCD camera are then correlated to lubricant film thickness measured at the same conditions.

In 1997 Hartl et al. (1997) presented their approach to 3D film thickness mapping, named as Colorimetric Interferometry. In this method a differential colorimeter is used for evaluation of interference colour and images of lubricant films are captured with a photographic camera. This approach, rather than using a RGB video camera, allowed higher spatial resolution of the images to be obtained. A digital colour chart was constructed using Newton's rings for the static contact and colours were defined according to CIE (Commission internationale de l'éclairage - International Commission on Illumination) reference system. The authors performed film thickness measurements in the range from 60 to 800 nm showing good agreement with theoretical predictions. They showed the possibility of extracting full 3D film thickness maps (Figure 4.20) showing EHD film thickness distribution in detail.

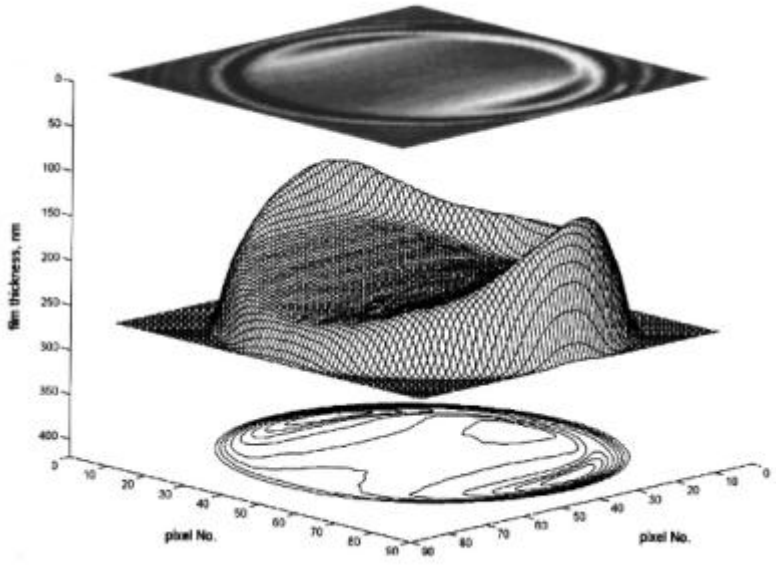

Figure 4.20: Grey scale interferometric image with corresponding 3D profile and contour map (Hartl et al., 1997)

The system has been further improved to allow fully automatic measurements (Hartl et al., 1999) and also the measurable lubricant film range has been extended down to even below 1 nm with silica spacer layer discs. The method was subsequently used to study the behaviour of fluids on the borderline between full-film EHD and boundary lubrication regime (Hartl et al., 2001).

Thin-film interferometry and SLIM methods have been extensively used over the years to study various aspects of lubrication, including grease lubrication and starvation (Cann, 1999), boundary lubrication (Ratoi et al., 2000), influence of roughness on film formation (Guangteng et al., 2000) and many others.

SLIM can also be applied for out-of-contact imaging allowing observation of additive derived antiwear films developed on the surface of a steel ball during friction tests (Taylor et al., 2000). The build-up of the reaction layer can be monitored and film morphology analysed. The use of steel-on-steel contact gives more severe rubbing conditions leading to much thicker (estimated around 200 nm in contact) ZDDP films than can be obtained if standard interforemetric setup with a glass disc is applied and rather thermal films are developed (up to 50 nm (Gunsel et al., 1993)). It also allows the study of more realistic material-pair combinations. The authors mention a potential inaccuracy coming from the assumed value of refractive index of the layer (1.4), where most of glasses, including phosphate glasses fall in the range between 1.35 and 1.55. Initially, the ball had to be removed from the MTM (Mini-Traction Machine) and transferred to a separate measurement setup which may lead to some micron-level misalignments when the ball is mounted again. This disadvantage was soon eliminated by using an in-situ spacer layer probe being a part of the MTM arrangement (Fujita and Spikes, 2004). Based on literature data the authors also refined the value of the refractive index used for film thickness evaluation. Given the range from 1.50 to 1.65 (Brow et al., 1995) 1.60 was chosen and uncertainty was estimated to be lower than 7 percent. Examples of interferometric images of ZDDP-derived reaction layer and film thickness measured at a range of temperatures (same lambda ratio) are shown in Figure 4.21 and Figure 4.22, respectively, both in rubbing tests.

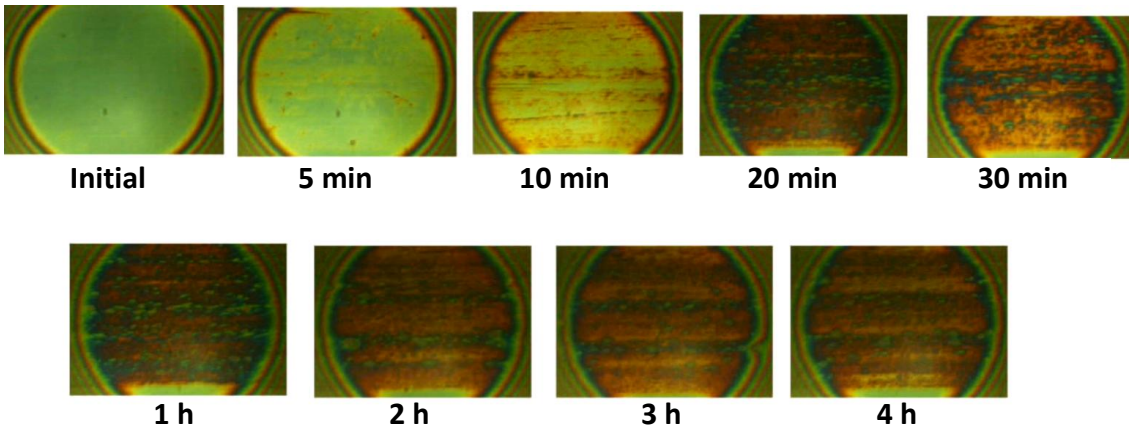

Figure 4.21: Interference images showing development of ZDDP film in the wear track (Fujita and Spikes, 2004)

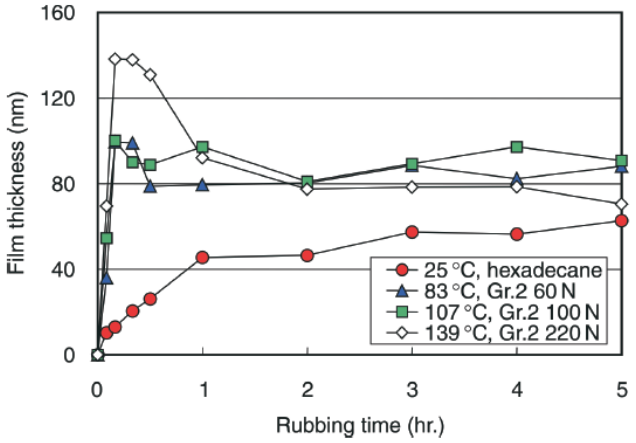

Figure 4.22: Film thickness of ZDDP-derived layer at different temperatures (same lambda ratio) (Fujita and Spikes, 2004)

An alternative approach allowing the measurement of films below one-quarter of the wavelength thickness, based on monochromatic interferometry, was proposed by Roberts and Tabor (1971). It is based on the fact that if the change from dark to bright interference corresponds to one-quarter of the wavelength then the values in between can be determined from the interference intensity.

Even though the experiments presented in this publication concern highly elastic solids (i.e. rubber) and were used to study the formation of electrical double layer by ionic solutions on the surfaces mostly in static conditions, the idea was later used by other researchers to develop a method applicable for situations simulating hard-EHD conditions, where contacts between steel ball and a glass disc were studied.

It took 25 years for this concept to be used by Luo et al. (1996) who in 1996 presented their first publication on this subject. The relative optical interference intensity (ROII) technique is used to study the transition from full-film EHL to so-called thin film lubrication (TFL) regime with a number of lubricants in a range of testing conditions. Film thickness is calculated using the formula:

$$h = \frac{\lambda}{4n\pi}[arccos(\bar{I}) - arccos(\overline{I_0})] \quad (13)$$

Where n is a refractive index of lubricant, $\bar{I}$ is the relative intensity of oil film and $\overline{I_0}$ is relative intensity of zero film.

The results show that film thickness dependence on speed is different than expected for EHL regime (Figure 4.23). The transition point does not occur at certain film thickness but depends on the molecular structure of the lubricant. In all experiments, however, it took place in films below 30 nm. The effect of load and ball diameter is similar as in classical EHL. The influence of viscosity, on the other hand, is weaker than in EHL, but affects film thickness more significantly that the variation of speed. The authors explain their findings using the model of lubricant film consisting of: a fluid layer, liquid layer with ordering of molecules and an adsorbed layer.

Several years later Guo and Wong (2002) performed an extensive theoretical analysis including the effect of optical absorption in chromium-layer and multi-beam interference approach.

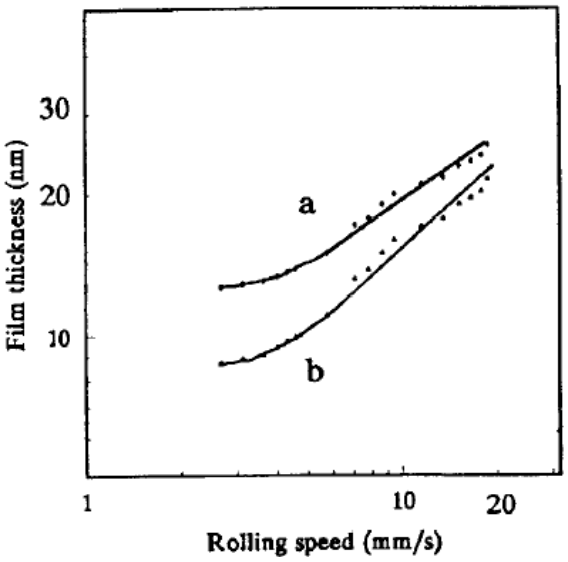

Figure 4.23: Film thickness results showing transition between EHL and TFL (Luo et al., 1996)

Experimental results in oil lubricated pure-rolling conditions allowed a comparison of film thickness obtained using a simplified two-beam interference approach, and more complex multi-beam interference (Figure 4.24). It can be seen that ROII gives lower film thickness and also smaller depth of constriction at the exit. The authors also comment on the influence of exposure time on an apparent smoothness of the film profiles extracted.

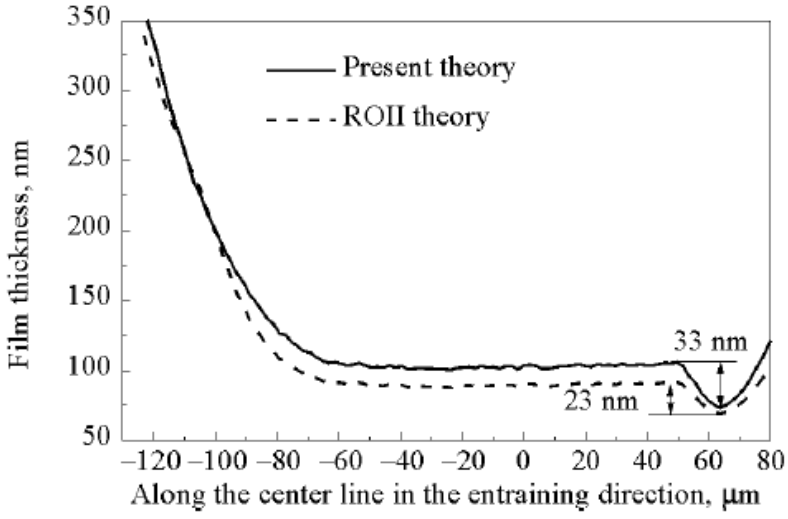

Figure 4.24: Effect of multi-beam interference on film thickness (Guo and Wong, 2002)

4.3 Ultrasound

Apart from techniques based on optical interferometry principles, or electrical measurements (capacitance, resistance) there are other that are used for the study of lubrication. Among those, the most relevant for the subject of the current study is a method based on ultrasound published by Dwyer-Joyce et al. (2003).

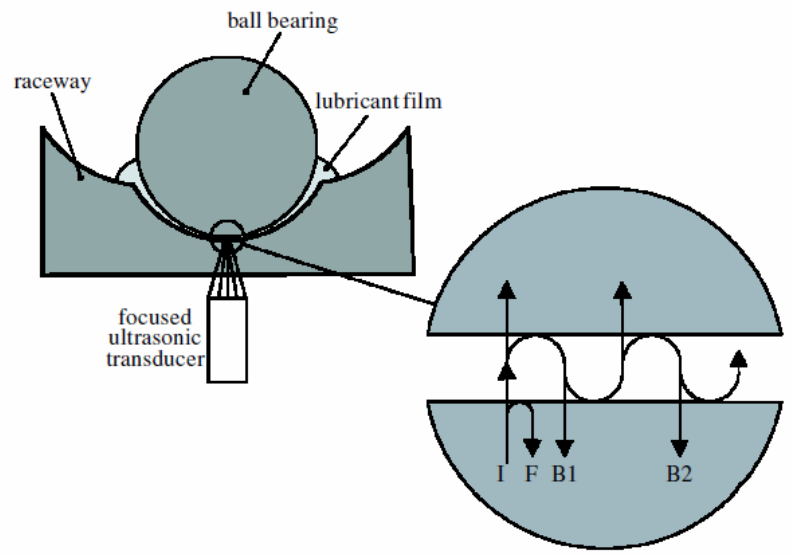

Figure 4.25: Ultrasonic beam paths in a lubricated contact (Dwyer-Joyce et al., 2003)

The method, of which the principle is shown in Figure 4.25, allows measuring lubricant layer thickness in steel-on-steel contacts based on a reflection coefficient (R) using the following equation:

$$h = \frac{\rho c^2}{\pi f z'}\left(\frac{R^2}{1-R^2}\right) \quad (14)$$

Where ρ is the density of the layer, c the speed of sound in the layer, z' is acoustic impedance of the contacting material and f the resonant frequency of ultrasonic wave. A focused ultrasonic transducer emits a pulse of ultrasonic energy after being excited by a high-voltage pulse sent from an ultrasonic pulser-receiver (UPR). The ultrasonic pulse goes through the steel bearing material and after being reflected from the oil film is received by the same transducer. Before dynamic film thickness

measurements were performed, the method was validated in static experiments. First, a water wedge between two flat glass sheets and then the influence of curvature was examined by measuring the oil film between two eccentric cylinders loaded against each other. Dynamic measurements were carried out in two configurations: ball-on-flat contact and radially loaded ball bearing. Ball-on-flat experiments were done in pure sliding conditions and the results shown in Figure 4.26 show a fair agreement with theory. It should be noted that some film fluctuation was noticed by the authors using optical interferometry, the results, however, show a potential of the method.

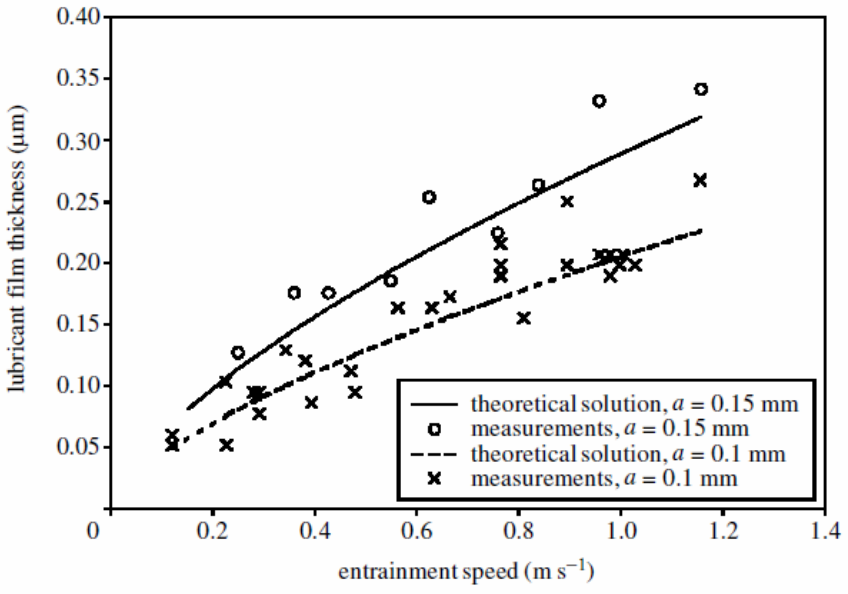

Figure 4.26: Comparison of measured and theoretical film thickness in ball-on-flat setup at two loads (Dwyer-Joyce et al., 2003)

Full-bearing measurements (Figure 4.27) show a scatter of the results and it is not clear at this stage whether it is due to the measurement procedure (some source of error) or the film thickness indeed fluctuates.

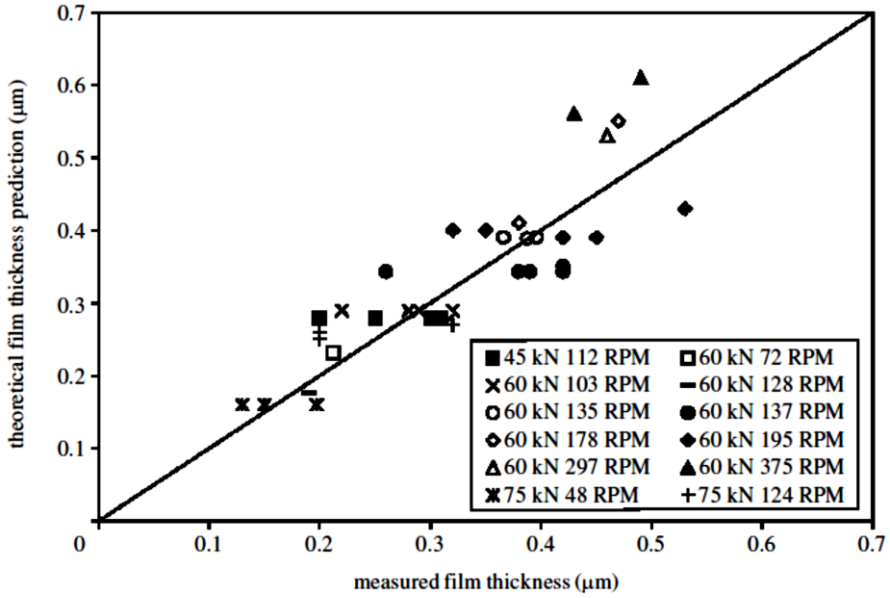

Figure 4.27: Comparison of measured and theoretical film thickness in a rolling bearing (Dwyer-Joyce et al., 2003)

Chapter 5: Lubrication of rolling element bearings

According to Lugt (2009) “more than 90% of all rolling element bearings are greased and sealed for life”. Nowadays grease is considered as one of the components of a bearing, which shows its importance to proper bearing functioning. Ineffective lubrication causes poor performance and in extreme cases may lead to a bearing failure. For these reasons this chapter will focus mainly on grease lubrication of rolling element bearings.

Since a direct monitoring of lubrication condition and prediction of film thickness in an operating bearing is difficult, most of bearings’ design and service-life predictions are based on modelling and tests run to failure. However, even though the main part of the research effort nowadays is put into theoretical studies, these still require experimental work to verify the findings and help establish new models.

The majority of experimental studies concerning grease lubrication have been carried out in a simplified ball-on-flat setup. Thanks to the improvements in optical interferometry techniques it is possible to accurately measure film thickness; however, due to differences in geometry and kinematics, some phenomena taking place in bearings cannot be reproduced. It is difficult to replicate all feed and loss mechanisms and also the effect of centrifugal force on grease redistribution cannot be taken into account.

Experimental studies on grease lubrication in ball-on-flat contacts are performed under either fully-flooded or starved conditions. In the first case either a grease reservoir or a plastic scoop that directs the grease pushed to the sides back into the track is used. In starved experiments, on the other hand, grease is applied before the experiment and no additional amount is added.

Full-bearing tests are mostly dealing with friction measurements (Wikström and Höglund, 1996), bearing-life evaluation (Franke and Poll, 1997), with some works

dealing specifically with grease behaviour (Lugt et al., 2009). Monitoring of lubrication condition in rolling element bearings, through either film thickness measurements (Leenders and Houpert, 1987) or estimation of amount of metal-metal contact (Heemskerk et al., 1982) has been a focus of many investigations.

Even though greases' structural and functional properties have been extensively studied, it was not until the early 1970s when it was recognized that grease lubrication makes bearings run under starved conditions. First experiments on a disc machine by Dyson and Wilson (1969) (Figure 5.1) and Poon (1972) revealed that greases initially form films thicker than their base oils; however when the amount of grease available in the inlet decreases, these films gradually become thinner and eventually fall below base oil film thickness values, reaching a stable value of around 40% of the initial thickness. A similar decrease of film thickness was also observed for the most viscous oil at higher speeds. The authors suggest that this is due to the centrifugal force acting against surface forces trying to keep the oil on the rolling track.

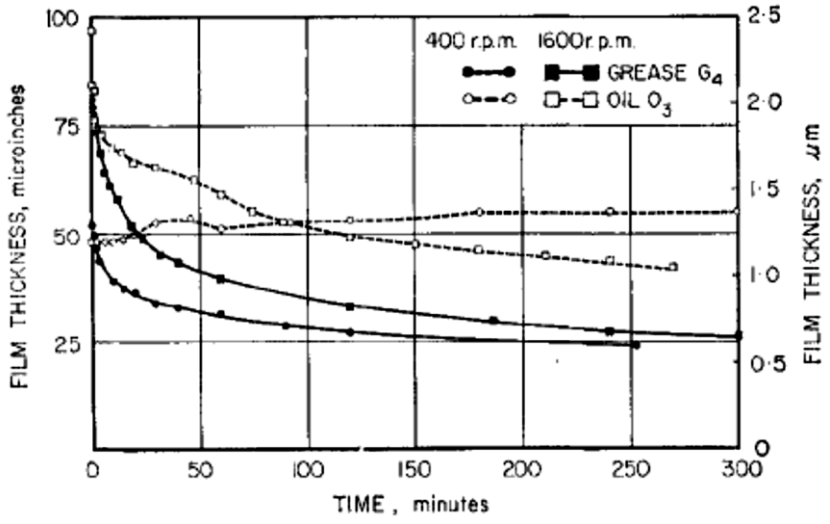

Figure 5.1: Film thickness measured for Grease G4 and its base oil (Dyson and Wilson, 1969)

One of the greases was an exception from this behaviour; film thickness decrease was less pronounced and also the film seemed to recover with time to almost the initial value.

It was also found that the higher the amount of thickener, the thicker initial film grease formed. The same conclusion came from full bearing tests carried out by Wilson (1979), who found that grease films initially reached values which would normally correspond to an oil with viscosity higher by 30-35% than the base oil viscosity. Based on bearing temperature measurements he also concluded that a partially starved condition has a beneficial effect of viscous friction reduction.

A very significant contribution to the understanding of lubricant starvation was due to Wedeven et al. (1971) who, based on optical film thickness measurements, established a relation between film thickness and the amount of oil available in the inlet using a meniscus distance. According to that, fully-flooded condition can be achieved if the minimum inlet distance (S_f) is filled with lubricant:

$$S_f = \frac{3.52 \cdot (R h_0)^{2/3}}{a^{1/3}} \tag{15}$$

Where *R* is the reduced contact radius; h_0 is central film thickness and *a* is Hertzian contact radius.
This was included in later numerical calculation of minimum film thickness by Hamrock and Dowson (1977) and further extended by Chiu (1974).

A vast amount of research effort was put into studying mechanisms and forces driving lubricant replenishment in starved conditions. The first experimental visualisation of lubricant flow around the contact is due by Pemberton and Cameron (1976), who used aerated oil and a television camera to observe the contact formed between glass disc and steel ball. The results of their work, seen in Figure 5.2, show the flow of lubricant from two side bands to form the oil meniscus with a typical “butterfly” shape of the oil boundary.

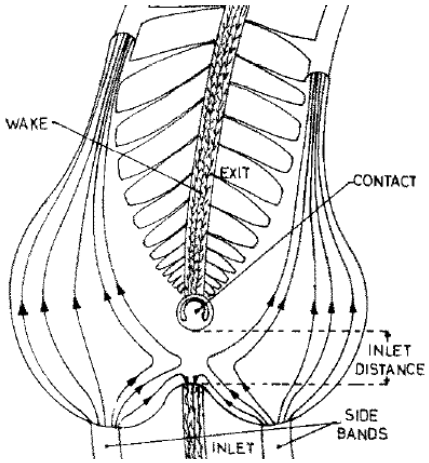

Figure 5.2: Visualisation of the flow around EHD contact (Pemberton and Cameron, 1976)

In his model Chiu (1974) considered that replenishment is only driven by the surface tension. Later Jacod et al. (1998) pointed out that this mechanism would be too slow and concluded that capillary forces must play a significant role.

Cann (1996) measured the time it takes for the lubricant to flow back from a grease reservoir to reform the meniscus after the motion is halted. The measurements were performed at three temperatures (25, 50 and 80^{o}C) and it was found that the reflow time decreased with temperature and number of over-rollings. This indicates that the worked grease releases the oil easier, and decreasing the viscosity improves the inlet replenishment. It was suggested that the same replenishment mechanism, due to capillary action, would be valid during running.

Other authors (Gershuni et al., 2008), however, expressed their scepticism that this would apply to working rolling element bearings, since based on their model a detrimental effect of the centrifugal force on the inner ring oil layer will make the reflow impossible as the oil will be thrown off. The reflow on the outer ring, on the other hand would benefit from centrifugal force action. Nevertheless, the time between successive over-rollings in an operating bearing is too short for a sufficient amount of oil to flow back and fill the inlet.

There are a few general types of film thickness variation for greases run without additional supply at constant speeds. These are schematically shown in Figure 5.3 after Mérieux et al. (2000), where (a) is fully-flooded; (b) is starved; (c) and (d) denote starved with stabilisation and recovery, respectively. The authors stress that operating conditions (e.g. temperature, speed and geometry) determine the type of behaviour as one grease can show either of them. Film thickness in a fully-flooded regime (a) is stable, and as already mentioned, slightly higher than for the corresponding base oil. Curve (b) is the other extreme, with film thickness dropping to very low values which eventually leads to direct contact between the surfaces. Grease film thickness, after an initial decrease can also reach a steady-state (c) value if an equilibrium flow condition is reached, or even increase (d) if lubricant replenishment is improving due to shearing of the grease.

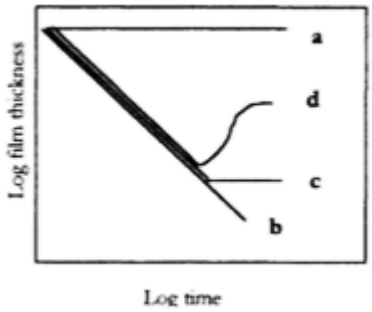

Figure 5.3: Possible starvation curves (Mérieux et al., 2000)

The most common view on grease lubrication in rolling bearings is that a thickener's function is to act as a reservoir releasing the oil onto the rolling track and that it does not take part in the lubrication process. This may be true for high-speed applications; however, for bearings operating at low speeds, such as those found in wind turbines, the role of the thickener in lubrication process should also be considered (Cann, 2007).

Recordings of interferometric images of grease lubricated contacts (without further resupply) registered by Åström et al. (1991), revealed lumps of grease thickener entering the contact zone and a significant film thickness fluctuation in an initial stage of the experiment. Improvements of optical interferometry technique later allowed for

more accurate film thickness measurements and Larsson et al. (2000) were able to evaluate the pressure distribution within the contact based on interferometric images, such as those shown in Figure 5.4. The authors found that thickener lumps entering the contact during fully-flooded experiments can cause severe pressure fluctuations.

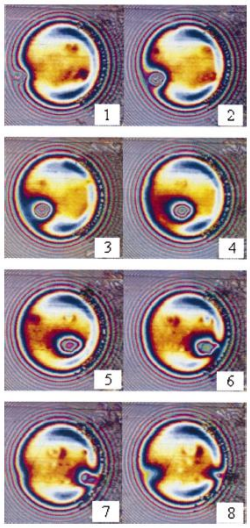

Figure 5.4: Interferometric images of a soap lump passing through the contact (Larsson et al., 2000)

Cann et al. (1992) used the infrared spectroscopy (IR) (details of the method can be found in Cann and Spikes (1991)) to analyse grease structure in the inlet region during a fully-flooded experiment. The IR spectra confirmed the presence of thickener. It was also seen that the structure and composition of grease changes during the run, and that the thickener's structure is degraded due to shear.

The authors also used optical interferometry to measure the thickness of grease films and found that film thickness increases approximately linearly with lithium soap concentration.

Later, experimental work in which Cann (1999) compared the fully-flooded and starved behaviour of greases, revealed that with a sufficient amount of grease to fill in the inlet, greases behave similarly to base oils when the initial film thickness fluctuations stabilise (Figure 5.5). Under starved conditions the effect of thickener was the opposite

to that reported earlier (Cann et al., 1992) for 30 cSt viscosity base oil, where a higher thickener content lead to lower final film thickness. This correlated well with the oil bleeding ranking, according to which greases with lower thickener concentration release more bled oil. For a more viscous base oil (200 cSt), however, the effect of the thickener's amount on film thickness was not noticeable. Additionally, base oil's viscosity influence was different than in fully-flooded conditions. Here, a higher viscosity means that less lubricant can flow back onto the rolling track and therefore a thinner film will be formed.

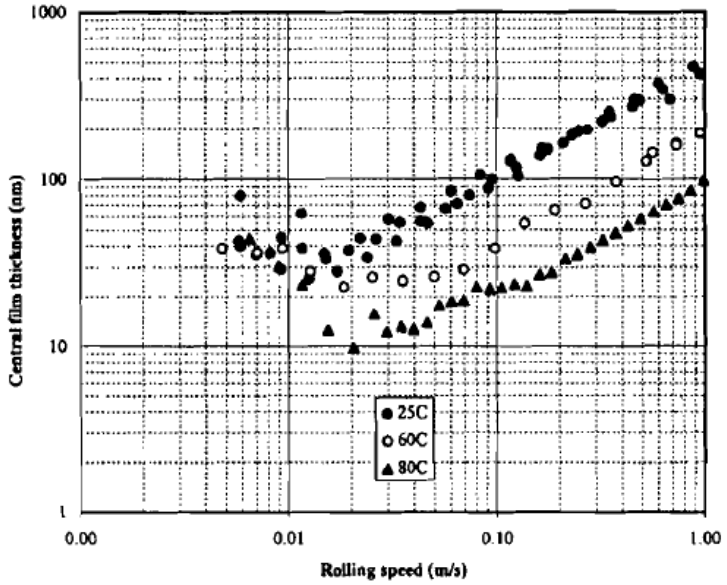

Figure 5.5: Fully-flooded grease film thickness (30 cSt base oil viscosity, 5% Lithium hydroxystearate thickener) (Cann, 1999)

Further infrared measurements (IR reflection-spectroscopy) performed by Hurley and Cann (2000) in a steel-on-steel contact under starved conditions at constant speeds revealed significant differences between lithium hydroxystearate soap and tetraurea thickener. Under the same operating conditions tertaurea grease showed either a stable (25^{o}C) or slightly declining (80^{o}C) film thickness, while the lithium soap grease starved quickly but showed some film recovery towards the end of the test. In the case of lithium soap grease, the residual film in the centre of the rolling track was too thin to allow IR analysis, while the tetraurea grease developed thick films (200 nm at 25^{o}C)

sufficient for infrared measurements. Analysis of the thickener's distribution across the track shows an opposite behaviour of the two greases. For the lithium soap grease much more thickener was found at the edge of the contact, while very little in the centre of the track. Tetraurea grease, on the other hand, showed high thickener content within the track, but the region near the edge consisted mostly of the base oil.

Cann et al. (2001), based on analysis of IR spectra of grease samples from various locations within the bearing (shown in Figure 5.6), studied grease degradation in operating rolling element bearings. The bearings were tested for up to 300 h under different temperatures, load and speed conditions and at the end of the test the lubricant samples were collected from different bearing areas and analysed with the IR spectroscopy. Here, a sample from the seal reflected the condition of grease reservoir, while that from the cage pocket was used to evaluate the condition close to ball bearings. It was found that the condition of grease strongly depended on the sample location. It varied from almost base oil with some thickener present in the inner raceway area, through heavily degraded grease with little amount of thickener in the samples collected from the cage pocket, to samples with variable amount of thickener depending on the position on the seal (high in the rear seal sample).

Additionally, as expected, grease degradation was more severe in the conditions of higher temperatures and operating speeds. These experiments were reflecting the behaviour of grease during a normal operation. The study was further extended by the authors (Cann et al., 2007), where pairs of bearings were run up to the point where one of them failed. Bearing failure was defined as an increase of the outer ring temperature up to 130^{o}C.

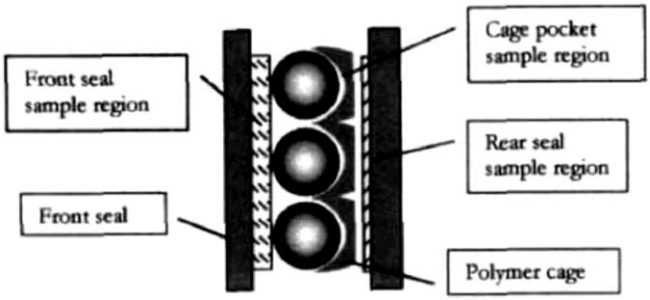

Figure 5.6: Schematic showing location of grease samples taken (Cann et al., 2001)

Comparisons of additized (including FM, EP, ZDDP and antioxidant) and non-additized greases showed a strong effect of additives on grease's life. Depending on the testing conditions, up to 700% longer grease life was obtained.

The amount of grease reservoir present on the seals decreased with running time and increasing temperature. Contrary to the first part of the study, in the run-to-failure experiments lubricant oxidation was clearly noticed. As expected, oxidation was more severe at higher temperatures and the amount of oxidation-related species was increasing with time.

The influence of grease's composition on the bearing performance was also studied by Franke and Poll (1997), through the measurements of film thickness, friction and bearing temperature. The type and content of thickener, type and viscosity of base oil and also presence of antioxidants were varied in these experiments. Based on the experiments carried out, the authors concluded that for the non-additivated greases high operating temperature and high friction lead to a short bearing life. A grease's life can be extended if synthetic oils, such as PAOs or esters, are used instead of mineral base stocks and if the greases are treated with additives preventing thermal-oxidation. Interestingly, when the greases with lithium and calcium soap thickeners were compared, the former showed longer service life, even though their operating temperature was higher.

In another study by Gatzen et al. (2009) the authors tested different polymer additives. The comparison of film thickness of the five greases investigated, displayed in Figure

5.7, clearly shows a much thicker film for grease III, which contains a low molecular weight dispersing polyalkylmethacrylate (PAMA). Apart from that it also had the lowest running temperature, suggesting the lowest friction, and additionally the longest service life from polymer-blended greases. Despite the presence of thick polymer-originating boundary reaction layers the service life was however lower than the plain grease.

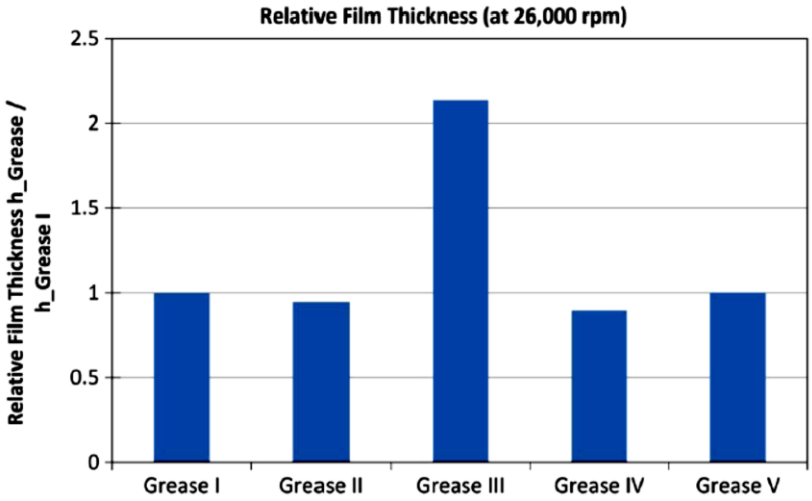

Figure 5.7: Relative film thickness of greases at 26000 rpm (Gatzen et al., 2009)

Despite the importance of full-bearing experiments, the simplified ball-on-flat setup still provides very valuable information because the number of parameters influencing grease's behaviour can be limited, and different effects can possibly be separated. Some attempts of introducing phenomena found in bearings into the ball-on-flat rig, such as ball spin (Baly et al, 2006) have been reported. In experiments with the ball spin introduced, a very strong effect on grease film thickness has been seen (Figure 5.8). Ball spin is clearly an important inlet replenishment mechanism. The contact was either fully-flooded during the entire experiment (grease A and the first run with grease B) or the starvation speed was much higher than without the spin (third run with grease B).

Another example is the work by Cann and Lubrecht (2003) who studied the effect of cyclic loading, as experienced by radially loaded bearings, on contact replenishment. The authors observed that immediately after unloading, the film thickness increased. In comparison with the grease, high-viscosity PAO base oil showed a stronger change, where the film thickness reached almost the fully-flooded value. However, this film recovery was only temporary, and the film thickness gradually decreased following the trend prior to unloading.

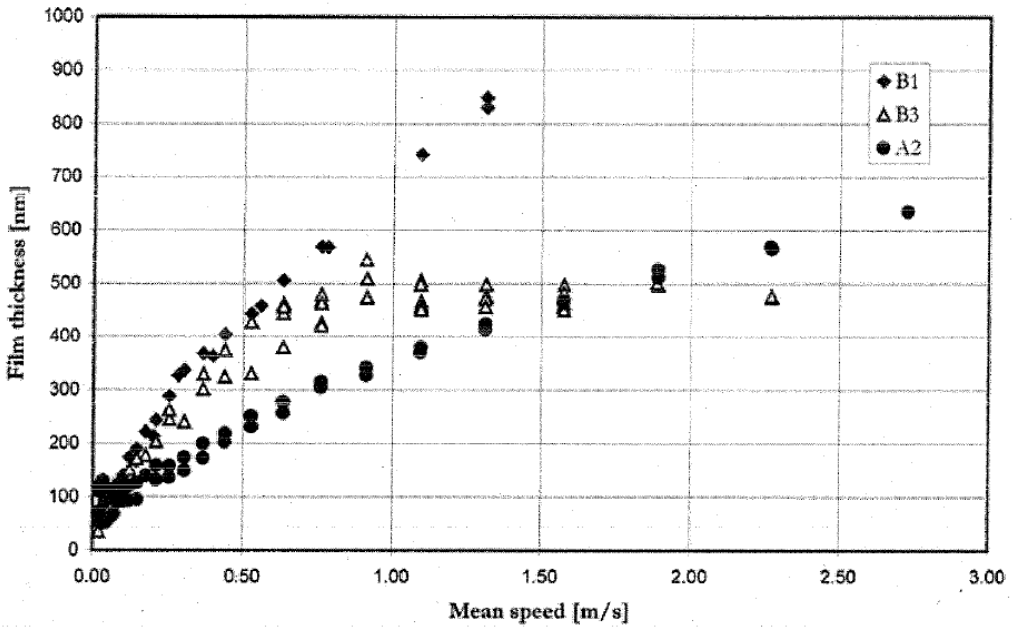

Figure 5.8: Grease film thickness measured in ball-on-flat setup with ball spin introduced (Baly et al., 2006)

Additionally, the effect of the lateral vibration has also been reported (Nagata et al., 2012), and so was the effect of a preceding rolling element on film thickness (Svoboda et al., 2013).

Unfortunately other aspects of bearing operation, such as cage effects and centrifugal force, cannot be easily reproduced in a simplified bearing-simulating device. An alternative approach would be to simplify a bearing, such as Cen et al. (2014) have done, and limit a number of studied contacts to one (inner and outer raceway).

Chapter 6: Properties of lubricants

Knowledge of the high-pressure behaviour of lubricants, via measurements of properties such as density and viscosity, has always been considered crucial to a complete understanding of EHD lubricated contacts, and also necessary for film thickness calculations. There are a number of models used to simulate viscosity- and density-pressure response; however all must be based on the experimental data.

6.1 Variation of viscosity with pressure

The Barus equation (Cameron, 1966) is the simplest formula describing viscosity dependence on pressure:

$$\eta = \eta_0 e^{\alpha p} \tag{16}$$

Where α is the viscosity-pressure coefficient. The formula can be used up to around 500 MPa and only as an approximation. Better suited for higher pressures, up to 1 GPa, and also including the effect of temperature, is the equation by Roelands (1966):

$$\eta_R = \eta_0 e^{\alpha^* p} \tag{17}$$

Where α^* is the Roelands' pressure-viscosity coefficient calculated according to:

$$\alpha^* p = [ln(\eta_0) + 9.67]\left\{\left(\frac{T-138}{T_0-138}\right)^{-S_0} \times (1 + 5.1 \times 10^{-9} p)^Z - 1\right\} \tag{18}$$

Where η_R is at T temperature. The dimensionless constant Z can be calculated from the formula:

$$Z = \frac{\alpha}{5.1\times10^{-9}(ln(\eta_o)+9.67)} \quad (19)$$

The pressure-viscosity coefficient strongly depends on temperature and also on the molecular structure, as can be seen based on comparison shown in Table 3, taken from Höglund (1999).

Table 3: Typical values of pressure-viscosity coefficients for a range of lubricants (Höglund, 1999)

Lubricant	**Pressure-viscosity coefficient, α (GPa^{-1})**			
	20°C	**40°C**	**60°C**	**80°C**
Naphthenic mineral oil	26.5	23.4	20.0	16.4
Mix of paraffinic/naphthenic oil. 50-50	23.0	20.8	18.5	16.1
Paraffinic mineral oil	19.8	18.2	16.6	15.0
Rapeseed oil	18.9	17.5	16.3	14.6
Polyglycol	18.7	16.0	13.2	10.5
Pine tree oil	17.2	15.6	13.7	12.5
TMP-ester	15.5	14.4	13.1	12.2
Diester	14.6	13.6	12.8	11.6
Polyalphaolefin	15.5	13.8	12.2	10.5

Larsson et al. (2000) presented some measurements of the dynamic viscosity for several base oils, up to a pressure of 500 MPa, and based on the results he determined temperature dependence of constant Z fitting into Roelands' equation (Eq. 18):

$$Z(T) = D_Z + C_Z log\left(1 + \frac{T}{135}\right) \quad (20)$$

Additionally, a variation of dynamic viscosity with temperature for a range of lubricant chemistries can be obtained with the formula:

$$log(log\eta_0 + 4.2) = -S_0 log\left(1 + \frac{T}{135}\right) + logG_0 \quad (21)$$

Coefficients for both equations can be found in Table A.1.

6.2 Variation of density with pressure

Density-pressure variation is most commonly described with the Dowson and Higginson equation (Hamrock et al., 2004):

$$\bar{\rho} = \frac{\rho}{\rho_0} = 1 + \frac{0.6p}{1+1.7p} \tag{22}$$

Where ρ_0 is the density at atmospheric pressure and measurement temperature, and ρ is high pressure density, at pressure p expressed in GPa.

This equation was developed based on the measurements of one mineral oil, and therefore does not take into account the differences due to chemical structure. Also, since these measurements were performed only up to 400 MPa, the formula predicts that the maximum increase from the atmospheric values is around 35 percent. These two limitations lead to a vast amount of research effort to find a more accurate description of the high-pressure behaviour.

Hamrock et al. (1987) investigated six base fluids over a range of pressures from 0.42 to 2.20 GPa at a fixed temperature of 20^{o}C. The authors mention that the accuracy of measurements at pressures lower than 0.42 GPa was not satisfactory and also it was not possible to study the influence of temperature on high pressure density.

Based on the experimental data they developed two equations of state characterising oils at pressures below and above the solidification pressure (or glass transition):

$$\bar{\rho} = \frac{1}{1-C_1 p^2 - C_2 p} \qquad \text{for } p \le p_s \tag{23}$$

$$\bar{\rho} = \frac{1}{1-C_3 p - C_4} \qquad \text{for } p \ge p_s \tag{24}$$

With constants shown in Table A.2. The density calculated based on these equations and extrapolated to even higher pressures is shown for two fluids in Figure 6.1. The difference between these measurements and Dowson-Higginson model clearly shows the influence of chemical structure of the fluid.

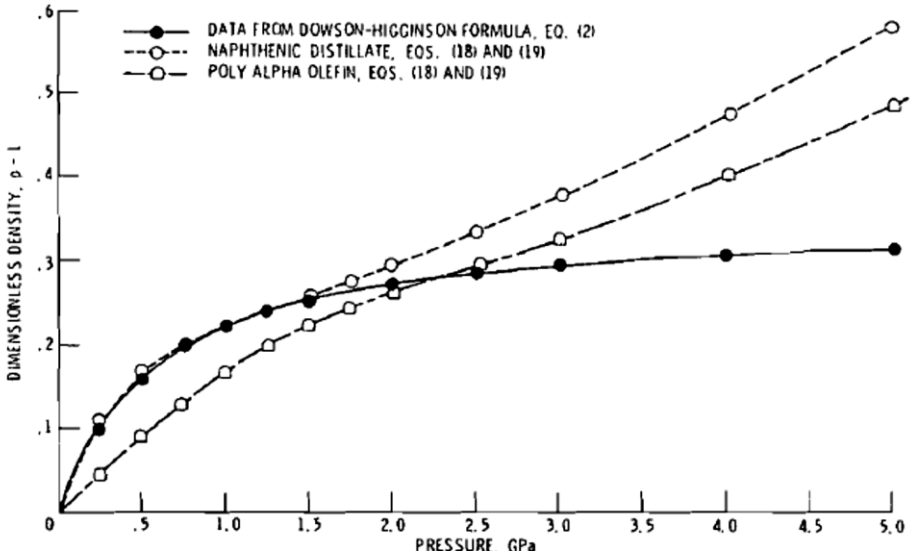

Figure 6.1: Variation of density of pressure for PAO and naphthenic distillate (Hamrock et al., 1987)

After some improvements to the high pressure chamber design, including the seals preventing leakage of the lubricant at lower pressures, Ståhl and Jacobson (2003) published more experimental work up to pressures of 2.7 GPa, based on which another equation of state was developed:

$$\frac{\overline{\rho}(p)}{\rho_0} = c_1 + c_2 - c_3 e^{-c_4 p} \tag{25}$$

With coefficients of the equation shown in Table A.3. The curve-fitted data for all five fluids tested, compared with Dowson-Higginson formula, are displayed in Figure 6.2. They indicate that the effect of pressure on density in high pressure conditions would be underestimated if the Dowson-Higginson model was used. The results suggest an increase of density around 5-7 % per 1 GPa of pressure in the high pressure range, where the solidification of fluids is likely to occur.

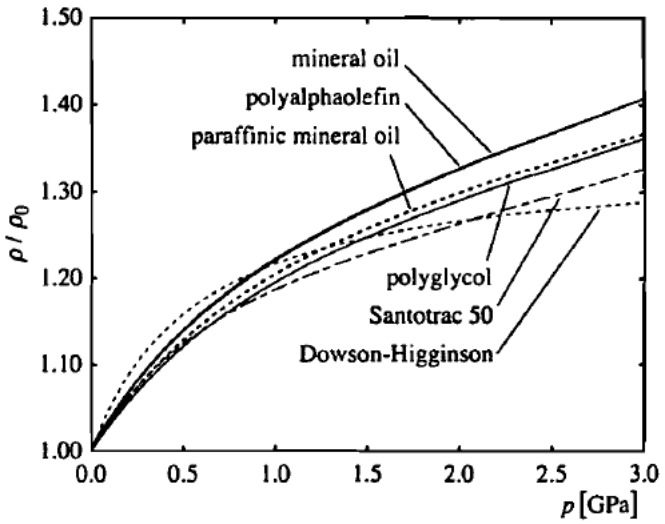

Figure 6.2: Variation of density with pressure for the lubricants tested (Ståhl and Jacobson, 2003)

All of the above results were obtained under steady state conditions; an alternative approach was developed by researchers from Luleå University of Technology, Höglund and Larsson (1997), who performed their measurements with loading-unloading time in the range between 100 and 300 μs. Seven lubricants were tested at pressures up to 1.9 GPa giving foundation for formulation of the following empirical formula:

$$\frac{\rho}{\rho_0} = \left\{1 + \frac{C_1}{2C_2}\left[1 + s\sqrt{1 + \frac{4C_2(p - C_3)}{C_1^2}}\right]\right\}^{-1} \tag{26}$$

This dependence can also be expressed in terms of the volume change:

$$p = C_1 \frac{\Delta V}{V_0} + C_2 \left(\frac{\Delta V}{V_0}\right)^2 + C_3 \tag{27}$$

The dilatation-pressure behaviour can be calculated using appropriate coefficients (Table A.4) and shown in the form as in Figure 6.3.

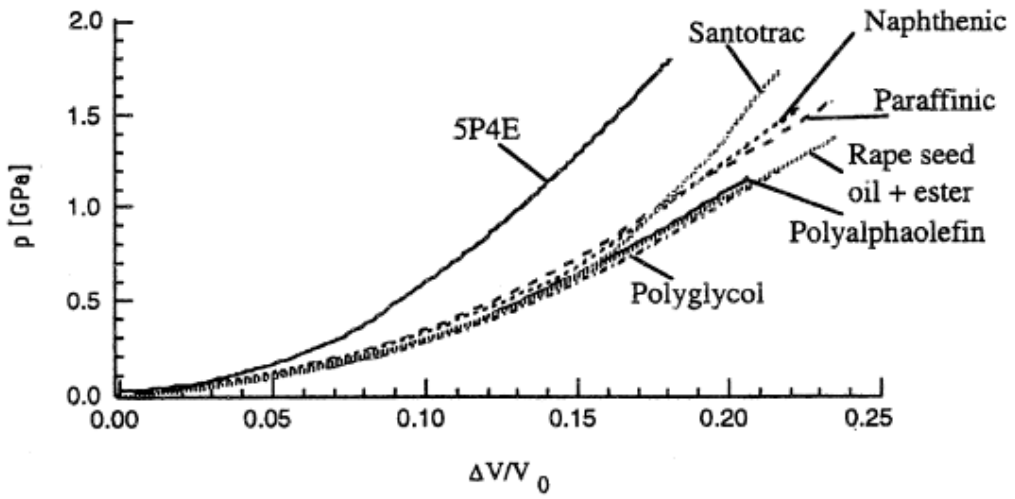

Figure 6.3: Dilatation-pressure relationship for various oils (Höglund and Larsson, 1997)

Larsson and co-workers also measured the high-pressure density and presented a refined version of Dowson and Higginson formula, which also includes the effect of temperature (Larsson et al., 2000):

$$\rho(p,T) = \rho_0 \left(1 + \frac{D_1 p}{1+D_2 p}\right)[1 - \varepsilon(T - T_0)] \quad (28)$$

All needed constants can be found in Table A.5 and Table A.6.

6.3 Dielectric properties of lubricants

6.3.1 Introduction

In order to fully understand dielectric properties of lubricants it is necessary to first establish some of the terms which will be used further throughout this chapter (based on Israelachvili (2011) and Atkins and de Paula (2006).

Polarity of a molecule is a result of an uneven internal charge distribution and gives the molecule a *permanent* dipole moment. This uneven partial charge distribution within a

polar molecule may arise from the differences in electronegativity of the atoms and/or asymmetrical structure of the molecule.

Nonpolar molecules, on the contrary, do not possess a *permanent* dipole moment, but under the effect of an external electric field acting to shift their partial charges, a dipole moment can be *induced*.

When a dielectric (nonconductive) material is exposed to the electric field its molecules align according to the direction of the field causing a *polarization*. There are a few types of polarization mechanisms which can be distinguished based on the frequency at which they occur, as shown in Figure 6.4. At low frequencies permanent dipoles (polar molecules) have sufficient time to rotate and align to oppose the electric field. This mechanism is called *orientation polarization* (or *dipolar*). As the frequency of the field direction changes increases, the molecules are no longer able to adjust their orientation and this polarization mechanism is suppressed. This is observed around 10^{11} Hz and since this component of polarization has a very strong contribution to the dielectric constant, after passing the limiting frequency, a significant decrease of the dielectric constant is observed. Another type of polarization, called *distortion* polarization, is seen for both, polar and nonpolar molecules. Depending on the frequency it includes either stretching or bending of bonds (*atomic* polarization), or shifting electron clouds in the opposite direction than nuclei (*electronic* polarization), thus creating an induced dipole. Atomic polarization occurs between 10^{11}–10^{14} Hz, which corresponds to the infrared radiation, while electronic polarization covers the visible and ultraviolet range (10^{14}–10^{17} Hz).

For nonpolar molecules, or for polar ones with supressed dipolar polarization, the dielectric constant can be calculated using the Clausius-Mossotti equation (Atkins and de Paula, 2006):

$$\frac{\varepsilon_r-1}{\varepsilon_r+2}=\frac{N_A\alpha_d\rho}{3M} \tag{29}$$

Here N_A is the Avogadro constant, α_d is molecular polarizability, M molecular weight and ρ is density. According to Eq. 29, the ratio $\frac{\varepsilon_r-1}{\varepsilon_r+2}$ for any given substance is

proportional to the density of that substance. The factor $\frac{N_A \alpha_d \rho}{3M}$ can be deduced from the value of the dielectric constant and density at atmospheric pressure and used to calculate the dielectric constant under different conditions, if the density is known.

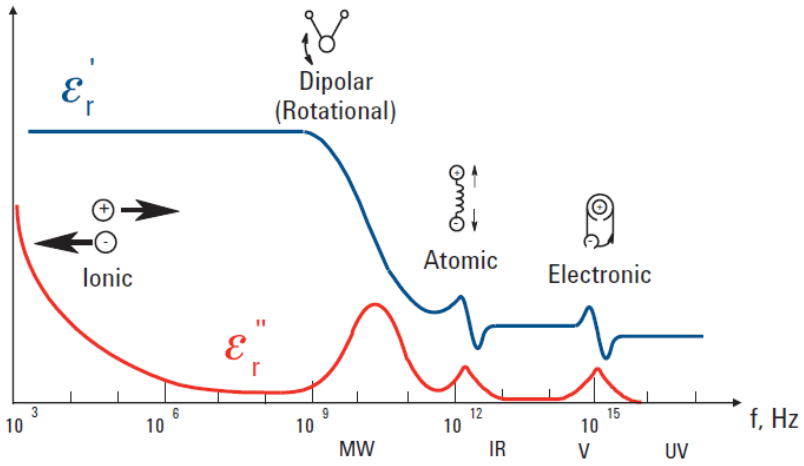

Figure 6.4: Dielectric mechanisms (Agilent Technologies)

Dielectrics are mainly used in capacitors, because they increase the amount of charge which can be stored. A high dielectric constant is crucial in this case, as the higher the dielectric constant of the medium, the higher the charge storage capacity, as seen in the following equation, known as a parallel-plate capacitor formula:

$$C = \frac{\varepsilon_0 \varepsilon_r A}{d} \tag{30}$$

There are two more variables which influence capacitance, namely area, *A*, and distance between the plates, *d*. The equation also includes a constant ε_0, which is the vacuum permittivity.

Since real dielectrics are not ideal and some of the energy is always lost, the dielectric constant is expressed as a complex number allowing the inclusion of a loss factor (imaginary part):

$$\varepsilon_r = \varepsilon_r' - j\varepsilon_r'' \tag{31}$$

6.3.2 Dielectric constants of lubricants

From the point of view of tribology and lubrication there are several reasons why the researchers have been interested in measuring dielectric constants of lubricants.

One of the reasons is the fact that the dielectric constant is a direct indication of molecule's polarity. From the early days of tribology research it has been recognized that polar fluids, such as esters, due to their higher "lubricity", in comparison to mineral oils, offer a reduced boundary friction. Dielectric constant can therefore be used to differentiate the oils and together with other properties may help explaining observed lubricant's behaviour. Table 4 shows, as an example, dielectric constants for a range of lubricants with different chemistries, covering hydrocarbon-based stocks, as well as polyol esters (POE) and polyalylene glycols (PAG).

Table 4: Atmospheric pressure dielectric constants of lubricants (based on Han and Masuko (1999))

Type	**Name**	**Dielectric constant at 23°C**
Hydrocarbon	Hydrotreated super-refined paraffinic mineral oil	2.034
	Alkyl Naphthalene	2.241
Polyol Ester (POE)	Trimethylolpropane tri 2-ethylbutanoate	3.722
	Trimethylolpropane tri 2-ethylhexanoate	3.456
	Trimethylolpropane tri 3,5,5-trimethylhexanoate	3.263
	Pentaerythritol tetra 2-ethylhexanoate	3.046
	Pentaerythritol tetra 3,5,5-trimethylhexanoate	2.767
Polyalkylene Glycol (PAG)	R-$(PO/EO=5:5)_n$-R dialkylether of random co-polymerized propyleneoxide and ethyleneoxide	5.909
	R-$(PO/EO=9:1)_n$-R dialkylether of random co-polymerized propyleneoxide and ethyleneoxide	4.922
	R-$(PO)_a$-R polypropyleneoxide dialkylether	4.789
Additive	Trictresyl phosphate	4.859

Another reason is using the dielectric constant as one of the parameters in oil condition monitoring, mostly for engine lubricants. Due to its high sensitivity to changes in chemistry, resulting from either oxidation or oil contamination, with for

example glycol or water, it can help with determining potential sources of engine oil performance deterioration.

In both areas of interest only the atmospheric pressure value of dielectric constant is concerned. The third important area requires knowledge of high-pressure variation of the dielectric constant. Understanding pressure dependence is necessary for correct evaluation of lubricant film thickness from measurements of electrical capacitance, as discussed in subchapter 4.1.1.

Galvin et al. (1963) measured a range of different lubricating oils' chemistries up to 345 MPa pressure at 20 and 100^{o}C (Table A.7). They observed that two of the oils (D and F) after an initial increase of the dielectric constant with increasing pressure, show a negative gradient. This behaviour is unexpected, however it should be noted that this trend was only found at the lower temperature and both fluids are characterised by high viscosity and low viscosity index, with one of them additionally containing a methacrylate polymer.

The authors also calculated dielectric constants theoretically with the Clausius-Mosotti relation (Eq. 29) using the oil's density at 345 MPa and compared this data with their measurements. Based on the results shown, it can be concluded that for the majority of the oils the calculated values were within 10% from the measurement results, with many showing a difference smaller than 5%. Apart from the two oils already mentioned (D and F), all other mineral-based oils show a very good agreement. A higher difference is expected for more polar oils as the equation is considered to be accurate only for nonpolar substances.

The trend of a decreasing dielectric constant at higher pressures for a viscous oil was reproduced by the same research group few years later (Dyson and Wilson, 1969). As seen in Figure 6.5, one of the oils (O_3) shows a strong drop of the dielectric constant above 150 MPa pressure. The same authors also measured dielectric constants of greases (shown in Table A.8).

Due to a difficulty and potentially high uncertainty of dielectric constant measurements of greases under pressure, the values are often obtained by an extrapolation of the atmospheric pressure results. A rate of change can be estimated with the use of the base oil.

It is also important to note that due to breaking of the thickener's structure under shear, a decrease of dielectric constant occurs (Bondi and Penther, 1953). This effect is difficult to estimate by calculation, therefore actual measurement is preferred.

Wilson (1979) examined the static dielectric constant of an unused grease and compared it with results after shearing the grease in a twin-disc machine. The conditions of speed and contact pressure were adjusted to replicate those found in the bearing tests. The initial dielectric constant of 3.07 decreased to a value of 2.60, while the base oil's dielectric constant was equal to 2.32.

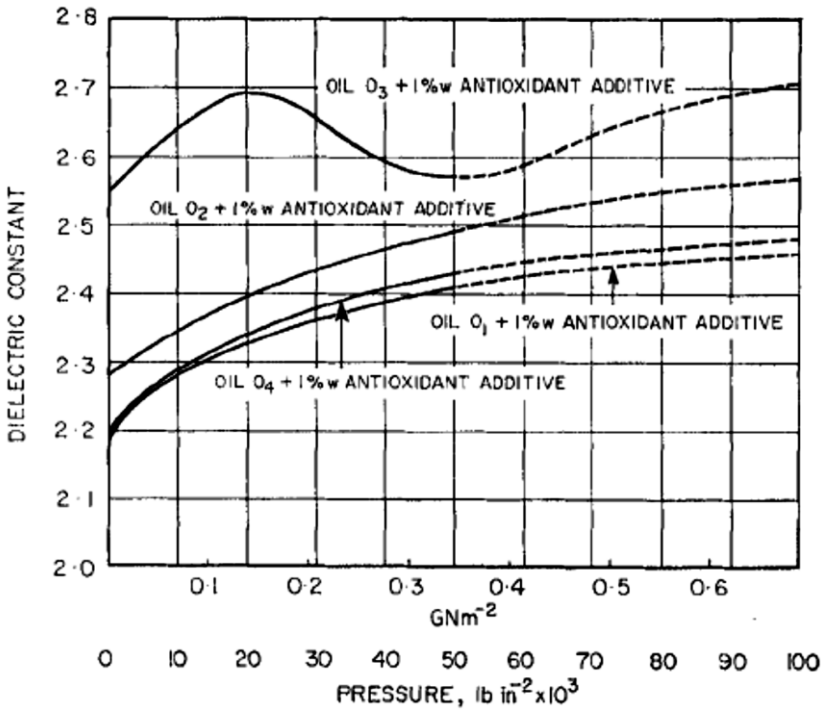

Figure 6.5: High-pressure measurements of dielectric constants of base oils (Dyson and Wilson, 1969)

6.3.3 Dielectric properties of glycerol

Dielectric properties of glycerol have been widely studied over the years due to its unique properties. Small molecule size, very high polarity and viscosity, miscibility with water in all proportions, as well as a low price and availability have made it a very interesting subject of research starting in the early 1930s.

Danforth (1931) was the first who investigated dielectric properties of liquids at truly high pressure conditions, reaching 1.2 GPa, which was up to four times higher than any other investigator before him. He tested a number of liquids (including hydrocarbons, ethers, halogen compounds and alcohols) at two different frequencies.

An unexpected behaviour was reported for glycerol, eugenol and isobutyl alcohol in high frequency measurements (247 kHz). These results are shown as solid lines in Figure 6.6, while the dashed lines correspond to the audible frequency (20 – 20 kHz) measurements.

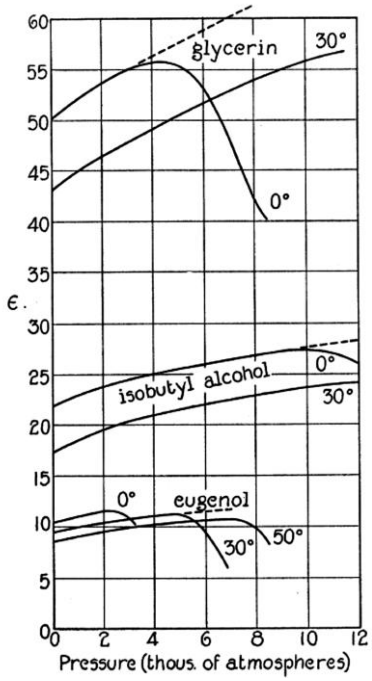

Figure 6.6: Dielectric constant measured at 247 kHz (Danforth, 1931)

The author concluded that the decrease of dielectric constant from a certain pressure for the three fluids results from the supressed orientation of molecules due to viscous

resistance. According to the authors the lack of this phenomenon at an audible frequency means that freezing as a possible cause, can be excluded. The fact that the value of pressure at which a decrease of dielectric constant begins is increasing with temperature, as can be clearly seen for eugenol, supports the idea of the viscosity effect. It should be noted, however, that no decrease of dielectric constant was noticed at 30^{o}C for glycerol in the pressure range studied.

Similar results were obtained by Scaife (1955) who measured real and imaginary parts of complex permittivity of glycerol at 5^{o}C up to 0.9 GPa at two different frequencies (Figure 6.7).

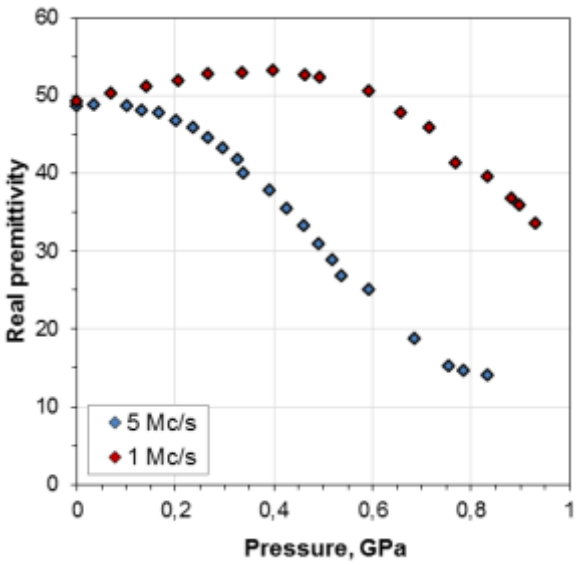

Figure 6.7: Real part of permittivity of glycerol at 5^{o}C (reproduced based on Scaife (1955))

It can be seen that both, the temperature and the measurement frequency, affect the position of the inflection point, with lowering temperature and increasing frequency acting to shift it towards the lower pressures.

Later Scaife W (1976) commenting on Danforth's (1931) results said, that “an anomalous dispersion in permittivity was observed for both liquids, but there were hidden errors in the data due to electrode double-layer effects”. In his own work he

also measured the electrode polarization and showed that, as expected, it will strongly affect overall capacitance at low frequencies (below 1 kHz). He mentions, however, that in case of glycerol the effect of double-layer and dielectric relaxation may overlap under certain conditions, making the evaluation of dielectric constant difficult. Unfortunately he does not provide more details.

An alternative approach to study dielectric properties of liquids at high-pressures is to perform measurements in the supercooled-state in order to shift the dispersion process to lower frequencies. This has been done by Davidson and Cole (1951), who studied dielectric relaxation at atmospheric pressure and over temperature range between 40 and -75^{o}C (Figure 6.8).

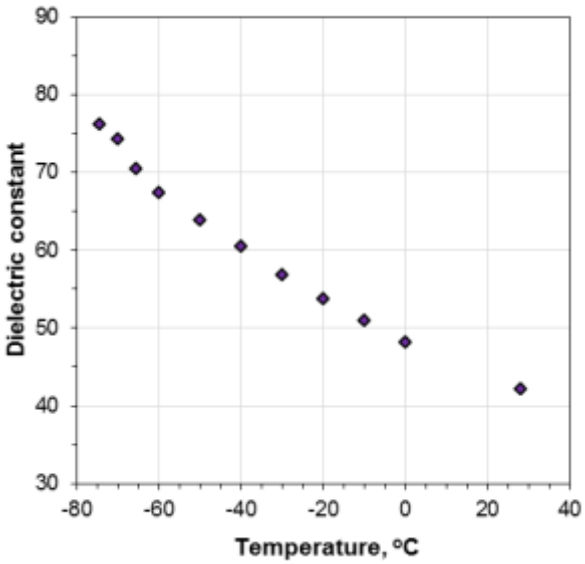

Figure 6.8: Static dielectric constant of glycerol over the range of temperatures at atmospheric pressure, reproduced based on data from Davidson and Cole (1951)

For the current study it is necessary to know the dielectric constant of lubricants under the testing conditions and for this purpose the effect of pressure on molecular reorientation of glycerol must be understood. In order to determine if the static dielectric constant can be used in the calculations, dielectric relaxation data found in literature were analysed.

Johari and Whalley (1972) presented an extensive work covering a very wide range of temperature (218-357 K), pressure (0-53 kbar) and frequencies (0.1-10^5 Hz). By using their diagram (shown in Figure 6.9) it is possible to determine the location of the maximum of dielectric loss curve for certain conditions. It is clear that over the range of pressures used in the current study (up to 1GPa), if the experiments are performed at temperatures above 0^oC, the static dielectric constant can be used as the dipolar polarization mechanism will not be supressed.

In order to gain absolute certainty, additional data was studied for comparison. Results of experiments performed by Forsman et al. (1986) (Figure A.1), as well as by Paluch et al. (1996) (Figure A.2), confirm the initial assumption.

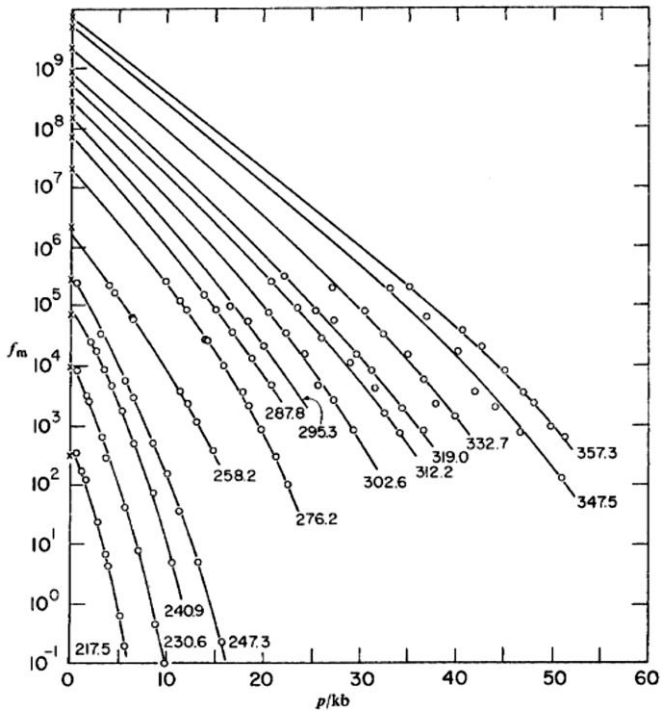

Figure 6.9: Maximum loss frequency of glycerol as a function of pressure (Johari and Whalley, 1972)

The values of static dielectric constant were extrapolated from the results by Johari and Whalley (1972) (Figure 6.10), as they also showed an excellent agreement with a later study by Forsman et al. (1986).

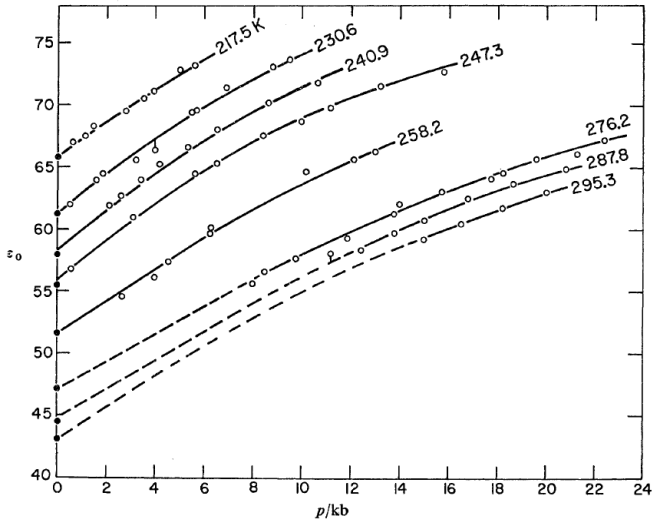

Figure 6.10: Static dielectric constant of glycerol measured over the range of pressures and temperatures (Johari and Whalley, 1972)

Chapter 7: Experimental methodology

7.1 Properties of lubricants tested

The lubricants used for experimental work in the current research can be divided into a few groups:

- base oils: polyalphaolefins of various viscosity (PAO4, PAO40, PAO VG48) and their blends
- polar fluids: glycerol, polyethylene glycol (PEG400) and synthetic ester (base oil for SRL grease by Kyodo Yushi)
- organic friction modifier solution (1 wt% of glycerol monooleate (GMO) in PAO4)
- fully formulated mineral oil (Shell Turbo T100)
- SRL grease manufactured by Kyodo Yushi

Viscometric characteristics of the oils, as well as their dielectric constants and viscosity pressure coefficients necessary for the current study, are listed in Table 5, while details of the grease are found in Table 6.

Table 5: Properties of lubricants tested

Lubricant	**Viscosity at 40°C mm^2/s**	**Viscosity at 100°C mm^2/s**	**Pressure-viscosity coefficient at 25°C GPa^{-1}**	**Dielectric constant at 25°C**
PAO4	17.2	3.9	15	2.1
PAO40	396.0	39.0	-	2.1
PAO4:PAO40 1:3	150.0	19.0	-	2.1
PAO VG48	46.4	7.8	16.5	2.1
Mineral oil	99.0	11.4	24.5	2.3
Glycerol	224.8	12.2	-	41.9
Polyethylene glycol	40.2	6.8	-	17.3
SRL ester	26.0	4.7	-	-

Two additional blends of PAO with synthetic ester were prepared with a targeted dynamic viscosity at test temperature, 30^{o}C:

- SRL:PAO4 1:1 with a dynamic viscosity of 24.6 mPa·s
- SRL:PAO mix 1:1 of the same dynamic viscosity at 30^{o}C as SRL (33.3 mPa·s), where PAO mix was obtained by mixing PAO4 and PAO40 in mass proportion 94:6

Table 6: Properties of the grease tested

Oil	**Kyodo Yushi SRL**
Base oil type	Synthetic ester
Base oil viscosity at 40^{o}C, mm^{2}/s	26
Thickener type	Lithium Stearate
Worked penetration	250
Thickener content	5-15%
Additives	Barium compound (5%)

As glycerol is a highly hygroscopic liquid, it easily absorbs moisture from the atmosphere. Therefore it is necessary to establish the influence of water content on viscosity and dielectric constant of glycerol used in current experiments. Relevant data was found in literature and is shown in Table 7. It can be seen that the dynamic viscosity reduces to less than half of the initial value for 5% water content. This is equivalent to a reduction of more than 40% of the EHD film thickness. Thus, in order to avoid errors due to a change of viscosity, the viscosity of glycerol was always measured after each test. These measurements showed that the maximum water concentration in all samples was around 1%.

From the data in Table 7 it can also be noticed that for this concentration the change of dielectric constant due to the presence of water is negligible.

Table 7: Dependence of glycerol viscosity (Segur and Oberstar, 1951) and dielectric constant (OPTIM Synthetic Glycerine) on water content

Glycerol content, %	Viscosity at 30°C, mPa·s	Dielectric constant at 25°C
100	612	40.1
99	500	–
98	409	–
97	340	–
96	281	42.3
95	237	–
90	109	45.5

7.1.1 High-pressure properties

Dielectric constants of PAO oils and the mineral oil were calculated using the Clausius Mossotti relation (Eq. 29). As already discussed in section 6.2, there are a number of equations describing density-pressure variation for lubricants. For this study a model-based on experimental data by Ståhl and Jacobson (2003), was chosen. Figure 7.1 shows the predicted dielectric constant for PAO4, while the results for mineral oil are displayed in Figure 7.2. In both cases a reference line obtained with the Dowson-Higginson formula (Eq. 22) is included for comparison.

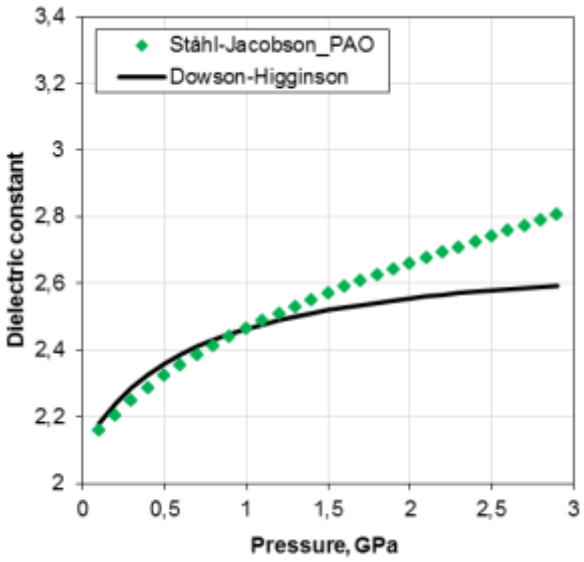

Figure 7.1: Dielectric constant of PAO4 as a function of pressure calculated based on different density-pressure models

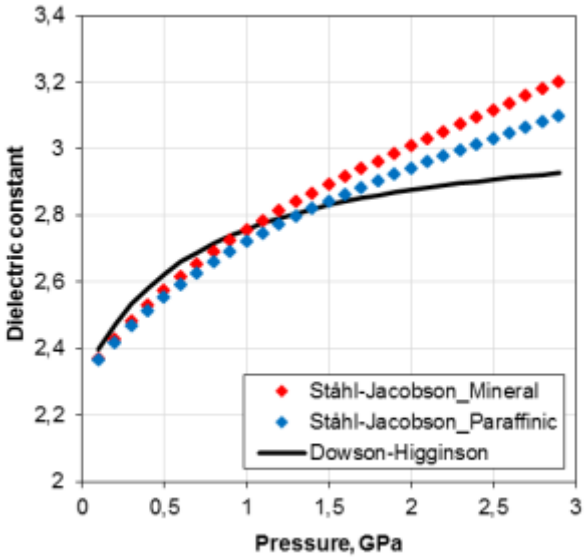

Figure 7.2: Dielectric constant of Mineral oil as a function of pressure calculated based on different density-pressure models

The dielectric constant of glycerol at atmospheric pressure and 30^{o}C was based on the experimental data by Davidson and Cole (1951), also shown in Figure 6.8. The value at 60^{o}C was obtained by extrapolation of those results. In order to calculate dielectric constants at contact pressure, a correction based on results from publication of Johari and Whalley (1972) (Figure 6.10), was applied.

In the case of polyethylene glycol only atmospheric pressure values of dielectric constant could be found in literature (Sengwa et al., 2000), and to obtain the high pressure value the same correction for estimating increase of dielectric constant with pressure as for glycerol, was used.

Apart from the dielectric constant at contact pressure, it is also necessary to know the high pressure refractive index of lubricants to correctly evaluate film thickness with optical interferometry methods.
This can be obtained with the Lorentz-Lorenz equation (Foord et al., 1968):

$$n_p = \left(\frac{1+2A}{1-A}\right)^{1/2} \quad (32)$$

where:

$$A = \frac{\rho_p}{\rho_0}\left(\frac{n_0^2-1}{n_0^2+2}\right) \quad (33)$$

n_0 and ρ_0 are atmospheric pressure refractive index and density, while symbols denoted with "p" subscript correspond to high-pressure values.

7.2 The EHD film thickness measurement rig

Experiments were performed on an EHD rig by PCS Instruments. The rig has been originally designed for film thickness measurements with ultra-thin film interferometry (UTFI), according to the method described by Johnston et al. (1991). More details on the optical interferometry can be found in e.g. Francon (1966).

The system uses a 19.05 mm diameter steel ball and a 100 mm diameter disc, which can be independently driven at various slide/roll ratios. The temperature of the oil bath can be set to within ±1^{o}C.

In order to avoid excessive splashing of the lubricant, speeds above around 0.5 m/s were avoided and it was always intended to run the tests at a lower speed range. The lowest speed feasible on the current rig was around 0.010 m/s as below that value the motors were not running smoothly. For that reason the targeted film thickness range was adjusted by varying either test temperature, or base oil's viscosity.

A simplified schematic of the optical measurement system, using a two-beam interferometry principle, is shown in Figure 7.3. White light is shone onto the contact formed between a steel ball loaded against a glass disc. The disc has a thin, semi-reflective layer of chromium coated on the contacting surface, on top of which a layer of silica of around 500 nm thickness is deposited.

The light passes through the glass and is partly reflected from the Cr film. The remaining part travels through the chromium layer, silica spacer layer and the lubricant film and is then reflected from highly polished surface of the steel ball.

As these two rays come from the same source and have travelled different distances, they interfere, either constructively or destructively depending on the separation between the surfaces, which is given by the thickness of lubricating film.

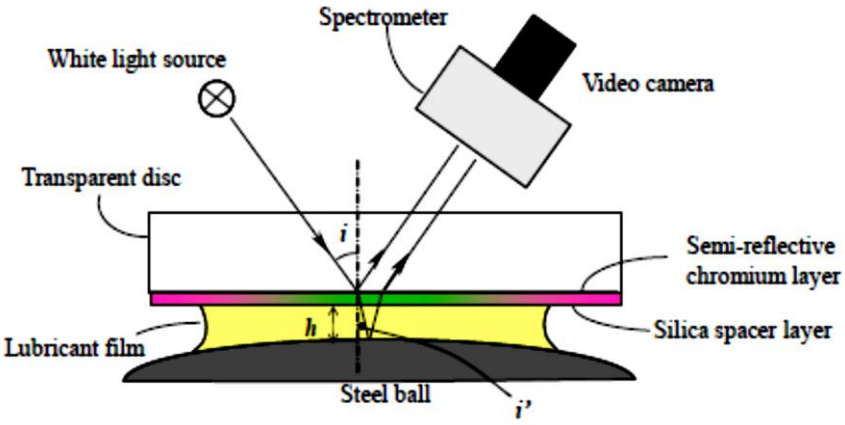

Figure 7.3: UTFI measurement system

The lubricant film thickness is determined by finding the wavelength corresponding to a maximum constructive interference and by taking into account the influence of the silica layer. The following equations can be used for either constructive or destructive interference (Spikes and Cann, 2001):

$$2n_{oil}h_{oil} + 2n_{silica}h_{silica} + \omega\lambda = N\lambda \qquad N = 1, 2, 3, \ldots \qquad (34)$$

$$2n_{oil}h_{oil} + 2n_{silica}h_{silica} + \omega\lambda = \left(N - \frac{1}{2}\right)\lambda \qquad N = 1, 2, 3, \ldots \qquad (35)$$

7.2.1 Relative intensity optical method

In order to be able to directly measure the optical film thickness of a lubricating film, and the electrical capacitance of an EHD contact, a method based on the dependence

of relative intensity of the interfered light on separation has been established. The idea of using interference intensity (grey level) originates from Roberts and Tabor (1971), who demonstrated that measurements of films having a thickness below a quarter of monochromatic light wavelength were possible. This concept was further used by Luo et al. (1996), under the name of the Relative Optical Intensity Interferometry (ROII). Film thickness is calculated assuming that the intensity versus film thickness function follows a cosine trend (Eq. 13), which depending on the optical and experimental setup may not be the case.

An attempt to apply the ROII variant and calculate film thickness based on interference intensity has not been successful. It is believed that the reason for that was the specifics of the optical system used in the current study (i.e. Cr layer thickness, multi-beam reflections, optical components and arrangement). The work by Guo and Wong (2002) confirms this explanation as it shows how the thickness of the chromium layer itself may cause a deviation from the cosine trend, due to absorption (Figure 7.4).

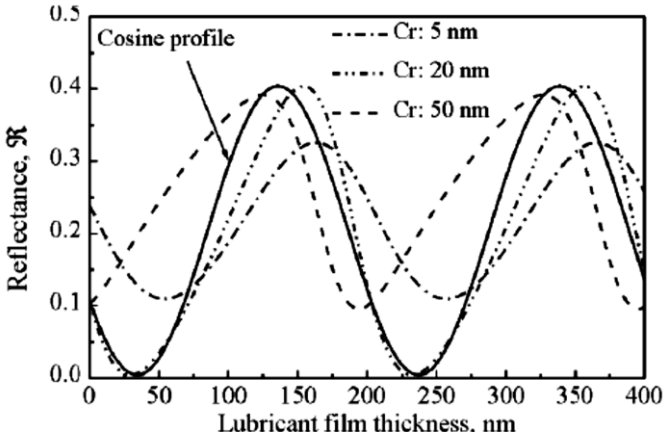

Figure 7.4: Deviation from the cosine trend depending on the Cr thickness (Guo and Wong, 2002)

During the initial experiments it has been noticed, however, that even though the relationship between the intensity and film thickness does not follow the exact cosine trend, the shape of the curve is repeatable and reproducible even under different operating conditions (temperature, lubricant viscosity). It was therefore decided that a

calibration curve that correlates intensity to a known film thickness measured with the ultra-thin film interferometry can be prepared. In order to compensate for different intensity of the light used for measurements, a normalized value of intensity has been used. This was obtained by dividing intensity of an area of interest (central plateau, profiles along or across rolling direction and full maps) by a maximum intensity for each image analysed. It should be noted that chromium discs used in this study varied with sputtered chromium thickness, although they were all in the range approximately between 10 and 35 nm, the exact thickness for each is not precisely known. This slight difference in chromium thickness will lead to a different response of the system, and slight variation in the relative intensity-film thickness curve shape. For that reason, whenever a new disc was used, a new calibration curve was obtained.

The experimental procedure was as follows: white light filtered by a narrow band-pass filter, with a centre wavelength of 550 nm and a full-width at half-maximum (FWHM) of 10 nm, was directed onto the EHD contact under investigation and the interferometric image after passing through a microscope was recorded by a high resolution black and white camera. To allow more accurate film thickness mapping and observation of lubricating film features, a 10x magnification objective lens was used. That limited the maximum load which could be applied, as above 25N the entire contact area was not visible. To obtain film thickness maps at loads higher than 25N lower magnification lens, 5x, was required.

Figure 7.5 gives an example of optical images showing an interference pattern over a range of film thicknesses. Relative intensity extracted from the central plateau of EHD contact images can then be plotted as a function of optical film thickness, as in Figure 7.6. The optical film thickness is obtained by multiplying the film thickness measured with UTFI method by the refractive index of lubricant at testing conditions (test temperature and maximum Hertzian contact pressure). The refractive index at contact pressure is calculated as described in section 7.1.1.

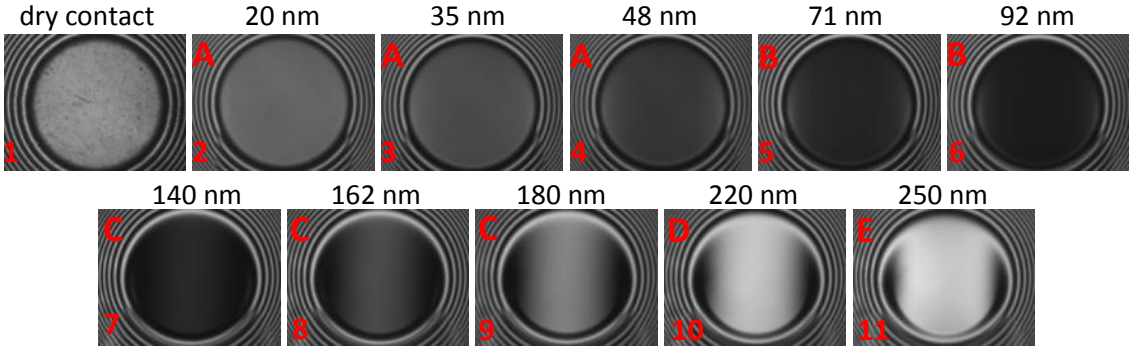

Figure 7.5: Interference pattern of the contact for a range of lubricant film thickness (actual, not optical film thickness shown)

The first image in Figure 7.5 shows an interference pattern for dry contact at a 20N load, with the gap between the glass disc and curvature of the steel ball filled with air. The following images (2-11) were recorded when the contact was lubricated and run at an increasing speed.

It can be seen that when the film thickness is very low, i.e. at low speeds, the contact area has a uniform light-grey colour (image 2), which becomes darker as the speed, and film thickness, increases (images 3-5). This corresponds to the first slope of the curve, described as “A” in Figure 7.6. When the curve approaches its minimum (part “B”; images 5 and 6) the resolution of the method decreases. In this region the contact area has a very dark grey, to black colour. As the film thickness increases further, the central region becomes brighter (part ”C” of the curve; images 7-9), with the side lobes and the exit side having darker-grey colour. The curve now has a steep shape, giving a high resolution until the relative intensity reaches its maximum (part “D”, image 10). Further increase of the film thickness results in the central area of contact getting darker (part “E”). This cyclic change of the central region colour from light grey, through dark grey and black and getting brighter again repeats itself. With further increase of speed the images get more complex, also the side lobes and constriction at the exit are much more pronounced.

Due to a specific shape of the curve and relatively large area of lower resolution (part “B”), the method should preferably be used in thin film region (part “A”), which was the focus of current work.

In order to determine the lubricant film thickness from relative intensity extracted from black and white images of EHD contact, a calibration curve is needed. An example of such a curve (for one of the chromium-coated discs used) is shown in Figure 7.7. As can be noticed, the same value of relative intensity corresponds to several film thickness conditions. It is therefore necessary to determine the interference order and to specify in which part of the curve the measured film thickness approximately is.

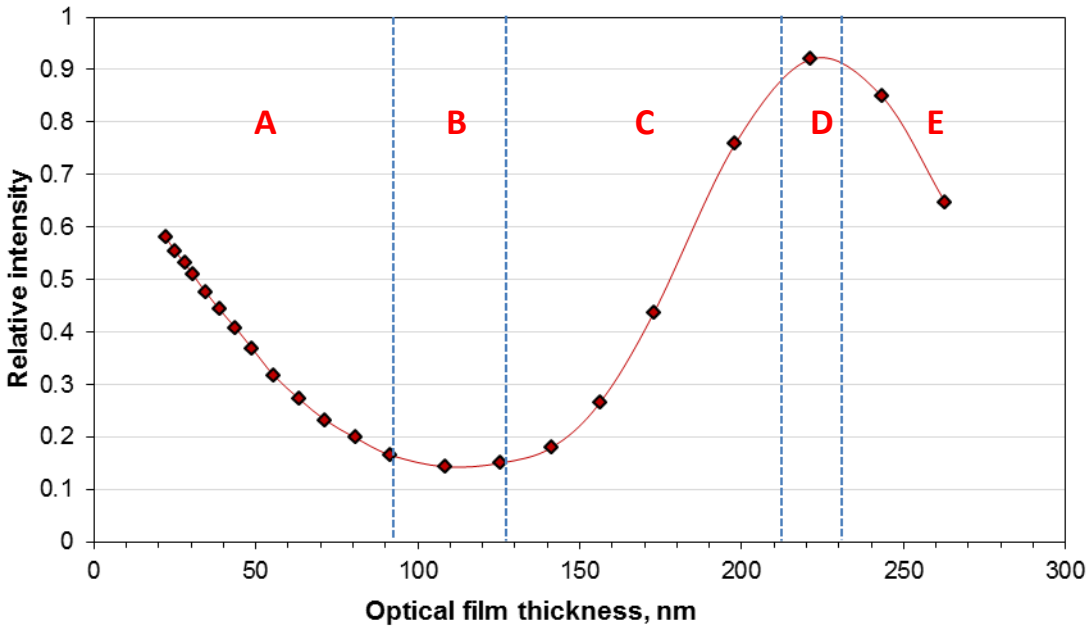

Figure 7.6: Relative intensity as a function of optical film thickness

This can be done based on the appearance of the contact area. If the whole contact area is almost uniform in shades of grey, the expected optical film thickness is below around 115 nm. If the central area is of a brighter shade than the sides and side lobes can be clearly distinguished, then the optical film thickness will be between 115 and 225 nm.

For the purpose of reading relative intensity values from the images taken, and calculating corresponding optical film thickness, a Visual Basic computer program has been used. It allows analysing an area of interest, such as central film thickness, film profiles or film thickness maps and extracts the result (optical film thickness) in the

form of a text file. It is then necessary to divide the optical film thickness by a refractive index of lubricant at testing conditions.

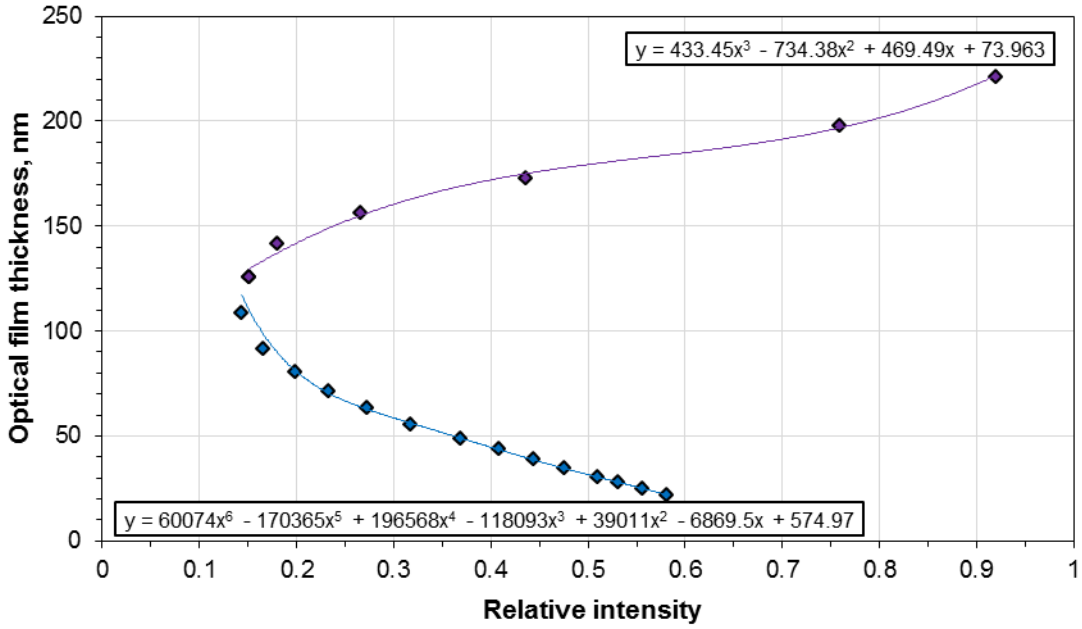

Figure 7.7: Example of a calibration curve

As the thin film region, covering part "A" of the curve, is crucial for the current study, much attention was given to study the resolution of film thickness evaluation in this range. At first it was necessary to establish whether or not, such an approach can indeed give repeatable and reproducible results. Figure 7.8 shows relative intensity as a function of optical film thickness for three tests performed in the same conditions. An excellent repeatability of the results can be observed. In addition to that, in order to verify if the shape of the curve depends on the operating conditions of temperature and speed, a blend of PAO4 and PAO40 in proportion 1:3 was compared with PAO40 tested at 30^{o}C and 60^{o}C. A significant difference in viscosity at test temperature results in a different range of entrainment speeds for each of the lubricants tested. Nevertheless, the data in Figure 7.9 also show a very good correlation.

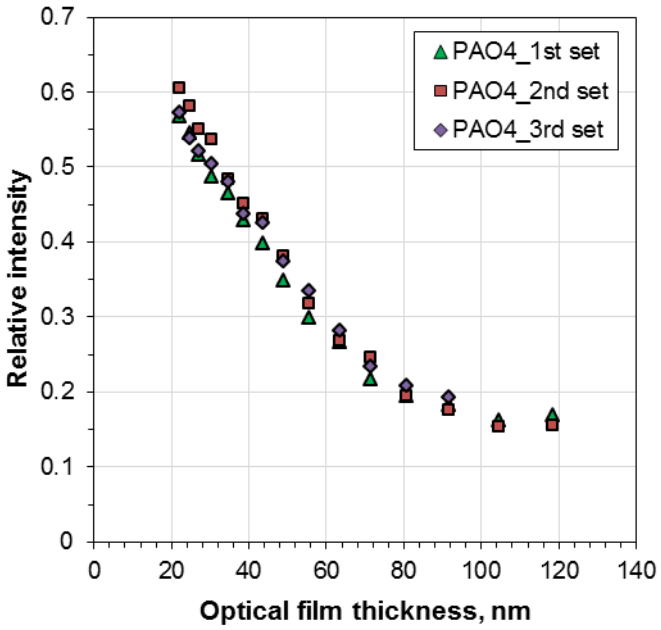

Figure 7.8: Relative intensity repeatability with PAO4 and 25°C

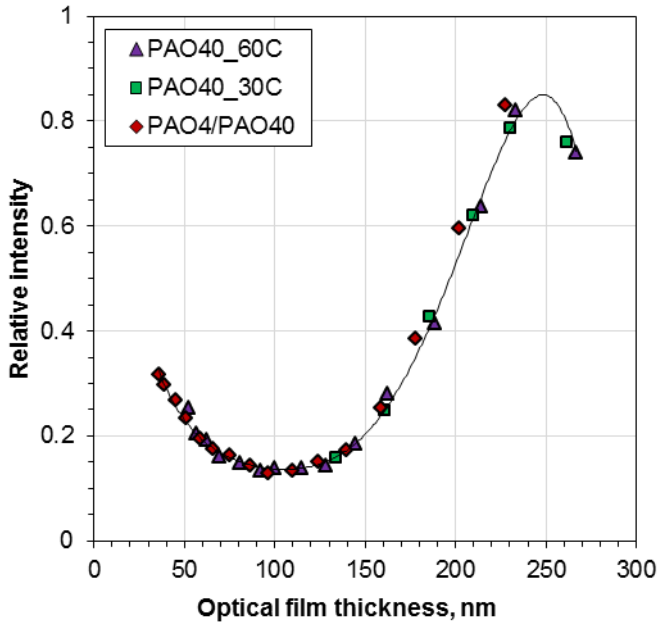

Figure 7.9: Relative intensity repeatability at different temperatures

Even though the lubricants tested have different refractive indexes at test temperatures, it is easy to compensate for that by using optical film thickness in calibration procedure and data extraction. The same applies to refractive index

variation due to pressure. The calibration curve can therefore be used for various conditions of temperature and load.

It should be noted that the curve from Figure 7.9 cannot be directly compared with the curve in Figure 7.6, as the two were obtained with two different chromium-coated glass discs of slightly different Cr layer thickness.

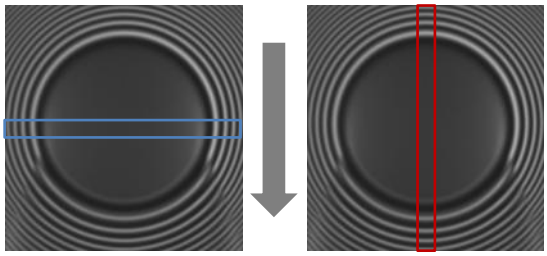

Figure 7.10: Interferometric images showing rolling direction and areas taken for film profiles

Apart from the central film thickness, the method allows extracting film thickness profiles across and along the rolling direction, as schematically shown in Figure 7.10.

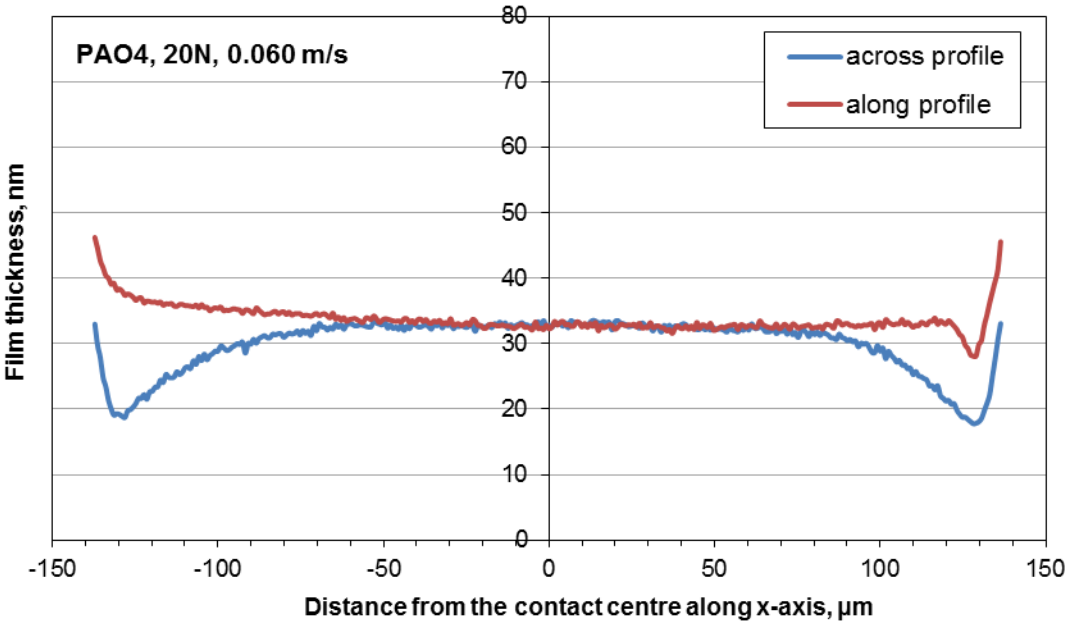

Figure 7.11: Film thickness profiles extracted from relative intensity (PAO4, 20N, 25°C, 0.060 m/s)

Film thickness profiles extracted from similar images, for two different speeds (0.060 and 0.104 m/s) with PAO4 are shown in Figure 7.11 and Figure 7.12, respectively. Both figures show clearly the presence of minimum film thickness at the side lobes and decreased film thickness at the exit, even though by visual examination the contact area seems to have uniform film thickness.

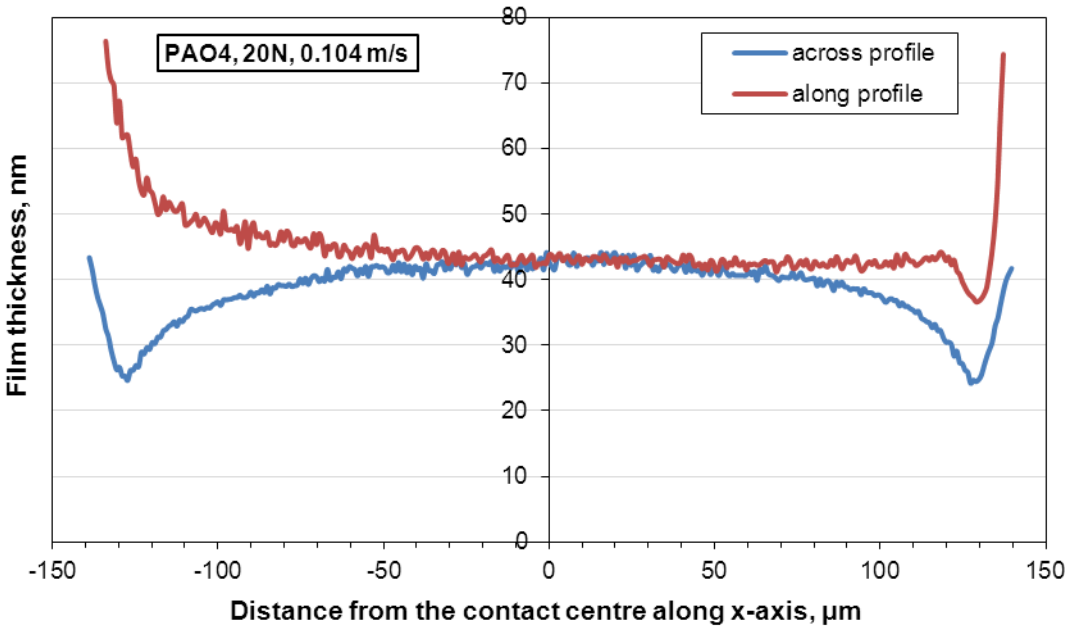

Figure 7.12: Film thickness profiles extracted from relative intensity (PAO4, 20N, 25°C, 0.104 m/s)

Apart from film thickness profiles, also full maps showing the distribution of separation within the contact can be obtained. Figure 7.13 shows three images taken at increasing loads of 10, 15 and 20N. In these conditions the maximum Hertzian contact pressure is 0.41, 0.47 and 0.51 GPa, respectively. As known from the EHD theory, film thickness depends very weakly on load parameter (power of 0.053), therefore only a small variation is seen in the figures.

Variation of speed brings, as expected, higher increase of film thickness as can be observed by comparing film maps in Figure 7.14.

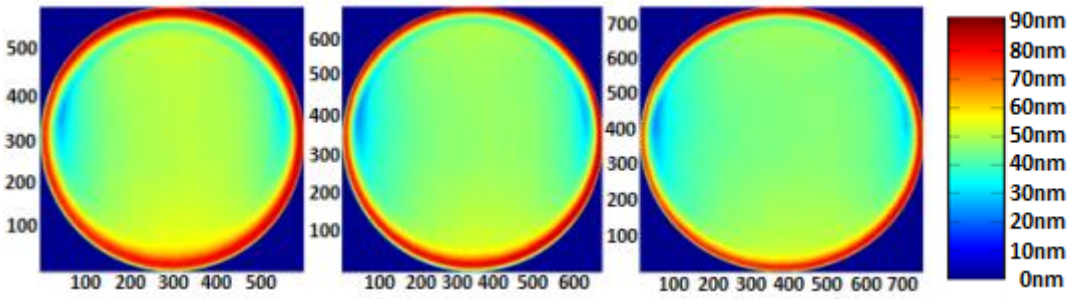

Figure 7.13: Effect of load on film thickness; 10, 15 and 20N at 0.072 m/s with PAO4 at 25°C

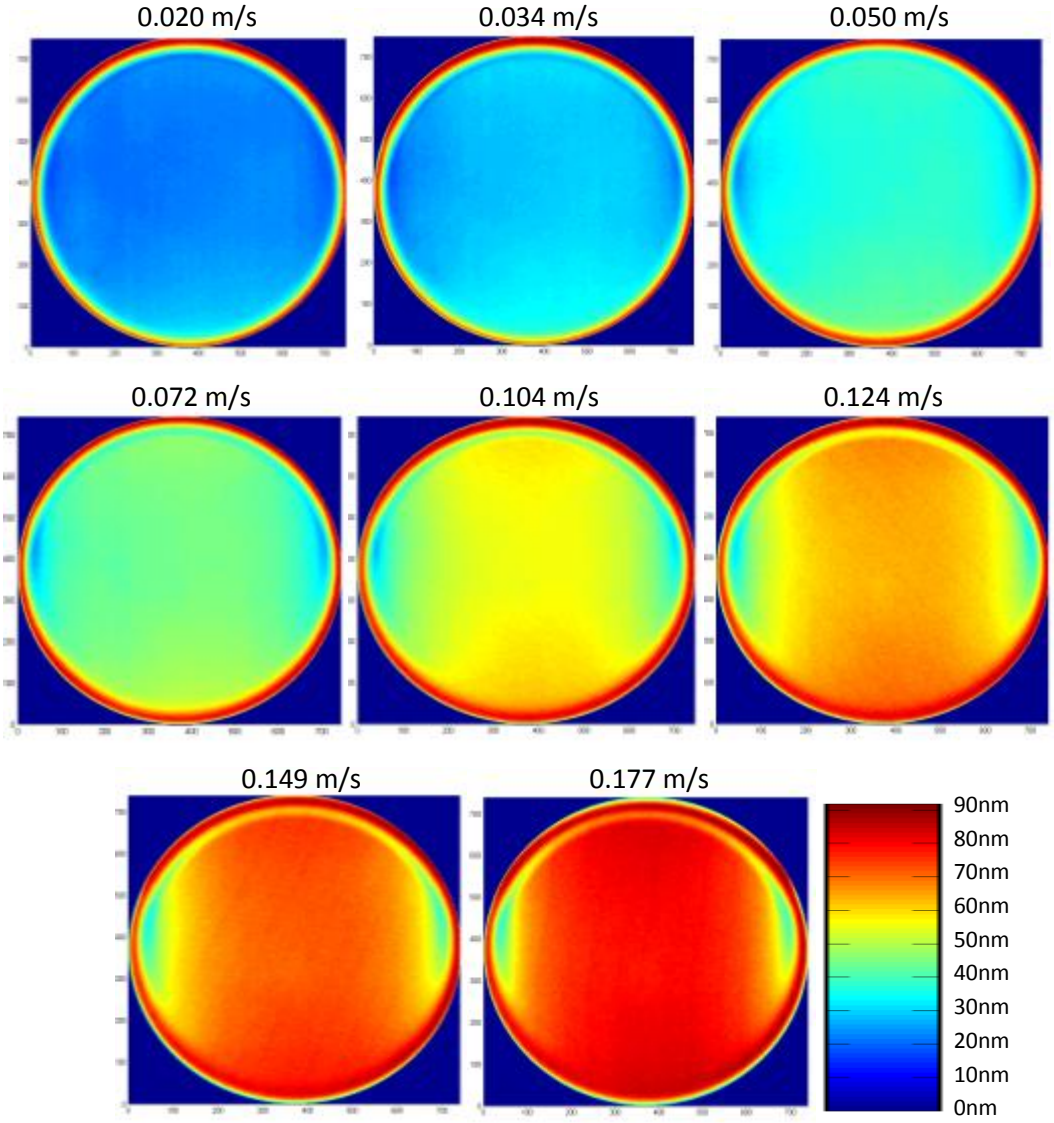

Figure 7.14: Film thickness maps extracted from relative intensity measurements (20N, PAO4, 25°C)

7.2.2 Modifications to the rig to allow capacitance measurements

Since the rig currently used has been designed for optical measurements of lubricant film thickness in order to be able to measure electrical capacitance, some modifications were necessary, schematically shown in Figure 7.15.
Both specimens are electrically insulated from each other and all other parts of the rig. This includes fitting an insulating sleeve on the top part of disc shaft, insulating the bottom surface of the disc with plastic sheets and also insulating the bearings supporting the ball from the ball carriage.

Several variants of electrical connections for collecting the signal from the ball were examined. Since the ball is immersed in lubricant, and constantly rotating, any type of a brush is not ideal, as there would always be a layer of lubricant between the contact points, and that would introduce additional capacitance in the circuit. It was therefore decided that the signal from the ball would be transferred through the ball shaft and further through the connections initially used for strain gauges in traction measurement system. To increase the signal to noise ratio, four brushes were connected in parallel. On the disc side, a carbon brush allowing a sliding contact with the copper nut, used to secure the disc on the shaft, was fitted.

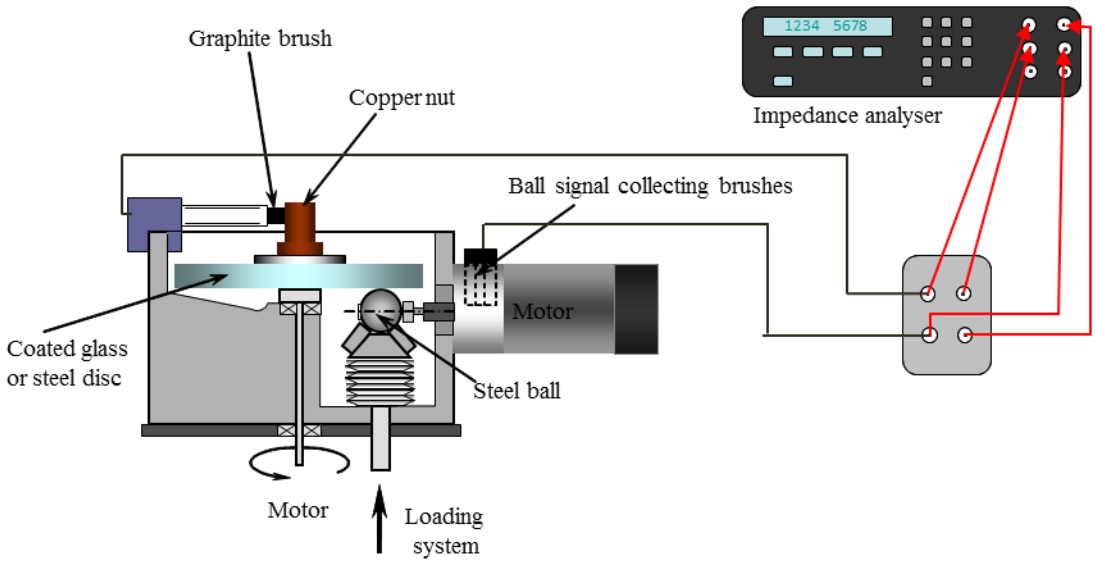

Figure 7.15: Experimental setup for capacitance

The electrical capacitance was extracted from the impedance measured with the Solartron 1260 Impedance Analyser. It should be noted that parameters, such as frequency and voltage strongly affect the measurement quality.

The frequency chosen for the measurement cannot be too low, as the capacitance would show fluctuations due to short-circuiting. On the other hand too high carrier frequency may lead to electromagnetic interferences. Based on literature and preliminary data, where a range of frequencies were tested, it was decided to choose 100 kHz for the measurement frequency.

The voltage applied is another very important parameter. Too high voltage may cause current leakage or eventual breakthrough through the thin lubricating film. It was observed that 0.1 V gave stable readings but with some higher conductivity samples it was necessary to lower the voltage even further as the current leakage caused instability of the signal.

The impedance analyser allows setting an integration time (1 s in this case) over which the impedance is measured (number of cycles depends on the frequency chosen). In the current study 50 measurement points (each being an average over 1 s) were collected, and the average was then used for film thickness calculations. Longer term measurements with grease were an exception here, as these were covering far more than 50 measurements and their integration time was lowered to 0.1 s to capture rapid variations of capacitance.

7.2.3 Film thickness evaluation procedure

During the initial course of this work, an approach for the film thickness evaluation based on measurement of electrical capacitance has been developed. It should be first established, that the capacitance measured by the impedance analyser in the current circuit (C_{total}), includes not only the Hertzian contact capacitance ($C_{contact}$), but also the

capacitance corresponding to a region outside of contact ($C_{outside}$) and some background capacitance ($C_{background}$). The latter was evaluated by measuring the capacitance of the system without the ball connected and it was found to be of the order of femtofarads (fF), which can be neglected due to a very small effect on the total measured capacitance, which is of the order of tens to hundreds of picofarads (pF).

The first step in the current approach, which is schematically shown in Figure 7.16, is a rough estimation of lubricant film thickness; with either an optical measurement, as in the initial part of the study, or by theoretical calculation, as for the tests with steel discs. This is necessary for correct calculation of capacitance of the area surrounding EHD contact ($C_{outside}$), which depends on separation between the surfaces (film thickness), size of the area included in the calculation (corresponding to ball radius), and also the composition of a medium between the surfaces (lubricant or oil/air mixture).

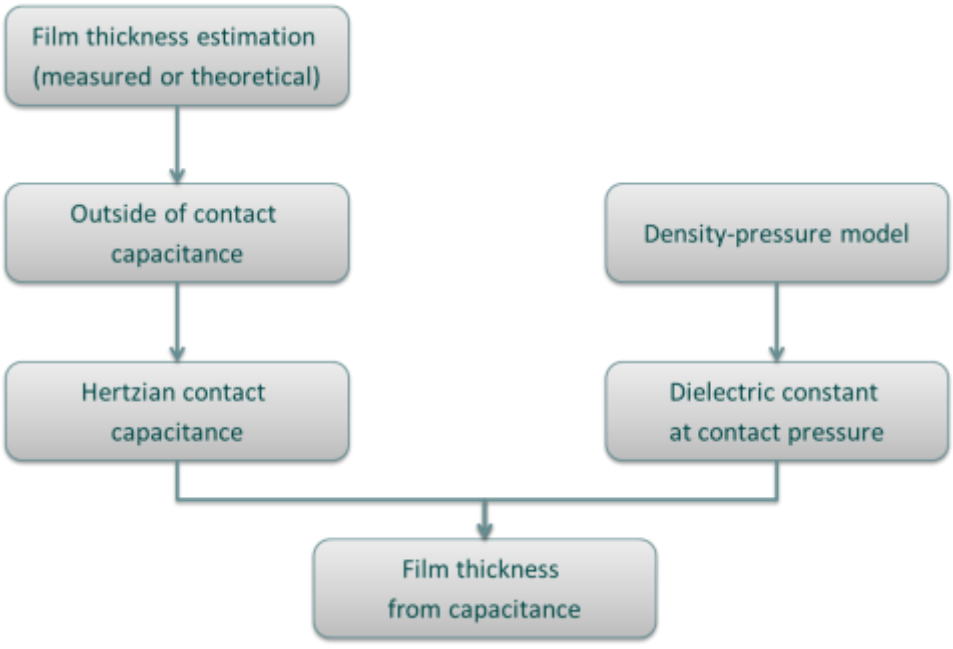

Figure 7.16: Film thickness evaluation procedure

In order to calculate the outside of contact capacitance, the area surrounding the Hertzian contact is divided into two regions: flooded and cavitated region, as seen in Figure 7.17, with corresponding capacitances: $C_{flooded}$ and C_{cav}, respectively.

Capacitance of the flooded region is calculated with formula:

$$C_{flooded} = \int \frac{\varepsilon_0 \varepsilon_{oil}}{h_c + h_{gap}(x,y)} dxdy \tag{36}$$

Where ε_{air} is 1, h_c is the central film thickness and h_{gap} is the gap between the solid bodies, given by the Hertzian deformation for dry contacts.

In the cavitated region it is assumed that the lubricant film splits in two and adheres to the solid surfaces, which is included in the following formula:

$$C_{cav} = \int \frac{\varepsilon_0}{\frac{h_c}{\varepsilon_{oil}} + \frac{h_{gap}(x,y)}{\varepsilon_0}} dxdy \tag{37}$$

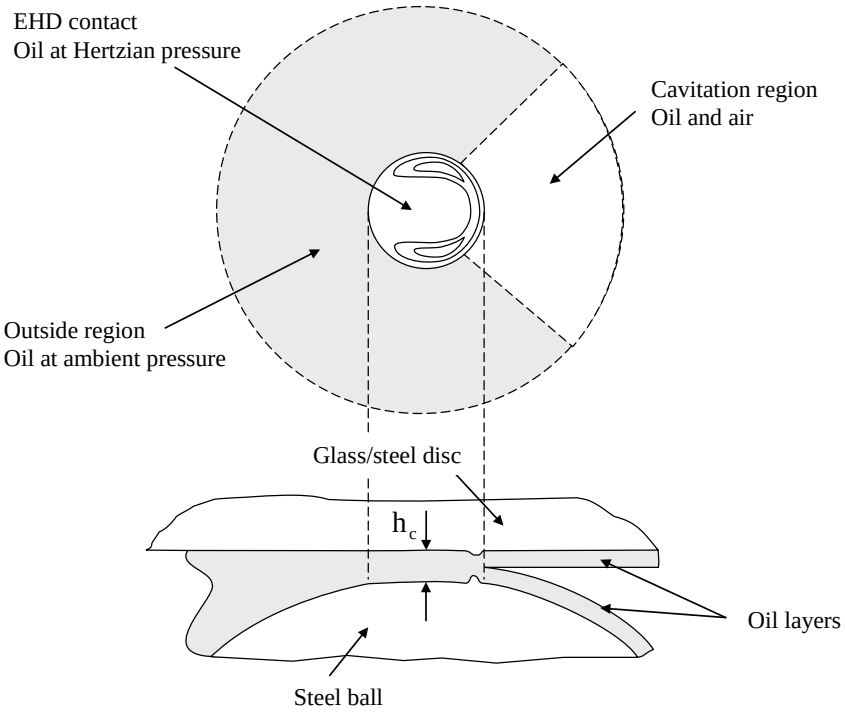

Figure 7.17: Schematic indicating the Hertzian contact area, the outside of contact region, and the assumed distribution of oil around the contact

The extent of the area of the cavitated region, A_{cav}, was estimated from images of the contact, such as those shown in Figure 7.10, and was found to be slightly speed-dependent. For simplification it was assumed that 75 percent of the total area surrounding the contact is fully-flooded with lubricant.

Since the cavitated and flooded regions are two capacitors in parallel, their capacitance is simply added giving:

$$C_{outside} = C_{flooded} + C_{cav} \quad (38)$$

The size of the area to be taken into account to calculate $C_{outside}$ is the area corresponding to the projection of the ball onto the disc.

Correct evaluation of the capacitance outside the contact is crucial for the accuracy of film thickness calculations using the capacitance technique.

When $C_{outside}$ is determined and subtracted from C_{total}, the remaining capacitance is then equal to the capacitance of the Hertzian contact $C_{contact}$. This can be used to calculate the film thickness assuming the parallel-plate geometry approximation (Eq. 30) and considering the dielectric constant at Hertzian pressure.

Figure 7.18 shows the pressure and the dielectric constant variation with pressure along the rolling direction, for 20 N load. The pressure distribution was obtained from film thickness maps using an inverse elastic approach and subsequently, the dielectric constant variation with pressure over the EHD contact has been calculated. Within most of the central region of the contact the dielectric constant varies only between about 2.30 to 2.36. This justifies the use of the maximum pressure for the calculation of the correction of the dielectric constant with pressure.

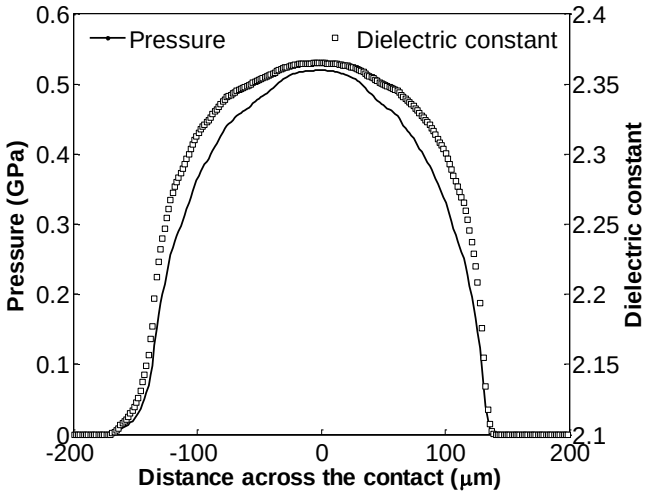

Figure 7.18: Distribution of pressure and dielectric constant in EHD contact across rolling direction

7.3 Test rig for capacitance measurements in rolling element bearings

Capacitance measurements on a rolling element bearing were carried out at SKF Engineering and Research Centre in Nieuwegein in the Netherlands. The bearing under study was a 6306 ETN9 Deep-Grove Ball Bearing (DGBB) with a 30 mm inner diameter and 72 mm outer diameter. Six out of seven steel balls were replaced with ceramic balls (silicon nitride, Si_3N_4), and therefore only the contacts between the remaining steel ball and the raceways were measured. This is the first time such approach has been reported in the literature and despite being a simplification; it allows a validation of the method and determination of uncertainties and possible error sources.

The schematic of experimental setup is shown in Figure 7.19. Capacitance measurements were performed using a Lubcheck instrument developed at SKF. This device was used in previous studies by Heemskerk et al. (1982), Leenders and Houpert (1987), as well as by Wikström and Jacobson (1997). All these references are described in more detail in section 4.1. Lubcheck is a commercially available device allowing monitoring of the lubrication condition. In this study, however, instead of using average capacitance value calculated by the instrument, real-time data was displayed

and recorded with an oscilloscope. In this way it was possible to observe capacitance variations as the steel ball follows the full rotation of the inner ring, with clear differentiation between unloaded and loaded zone.

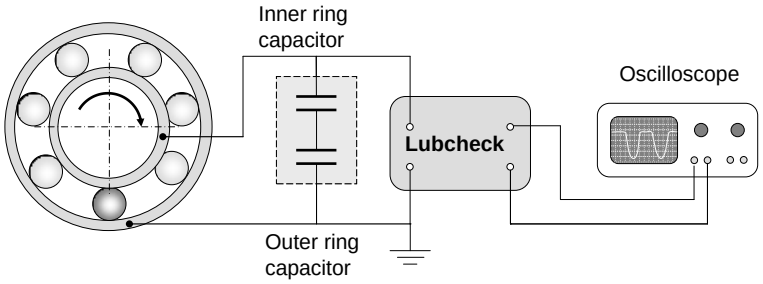

Figure 7.19: Bearing tests experimental test rig

An example of data displayed on the oscilloscope is shown in Figure 7.20. The presence of an inductive sensor allows detecting the moment when the steel ball is in the maximum load position.

For each speed setting five measurements were taken, each consisting of three or four rotation cycles, depending on the speed. The Lubcheck voltage is inversely proportional to capacitance, meaning that low voltage corresponds to high capacitance and hence a thin lubricant film or a large surface area. The Lubcheck signal on the left side of Figure 7.20 corresponds to the position where the steel ball is around the centre of the unloaded zone (top position in Figure 7.19). The ball then moves clockwise through the unloaded zone (flat region) and when it enters the loaded region, the voltage decreases (capacitance increases) as the load on the steel ball increases up to the maximum value at the point in the centre of the loaded zone (bottom position in Figure 7.19). For this position minimum voltage reading (maximum capacitance) is recorded. From this point forward the load on the steel ball is gradually decreasing causing increased voltage (decreasing capacitance) up to the point when the steel ball leaves the loaded zone and the voltage signal remains almost constant. In Figure 7.20 almost five full cycles are seen.

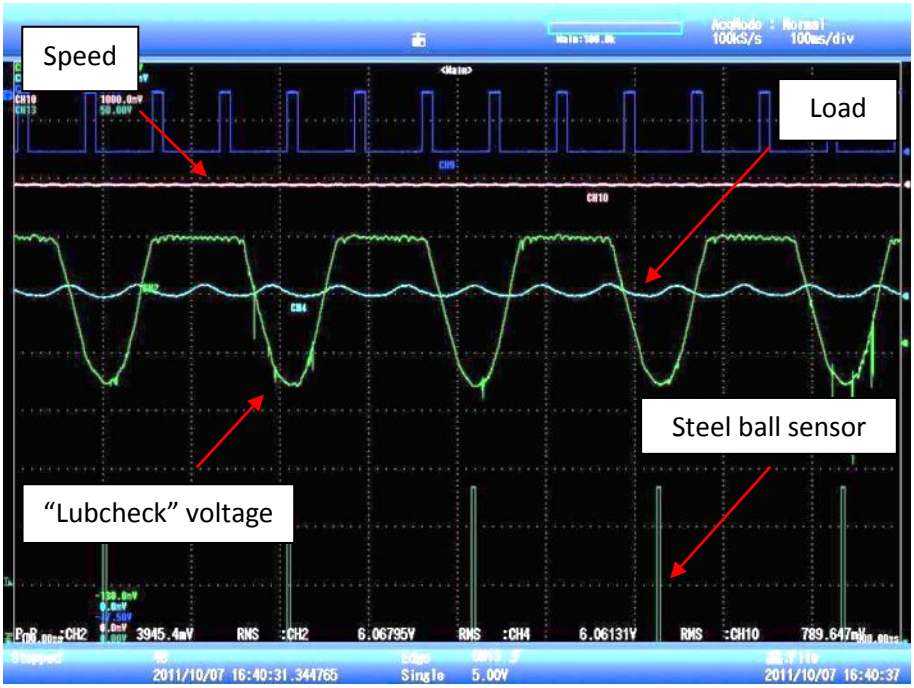

Figure 7.20: Example of data displayed by oscilloscope

7.3.1 Film thickness evaluation procedure

Theoretical central film thickness for the steel disc experiments in ball-on-flat setup, as well as for the ball bearing case was calculated using the Hamrock-Dowson isothermal formula for an elliptical contact (Eq. 10). Additionally, the film thickness decrease due to the inlet shear heating was included by applying a correction factor according to Gupta (1992).

Film thickness calculations for the ball bearing are based on the same principles as for the ball-on-flat setup; however there are few points that must be highlighted here.

From an electrical point of view the capacitance of the bearing consists of the capacitance between the steel ball and the raceways, the capacitance between inner and outer ring, and some background capacitance. The last two were evaluated using a bearing with all ceramic balls and an open circuit, and the obtained values were subtracted from all the measured data.

The capacitance between the steel ball and the raceways consists of the capacitance of the inner ring and the outer ring contacts, which are in series and therefore:

$$\frac{1}{C_{steel\ ball}} = \frac{1}{C_{inner}} + \frac{1}{C_{outer}} \tag{39}$$

Each of those contains the Hertzian contact capacitance and the capacitance of the region outside the contact, which are in parallel. For inner ring capacitance:

$$C_{inner} = C_{inner}^{contact} + C_{inner}^{outside} \tag{40}$$

Contact capacitance can then be expressed with parallel-plate formula:

$$C_{inner}^{contact} = \varepsilon_0 \varepsilon_r^{p_i} \frac{A_{inner}}{h_{inner}} \tag{41}$$

To solve Eq. 39 one of the unknowns, either outer ring film thickness or inner ring film thickness has to be eliminated. For this purpose a ratio of theoretical film thickness of inner and outer ring is used:

$$h_{outer} = h' h_{inner} \tag{42}$$

With this Eq. 39 can be written as:

$$\frac{1}{C_{steel\ ball}} = \frac{1}{\varepsilon_0 \varepsilon_r^{p_i} \frac{A_{inner}}{h_{inner}} + C_{inner}^{outside}} + \frac{1}{\varepsilon_0 \varepsilon_r^{p_o} \frac{A_{outer}}{h' h_{inner}} + C_{outer}^{outside}} \tag{43}$$

In order to calculate lubricant film thickness several assumptions, similar to those proposed by Wilson (1979) and Leenders and Houpert (1987), have been made:

- film thickness was calculated for the maximum load position,
- the ratio between inner and outer ring Hertzian contact area and film thickness was taken from Hertz's theory and Hamrock-Dowson formula,
- capacitance of the region outside the contact on the inlet side was calculated up to the point where separation between the surfaces reaches nine times the central film thickness and fully flooded condition was assumed (Wedeven, 1971). The capacitance on the sides of the contact was calculated assuming that oil fills the entire gap up to the shoulder of the rings. Finally the area at the exit of the contact was assumed to consist of a mixture of oil and air.

Static distribution of load for the modified bearing was carried out numerically following the analysis of Hamrock and Anderson (1983). However in the present case the difference in elastic modulus of steel and silicon nitride had to be taken into account. Details of this analysis are shown in the Appendix.

It is also important to note that the bearing's clearance strongly influences the load distribution in the bearing. The bearing under study has a C3 clearance which is in the range between 13 and 28 μm (radial clearance). For the calculations the middle clearance value was used.

Chapter 8: Results and discussion

8.1 Method development and validation

In the initial part of the study it was crucial to ensure that electrical capacitance can be measured in the current configuration in a repeatable manner and that the values measured reflect the changes in operating conditions of speed and load. For that purpose a synthetic, nonpolar polyalphaolefin base oil was chosen.

Since the main focus of the current project was on the thin-film conditions, in the majority of the experiments a low-viscosity PAO4 lubricant was used. In order to extend the range of film thickness studied, its blend with a high-viscosity PAO40, in mass proportion 1:3, was also examined. Properties of both can be found in Table 5.

At first, it was necessary to validate the repeatability of capacitance measurements. Figure 8.1 shows three repetitions of the PAO4 test, and additionally a test with PAO4 and PAO40 mixture. All experiments were performed at a temperature of 25^{o}C and 20N load, in pure rolling conditions, with a chromium-coated glass disc. The tests shown here were completed with approximately one-month intervals, and a fresh batch of oil was used every time.

As the PAO4 and the PAO4/40 mixture have a different viscosity, in order to verify if the capacitance measured (C_{total}) is indeed dependent only on the separation between the ball and the disc, the values of C_{total} are plotted here as a function of film thickness, rather than entrainment speed. From the analysis of Figure 8.1 it is clear that both, PAO4 and PAO4/40 mixture follow exactly the same trend, proving that there are no distortions related to speed. The results also show a very good repeatability of the capacitance measurements of PAO4 oil.

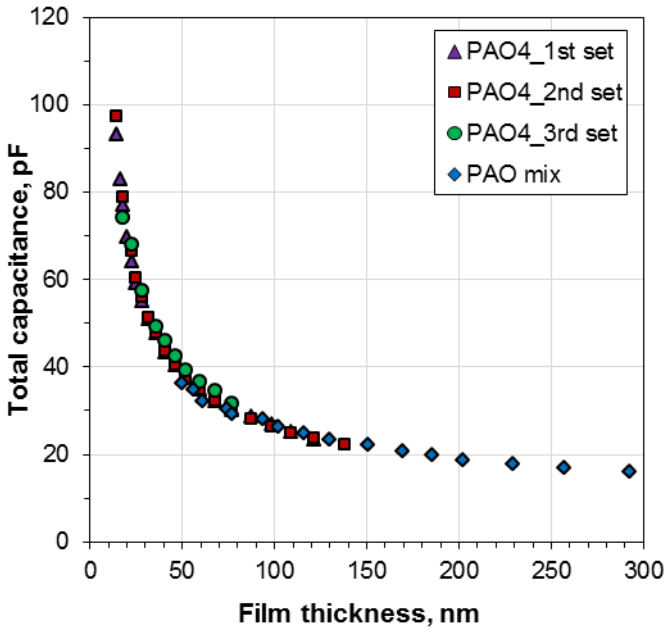

Figure 8.1: PAO capacitance measurements (Cr-coated glass disc, 20N, 25°C)

Figure 8.2 allows a detailed analysis of the components that contribute to the total capacitance (C_{total}), which can be determined according to the methodology described in subchapter 7.2.3.

It can be seen that as the film thickness increases, the contribution of the contact capacitance in the total capacitance decreases, and at a certain point (depending on the contact area) the contact capacitance will eventually fall below the value of C_{out}. Additionally, a slight variation of C_{out} with film thickness can be noticed, changing from around 16 pF for film thickness of 14 nm, down to around 10 pF at thicker films of around 230 nm. This difference may seem small, however, as the film thickness increases and as a consequence, the capacitance goes down, it becomes significant. It is therefore necessary to always estimate outside of contact capacitance separately for all conditions of speed and load.

In order to quantify the contribution of contact capacitance in the total capacitance it is useful to look at the $C_{total}/C_{contact}$ ratio. The idea of showing these two quantities as a ratio originated from the "correction factor" used by Franke and Poll (1997) to extract the Hertzian contact capacitance from the total measured capacitance in their work on

axially loaded rolling bearings. While a constant value describing this ratio can certainly work for that bearing geometry, it would lead to significant errors in a ball on flat arrangement.

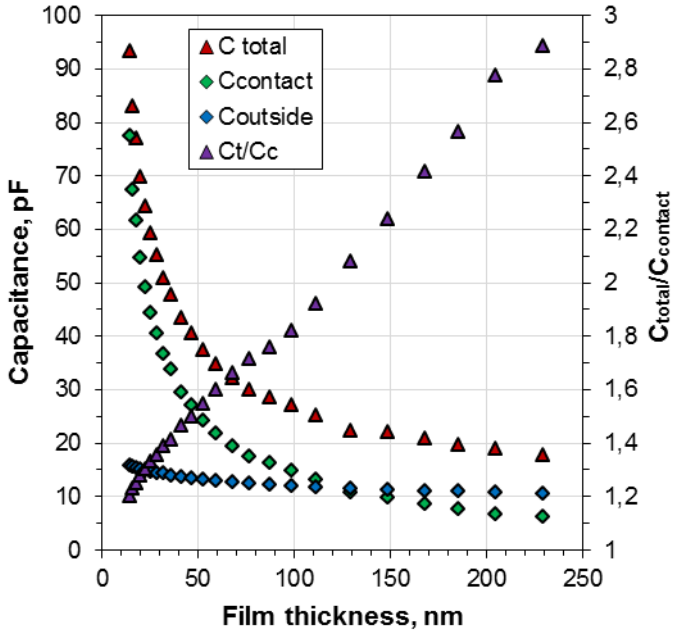

Figure 8.2: Contribution of contact and outside capacitance in total capacitance (Cr-coated glass disc, PAO4, 25°C, 20N)

When one looks at the dependence of capacitance on film thickness, it becomes clear that the rate, at which the capacitance changes with film thickness, decreases significantly. The graph in Figure 8.3 shows the resolution of the method defined as a change of capacitance for a certain film thickness change $(C_2-C_1)/(h_2-h_1)$.

Based on this it can be concluded that the method should preferably be used in the region of thin films, where its resolution is high. It should be noted, however, that the limiting film thickness value, determining the useful measurement range of the method, will also depend on the contact area and the dielectric constant of the lubricant.

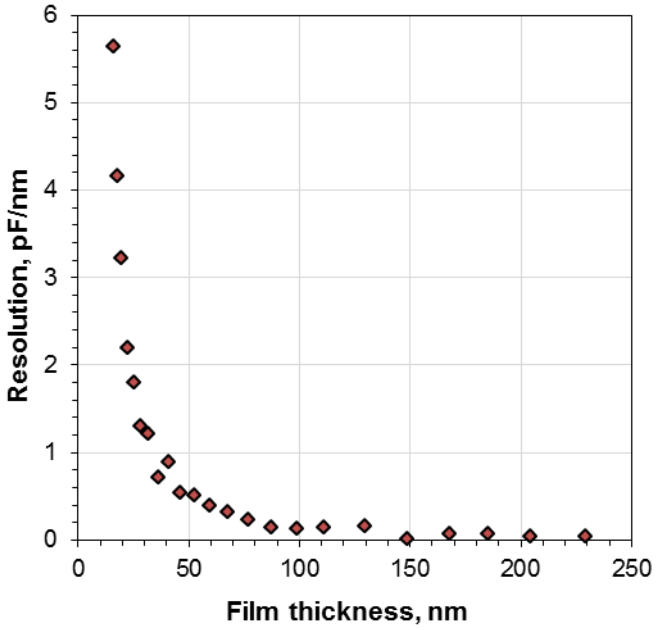

Figure 8.3: Resolution of capacitance measurement (Cr-coated glass disc, PAO4, 25^{o}C, 20N)

Using the capacitance measurements with the chromium-coated glass disc for PAO4 base oil, and following the procedure described in subchapter 7.2.3, film thickness extracted from the measured capacitance is depicted in Figure 8.4.

For comparison, the plot also shows the film thickness calculated based on the Hamrock and Dowson elliptical contact formula (Eq. 10), and the film thickness measured with an optical interferometry method described in subchapter 7.2.1.

It can be seen that all three data series follow the same trend and the agreement is generally very good. It is believed that a slightly different slope of the capacitance film thickness, relative to optical measurements, is a consequence of a number of simplifying assumptions included in the film thickness evaluation procedure.

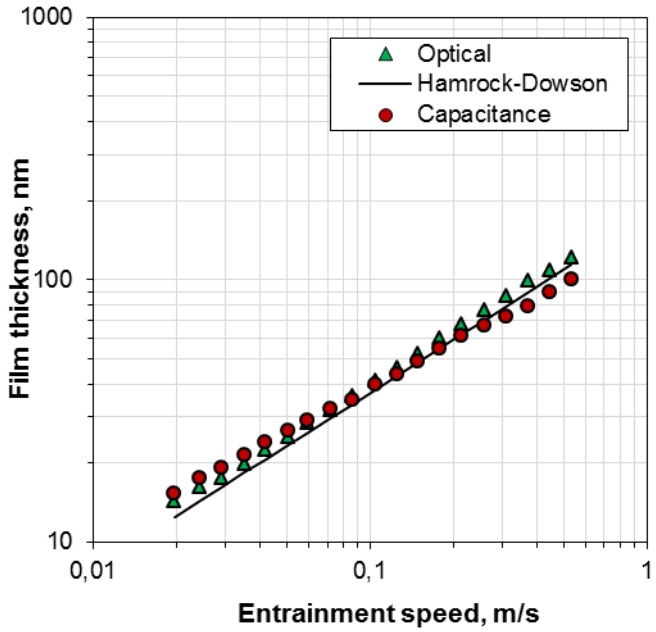

Figure 8.4: Film thickness extracted from capacitance, together with values from optical interferometry and theory (Cr-coated glass disc, PAO4, 25°C, 20N)

The aim of the experiments with the chromium-coated glass disc was to verify if accurate measurements of film thickness can be obtained from the measured capacitance. As a result of the ability of using an optical method to measure film thickness simultaneously with capacitance of the EHD contact it was possible to establish a step by step procedure which results in lubricant film thickness extracted from the measured capacitance.

The overall aim of the study was, however, the development of an approach that would enable studying lubrication condition where the optical methods cannot be used, i.e. in steel-on-steel contacts. For this purpose the glass disc was subsequently replaced with a steel disc and the same procedure for film thickness calculation was applied.

Figure 8.5 shows the results of this experiment for PAO4 tested with the steel disc, at 40N load and 25°C. The load was chosen for these experiments to give a similar contact area and film thickness as in the chromium-coated glass tests at 20N load.

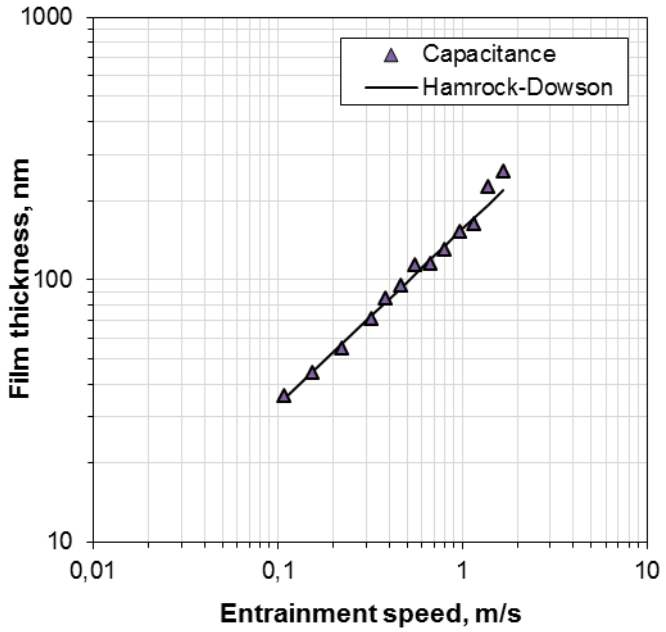

Figure 8.5: Film thickness from capacitance compare with theoretical values (steel disc, 40N, 25°C)

The results are very promising as the agreement with the theoretical predictions is excellent and shows a high potential of the method. Comparison with Figure 8.4 reveals that the lowest film thickness measured with the steel disc was around 35 nm, while with chromium-coated glass disc films as thin as around 15 nm could be measured. It should be noted that the steel disc in this case had a slightly higher surface roughness.

Figure 8.6 shows the film thickness extracted from the measured capacitance (markers) and compared with theory (dashed line), measured over a range of loads (10–40 N) at three speeds: 0.155 m/s, 0.224 m/s and 0.386 m/s. Error bars indicating ±10% from the Hamrock-Dowson film thickness are added for guidance. It can be seen that all the measurement points are within this range, and also that at the highest speed and the lowest load, corresponding to a thicker film and smaller contact area, the difference between the measurement and theory is the highest. Nevertheless the agreement is fully satisfying.

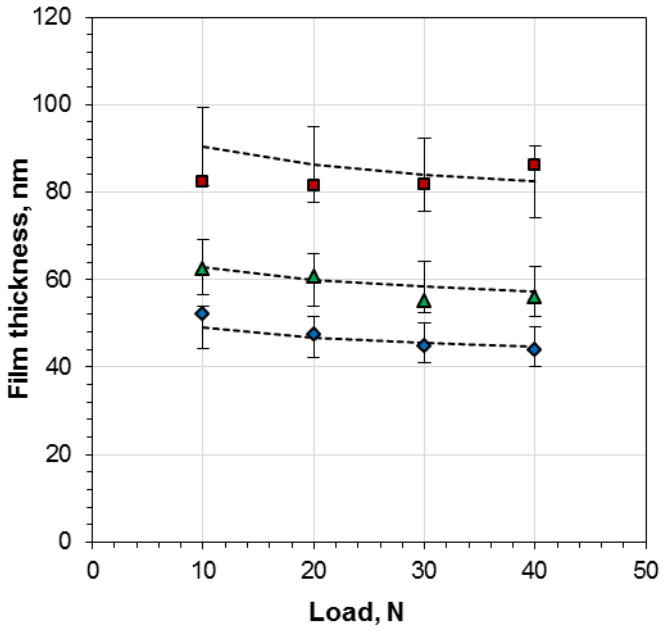

Figure 8.6: Film thickness as a function of load. Error bars indicate ±10% from the Hamrock Dowson film thickness shown as a dashed line

8.2 The effect of polarity of the lubricant upon capacitance measurements

All lubricants contain polar species in various amounts (e.g. additives), or are polar themselves, hence it is essential for the current study to investigate how lubricants' polarity affects their behaviour in elastohydrodynamic conjunctions. There does not appear to be a better method for that purpose than the electrical capacitance. In order to simplify the situation, base oils, rather than more complex mixtures, such as fully formulated oils, were chosen for the first part of this research.

8.2.1 Base oils

Due to a higher ambient temperature it was not possible to sustain a stable test temperature of 25^{o}C, as used in the previous subchapter, therefore in this part of the

investigation the experiments were performed at the temperature of 30^{o}C. Some additional tests with glycerol were completed at 60^{o}C in order to study further the observed behaviour.

In the previous subchapter (8.1), covering the validation of the method, PAO4 base oil was used as a model fluid. It appeared to be a perfect candidate, since due to its nonpolar nature, any interaction of either polar or ionic species, which may affect the measured capacitance, is eliminated. For that reason it was also used in this part of the study, as a reference nonpolar fluid.

In order to cover a wide range of base oils polarity, two more fluids were chosen: glycerol, with a very high dielectric constant (41.9, as shown in Table 5), and polyethylene glycol (PEG) (17.3, as seen in Table 5). Even though the dielectric constant of PEG is much higher than found in commercial lubricants, it serves as a fluid with intermediate properties between the nonpolar PAO and strongly polar glycerol.

As the first step of this work, before examining the polar fluids, it was necessary to establish the behaviour of the reference oil, nonpolar PAO4. Since the experiments temperature was set to 30^{o}C (and 60^{o}C) these results cannot be directly compared with the data from the previous subchapter.

Depicted in Figure 8.7 is the total capacitance measured for the PAO4 base oil with the chromium coated glass disc at 20 and 40N load. The error bars indicating the standard deviation (SD) of 50 measurements for each point of speed are also included. It can be seen that both series follow a similar straight-line trend (in logarithmic scale) over the entire range of speeds tested. From the error bars it can be concluded that the measurements are very stable, even at low speeds where the film thickness is the lowest.

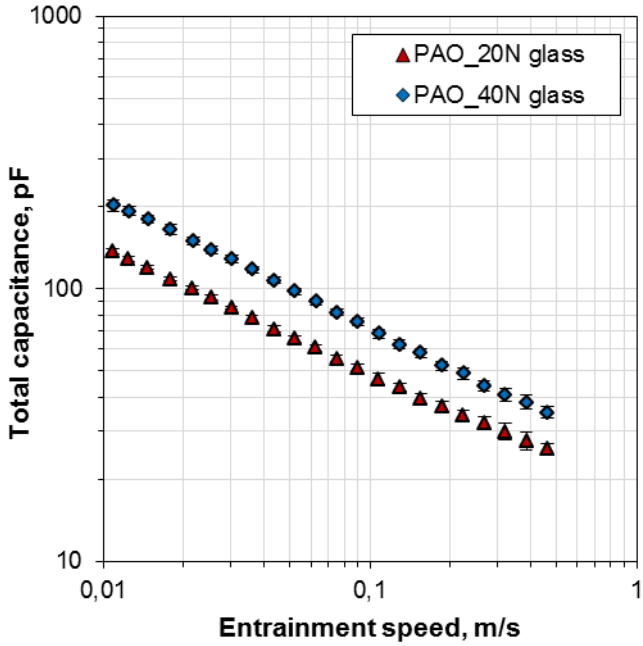

Figure 8.7: Measured capacitance as a function of entrainment speed for a glass disc (PAO4, 30°C, 20 and 40N)

A similar graph for polyethylene glycol, showing the total capacitance measured with the same disc as a function of entrainment speed, is seen in Figure 8.8. In this case however, the behaviour is different, as the straight-line (in a logarithmic scale) power law trend is not followed over the whole range of speeds. It can be observed that for both loads examined, as the speed is decreased, at a certain point the curves fall below the power-law trend and capacitance values lower than expected are registered. This behaviour is not a result of a high scatter of the measurement points, since the error bars shown in the graph (again based on SD of 50 measurements points for each speed) indicate stable readings. It can be clearly seen that the error bars are lower than the deviation from the general trend.

It was initially thought that such a deviation from the trend could be explained by the existence of a thicker than expected elastohydrodynamic film, hence the interferometric images of the contact were analysed.

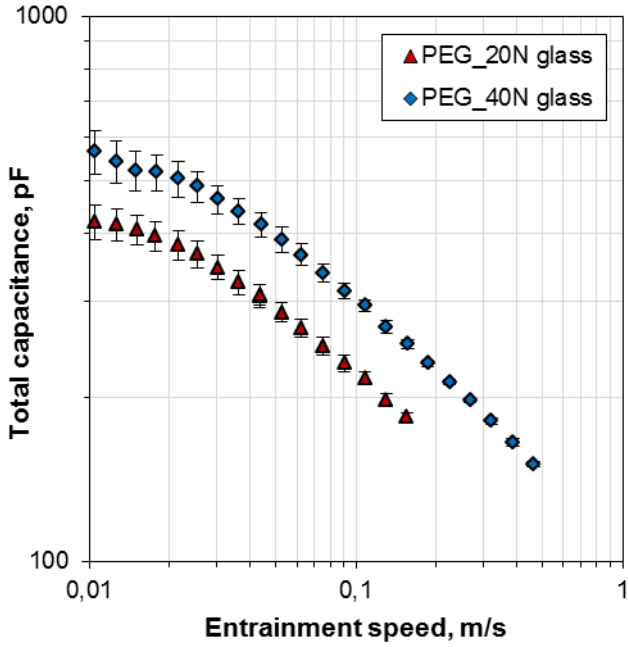

Figure 8.8: Measured capacitance for polyethylene glycol tested with chromium-coated glass disc at 20 and 40N

Figure 8.9 shows a series of images from the 40N test, covering the low speed region. It can be seen that, according to the principles of the method described in subchapter 7.2.1, as the speed decreases, the intensity of the central region of the contact increases (transition towards lighter shades of grey), which indicates a decreasing film thickness.

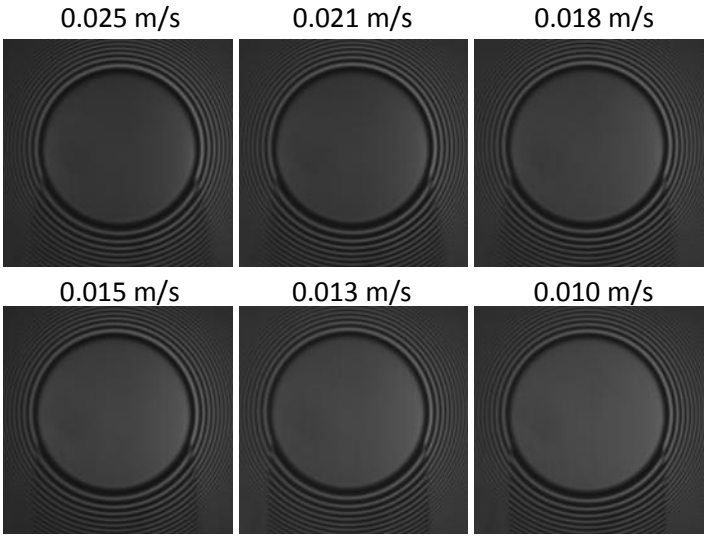

Figure 8.9: Interferometric images from polyethylene glycol test at 40N load

It can be therefore concluded that film thickness in the range of speeds where the unexpected capacitance variation was observed, follows the speed dependence known from the EHD theory.

The experiment was then performed for the third, and the most polar fluid - glycerol, at the same operating conditions, and the results are displayed in Figure 8.10. The results show that both, 20N and 40N series follow power-law in the entire range of speeds tested, however, if compared with PAO4 data shown in Figure 8.7, it can be noticed that glycerol's data show in general a lower gradient.

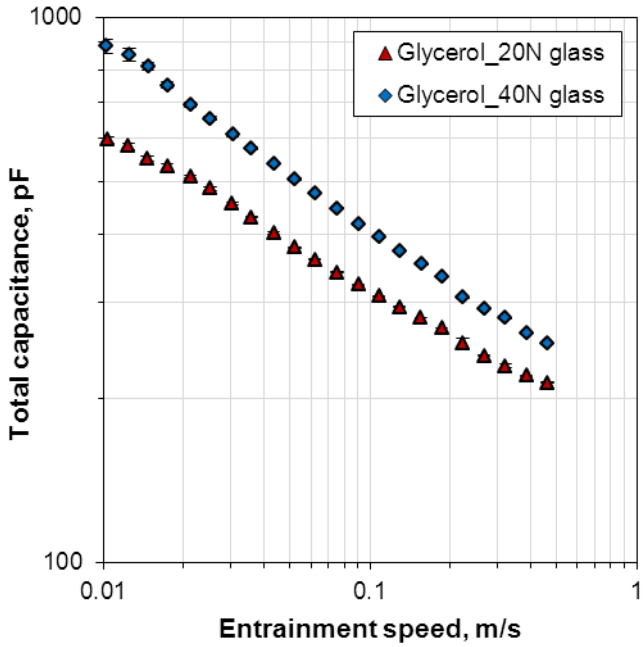

Figure 8.10: Measured capacitance for glycerol at 30°C with glass disc (20 and 40N)

It should be noted that these points would correspond to a different film thickness range as the fluids have a significantly different viscosity. Nevertheless, a clear deviation from the trend, as seen for polyethylene glycol, is not observed here.

It was interesting to see what film thickness values would be extracted from these capacitance measurements. In order to compare the results for all three fluids, the film

thickness was evaluated following the same approach as used in the previous subchapter for PAO4.

Figure 8.11 shows a film thickness comparison between the capacitance and optical interferometry methods for the tests performed at 20N load. The solid lines represent optical measurements, while capacitance data are displayed as markers. Since the results are displayed as function of entrainment speed, significant differences between fluids' viscosity leading to a different film thickness range for all three, are obvious.

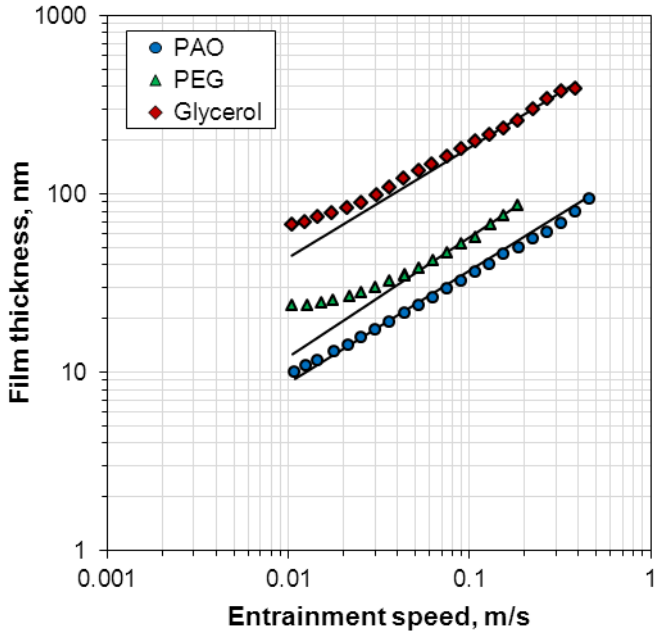

Figure 8.11: Film thickness extracted from capacitance compared with optical film thickness (glass disc, 20N, 30°C)

The nonpolar fluid, PAO4, shows a very good agreement between the optical and capacitance values (as previously shown for experiments in subchapter 8.1); however, for the other two lubricants a deviation at lower speeds can be clearly observed.

In the case of polyethylene glycol it is somehow not surprising after the analysis of Figure 8.8, where the measured capacitance was lower than expected. For glycerol, on the other hand, data presented in Figure 8.10, show only a different gradient than PAO4, and only now it can be realized how strongly it affects film thickness evaluation.

The difference between the capacitance and optical values seen for PEG at the lowest speed appears higher than for glycerol, but if same film thickness is compared, for example 45 nm (the lowest optical film thickness for glycerol) it is clear that in this range PEG already follows the power law relationship.

It was therefore essential to see what happens with glycerol at even thinner films. In order to investigate this matter, additional experiments at higher temperature (60^{o}C) were conducted. To examine whether the observed behaviour is related to the voltage level used for measurements, apart from typically used 100 mV signal, additional tests at 10 mV were included.

Figure 8.12 shows the capacitance measured at 60^{o}C with glycerol tested using the same disc material and under the same load conditions. This time, instead of following the power-law trend, and further increasing as the speed decreases, the measured capacitance first starts deviating from it, similarly as for polyethylene glycol, and from a certain point it even gradually decreases.

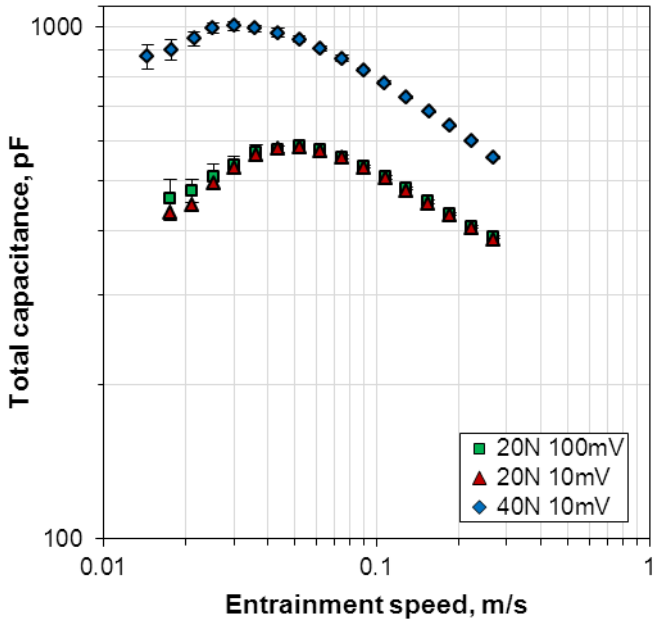

Figure 8.12: Total capacitance of glycerol measured with Cr-coated glass disc at 20 and 40N at 60^{o}C

Here as well the error bars, defining the standard deviation, confirm that the measurements were stable down to the lowest speed, which means that no current leakage through the film or occasional breakthrough occurred. It should also be noted that the same trend was observed at both loads, and that the behaviour was not influenced by the voltage applied, as the two measurements, apart from the few lowest speeds, are practically identical.

In order to confirm that no actual changes of film thickness, affecting the measured capacitance took place, interferometric images showing film thickness variation with speed were analysed. A series of images covering the low speed region, where the capacitance drop was observed, is shown in Figure 8.13. Similarly as for polyethylene glycol, the variation of intensity with the rolling speed proves that the film thickness follows the theoretical predictions.

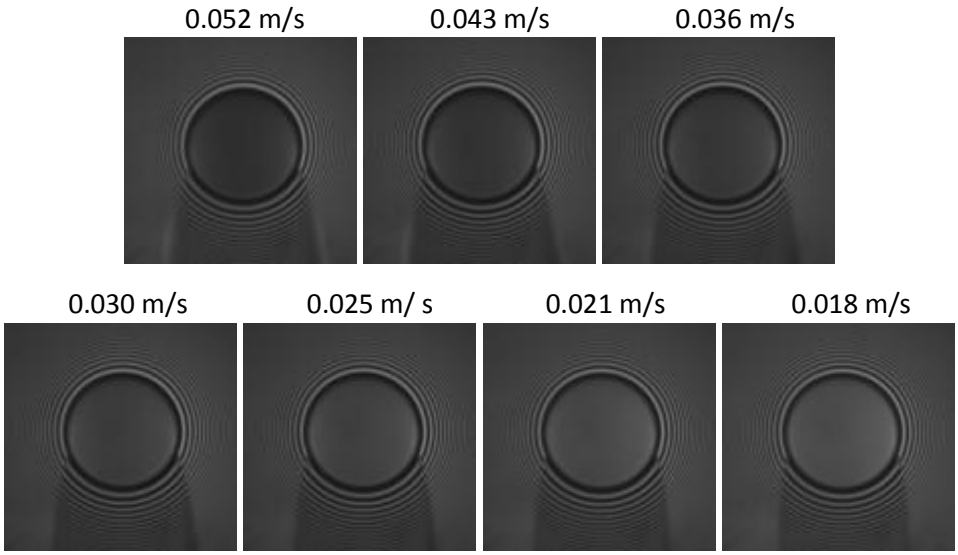

Figure 8.13: Interferometric images of EHD contact lubricated with glycerol at 60^{o}C and 20N load

In order to better illustrate the differences between the fluids, the contact capacitances (after excluding the outside of contact capacitance) are shown in Figure 8.14 as a function of film thickness.

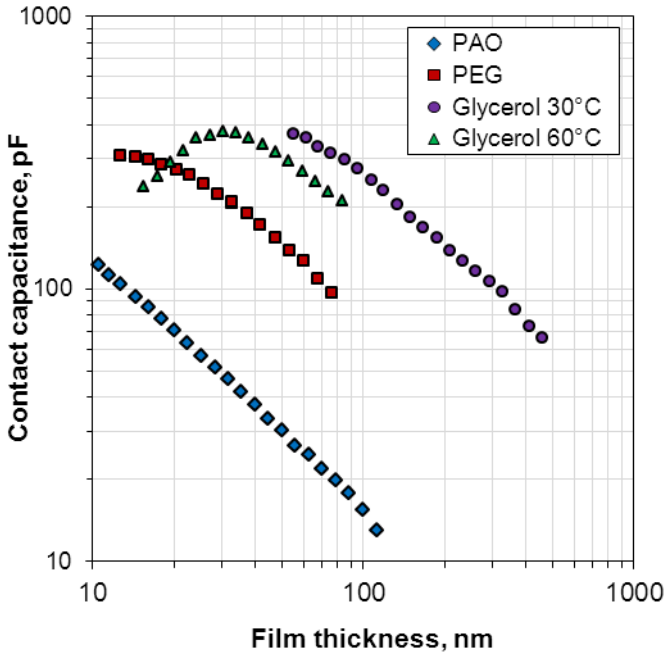

Figure 8.14: Contact capacitance as a function of film thickness for PAO, PEG and glycerol with Cr-coated glass disc at 20N

The difference between polyethylene glycol and glycerol can now be appreciated. The deviation from the power-law trend begins at much thicker films for glycerol. It is suggested that this may be related to a much higher dielectric constant of glycerol (42 in comparison to 17).

To summarise the findings presented and show a direct comparison of both polar fluids, a correlation between optical and capacitance film thickness is displayed in Figure 8.15. Error bars limiting ±10% from the point where the optical and capacitance values are equal, are shown for guidance. From the data presented here it is clear that in case of glycerol, the more polar fluid, the deviation is much stronger than for PEG.

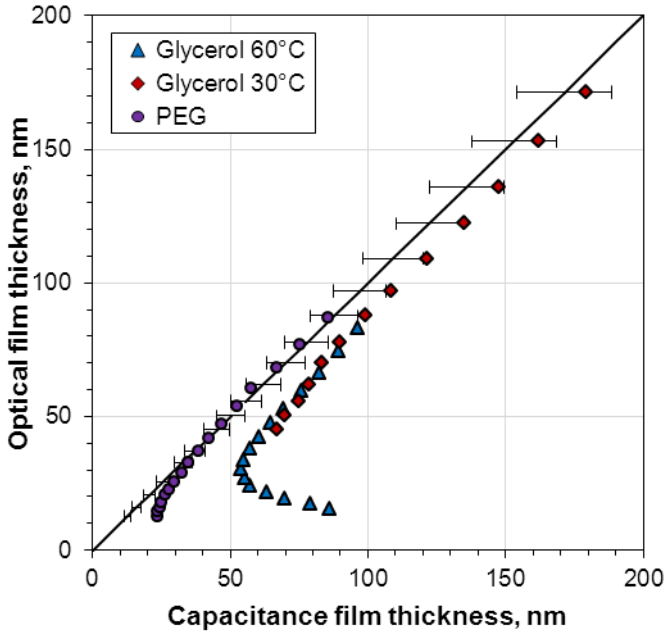

Figure 8.15: Correlation between film thicknesses extracted from measured capacitance with optically measured

Analysis of the parallel-plate capacitor formula (Eq. 30) indicates that only three quantities can influence the measured capacitance of an EHD contact. These are: film thickness, contact area and dielectric constant. To explain the trend observed with both polar fluids one of the following would have taken place:

- formation of a thick boundary film on the surfaces, causing an increased film thickness at low speeds, and thus a decrease of capacitance – discarded based on optical film thickness measurements,
- a decrease of the contact area – excluded as the load was kept constant during the tests and also the interferometric images confirm that the contact area did not change during the experiments,
- variation of the dielectric constant with film thickness – investigated further for glycerol, which showed more pronounced deviation.

Based on the contact area and film thickness, an “effective” dielectric constant can be back-calculated from the measured capacitance. The result is shown as a normalized value of the “effective” dielectric constant as a function of film thickness in Figure 8.16.

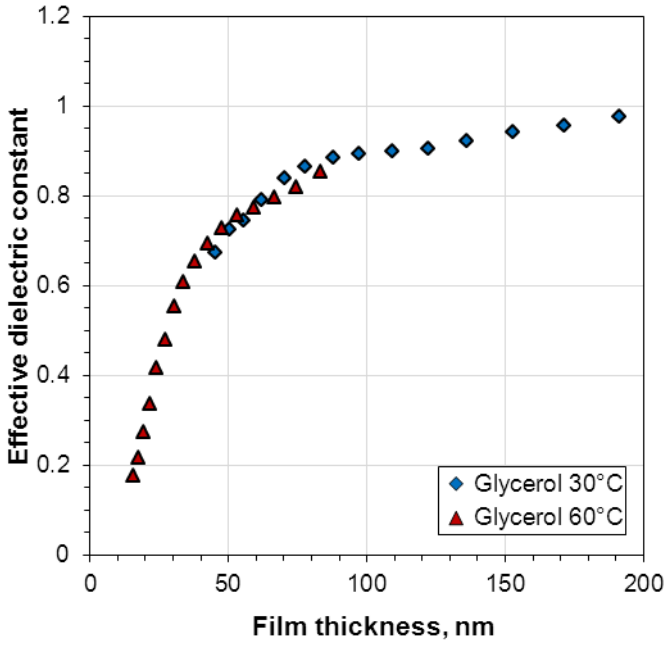

Figure 8.16: Relative effective dielectric constant calculated from contact capacitance for glycerol (Cr-coated glass disc, 20N)

It can be seen that up to around 150 nm thickness, the calculated value is much lower than the bulk dielectric constant. In the thin film region it falls to as low as 20% of the bulk value. Additionally, both series from measurements at different temperatures (30^{o}C and 60^{o}C) follow precisely the same trend. This suggests that the effect of speed and viscosity (temperature) can be excluded, and the observed behaviour is purely film thickness dependent.

As explained in subchapter 6.3.1, dielectric constants of polar liquids decrease if the dipolar polarization, contributing strongly to the dielectric constant of polar liquids, is supressed. This would happen when either the frequency of the electric field orientation change is too high and the molecules do not have sufficient time to rotate, or when the mobility of the molecules is restricted and they are not able to freely rotate and align according to the direction of electric field.

Exceeding the limiting frequency for dipolar polarization can be excluded as the behaviour would not be film thickness dependent, but rather much lower values of

capacitance, due to a lower bulk dielectric constant, would be measured over the entire speed range.

The second possibility, of somehow impeded mobility of the molecules was therefore further analysed. This can happen when the viscosity or density significantly increases, as during a temporary solidification of the fluid inside the EHD contact. To verify this hypothesis a phase diagram, based on data from Herbst et al. (1993) and Ohno and Yamada (2007), was prepared.

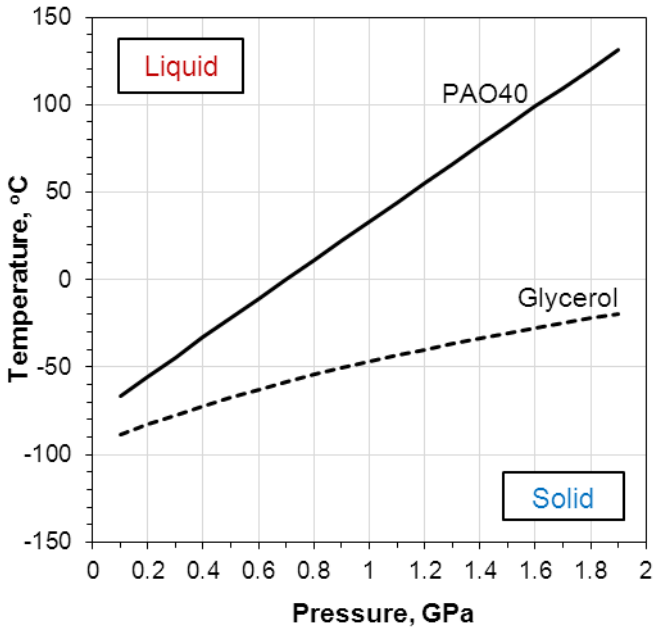

Figure 8.17: Phase diagram for PAO40 and glycerol over the range of temperature and pressure

The comparison of data for glycerol and PAO40 is displayed in Figure 8.17. According to this, solidification of glycerol at test temperature (30 or 60^{o}C) and Hertzian contact pressure (0.5 – 0.6 GPa), is not possible and therefore cannot explain the gradual decrease of the effective dielectric constant in thin films. In fact it can be concluded that PAO40 oil is more likely to solidify under the conditions experienced within an EHD contact.

Additionally, if solidification of polar fluids was indeed taking place, the effect would be similar to using a too high frequency, as effectively in this case the dipolar component would also be supressed.

Since the change of capacitance observed in the experiments is gradual, and any change of the bulk dielectric constant would simply result in lower capacitance measured over the full speed range, the possibility of the existence of a thin layer with a reduced mobility, and therefore lower dielectric constant, was considered. In this case as the film thickness is decreased, the layer would contribute more to the dielectric constant of the whole film, possibly even causing a drop as seen in Figure 8.16.

To test this hypothesis, simplified calculations were carried out to provide a comparison with the experimental results. At first, theoretical capacitance of a layer with uniform dielectric constant between the ball and the disc, based on a known separation (measured film thickness), was calculated. This case is referred to as the "one-layer model" and serves as a reference. Additionally, a "three-layer model" was used, which assumes the presence of a reduced mobility, and thus lower dielectric constant, layer close to or attached to each of the contacting surfaces. Two variants were considered here, one where the thickness of that layer is equal to 1 nm, and the second with 3 nm thickness.

Capacitance for the "three-layer model" was calculated according to the following equation:

$$C = \frac{\varepsilon_0 A}{\frac{h_l}{\varepsilon_l} + \frac{h_c - 2h_l}{\varepsilon_b}} \tag{44}$$

Where h_l is the thickness of the reduced mobility layer, and ε_l is its dielectric constant. constant. The two models are schematically shown in Figure 8.18.

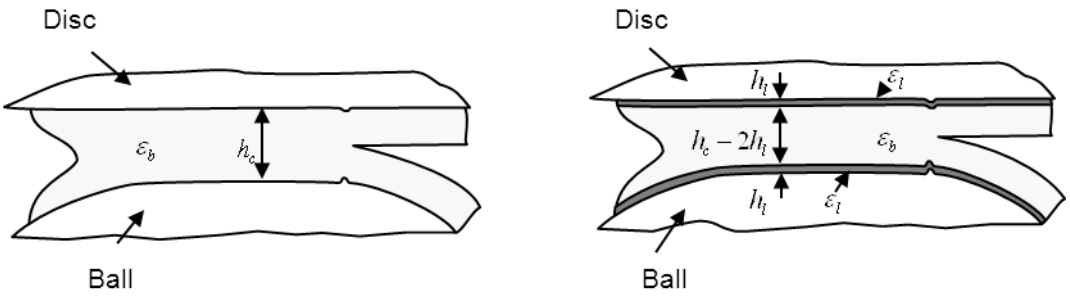

Figure 8.18: Contact model with one and three dielectric layers

The dielectric constant of the reduced mobility layer was chosen as 10, in order to fit the experimental data with the 3 nm layer thickness series at higher speeds.

The results in Figure 8.19 clearly show that the capacitance calculated based on optically measured film thickness and bulk dielectric constant (one layer model) differs significantly from the measured capacitance. The experimental results are much lower than theoretical, and they approach the predicted trend only at relatively thick films, above 80 nm.

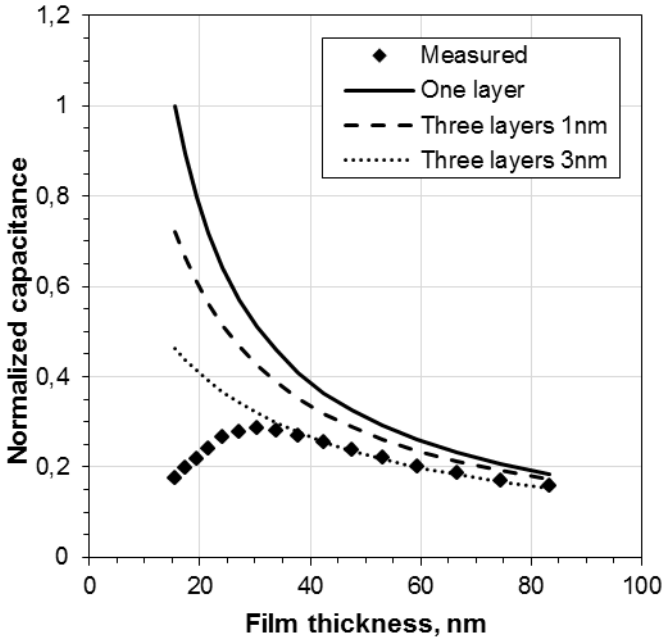

Figure 8.19: Normalized capacitance calculated considering three-layer mode compared with one-layer model and measurement

Now, if the three-layer model is considered, the capacitance is strongly affected, with the rate of change of capacitance with film thickness being much lower than theoretical, which in a logarithmic scale would be seen as a smaller gradient. Additionally, the effect is much stronger if the low dielectric constant layer is thicker (3 nm). It can also be seen that the 3 nm thick reduced dielectric constant layer model correlates well with the measured values down to around 35 nm film thickness.

Such a fit above a certain film thickness value could also be obtained for the layer with 1 nm thickness, if the value of the dielectric constant of that layer was taken as 4. This means that the three-layer model points can be shifted to match the experimental results at higher film thickness range, if the right combination of layer's thickness and its dielectric constant is chosen.

Nevertheless, none of them would predict a decrease of theoretical capacitance in thin film region (below around 35 nm).
This does not eliminate the possibility of the existence of such layer. On the contrary, it suggests that the change in the dielectric constant might not be as rapid, and the boundary between the reduced mobility and the bulk film is not well defined. It follows that the change would have to be gradual, increasing towards the bulk value with distance, which cannot be reflected in this simple model.

It is known (e.g. Israelachvili (2011)) that hydrogen-bonding molecules (such as water or glycerol) at an interface with a charged or polar surface will be forced to align in a certain direction. This in turn will affect their interaction with the neighbouring molecules and therefore their ability to form the hydrogen bonds, which highly contribute to the polarizability and as a result also to the dielectric constant.

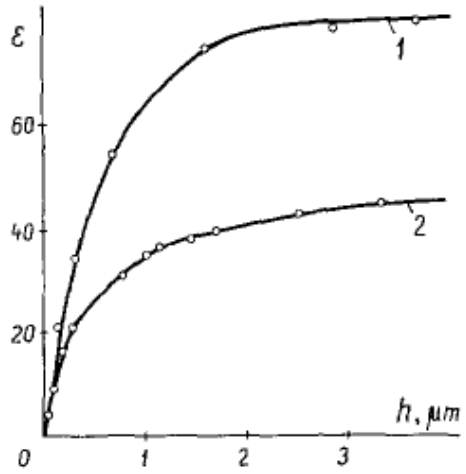

Figure 8.20: Variation of dielectric constant of water with distance between two mica platelets (Series 1 – $2x10^4$ Hz and 8°C; Series 2 – 10^{10} Hz and 20°C) (Metzik et al., 1973)

This is well documented for water e.g. Metzik et al. (1973) and Teschke et al. (2001), where the dielectric constant measured between two mica surfaces at separations up to few micrometres was dependent on the distance, as shown in Figure 8.20. The resemblance to the effective dielectric constant calculated for glycerol, shown in Figure 8.16, is striking.

The same dependence of dielectric constant on thickness was also found for thin-film solid capacitors e.g. Natori et al. (1998) and Stengel and Spaldin (2006). Figure 8.21 shows the effective dielectric constant calculated based on a simulation of Lorentz' local field theory for a high dielectric constant material, such as (Ba,Sr)TiO_3. Here again an unquestioned similarity is seen.

The authors concluded that the defects of the material can be excluded from the possible explanations. Instead, they show that the layers of a low dielectric constant are formed adjacent to the electrodes and they dominate the total capacitance as the thickness decreases.

This hypothesis is also confirmed by Stengel and Spaldin (2006), who show that at an interface between the dielectric and the electrode there is a drop in permittivity. They

argue that ‘‘this sub-polarized region is an ‘intrinsic dead layer’, which stems purely from fundamental quantum-mechanical and electrostatic properties of the metal insulator interface’’. They estimate that, for a 75 nm thick dielectric layer, the capacitance is about 85% (of the value corresponding to bulk dielectric constant), which is remarkable as only one or two atomic monolayers are responsible for this drop.

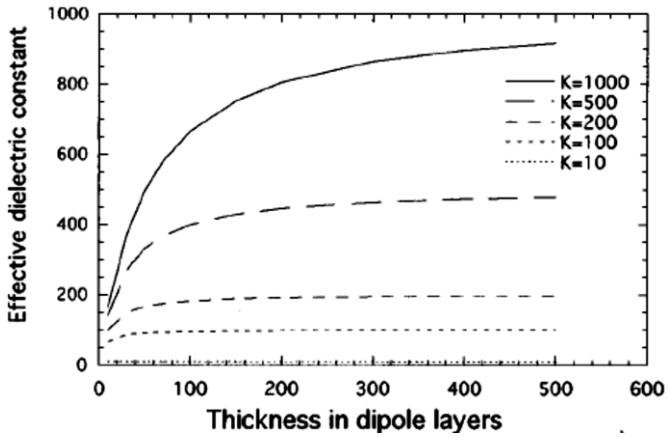

Figure 8.21: Effective dielectric constant calculated for a high dielectric constant material (Natori et al., 1998)

A more detailed analysis is beyond the scope of this work, however it is hypothesized that a similar ‘‘dead-layer’’ may be responsible for the observed reduction of the measured capacitance in the present experiments. The fact that the crude three-layer model shows that the presence of thin layers with reduced dielectric constant makes the capacitance depart from the one-layer prediction, supports this explanation. The continuous drop of the measured capacitance below the theoretical line, for film thickness below 30–40 nm, does not discount this hypothesis; on the contrary, it shows that in thinner dielectric films this effect is even stronger. The main conclusion is that dielectric properties of the lubricant layer seem to be dependent on the surface separation, without affecting its film-forming properties. The latter remark is evidenced by the fact that the film thickness values from optical evaluation follow well-established theoretical models.

The results presented in this subchapter, especially the film thickness values depicted in Figure 8.11, show the importance of this effect for an accurate film thickness evaluation, based on the measured capacitance. If polar fluids are used in EHD experiments and such behaviour occurs without being recognized and appreciated, it would lead to a significant overestimation of the actual film thickness. It is therefore recommended to always perform a full sweep of speeds if a new polar fluid is used, in order to detect any abnormal behaviour which may be misleading during the data analysis and interpretation.

8.2.2 PAO and ester mixture

Based on the results obtained with the polar fluids it was interesting to see if capacitance measurements can also provide additional information about the behaviour of binary mixtures of base oils of different polarity. Such mixtures, consisting of either esters or polyalkylene glycols mixed with PAOs or mineral oils, are commonly used in engine oils formulations, as well as in gear and compressor lubricants.

Guangteng and Spikes (1996) studied ester/PAO blends and showed that the film thickness in thin-film region (below 10 nm) is determined by the viscosity of a more polar component. They attributed this to a stronger interaction of an ester with the surface, and described it with the term “fractionation”. In an accompanying paper the authors also showed the implications of this phenomenon on friction control by possibility of shifting the lubrication regime towards either mixed or boundary lubrication (Guangteng and Spikes, 1997).

In this part of the study it was attempted to replicate a similar behaviour and verify if it can be deduced from the capacitance measurement of an EHD contact.

Even though from the point of view of capacitance, the biggest difference in polarity between the two base oils is beneficial; it should be noted that the choice of fluids for a blend is limited by their miscibility.

Hence for the experiments presented in the current chapter an ester and a polyalphaolefin base oil were chosen. The ester is the base oil used in SRL grease formulation. From the information provided by Kyodo Yushi it is known that it contains a mixture of a diester and polyolester, however, the details of the chemistry have not been revealed.

Two blends of the SRL ester with PAO base oil were prepared. At first, a blend consisting of SRL and PAO4 oils, in equal mass proportions, was made. Since the two components have a different viscosity (subchapter 7.1), another blend, where polyalphaolefin component (mixture of PAO4 and PAO40) has the same viscosity as the SRL ester, was also prepared. In order to examine the influence of the disc material, both, the Cr-coated glass and steel disc were used.

Figure 8.22 shows the capacitance measured during the tests with a glass disc for PAO4, SRL and the SRL:PAO4 blend. A similar graph from the steel-on-steel experiments is displayed in Figure 8.23. All three fluids have a different viscosity; therefore their capacitance cannot be directly compared when analysed as a function of entrainment speed. It can be however clearly seen, that despite the highest viscosity, and thus the thickest film formed at a certain speed, SRL ester always shows the highest capacitance.

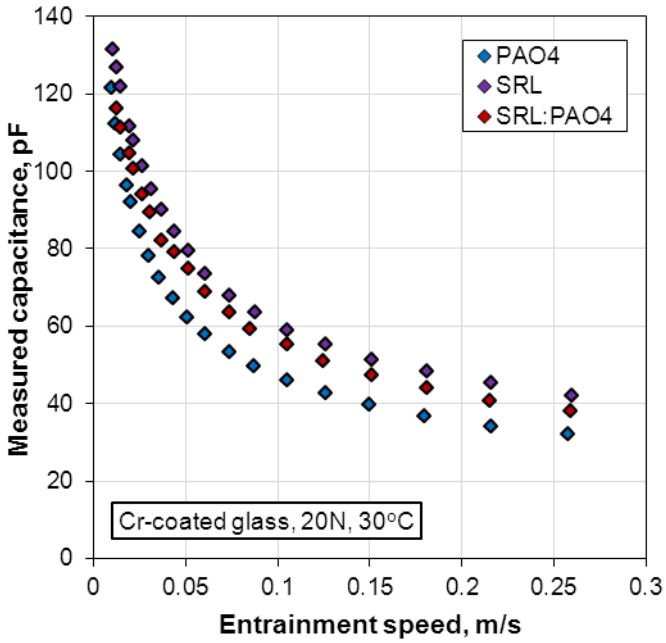

Figure 8.22: Measured capacitance for PAO4, SRL ester and SRL:PAO4 mixture (Cr coated glass disc, 20N, 30°C)

In order to take into account the effect of viscosity, the capacitance data can be displayed as a function of the product of entrainment speed and dynamic viscosity (u·η, [m·Pa]). Based on the literature data (Höglund, 1999), it can be assumed that pressure-viscosity coefficients are very similar for all fluids, and since the experiments have been performed at the same normal load, this parameter will essentially reflect the lubricant film thickness. If the capacitance results are then compared at a certain value, the difference between the series originates only from the different dielectric constant (as outside of contact capacitance contribution is assumed to be the same).

The results displayed in Figure 8.24 and Figure 8.25 demonstrate a clear difference between the fluids. As expected, the capacitance results of PAO4 are the lowest, SRL ester's capacitance is the highest, while the SRL:PAO4 blend falls in between the two base oils. Additionally, a deviation from the straight-line trend (in a logarithmic scale) is seen for SRL ester and also for the SRL:PAO4 blend.

In the Cr-coated glass disc experiments (Figure 8.24), at higher speeds (u·η above 10^{-3} [m·Pa]) SRL:PAO4 blend is exactly parallel to the PAO4 series, however, when the speed is lowered, the trend changes and resembles more that shown by the SRL ester.

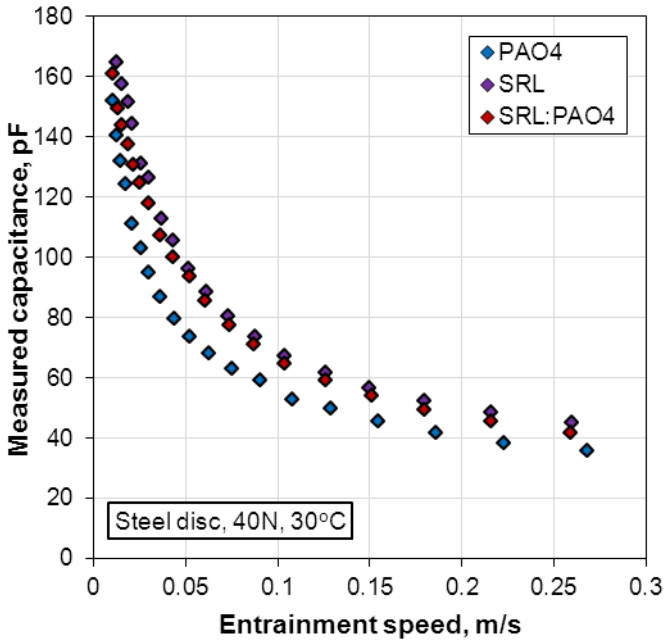

Figure 8.23: Measured capacitance for PAO4, SRL ester and SRL:PAO4 mixture (Steel disc, 40N, 30°C)

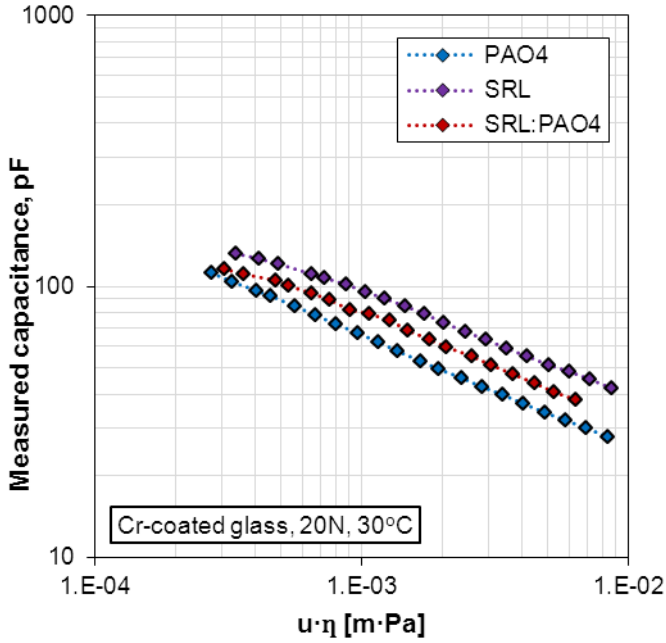

Figure 8.24: Measured capacitance as a function of product of speed and dynamic viscosity for Cr-coated glass disc tests

In the steel-on-steel experiments (Figure 8.25) the similarity between the ester and its blend with PAO4 is even stronger and extends practically over the whole range of the speeds tested.

This suggests that the ester present in the blend has a stronger effect on the blend's capacitance, especially as the film thickness decreases.

It can also be deduced that if the viscosity of a uniform mixture is considered, as in the Figures shown, the blend's results series will never reach the SRL line. If however, the fractionation was taking place and the film-forming viscosity was varying at thin films, when more ester was contributing to the lubricating film, the SRL:PAO4 blend series would approach that of the pure ester.

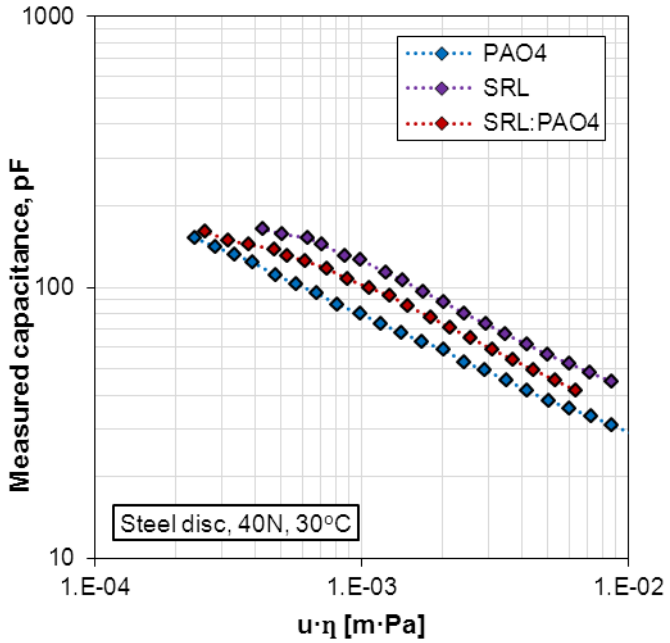

Figure 8.25: Measured capacitance as a function of product of speed and dynamic viscosity for steel disc tests

In order to determine whether or not fractionation of base fluids was indeed taking place in the current experiments, a blend consisting of equal parts of SRL and PAO mixture (of the same viscosity as the ester), was tested. The viscosity effect can therefore be excluded and the difference in composition of the lubricating film will only be reflected in capacitance.

Figure 8.26 shows the comparison between the capacitance measured in steel-on-steel tests with the SRL ester and the two blends.

The difference in capacitance between the SRL ester and SRL:PAO4:PAO40 mixture is only a result of a difference of dielectric constants. Hence the two series follow the same trend, with only a vertical shift.

The third series, SRL:PAO4, is placed between them. It is concluded that if the fractionation was indeed taking place, the SRL:PAO4:PAO40 data should approach the SRL trend as the speed is lowered, which has not been observed.

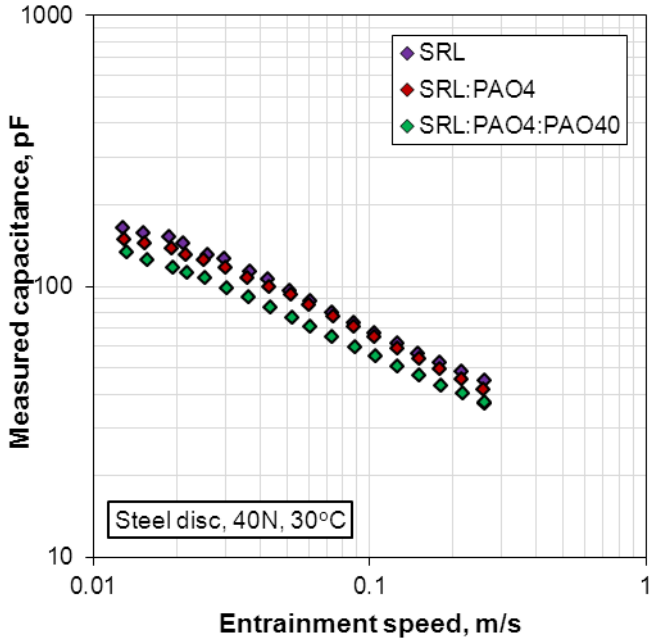

Figure 8.26: Measured capacitance as a function of speed for SRL ester and its blends with PAO

The analysis of the results including the viscosity influence, shown in Figure 8.27, confirm that SRL:PAO4 blend behaves like a uniform mixture of the two base fluids, without indication of any separation in the thin film region. This can be concluded based on the fact that it follows exactly the same trend as SRL:PAO4:PAO40 mix blend, for which fractionation due to a difference in viscosity would not be possible.

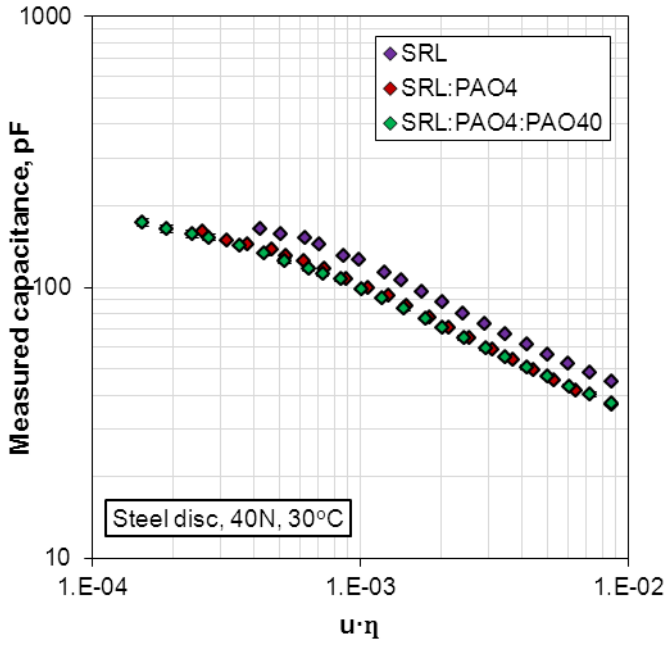

Figure 8.27: Measured capacitance as a function of product of speed and dynamic viscosity for SRL ester and its blends with PAO (error bars indicate STD of 50 measurements)

Nevertheless, a deviation from the straight-line trend (in logarithmic scale) is obvious for all tested fluids containing polar components. It is similar to that observed for polyethylene glycol and glycerol described in subchapter 8.2.1.

The film thickness range examined in these experiments covered films only down to around 10 – 15 nm. It is therefore possible, that if thinner films were measured, the effect of fractionation would be visible. The effect could also be more prominent if the components had significantly different viscosity.

The idea of lubricant fractionation was further explored by Bantchev and Biresaw (2008), who evaluated various mixtures of vegetable oils with polyalphaolefins and despite choosing components of significantly different viscosity, they were not be able to find any clear evidence of this phenomenon. In the following paper (Bantchev et al., 2012), however, they suggested that the behaviour might be time-dependent, and sufficient time should always be allowed for contact with the surface prior to film thickness measurements.

It is also possible that the choice of polar components' chemistry (e.g. type of ester) is very important here and simply not all of them would show this behaviour when blended with nonpolar fluids.

The results presented in this chapter, even though do not indicate the occurrence of fractionation directly, demonstrate the potential of the method for studying blends of base oils with different polarity. Blending mixtures with various proportions of the ingredients could provide additional information about the interaction of the polar species with the surfaces. Also the use of more polar, but still oil-soluble chemistries, such as polyalkylene glycols, would benefit from a better composition differentiation based on the measured capacitance.

8.2.3 Friction modifier solution

All of the experiments performed so far were concerning only pure base fluids; hence the current chapter is a step forward, aiming at a well-defined mixture of a single polar additive in a nonpolar base oil.

Some surface active components, such as carboxylic acids, esters, or aliphatic amines, are able to form a low-friction layer adsorbed on the surfaces and therefore show friction benefits in the boundary lubrication regime.
Friction reduction capability can be directly deduced from the friction measurements, and the presence of any boundary film can be confirmed by film thickness measurements with the optical interferometry.

The effect of the adsorbed layer on the film thickness is only evident for very thin films, below 10 nm, according to Ratoi et al. (2000); however the implication for capacitance is expected to be stronger due to a difference in dielectric constants of base oils and polar friction modifiers. It was interesting to see if the presence of such a layer can indeed be detected with the aid of capacitance measurements.

For this purpose a friction modifier, glycerol monooleate (GMO), widely used in the lubricants formulations, was chosen, and its solution in the PAO4 base oil, of 1 wt. % concentration, was examined.

The tests were performed at the temperature of 30^{o}C under pure rolling conditions. Two disc materials were used, a chromium-coated glass disc (at 20N load) and a steel disc (at 40N load). In all experiments performed, after the GMO mixture was poured into the lubricant reservoir, the disc and the ball were run unloaded for 30 min in order to allow the solution contact with the surfaces. The tests were always performed with the sweep of speeds starting from the highest value and decreasing towards the lowest.

In the first part of the experiments a Cr-coated glass disc was used. Lubricant film thickness was measured with the optical interferometry simultaneously with electrical capacitance. Over the range of speeds tested, no difference in film thickness was detected between PAO4 base oil and the GMO solution. The capacitance measured during both experiments is shown Figure 8.28.

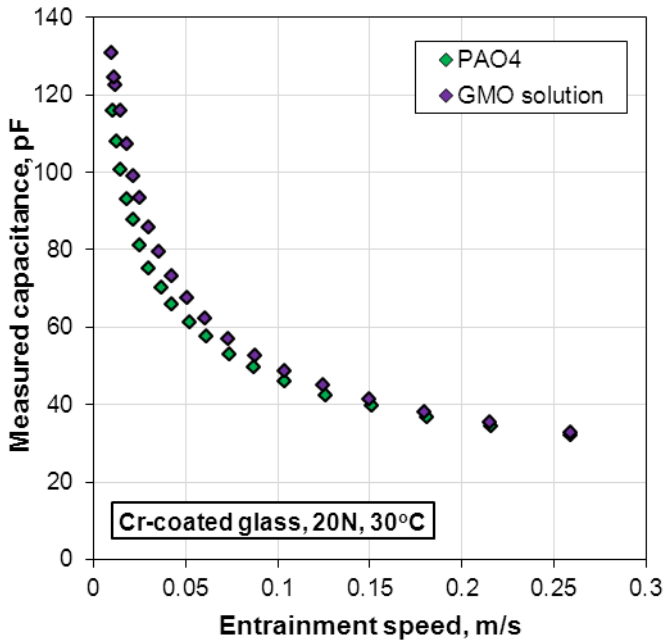

Figure 8.28: Capacitance of PAO4 and GMO solution measured with Cr-coated glass disc

A noticeable difference between the two can be observed, with the GMO solution showing higher capacitance values over the entire speed range. The difference becomes more significant as the speed, and film thickness, decreases. The presence of GMO, even if not seen as a boundary film formation in the optical measurements, clearly affects the dielectric constant of the lubricating film inside the EHD contact.

In order to verify if the type of the contacting surface (Cr-coated glass or steel) has any effect, additional experiments with the steel disc were carried out. Figure 8.29 shows the results for both fluids tested. This time the difference between them is even more pronounced.

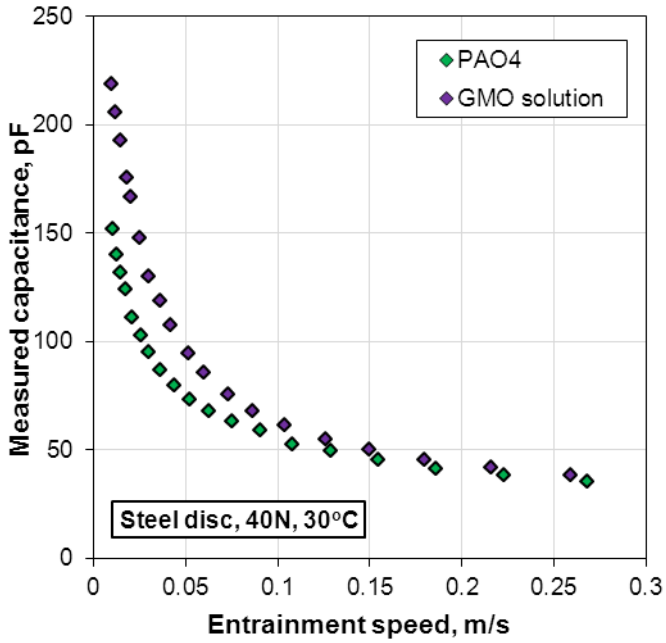

Figure 8.29: Capacitance of PAO4 and GMO solution measured in steel-on-steel test

When all the results are displayed in a logarithmic scale, as in Figure 8.30, and the variation of capacitance versus speed is compared, different gradients of the datasets can be noticed. Higher gradients of the GMO solution in comparison to PAO4 base oil, especially with the steel disc, are obvious. If the GMO mixture within the EHD contact had a uniform dielectric constant, equal to a bulk value, throughout the whole range of

speeds studied, the results would be exactly parallel to PAO4 data points, which is clearly not the case.

The behaviour observed here, a stronger than expected increase of capacitance with the film thickness decrease, is opposite to that reported earlier for the polar base oils and the blends.

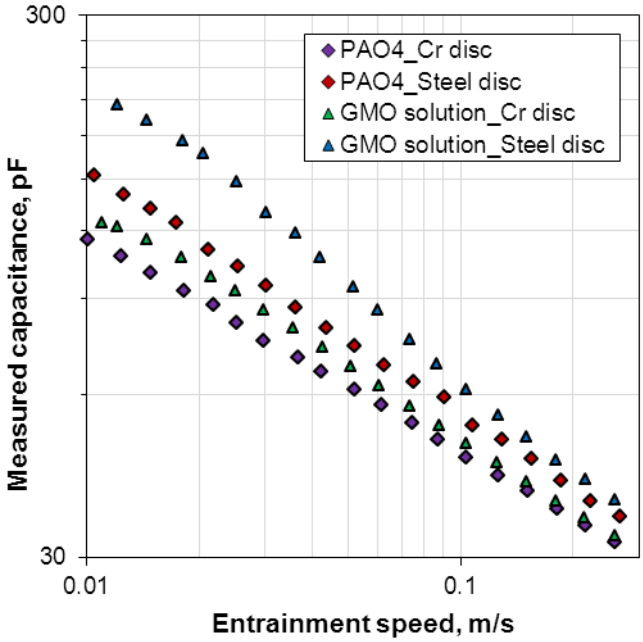

Figure 8.30: Comparison of measured capacitance for PAO and GMO solution

This means that as the speed, and film thickness decreases, the effective dielectric constant is higher than the bulk value, which implies an increased contribution of a more polar component, the friction modifier, in the EHD film. Not surprisingly, this effect appears even stronger when both contacting surfaces are made of steel.

In order to demonstrate the effect of the contacting surface type, the ratio of capacitance measured for GMO solution and PAO base oil, for both disc materials is displayed in Figure 8.31. This graph illustrates how much greater the capacitance of GMO solution is in comparison to PAO base oil.

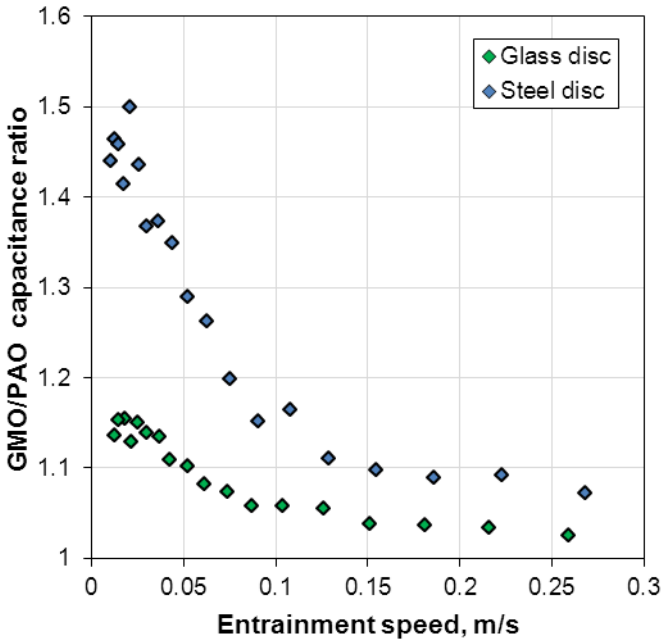

Figure 8.31: Ratio of GMO and PAO capacitance for glass and steel disc tests

The much larger difference between the capacitance values obtained in steel-on-steel experiments is striking. Based on these measurements it can be concluded that the friction modifier shows a much stronger interaction with the steel surfaces.

Similarly as in the case of polar fluids, the implication of this “artificially” changed, increased in this case, capacitance on the film thickness evaluation should be underlined.

Apart from that the results presented here also show a potential of capacitance measurements for studying interaction of polar additives with chromium-coated glass, and steel surfaces. The application would not be however limited to these two materials and other conductive metallic surfaces can be examined. Capacitance measurements can also be used to compare the effectiveness of various surface active components, such as other esters, amines and carboxylic acids.

The advantage over conventional interferometric film thickness measurements is the ability of detecting the presence of a film-forming additive at much higher film thickness than would be possible with the interferometric methods. It is also possible

to perform the tests at various slide/roll ratios to investigate ordering of the surface active species. Such measurements performed in parallel with friction evaluation can provide additional information that can help explain the observed behaviour.

8.3 Grease lubrication

Greases are widely used in the lubrication of rolling element bearings, therefore including experiments with this type of lubricant was of primary importance for the current study.

In this part of the experimental work two types of tests were performed:

- short-term measurements with a Cr-coated glass disc, where the interferometric images were captured simultaneously with capacitance measurements,
- long-term investigations with a steel disc, including introduction of ball movement which serves as an additional lubricant replenishment mechanism.

The unquestioned advantage of type (a) experiments is the ability to correlate capacitance response to changing conditions of the contact, including visual observation of the onset of starvation. Type (b) experiments, on the other hand, can be used for monitoring grease film variation over longer periods of time than it is feasible with the glass discs.

In order to avoid current leakage through the thin film in all experiments with the grease, capacitance was measured using a 10 mV voltage signal. Additionally, to accommodate observation of dynamic changes in capacitance of the EHD contact, the integration time was set to 0.1 s. All tests were performed at a room temperature, which was between 23 and 25^{o}C.

A commercial grease (SRL by Kyodo Yushi), with properties listed in subchapter 7.1, was used in this study. SRL grease is based on synthetic ester base oil with viscosity of 23 cSt at 40^{o}C, and contains the lithium stearate (LiSt) thickener.

At first it was essential to see if it is possible to measure a grease film in static conditions. An example of an interferometric image of a statically loaded contact with SRL grease film is shown in Figure 8.32.
It can be seen that in comparison to base oil, the thickness of the grease film within the contact area is not uniform; it generally appears to be around 150-200 nm with some areas showing lower or higher thickness.

For this investigation a generous amount of grease was first applied onto the ball. The presence of grease between the two surfaces is indicated by relatively high (8.2 pF) capacitance measured in unloaded conditions, as shown in Figure 8.33. The capacitance stayed on the same level until the loading started. It increased up to a value of around 100 pF when the load was gradually increased and 20N load was reached. The capacitance further increased by another few picofarads in the next seconds, suggesting that some of the grease might be pushed out from the contact.

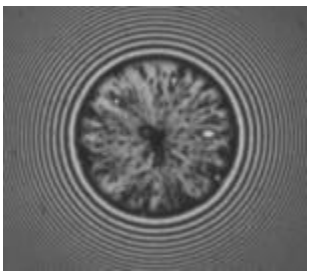

Figure 8.32: Interferometric image of statically loaded SRL grease (Cr-coated glass disc, 20N)

After that the capacitance showed only a very small change (around 2.5 pF) over the loaded period duration, suggesting no significant change in the structure or thickness of the film. A slightly lower capacitance after unloading (5.8 pF), in comparison to that of a freshly applied sample (8.2 pF), is most likely a result of a smaller amount of grease on top of the ball, as some of it has been pushed aside during the loading.

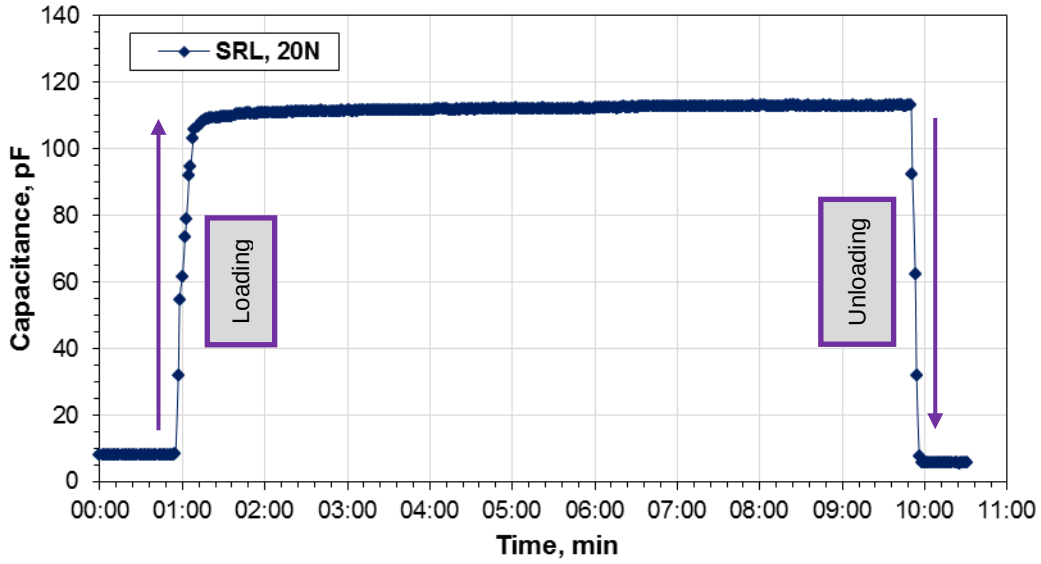

Figure 8.33: SRL grease static measurement at 20N load (Cr-coated glass disc)

Next, experiments under dynamic conditions were carried out, where the grease was applied onto the disc and run loaded at a fixed speed over a certain period of time. Optical images were taken simultaneously with capacitance measurements to help in interpreting capacitance behaviour during the development and the progress of starvation.

Figure 8.34 shows the capacitance recorded during the experiment run at 0.104 m/s rolling speed and 20N load. Here, capacitance variation can be correlated to optical images shown in Figure 8.35. It should be noted that due to a very dynamic nature of the grease film, the images chosen represent only a general behaviour.

The measurement begins in the unloaded condition with both, the ball and the disc rotating at 0.104 m/s. A few seconds after the start of the experiment, the load is applied and an increase of capacitance from around 8 pF to around 42 pF is registered. Over the first minute of the loaded run (0:30 min to 1:30 min) the capacitance oscillates around 42 pF and the images indicate a stable and uniform film. After that time (from 1:30 min) the capacitance drops and a slightly thicker film is seen in the interferometric images (2 min image).

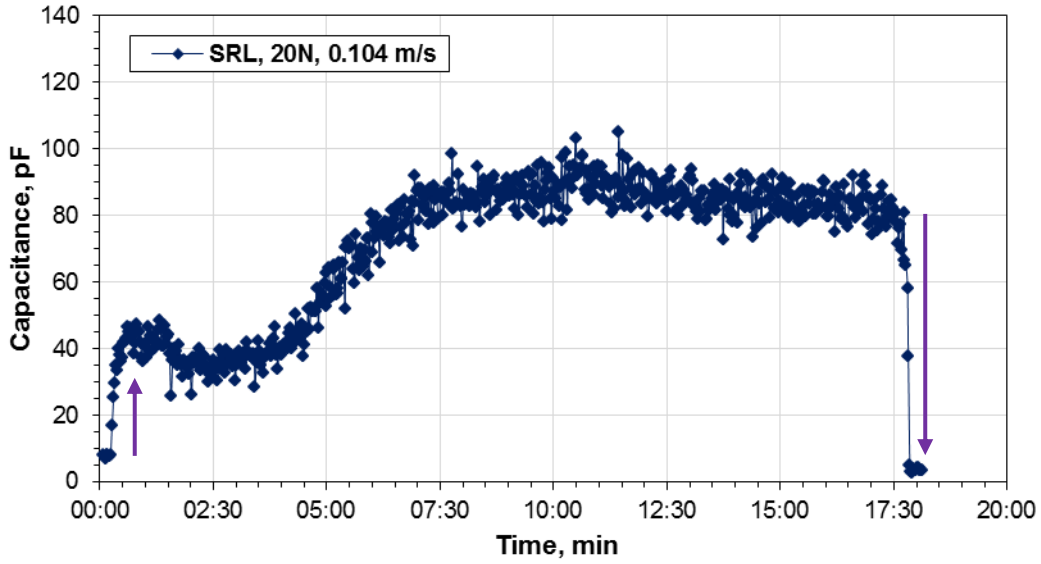

Figure 8.34: SRL grease, dynamic test at 20N and 0.104 m/s

Additionally, a meniscus in front of the contact becomes visible and more pronounced with time. Up to around 3:30 min fluctuations of the film thickness can also be noticed. From that moment on (after 3:30 min) lubricant shortage in the inlet is obvious, leading to starvation. Film thickness fluctuation is a consequence of an occasional "lump" of grease going through the contact. A further steep increase of capacitance is the result of a gradual decline of film thickness due to starvation, which can be clearly seen in the interferometric images. From around 7 min on, the film thickness stays relatively stable, with occasional fluctuations due to additional lubricant supplying the inlet. The speed and load are kept constant for another 10 min, and no significant change in the lubrication condition can be observed based on either capacitance measurement, or contact images. Capacitance decreases slightly at around 12 min duration of the experiment and stays around 85 pF (with some fluctuations).

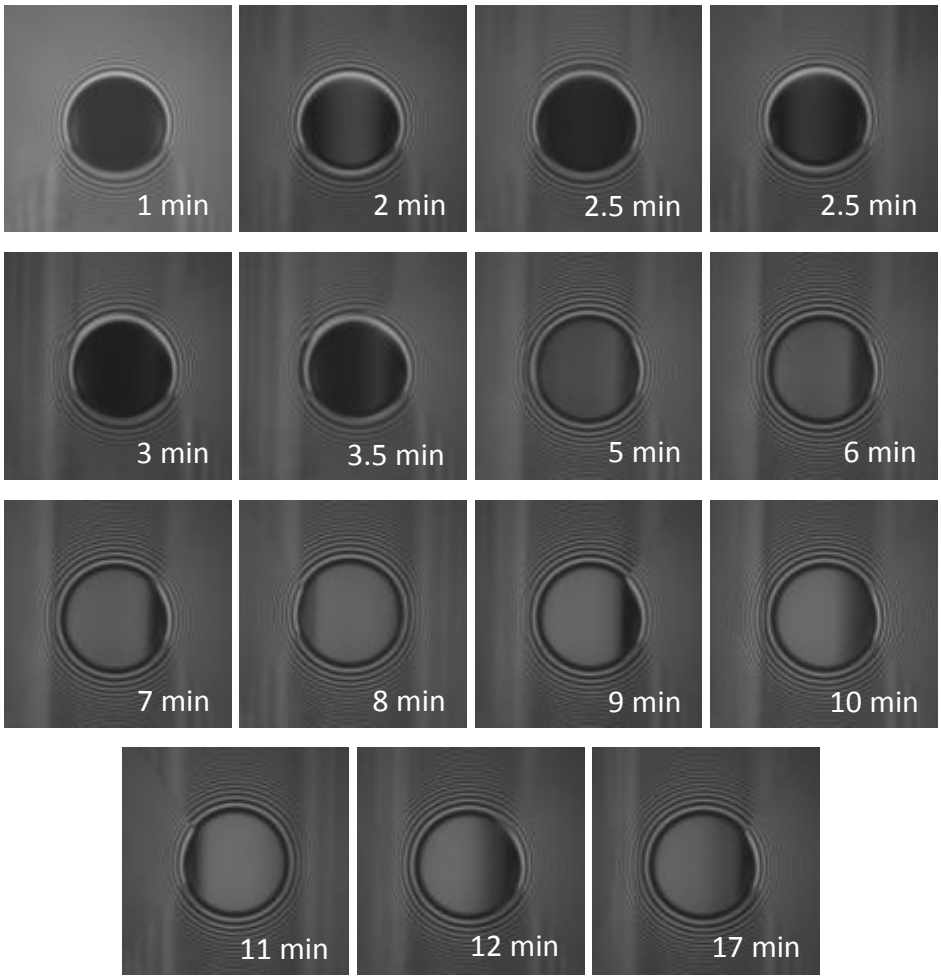

Figure 8.35: Interferometric images showing EHD film (corresponding to Figure 8.34)

The ball was then unloaded and the disc taken out from the rig. Grease was redistributed on the disc surface and removed from the ball with a paper tissue. The following experiment, at 20N load and 0.154 m/s, was therefore performed on the grease that has already been “worked”. The capacitance recordings are shown in Figure 8.36, while the interferometric images of the contact are displayed in Figure 8.37.

The test procedure was the same as in the previous experiment, excluding the speed. The unloaded ball and disc are first rotated at 0.154 m/s and when the load is increased up to 20N, the capacitance increases. It fluctuates around 38 pF and stays on that level for a couple of minutes.

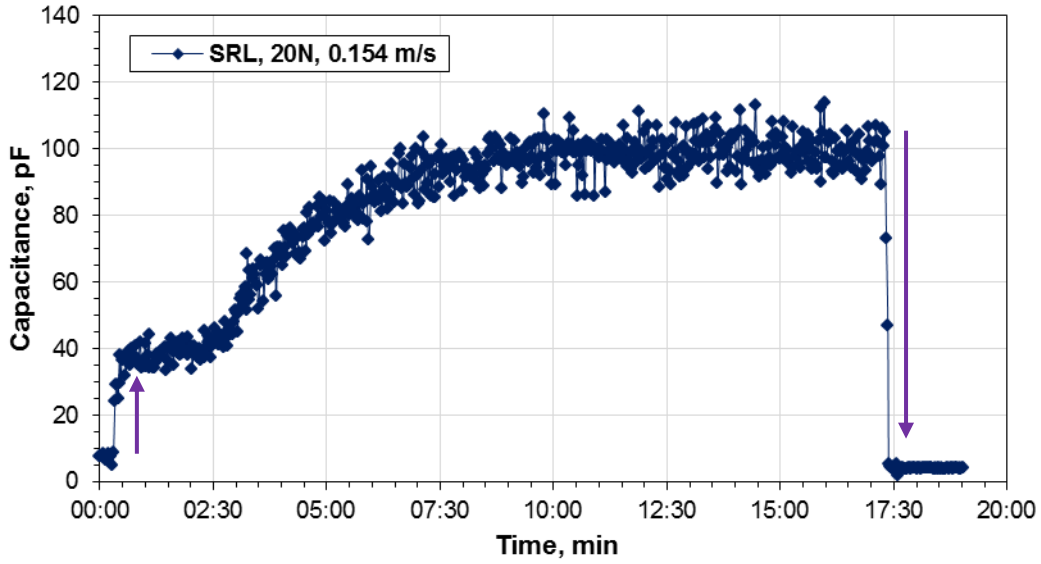

Figure 8.36: SRL grease, dynamic test at 20N and 0.154 m/s

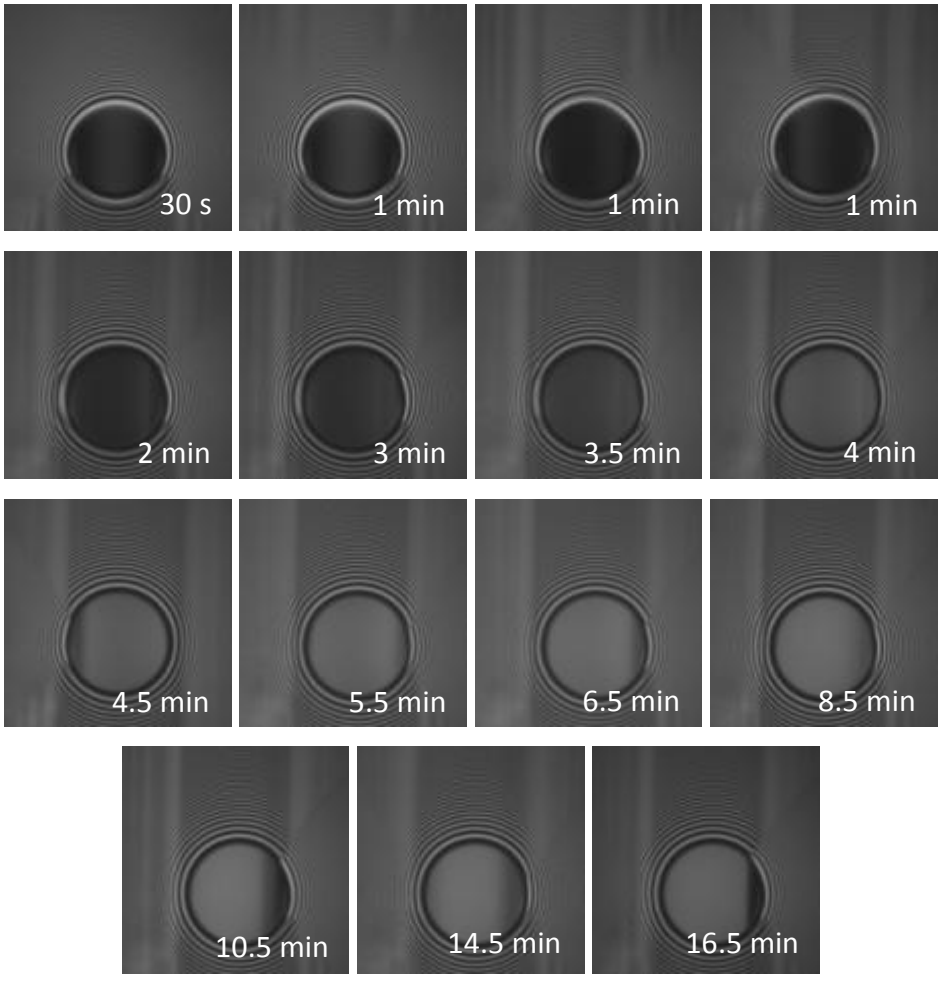

Figure 8.37: Interferometric images of contact area corresponding to data from Figure 8.36

The meniscus is visible from the beginning of the loaded period and some film thickness variation can be seen in the optical images as well. The steep increase of capacitance again corresponds to the film thickness decrease due to starvation. From around 8:30 min capacitance stabilizes at around 100 pF with variation in the order of ±10%. No further significant change in film thickness, apart from that due to an occasional grease lumps passing through the contact, is observed.

The third experiment, shown in Figure 8.38, was performed with a fresh sample of grease and after both the ball and disc have been thoroughly cleaned. In comparison with the results displayed in Figure 8.36, the time to starvation, showed with a blue arrow in Figure 8.38, is twice as long as in the test carried out under the same conditions, but with the grease that has been worked.

Even though it cannot be treated as an absolute quantitative parameter, as it strongly depends on the amount and distribution of the grease applied, the fact that the worked grease starves much quicker suggests a link to grease's structure or composition of lubricating layer changes during the running.

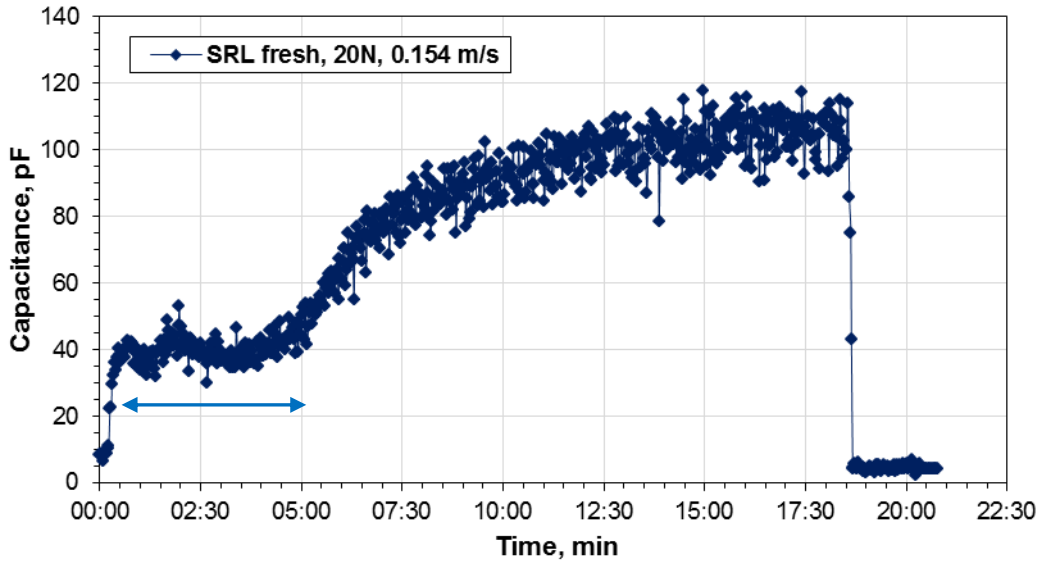

Figure 8.38: Fresh SRL grease tested in dynamic conditions at 20N load and 0.154 m/s

As it is known from the literature (Chapter 5) there are several factors, including vibrations and ball spin, acting in rolling element bearings, which promote additional lubricant replenishment. In order to carry out longer-term experiments without creating a severely-starved condition, it was attempted to introduce a similar contact replenishment mechanism in the ball-on-flat arrangement.

For that purpose a shorter connecting wire for capacitance signal was fitted, which was pulling the ball during half of its rotation. By doing so it was introducing a horizontal movement of the ball which was acting to redistribute the lubricant in the proximity of the rolling track.

Figure 8.39 shows the capacitance measurement of the run with the ball movement introduced, and the corresponding interferometric images are displayed in Figure 8.40. It can be seen than both, capacitance and film thickness, were stable over the whole duration of the experiment (around 20 min). No indication of starvation was noticed. It is also clear that capacitance level is in agreement with the fully flooded phase of previous experiments shown in Figure 8.36 and Figure 8.38.

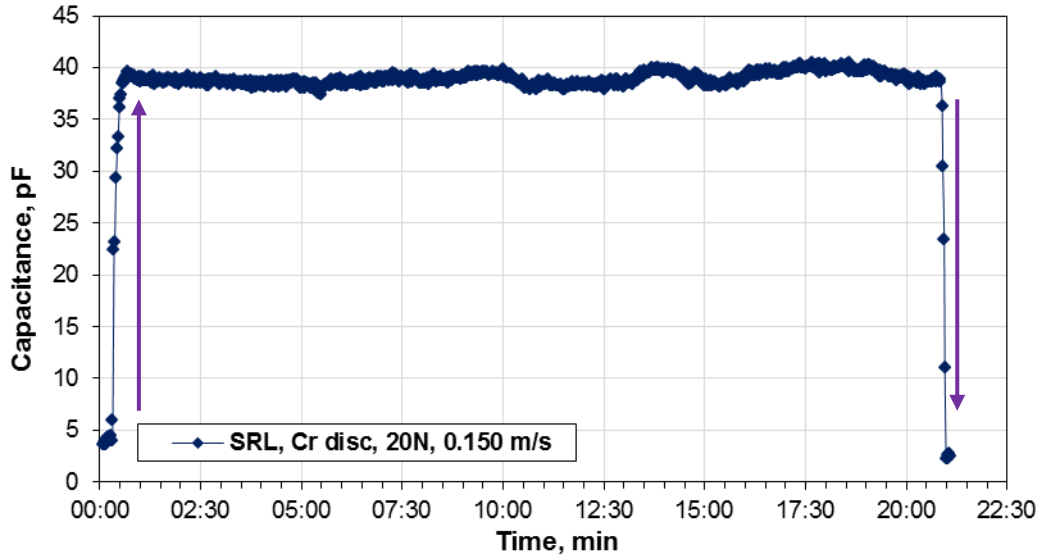

Figure 8.39: SRL grease tested with Cr-coated glass disc at 20N load and 0.150 m/s speed

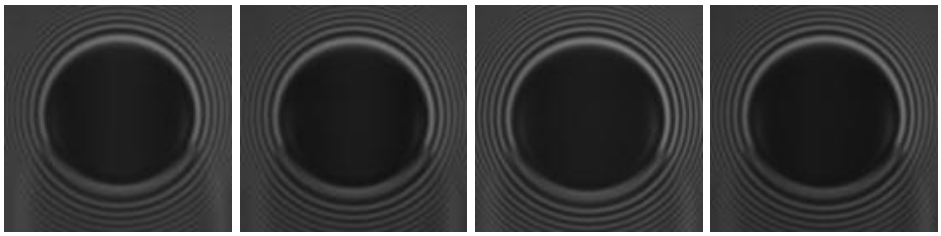

Figure 8.40: Interferometric images of SRL grease film taken at: 1 min, 5 min, 10 min and 15 min (Cr-coated glass disc, 20N, 0.150 m/s)

All experiments so far have been carried out at a fixed entrainment speed; hence it was interesting to examine how sensitive the capacitance measurement would be to a speed variation in grease lubricating contacts.

Capacitance data recorded during the variable speed experiment are shown in Figure 8.41. Some examples of images taken simultaneously are displayed in Figure 8.42. The ball and the disc were first rotated at 0.151 m/s speed and after few seconds the load was applied. An increasing load is seen as a sharp increase of the capacitance. The flat region with capacitance values around 39 pF corresponds to the lowest speed tested, 0.151 m/s, and highest film thickness. After around 30 s the speed was increased in two steps up to 0.258 m/s.

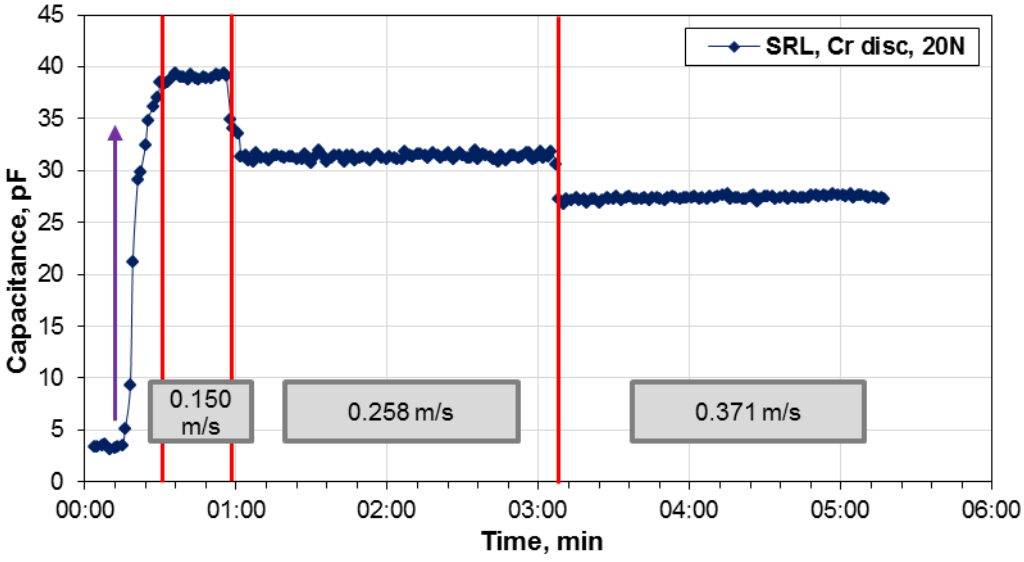

Figure 8.41: SRL grease speed variation at 20N load with Cr-coated glass disc

Optical images indicate an increasing film thickness and capacitance values show a drop down to around 31 pF. The speed is kept constant for several minutes and during that time, both the capacitance and film thickness are stable with no fluctuations. The next increase in speed up to 0.371 m/s is again accompanied by a decrease of capacitance as a result of increasing film thickness.

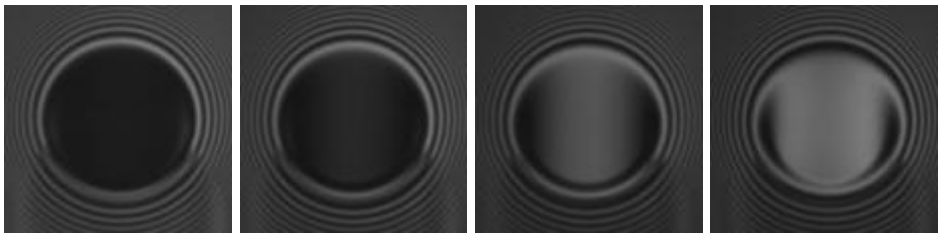

Figure 8.42: Interferometric images of SRL grease film taken at 20N load and 0.150, 0.216 (transition speed), 0.258 and 0.371 m/s

The results presented prove that thickness changes of the grease films are directly reflected in the capacitance measurements. Additionally, the ball movement introduced promotes lubricant replenishment and allows fully-flooded conditions to be studied.

The second part of the grease study was therefore focused on steel-on-steel contacts. Figure 8.43 shows capacitance measurement during a variable-speed experiment under fully-flooded conditions. The grease used in this experiment is the same as in the tests with Cr-coated chromium disc (SRL grease). The ball and disc were run unloaded at 0.150 m/s entrainment speed and then the load of 40N was applied.
The first entrainment speed is the same as in the previous test, shown in Figure 8.41, and since the contact areas in both cases are similar, it would be expected that the capacitance will also be similar. The comparison however, shows a slightly higher capacitance for the steel disc case, around 45 pF, while around 39 pF was recorded for the Cr-coated glass disc. The dielectric constant increase due to pressure cannot explain this difference on its own. It is therefore suggested that a stronger interaction of polar components in grease's formulation (i.e. thickener and additives) with steel as

opposed to chromium surface, can be a possible explanation. This is also in agreement with observations during the experiments with friction modifier (subchapter 8.2.3).

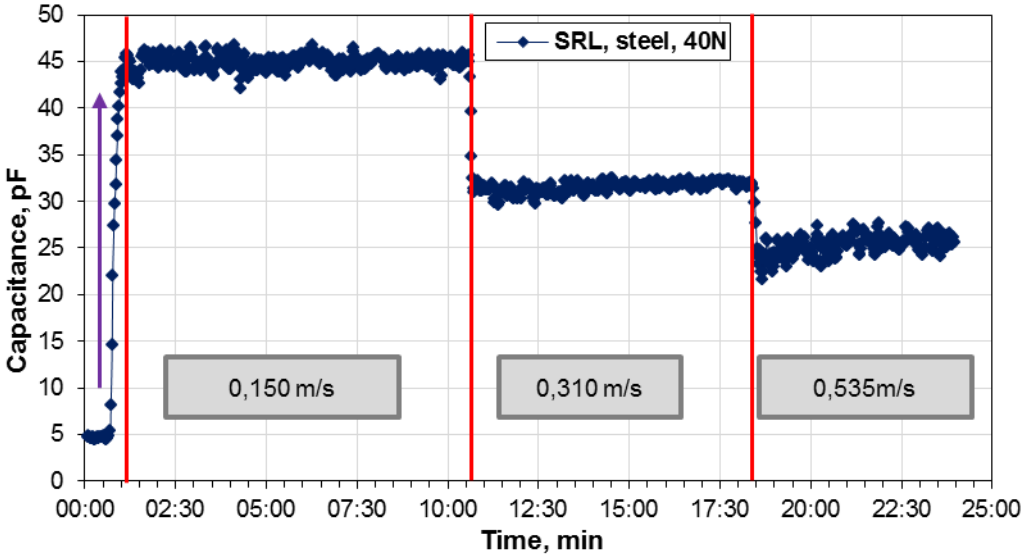

Figure 8.43: SRL grease with steel disc, speed variation at constant load

The difference is seen for the other two speeds as well. During the test with the glass disc, a capacitance of around 31 pF and 27 pF was measured at 0.258 and 0.371 m/s, respectively. That means that the capacitance of steel-on-steel contact at 0.310 m/s should be in between the two, it is however, higher again (around 32 pF).

Since long-term experiments in severely starved conditions are not feasible with a Cr-coated disc due to a high susceptibility of the chromium layer to scratching, they were performed with a steel disc only. In the following figures the response of capacitance to changing contact inlet conditions (fully-flooded or starved) can be seen. A variation of capacitance due to either additional supply or removal of grease can also be observed.

In Figure 8.44 capacitance recordings of a grease lubricated contact, running at fixed load and speed settings is displayed. In this experiment, in order to fully observe the starvation, a very small amount of grease was applied only onto the ball surface.

As a comparison, the capacitance recorded in fully-flooded conditions at the same speed can be seen in Figure 8.43, where the results show the level of around 32 pF.

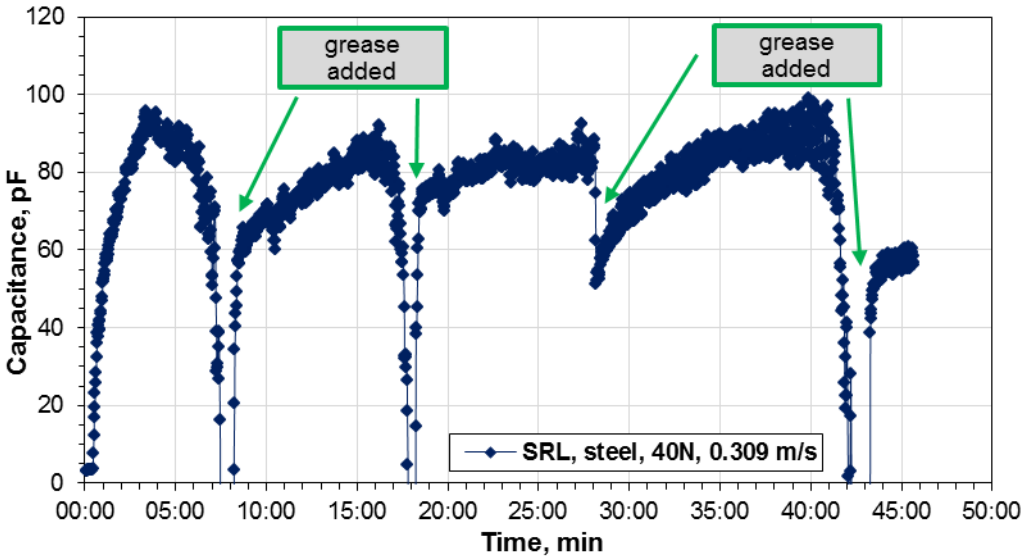

Figure 8.44: SRL grease starvation observation with steel disc at 40N and 0.309 m/s

In the current experiment it can be seen that the capacitance immediately and sharply increases up to around 95 pF, which reflects a lowering grease film thickness due to starvation.

When the film thickness becomes too thin for capacitance measurements, current leakage through the film is manifested by a decreased capacitance. As previously explained (subchapter 7.2.2), each capacitance value displayed as a result, is an average of measurements taken over a certain time, called the integration time, which is 0.1 s in the current tests. A decrease of capacitance seen in Figure 8.44 is due to increasing number of “negative” capacitance readings caused by the current leakage. At a point when the measurement is not possible anymore, only negative capacitance values are displayed.

It is difficult to estimate the film thickness based on these results, since the exact composition of the film between ball and disc is not known. The amount of ionic thickener, and possibly additives of ionic character, will influence the dielectric

constant and also the conductivity of the layer, determining the minimum film thickness which can be measured in these conditions. However, based on experience from the previous grease tests carried out with the Cr-coated glass disc, the lowest film thickness measured was around 10-15 nm.

When a small amount of fresh grease is added (grease on a spatula approaching the rotating ball), while the test is still running, the capacitance increases (from the negative values) up to around 60 pF, but it does not stabilize. It increases further to around 85 pF and decreases sharply again. An addition of a grease sample brings the capacitance back up to around 70 pF. The increase this time is less rapid, and the values never fall below zero. Another amount of grease introduced brings the capacitance down to around 50 pF, a slow gradual increase follows, which is accompanied by an increasing scatter of the data points. When the film eventually breaks, another grease sample lowers the capacitance again.

Another similar experiment is shown in Figure 8.45. Here as well, when the starvation occurs, an additional amount of grease is introduced to replenish the contact. This time however, starvation was not observed again and the contact retained the fully-flooded condition even when the speed was increased.

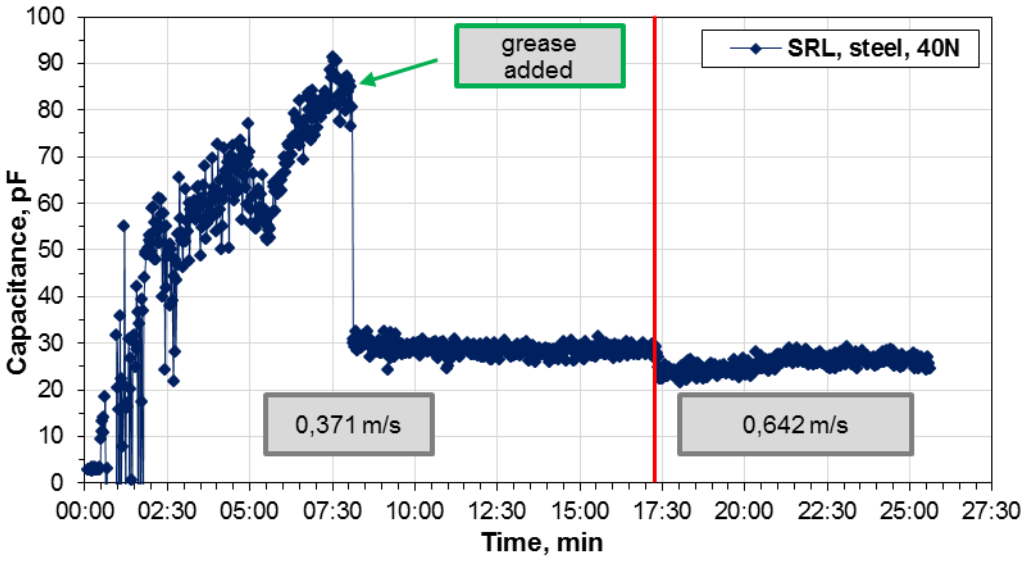

Figure 8.45: SRL grease tested with steel disc at 40N load

The same behaviour can also be seen in Figure 8.46, where in order to shorten the time before starvation occurs, some grease from the rotating ball was removed by touching it with a tissue. After the first attempt the grease film quickly recovered, and only the second attempt caused a clear increase of capacitance.

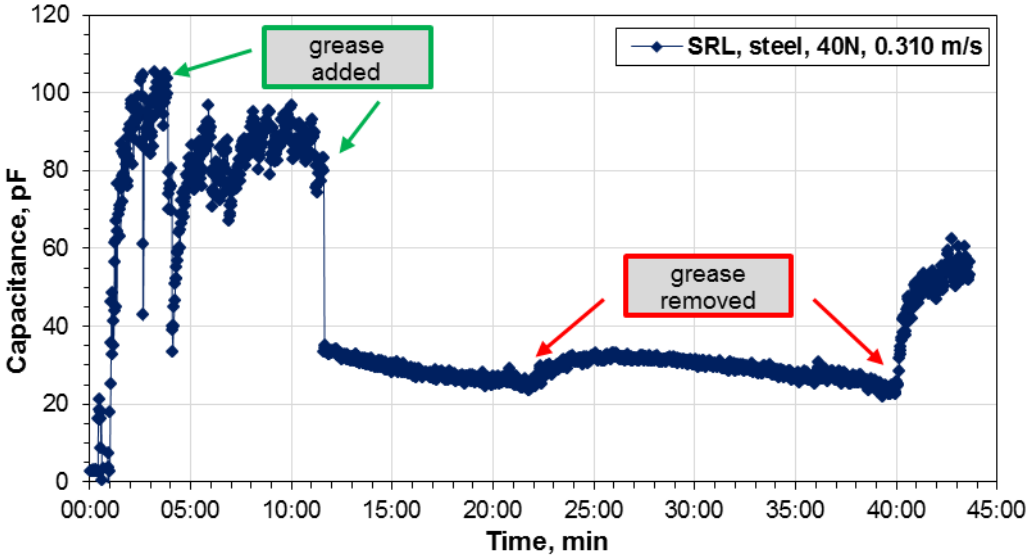

Figure 8.46 SRL grease tested with steel disc at 40N and 0.310 m/s

Capacitance recordings presented here should only be used on a semi-quantitative basis. The observed behaviour strongly depends on the amount of grease applied and the extent of track replenishment due to ball movement introduced. This, on the other hand, depends on the exact mounting and the ball alignment. The graphs shown here can be only used as guidance and to understand the meaning of the capacitance variation in grease lubricated ball-on-flat contacts.

The data presented here clearly show the high sensitivity of capacitance measurement to detect rapid changes in the grease lubrication condition. When the method is combined with optical interferometry the grease films can be also visually observed. This method enables a comparative study of different greases and their short- and long term behaviour with more realistic material combinations, such as steel on steel contacts.

8.4 Evaluation of film thickness in ball bearings by electrical capacitance

The final part of the experimental work was focused on the film thickness measurements in a rolling element bearing. The approach used is based on findings from the tests in a ball on-flat arrangement with some modifications allowing for a different geometry and the existence of two different EHD contacts (inner ring and outer ring), measured at the same time.

Two lubricants were used in the current experiments: PAO base oil and a fully formulated mineral oil. For the ball-on-flat tests PAO4 was chosen, while the measurements on a ball bearing were performed with a more viscous blend, corresponding to ISO viscosity grade 48. Details of both can be found in subchapter 7.1.

At first, these two oils were evaluated in the ball-on-flat arrangement to confirm that the procedure indeed provides accurate film thickness results in both glass/steel and steel/steel EHD contacts.

8.4.1 Ball-on-flat setup

Testing conditions for this part of the investigation are listed in Table 8. The experiments with chromium coated glass discs were performed at the highest load achievable in the current test rig, 40N.

Table 8: Testing conditions in the ball-on-flat experiments

Lubricant	Glass disc (0.65 GPa)	Steel disc (1.04 GPa)
Mineral oil	40N, 25°C, 0.10 V, 0.01-0.23 m/s	40N, 40°C, 0.05 V, 0.03-0.31 m/s
PAO4	40N, 25°C, 0.10 V, 0.01-0.46 m/s	40N, 25°C, 0.10 V, 0.01-0.46 m/s

Since glass and steel have different elastic moduli, at the same load the contact area will be much smaller with the steel disc ($5.75 \cdot 10^{-8}$ versus $9.26 \cdot 10^{-8}$ m^2), leading to a lower measured capacitance. Additionally, as a result of a higher viscosity, and therefore thicker film formed at the same entrainment speed, the mineral oil would show a much lower capacitance than PAO4.

In order to extend the range of film thickness, which can be accurately measured with the capacitance method, and also to improve the method's resolution, steel-on-steel experiments with the mineral oil were carried out at a higher temperature, namely $40^{o}C$, resulting in a lower film thickness, and therefore higher measured capacitance.

Due to a higher conductivity of mineral oil, related to the presence of additives, of presumably ionic character, some modifications were necessary to prevent current leakage or breakthrough occurrence during the measurements of capacitance.

First of all the measurement voltage was lowered down to 50 mV. This resulted in an improvement; however the measurements were still not stable enough.

Since this issue has not been observed with the chromium-coated disc, where the thin Cr-layer essentially acts as a resistor in series with the EHD contact, it was thought that introducing a resistor of a similar value (around 300 Ω), in the circuit with the steel disc might provide a solution.

This indeed allowed stable capacitance measurements over a wide range of speeds to be performed, nevertheless, it was not possible to measure films as thin as with PAO4 base oil.

The idea that the additives in the fully-formulated oil are responsible for this is supported by the fact that such behaviour has not been observed with any of the base oils, even the highly polar, or with the friction modifier solution. Current leakage through the film was only observed with very thin grease films, which contained both soap-type thickener and performance-enhancing additives.

The results of the capacitance measured for both lubricants with the chromium-coated glass and steel disc are shown in Figure 8.47. All series follow the straight-line power law (in a logarithmic scale) over the full range of speeds, as expected for nonpolar lubricants. Since the temperatures of both tests with the mineral oil are different, the values displayed cannot be directly correlated to film thickness.

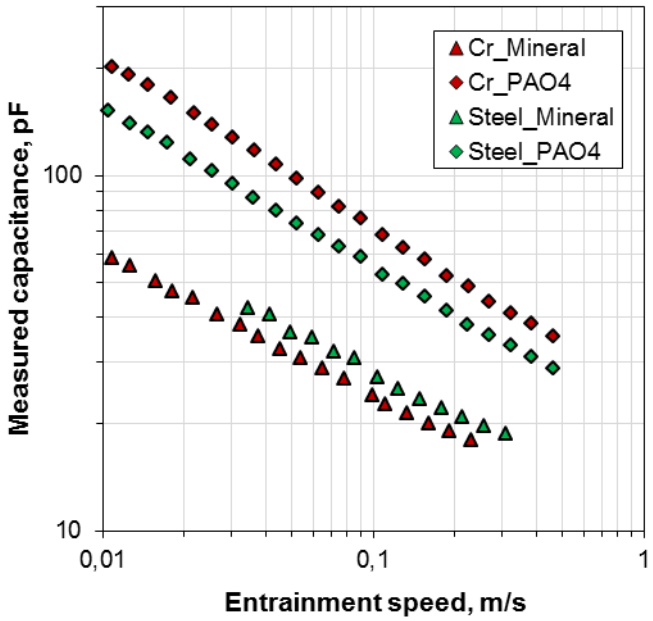

Figure 8.47: Measured capacitance as a function of speed in ball-on-disc setup (Mineral oil and PAO4, Cr-coated glass and steel discs, 40N load)

To allow for a direct comparison, the film thicknesses extracted from the measured capacitance are shown in Figure 8.48 and Figure 8.49, for chromium-coated glass and steel disc, respectively. The values obtained from optical interferometry measurement and calculated from the theory are also included. The dotted lines indicating ±10% from the optical or theoretical results are shown for guidance. The low-speed region is enlarged for clarity in the accompanying plots.

It can be seen that the capacitance results lie within the limits over the whole range of speeds tested, corresponding up to around 300 nm for the mineral oil film thickness in the Cr-coated glass disc experiment.

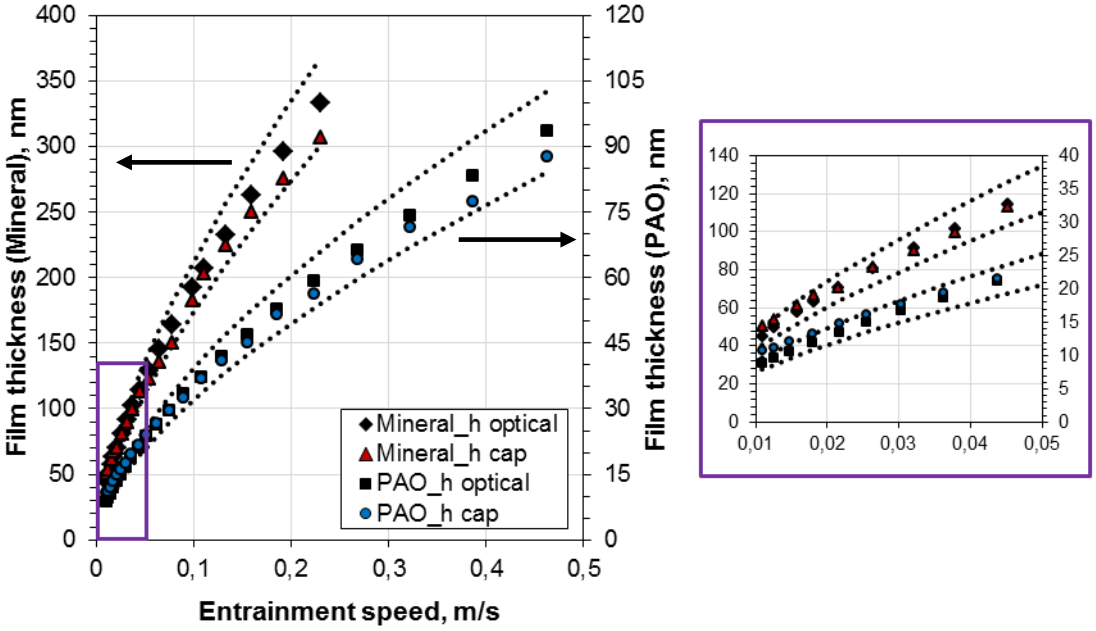

Figure 8.48: Film thickness measured with optical method and capacitance in ball-on-disc setup (Mineral and PAO oil, 40N, Cr-coated glass disc, 25°C, ±10% h_{opt} dotted lines)

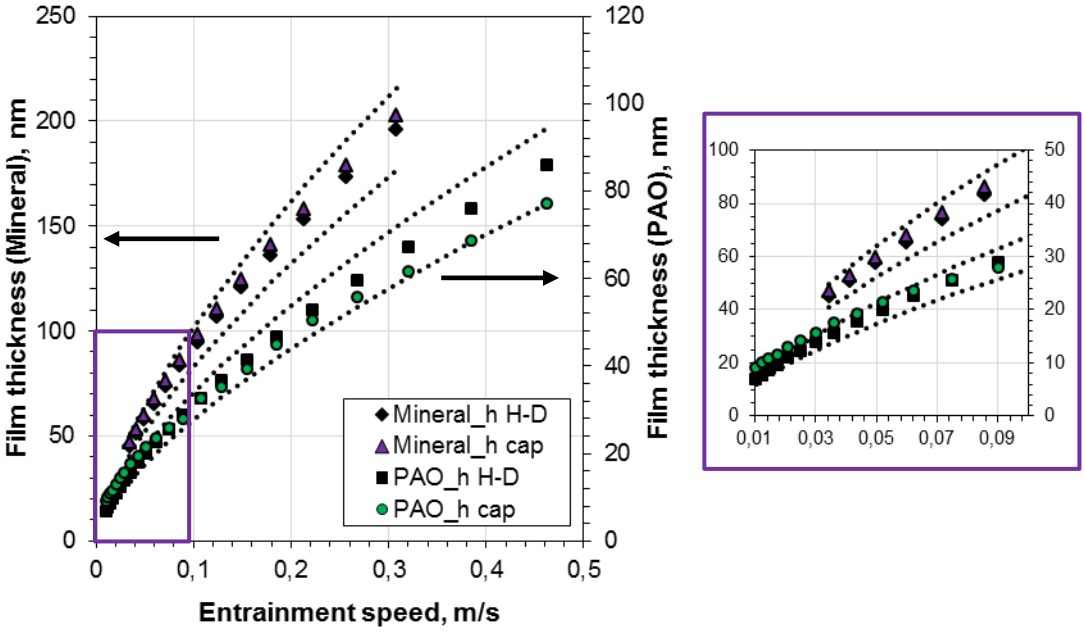

Figure 8.49: Film thickness calculated from theory and measured with capacitance in ball on disc setup (Mineral and PAO oil, steel disc, 40N, 25°C and 40°C, ±10% h_{theo} dotted lines)

When the results obtained with the steel disc are compared, it can be clearly seen that the lowest film thickness measured with PAO is smaller than in the case of mineral oil (10 nm in comparison to 46 nm). Nevertheless this is still in the range of thicknesses that would be considered as thin films.

In order to directly compare the two oils, the ratio of measured capacitance and dielectric constant of the lubricant at Hertzian contact pressures is shown as a function of film thickness in Figure 8.50.

By taking into account the difference in dielectric constants it can be seen that both lubricants follow the same trend for each disc. It should be noted that this is only possible when both lubricants have a low polarity.

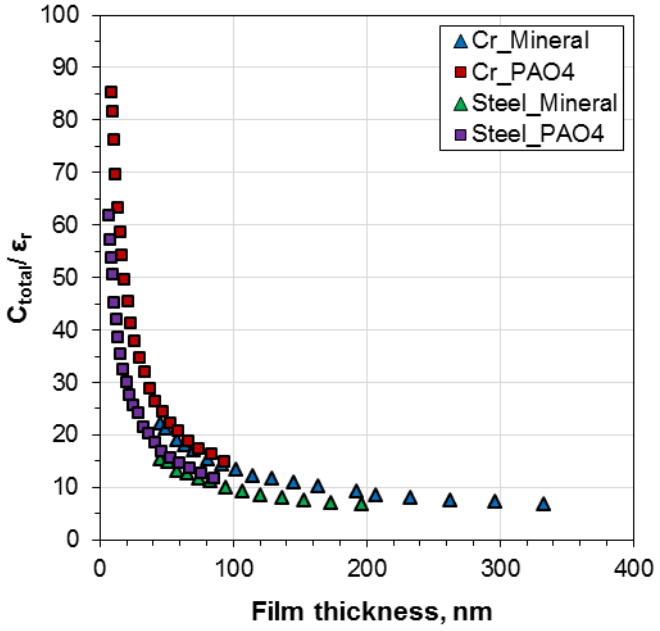

Figure 8.50: Ratio of the measured capacitance and dielectric constant as a function of film thickness in ball-on-disc setup

From these results it is also clear that the two disc materials show different trends. This is related to different contact areas and also the contribution of contact capacitance in the total measured capacitance. For this reason graphs similar to the one shown in Figure 8.50 can only be used to extract the film thickness for nonpolar

lubricants tested only under the same load conditions and with the same disc materials as reference oil.

In this section it has been proven that for both lubricants under investigation, the film thickness can be evaluated with a satisfying accuracy from the measured capacitance. The important implication of the presence of additives of ionic-character for capacitance measurements has been observed.
With that in mind it is now possible to proceed to the second part of the study, which involves applying the same approach to a rolling element bearing.

8.4.2 Ball bearing setup

The second part of the experimental work was performed in the bearing test rig presented in subchapter 7.3. A 6306 ETN9 deep-groove ball bearing (DGBB) with a polymer cage and inner and outer diameters of 30 and 72 mm, respectively, was used. A radial load between 1 and 6kN was applied and the tests were performed over a range of entrainment speeds from 0.12 m/s up to 0.91 m/s (95–737 rpm). Contact parameters at a maximum load position for both, inner and outer ring contacts are listed in Table 9.

Table 9: Contact parameters for the range of loads at the maximum load position

Load applied, kN	**Contact area, m^2**		**Maximum Hertzian pressure, GPa**	
	Inner ring	**Outer ring**	**Inner ring**	**Outer ring**
1	$8{,}9\cdot10^{-7}$	$1{,}0\cdot10^{-6}$	1,6	1,3
2	$1{,}3\cdot10^{-6}$	$1{,}5\cdot10^{-6}$	1,9	1,6
3	$1{,}6\cdot10^{-6}$	$1{,}9\cdot10^{-6}$	2,1	1,8
4	$1{,}9\cdot10^{-6}$	$2{,}2\cdot10^{-6}$	2,3	2,0
5	$2{,}2\cdot10^{-6}$	$2{,}5\cdot10^{-6}$	2,4	2,1
6	$2{,}4\cdot10^{-6}$	$2{,}8\cdot10^{-6}$	2,6	2,2

The bearing was lubricated with a few drops of lubricating oil applied with a pipette. In order to prevent starvation at high rolling speeds, a small amount of oil was added before a sweep of speeds at each load.

All tests were performed at room temperature and the bearing was run under self-induced temperature conditions. The temperature was measured on the outer ring before and after a sweep of speeds for each load.

The current setup, in which only the capacitance of the contacts between one steel ball and the raceways are measured (as described in subchapter 7.3), enables monitoring of the position of the steel ball as it travels through the full rotation cycle.

The Lubcheck signal and corresponding capacitance distribution within the bearing, measured with the mineral oil at a range of loads (1-6kN) and a single speed (0.41 m/s) is shown as an example in Figure 8.51.

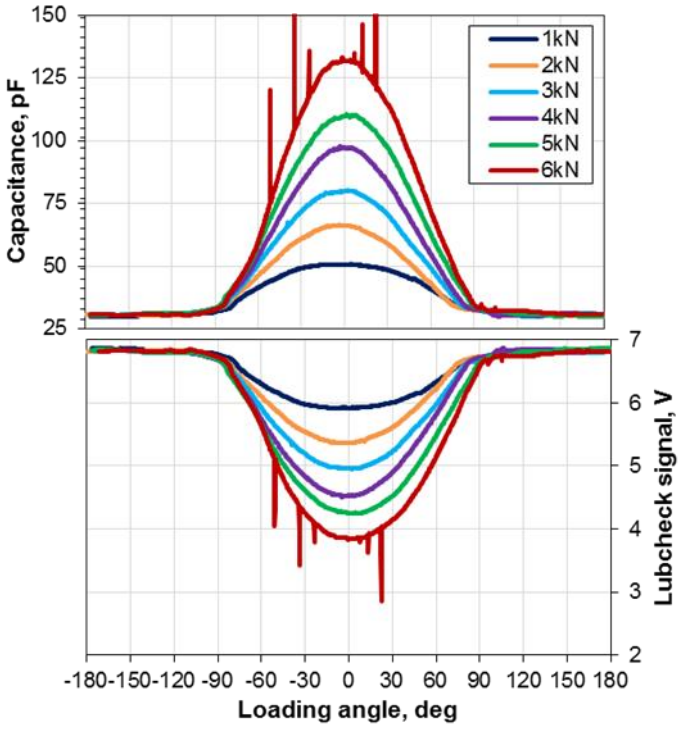

Figure 8.51: Lubcheck signal and corresponding capacitance measured over a full rotation at a range of loads (Mineral oil, 0.41 m/s)

According to the elastohydrodynamic theory (subchapter 2.2) lubricant film thickness is relatively insensitive to load changes. This is shown in Figure 8.52, in which the data was calculated based on the bearing's geometry for a randomly chosen condition of speed and lubricant viscosity (both were kept constant). The values displayed correspond to the inner ring contact.

It can be seen that the contact area varies significantly with the load, therefore it can be concluded that an increase of capacitance with load, as clearly seen in Figure 8.51 comes mainly from the change of the contact area and, in a lesser extent, from the variation of the dielectric constant with pressure (subchapter 7.1.1).

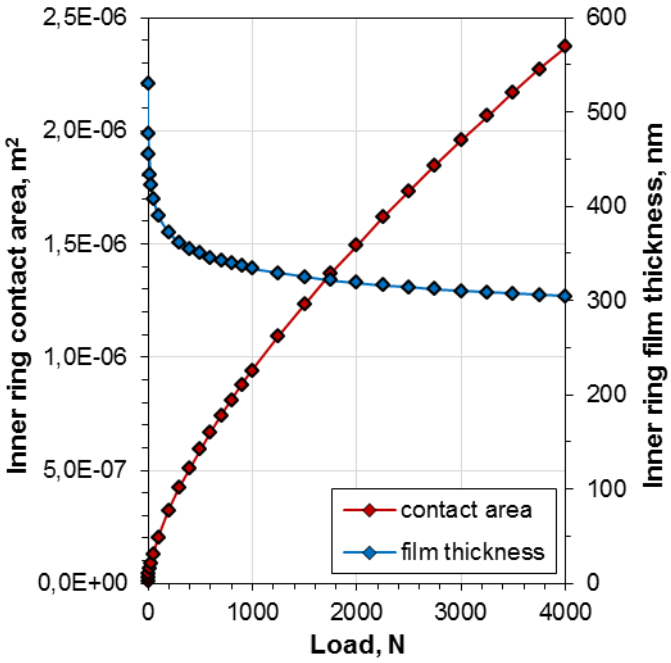

Figure 8.52: Variation of film thickness and contact area calculated for inner ring contact in the DGBB

Based on the capacitance distribution within the bearing, for the purpose of film thickness evaluation, the values corresponding to the position of the maximum load were taken. Since this point represents also the lowest film thickness, it provides valuable information about the lubrication condition in the most critical area in the bearing.

First, the capacitance recorded (at the highest load position) at a range of loads and speeds, is shown in Figure 8.53 and Figure 8.54 for mineral oil and PAO VG48, respectively. As expected, for both lubricants a significant increase of the total measured capacitance with the load is clear, as well as a decrease of capacitance with increasing entrainment speed.

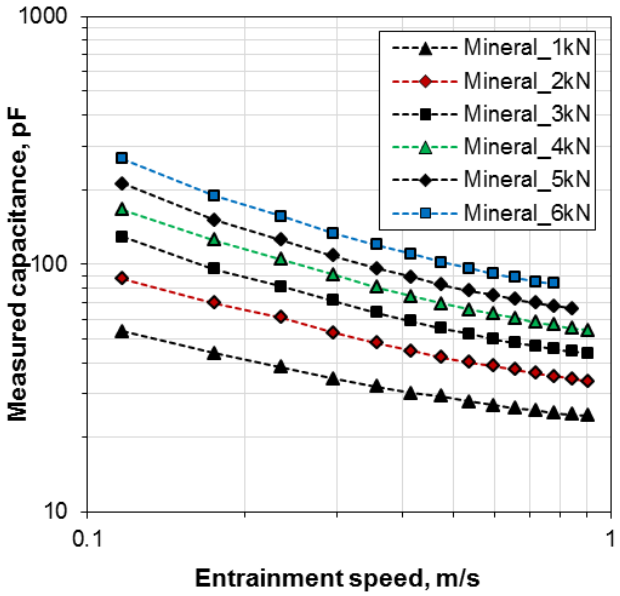

Figure 8.53: Measured capacitance as a function of speed for mineral oil in DGBB tests

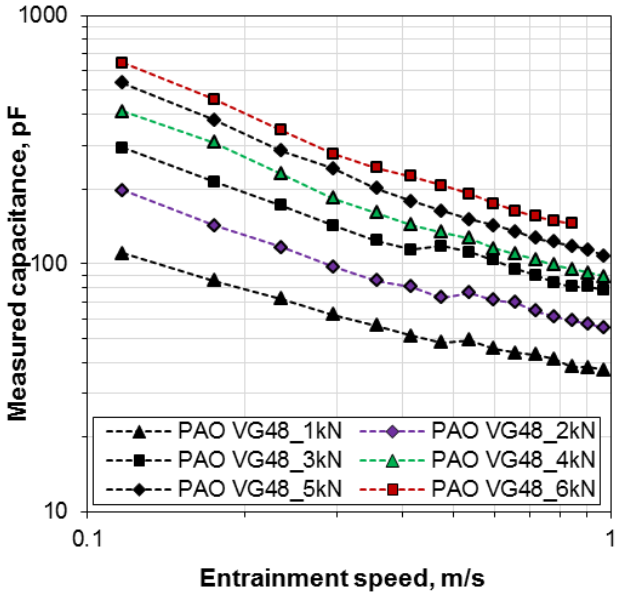

Figure 8.54: Measured capacitance as a function of speed for PAO VG48 oil in DGBB tests

The capacitance data points generally follow straight-line power law trend (in a logarithmic scale), which is in agreement with the findings from the ball-on-flat setup experiments. Slight deviations from that trend can be seen at high speeds, with much stronger deviations in the case of PAO VG48 lubricant, (Figure 8.54). It is believed that it is the result of an increasing temperature during the experiment. Thus, the film thickness is lower, leading to greater capacitance readings than expected.

Since the two lubricants tested have a significantly different viscosity (Table 5), in order to make a direct comparison, also taking into account different dielectric constants, the ratio of the total measured capacitance and the dielectric constant is displayed as a function of theoretical inner ring film thickness in Figure 8.55.

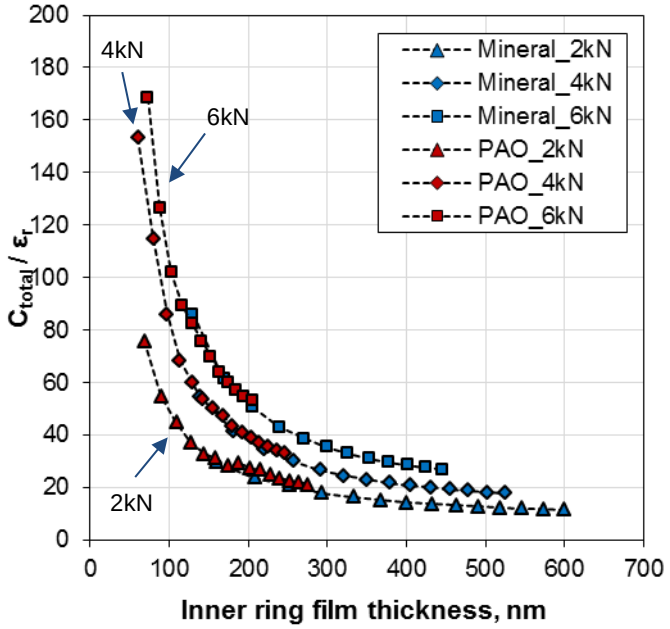

Figure 8.55: Ratio of the measured capacitance and dielectric constant as a function of inner ring film thickness in DGBB tests

This result is in agreement with the previous findings for the ball-on-flat case (Figure 8.50). However here, instead of two different disc materials, variable load conditions are shown. It can be concluded that for a certain bearing geometry, nonpolar lubricants follow the same trend at each load if the difference in dielectric constants is

taken into account. This means that if the capacitance variation for a reference nonpolar fluid is established, it can be then used for other nonpolar oils.

With this in mind, the film thickness values of mineral oil calculated from the measured capacitance, together with the theoretical values for 6kN load are shown in Figure 8.56. Theoretical predictions displayed here include a thermal correction factor to allow for inlet-shear heating effect, calculated according to Gupta et al. (1992).

In the absence of separate capacitance measurements for the inner and outer ring contacts, the partition of the measured capacitance attributed to each contact was done by the ratio of the theoretical areas. By doing so it was possible to calculate separate film thicknesses for each of the contacts, rather than assuming the two are equal.

Capacitance film thickness values below the theoretical line are seen for both, the inner and outer ring. This deviation is about 9% for the inner ring and 6% for the outer ring at low entrainment speed (thin films), and about 8% for both rings at higher speeds.

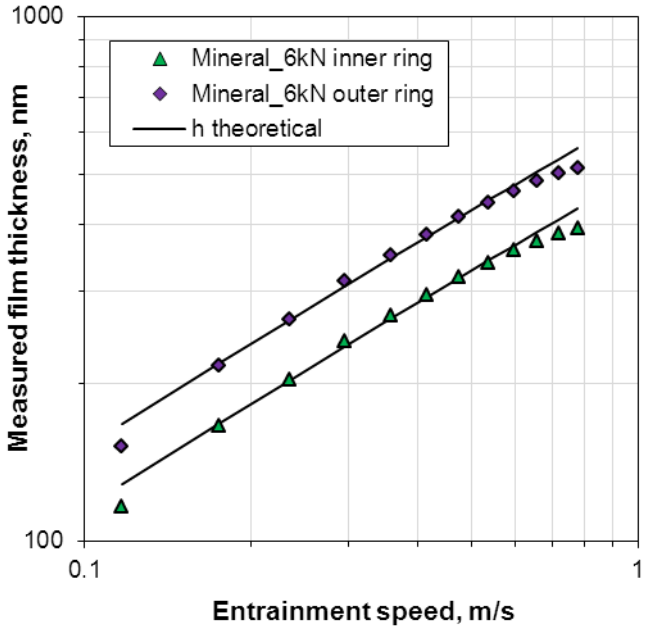

Figure 8.56: Film thickness measured with capacitance compared with theoretical values for the inner and outer ring in DGBB tests (Mineral oil, 6kN)

The difference between the film thicknesses of the two rings is due to geometry of the convergent region. The outer ring gives better conditions for lubricant entrainment; thus a thicker film is formed. Since the film thickness is extracted from the combined capacitances between the ball and inner and outer ring, the same trend for both contacts is observed. This is the case for all experiments, and from this point only the film thickness of the ball inner ring contact will be shown.

The comparison of film thickness extracted from the measured capacitance and calculated from Hamrock and Dowson formula (Eq. 10), is shown in Figure 8.57 for 2, 4 and 6kN radial load (figures a, b and c, respectively). Additional plots enlarging the region up to 300 nm are also included for clarity.

Since it is difficult to estimate the accuracy of film thickness evaluation based on the electrical capacitance (subchapter 8.4.2.1), it was decided to choose an arbitrary level, which would be considered as acceptable in an experiment on a real machine component. Therefore, the dotted lines limiting ±15% from the theoretical predictions are displayed only for guidance and are not a claim of the method's accuracy.

It can be seen that the majority of the film thickness results are within those limits over the whole film thickness range. The general position of the capacitance results relative to theoretical ones slightly varies with the load. It is believed that the reason for this lies in the accuracy of the contact area evaluation, which is strongly dependent on the value of the load in the centre of loaded zone in the bearing. The influence of clearance and load calculation approach would be the strongest for the lowest load (1kN) and the least relevant for the highest load (6kN).

Additionally, slightly different trends can be seen for PAO VG48 and the mineral oil. The capacitance results of the mineral oil show a gradual decrease below the theoretical film thickness trend, which is not seen with PAO VG48 oil. It should be noted that the mentioned deviation occurs at much higher film thickness than the range studied with PAO VG48.

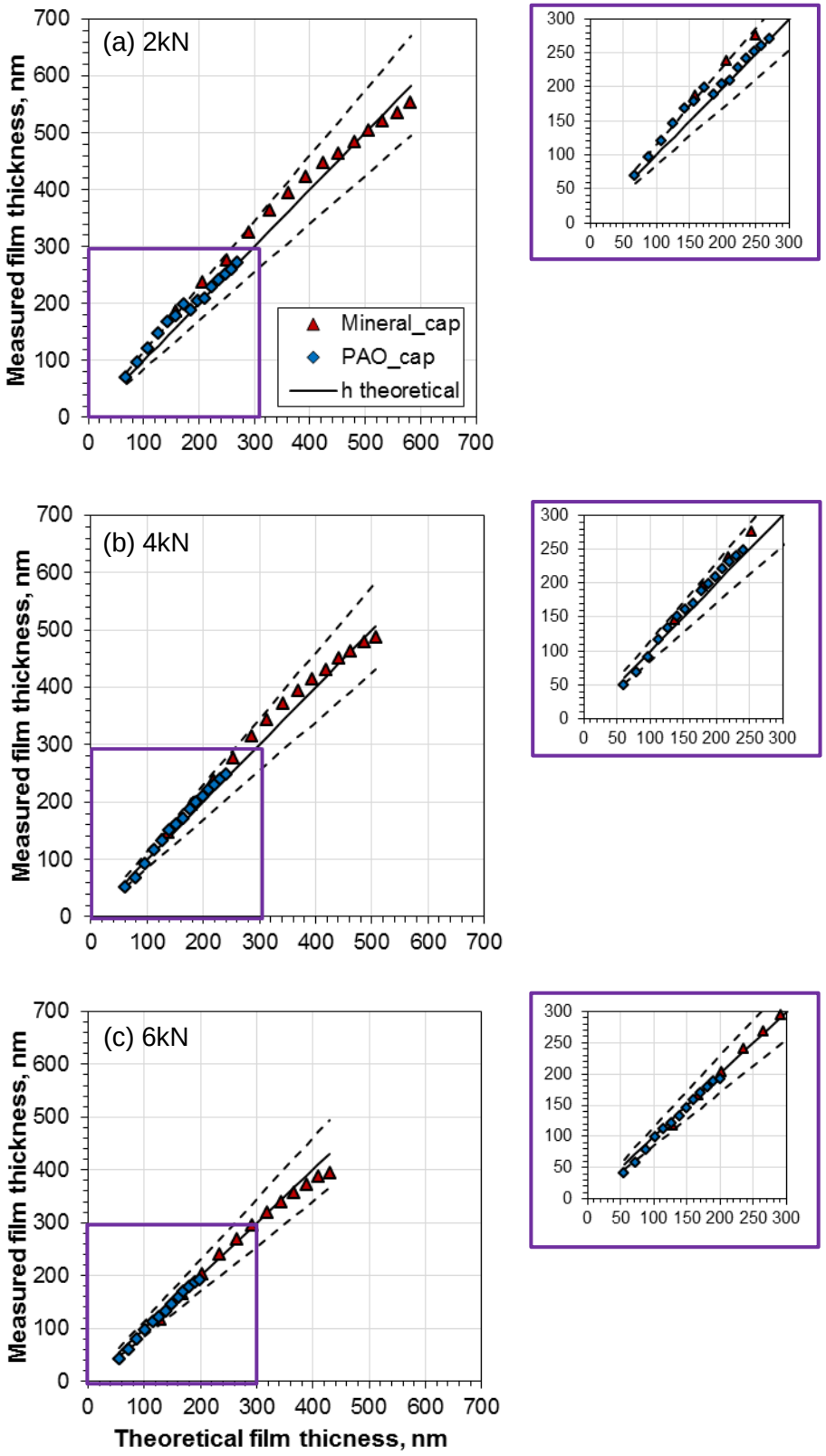

Figure 8.57: Mineral and PAO VG48 oils in DGBB tests (inner ring film thickness, ±15% h_{theo} dotted lines) with the thinner-film thickness range enlarged

In order to explain this difference, an analysis of temperature increase and inlet shear heating influence was carried out. The two lubricants studied significantly differ in terms of viscosity and their viscosity-temperature characteristics. PAO has a higher viscosity index (Table 5) and thus shows a smaller viscosity change with temperature than the mineral oil.

According to Gupta et al. (1992) thermal reduction factor can be calculated with the formula:

$$\Phi_T = \frac{1-13.2\left(\frac{p_0}{E'}\right)L^{0.42}}{1+0.213(1+2.23S^{0.83})L^{0.640}} \quad (45)$$

Where p_0 is the Hertzian pressure, K_f is the thermal conductivity, and thermal loading parameter (L) and slide-to-roll ratio (S) can be calculated according to:

$$L = \left(-\frac{\partial\mu}{\partial T}\right)\frac{U^2}{K_f} \quad (46)$$

$$S = 2\frac{U_1-U_2}{U_1+U_2} \quad (47)$$

Figure 8.58 shows the theoretical film thickness calculated for 1kN load tests with both oils. The isothermal Hamrock and Dowson film thickness for starting temperatures is shown with symbols. The dotted lines depict the same film thickness but corrected for the inlet-shear heating. Additionally, Hamrock Dowson film thickness with the thermal correction at temperatures higher by one and two degrees from the start of test temperatures, are included.

The temperature measurement before the sweep of speeds for that load was 24^{o}C for the mineral oil, and 23^{o}C for the PAO VG48 lubricant. After completing the test, an increase of 1^{o}C was registered; however, since the temperature was only measured on the outer ring, the actual temperature of the lubricant going through the EHD contact may be higher.

In most of the work already published, for practical reasons the bearing temperature was measured on the outer ring; however, as shown by Joshi et al. (2001), the cage

temperature may be more representative, as the cage's response to a change of operating conditions is much quicker.

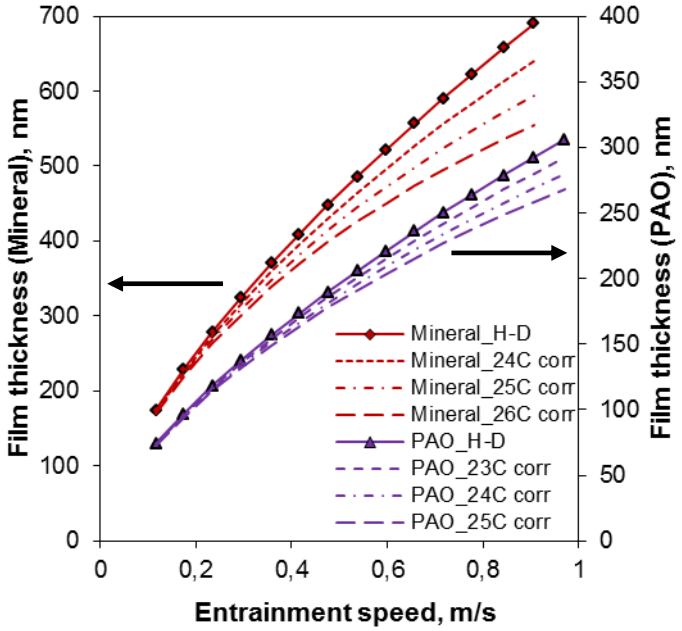

Figure 8.58: Influence of the inlet shear heating correction on theoretical film thickness form mineral and PAO base oil in DGBB tests (1kN)

In Figure 8.58 it can be seen that the influence of temperature, in this very small range, on theoretical film thickness corrected for inlet shear heating, is much stronger for mineral oil, due to already mentioned lower viscosity index. It can also be seen that for high speeds even such a small change of temperature as 2^{o}C can cause a significant decrease of film thickness for mineral oil, up to 20%.

It can be therefore concluded that the underestimated lubricant temperature is the most likely reason for capacitance film thickness being below theoretical predictions, as seen in Figure 8.57. The application of a different and more accurate temperature monitoring method thus can be advantageous. Nevertheless, an overall good agreement was obtained for both lubricants tested over the range of speeds and loads.

8.4.2.1 Additional analysis

Effect of lubricant's conductivity

During the course of this work it has been realized that, similarly to the ball-on-flat configuration, conductivity of the lubricant tested plays a very important role in the interpretation of capacitance data.

From the comparison of the Lubcheck voltage measured for mineral and PAO VG48 oil, shown in Figure 8.59, it is clear that for the same load and film thickness conditions a significantly different behaviour is observed for the two lubricants. The signals from mineral oil tests show much more noise in the loaded region, than the corresponding recordings for the polyalphaolefin base oil. If a direct comparison at the same film thickness, such as that shown in Figure 8.59, was not possible, it would be assumed that the "noise" observed on the oscilloscope's display originates from the asperity contacts, causing short-circuits.

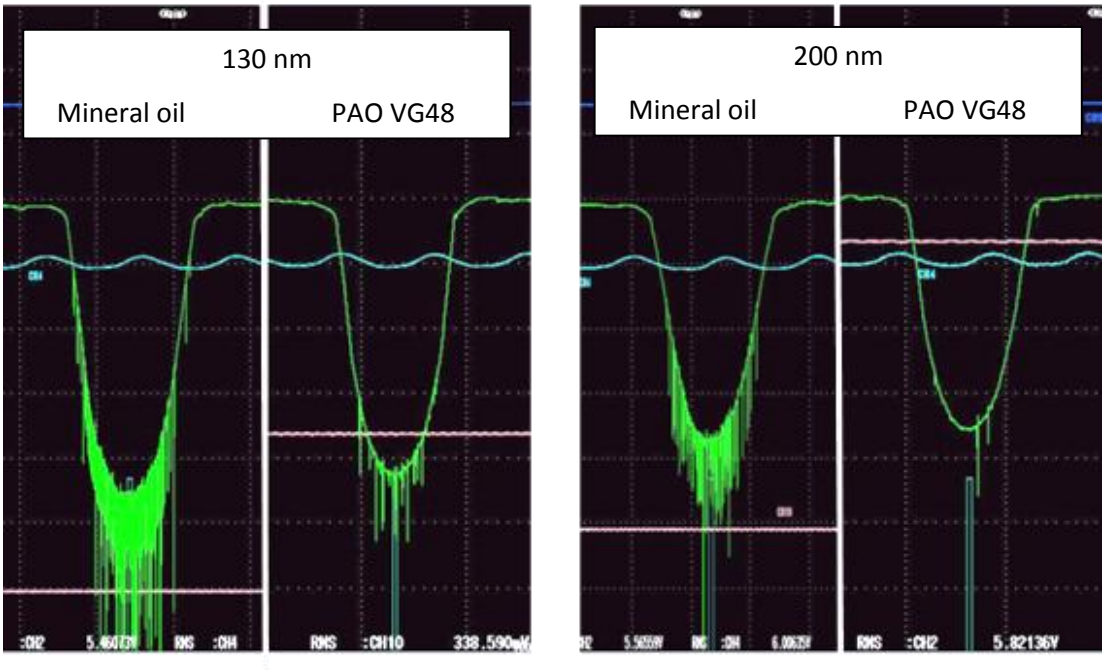

Figure 8.59: Influence of additives on capacitance measurements in DGBB tests (inner ring film thickness, 6kN)

However, since both lubricants were tested on the same bearing, it becomes obvious that this cannot be the only reason, as the surface roughness was the same in both experiments. Thus the explanation must come from the oils' chemistry, namely from the higher conductivity of the mineral oil due to the additives it contains.

This is in agreement with the observations from the ball-on-flat setup tests, where the voltage had to be lowered for the measurements with the mineral oil and steel disc, in order to avoid current leakage through the film. Literature data to confirm this hypothesis were sought.

According to the measurements by Harvey et al. (2004) polyalphaolefin base oil (PAO6 in that case) exhibits, as expected, a very low conductivity, because it is a purely synthetic hydrocarbon base oil without heteroatom-containing species, which are found in mineral oils. Mineral base oils generally show a higher conductivity than PAOs, however, the level of conductivity depends on the API Group as it varies with the refinement level. Harvey et al. (2004) also measured the conductivity of fully formulated and commercial oils, which showed much higher conductivity than the base oils.

It is therefore concluded that the "noise" observed in the Lubcheck signal (which then translates into capacitance) in mineral oil tests, is not only due to the surface roughness but is also caused by the current leakage through thin lubricating film due to an increased conductivity (or lower resistivity) of the oil layer.
The conclusion presented may seem obvious, however, if the origin of this behaviour is not fully understood and appreciated, significant errors when interpreting the data are inevitable. The assumption that the noise is a result of only metal-metal contact may lead to underestimation of lubrication condition in rolling element bearings. The same principle applies when only the average capacitance values are used for data analysis, because the presence of the noise artificially increases capacitance value, thinner than actual film would be deduced.

Loaded zone analysis

The maximum load in the centre of the loaded zone, as well as the load distribution within the bearing strongly depends on the bearing's clearance considered in the calculations. For the bearing tested in the current study, C3 clearance covers a range from 13 to 28 µm radial clearance. In the modified bearing with only one steel ball, the effect of elastic properties of the ceramic material needs to be taken into account.

This can be seen in Figure 8.60, which shows a comparison between the load calculations for a bearing with all steel balls (a), and the case with one steel ball and the rest made of silicon nitride (b), for 4kN load applied.

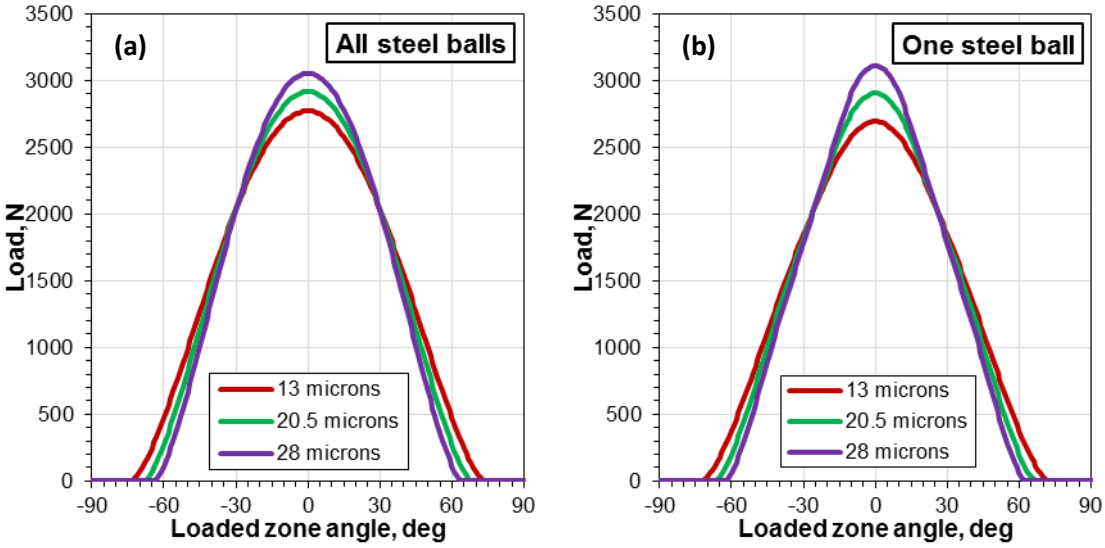

Figure 8.60: Load distribution throughout the loaded zone at 4kN load applied

It can be seen that in both examples a smaller clearance results in a lower maximum load in the centre of the loaded region, and also that the loaded zone extends over a bigger bearing angle (147^{o} for 13 µm clearance, versus 127^{o} for 28 µm clearance). Additionally, the load distribution is different for a full-steel bearing (a) and a hybrid (steel and ceramic balls) bearing (b).

If the capacitance data recorded during the full rotation, as those seen in Figure 8.51, are compared with the load distribution, it is clear that regardless of the approach

used for the load calculation, or the bearing clearance considered, the two do not match.

It was therefore thought that the load distribution can be calculated based on the measured capacitance and compared with the assumed load profile.
Experimental data from the 4kN test with the mineral oil was used for that purpose. The procedure was as follows:

- capacitance values were taken at 10^{o} intervals, starting from the centre of the loaded zone,
- film thickness values were calculated based on those capacitance readings and the contact load was adjusted up to the point where an agreement with the theoretical film thickness was obtained. This will only happen if the correct contact area, and therefore load, is considered,
- the procedure was then repeated for two more speeds leading to the same load distribution.

The result of this process is displayed in Figure 8.61, and compared with a theoretical load profile calculated for the 20.5 μm radial clearance and all steel balls case. It can be seen that the two agree well in the centre of the loaded zone, however they clearly diverge when the steel ball leaves the maximum load area.
The third series in this Figure was obtained by excluding the clearance from the load calculation. The maximum load is lower by around 8% from the value based on the capacitance measurement. Apart from that, the profile shows an excellent agreement.
This suggests that due to a different stiffness of ceramic and steel balls the load distribution within the bearing is somewhere in between these two cases.

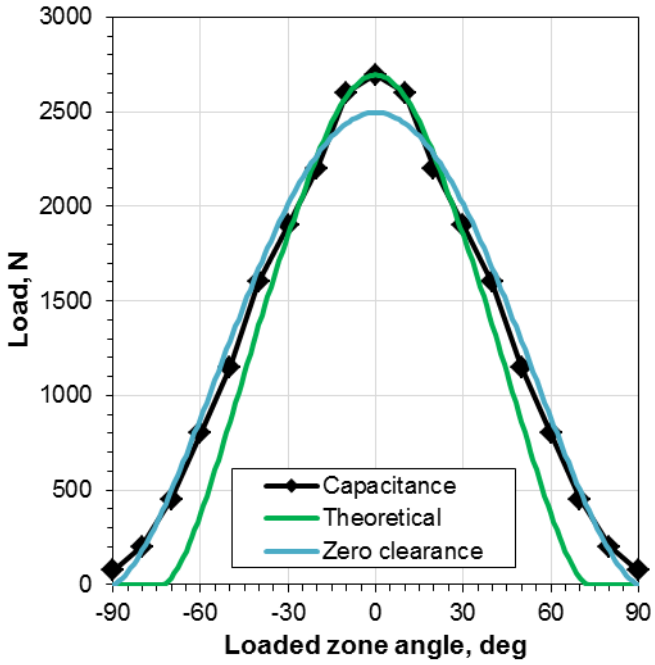

Figure 8.61: Load distribution calculated based on capacitance measurement at 4kN load applied

Starvation

Lubricant starvation can strongly affect capacitance measurements thus it should be ensured that a sufficient amount of oil is available to supply the inlet. The occurrence of starvation can be deduced from capacitance readings, as will be shown in the following images.

Two sets of measurements are shown here, both with the PAO VG48 oil. The first set comes from an experiment where the lubricant was added only once, at the start of the test at 1kN. When the test reached the 4kN stage, from a certain speed the capacitance values instead of further decreasing (because of increasing film thickness with speed), started increasing, and the signal became much noisier.

Starvation was considered as a possible reason for this behaviour. In order to confirm this hypothesis, the bearing was re-lubricated and the sweep of speeds at 4kN was repeated. This is shown in the second set of images.

It should be noted that these oscilloscope print screens show the Lubcheck voltage, which is inversely proportional to capacitance, therefore a decreasing capacitance corresponds to an increasing Lubcheck signal.

Figure 8.62: Oscilloscope data comparison between starved and fully-flooded contact (PAO VG48, 4kN, 0.358 m/s)

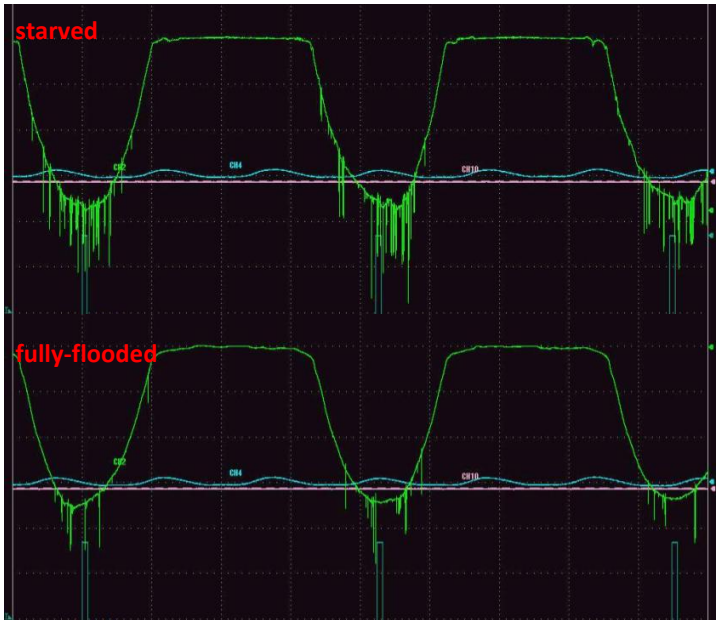

Figure 8.63: Oscilloscope data comparison between starved and fully-flooded contact (PAO VG48, 4kN, 0.476 m/s)

Figure 8.62 shows a comparison of the two tests at 0.358 m/s. It can be seen that both contacts are fully-flooded since the capacitance values are very similar. The general appearance of the signal is also the same.

As the speed is increased (Figure 8.63), a clear difference between the two sets of data can be seen. The upper image shows a lower Lubcheck voltage, indicating a higher capacitance, and a much noisier signal in the loaded zone.

Further increase of the speed (Figure 8.64) shows an even stronger difference and allows a conclusion that starvation indeed occurred.

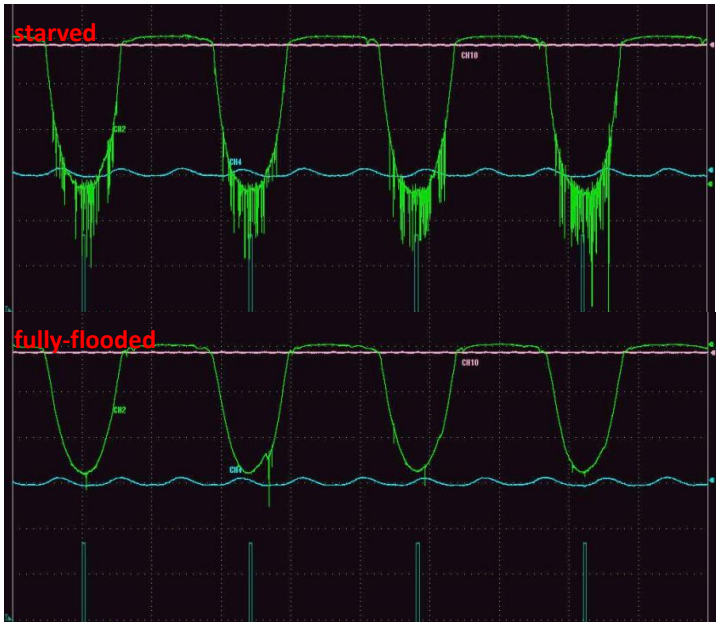

Figure 8.64: Oscilloscope data comparison between starved and fully-flooded contact (PAO VG48, 4kN, 0.843 m/s)

Accuracy and uncertainty of film thickness evaluation

The accuracy and uncertainty of capacitance film thickness evaluation is difficult to estimate due to a number of factors.

First of all such analysis would be based on the assumption that the theoretical value is the “real” film thickness in the bearing. This strongly depends on the actual temperature of the lubricant, which can be different from the temperature measured on the outer ring of the bearing.

The correct evaluation of the maximum load value also plays an important role. As shown, the load distribution within the bearing strongly depends on the clearance used for the calculations, and that will affect the Hertzian contact area especially at low loads.

The uncertainty coming from the assumptions included in the calculations of film thickness from the measured capacitance should also be considered. Since it would be difficult to evaluate the actual film thickness distribution within the EHD contact it is necessary to assume the flat shape (by using the parallel-plate capacitor formula (Eq. 30), and it is known that the contact has regions of thinner film which gives the lubricant film the well-known horse-shoe shape. The real film thickness distribution may diverge from the assumed shape even more at the conditions of high speeds. The same assumption applies to the pressure distribution and as a result the variation of dielectric constant within the contact area.

Some simplifying assumptions regarding the amount of lubricant in the bearing are needed in order to calculate the capacitance of the region outside the contact. Since in the current study it is considered that the bearing is operating under fully-flooded conditions, an area around the contact corresponding to separation equal nine times central film thickness is taken into account. This ensures that a minimum amount of lubricant required to supply the inlet is available. The amount of oil in the bearing will vary during the operation, with more oil present after re-lubrication and at low speeds.

To show how much the outside of contact capacitance affects the calculated film thickness, a comparison of two approaches for inner ring contact, is shown in Table 10. “Wedeven’s distance” corresponds to an area limited to a separation equal to nine times the central film thickness, while for the “Ball diameter” case, outside of contact capacitance was calculated over the area corresponding to the ball diameter.

Based on these results it can be seen that the higher the outside of contact capacitance considered, the higher the film thickness calculated from capacitance. It

can be therefore concluded that at low speeds, where there is more lubricant present in the bearing, the film thickness is likely to be underestimated with the current approach. It should be noted, however, that an alternative approach would lead to an overestimated film thickness which can result in a premature bearing failure.

Table 10: Effect of outside of contact capacitance on film thickness calculation

	Wedeven's distance	**Ball diameter**
Measured capacitance, pF	103	103
Outside of contact capacitance, pF	16	30
Hertzian contact capacitance, pF	204	186
Capacitance film thickness, nm	246	270
Hamrock-Dowson film thickness, nm	244	244

Chapter 9: Conclusions

9.1 Thesis' summary and conclusions

In the case of rolling element bearings, vast amount of work is based upon computer simulations and models used to predict thickness of the lubricating film during the operation. Experimental work is mostly focused on testing bearings to failure, and the information about lubricant effectiveness is usually deduced from friction and temperature measurements.
It is believed that in the light of the ever increasing demands on performance, there is a need for a quantitative method to allow for the monitoring of the bearings' lubrication, which can be used as both, an engineering and research tool.

The current work was therefore focused on the application of electrical capacitance measurements for studying elastohydrodynamic (EHD) lubricated contacts. It has been shown that in the absence of optical measurements, the method can be used for either film thickness evaluation, or monitoring the lubrication condition in long-term experiments. It has been proven that accurate film thickness values can be obtained from the measured capacitance of a lubricated EHD contact in a ball on flat experimental setup, as well as in a modified ball bearing by directly comparing the results with those obtained via the optical method and theoretical predictions.

9.1.1 Development of film thickness evaluation procedure

The majority of experimental work was carried out in a bearing simulating rig, in which a steel ball is loaded against either a chromium-coated glass, or a steel disc. For that purpose a commercial EHD rig, by PCS Instruments, was adapted to accommodate capacitance measurements. This involved the insulation of both specimens and providing an electrical connection for signal transfer between the measured parts and

the impedance analyser. All the experiments on the rig were carried out in pure rolling conditions where the ball and the disc were driven independently.

In order to develop a step-by-step approach, which allows for the extraction of lubricant film thickness from the measured capacitance, at first experiments with a nonpolar polyalphaolefin base oil (PAO4) and a chromium-coated glass disc were performed.

The thickness of the chromium layer was sufficient to make it possible to simultaneously measure film thickness with optical interferometry, and electrical capacitance of the lubricating film. To allow for film thickness measurements, an optical method, based on relative intensity dependence on film thickness, has been established. The method allows evaluation of lubricant film thickness in a chosen area within the EHD contact, including central film thickness, film thickness profiles along and across the rolling direction, as well as full film thickness maps.

Consequently, the capacitance data could be directly correlated to the oil film thickness measured at the same time.

Such simultaneous measurements of film thickness with an optical method, and electrical capacitance of the contact have not been reported before.

It has been shown that in order to obtain accurate film thickness results, careful evaluation of outside of contact capacitance is needed. The results indicate that this quantity must be calculated separately for each operating condition, as it depends on both, film thickness and contact area. Additionally, variation of dielectric constant with pressure has to be considered.

The procedure developed has been validated against both, optically measured film thickness, and theoretical predictions. It was shown that films down to around 10 nm thickness can be reliably measured. Since an excellent agreement has been found, the experiments were further successfully extended to cover steel on steel contacts.

During the course of this study it has been found that nonpolar lubricants follow a straight-line (in a logarithmic scale) trend of capacitance versus film thickness.

Additionally, if the dielectric constant is taken into account, for a certain contact area, determined by load and material pair, different nonpolar lubricants (e.g. PAO4 and mineral oil) follow the same trend. It is therefore possible to simplify the film thickness evaluation procedure if the behaviour of a reference nonpolar fluid is established under the same load conditions.

9.1.2 Effect of lubricant's polarity on capacitance measurements

However, as all lubricants either contain species of polar character, such as additives, or are polar themselves, it has been considered essential for the current work to evaluate the effect of polarity on evaluation of film thickness from electrical capacitance measurement.

Since capacitance strongly depends on the dielectric constant of the lubricant, it has been recognized that the method is very suitable for studying polar base oils, as well as their blends, or solutions of polar additives in nonpolar base fluids. Therefore the second part of the experimental work, dealing with polarity effect, covers all three groups.

It has been shown that the method is very sensitive to changes of capacitance due to composition variation, when the lubricant's components have different dielectric constants.

At first, two simple polar fluids of a well-defined structure and properties, namely glycerol and polyethylene glycol (PEG), have been tested under elastohydrodynamic conditions. In order to allow for a direct evaluation of film thickness corresponding to the measured capacitance and also to detect the presence of any boundary film formed, the chromium-coated glass disc was employed. The experiments were performed at two loads, 20 and 40N, and temperature of 30^{o}C. Nonpolar polyalphaolefin base oil was used as a reference fluid in these experiments.

Contrary to a well-established behaviour of nonpolar oils, in case of glycerol and PEG a deviation from the expected straight-line (in a logarithmic scale) power-law trend has been observed.

Based on additional experiments at a higher temperature, 60^{o}C, it has been shown that this behaviour was purely film thickness dependent and was not affected by either temperature or entrainment speed. The same result was seen in the measurements at a lower voltage, 10 mV as opposed to the usual 100 mV. It was also clear that the effect was stronger; the more polar was the oil.

Possible sources of this behaviour have been analysed, and it has been concluded that it must be directly related to the dielectric constant of the fluid.

It should be stressed at this point that, contrary to optical film thickness measurements which provide information about the lubricant state in the inlet zone, capacitance measurements reflect the behaviour of lubricants inside the EHD contact.

Capacitance measurements correlated to the corresponding lubricant film thickness implied that the dielectric constant decreases as the separation between the surfaces is lowered.

Similar behaviour has been documented for water, as well as for thin film capacitors, where the existence of a dielectric “dead layer” has been reported. This indicated that the presence of a reduced dielectric constant layer adjacent to the solid surfaces can be a possible explanation of the behaviour observed.

Simplified theoretical calculations were carried out and showed that a model considering two distinct layers of different dielectric constant cannot explain the reduction of the effective dielectric constant in the thin film. Instead, it suggests that such a layer of lower dielectric constant will also affect the neighbouring molecules and therefore the effect will extend up to a greater thickness. A detailed analysis of such approach is however beyond the scope of this thesis.

Nevertheless, an important implication for film thickness evaluation based on capacitance measurements can be drawn from these experiments. In case of polar

fluids such capacitance variation would lead to incorrect film thickness values if this behaviour occurs and is not recognised.

With this in mind it, tests with blends of a polar and nonpolar base oil were carried out. For that purpose polyalphaolefins of various viscosity and an ester were chosen. A similar deviation from the expected, straight-line power law trend was observed for both, the ester and its blends with PAOs. It has been clear that regardless of a blends' viscosity, the ester, as a more polar component, dominates the capacitance behaviour. Based on the capacitance measurements, it was not possible to confirm whether or not fractionation of the base oil has taken place. It is possible that the film thickness range in this study was simply too high for the effect to be seen, or that the contact time of the blend with the surfaces before capacitance measurements were taken, was not sufficient.

It was also interesting to examine the behaviour of a polar additive in a nonpolar base oil. Glycerol monooleate (GMO), widely used friction modifier, was chosen for that study. In the experiments performed a stronger interaction with the steel surface, in comparison to chromium-coated glass, was observed. Due to a higher dielectric constant than the base oil, the presence of GMO in the lubricating film can be deduced from capacitance measurements.

9.1.3 Grease lubrication

Since the lubrication of rolling element bearings was the focus of this study, experiments with grease were also conducted.
It has been demonstrated that the method can be successfully used to study transient behaviour of grease films and is capable of detecting rapid changes in lubrication condition due to either speed, or load.

It has been shown that experiments in both, fully-flooded and starved conditions can be carried out in the current rig.
Additionally, experiments with steel disc, in comparison to glass material, allow for the monitoring of grease films over extended periods of time, not achievable with glass discs. This also means that a more realistic material pair can be evaluated.

9.1.4 Measurements in a modified ball bearing

The final part of the experimental work, capacitance measurements in a ball bearing, can be seen as a transition step from the fundamental academic research into real industrial research application. The approach employed in this study is unique and it involves studying a modified ball bearing, in which all but one steel ball are replaced with elements made of an insulating, ceramic material.
The main advantage lies in the ability to eliminate some of the system's uncertainties and therefore allows for measurements of a much better controlled and defined setup. In the current configuration, by application of the oscilloscope, the steel ball signal can be followed through the full rotation, and therefore capacitance corresponding to the exact position of the steel ball within the bearing can be determined.

It has been shown that quantitative film thickness values at the maximum load position, and therefore lowest film thickness, can be extracted from the measured capacitance of the bearing. The results were in a good agreement with theoretical film thickness calculated from the Hamrock and Dowson formula over the range of loads (1-6kN) and speeds (0.12 m/s up to 0.91) tested.
It has been demonstrated that accurate temperature measurements are of primary importance, especially at test temperatures around ambient, where the change of lubricant's viscosity with temperature is significant.

Thanks to the accompanying ball-on-flat experiments with the same lubricants, it was possible to confirm observations regarding the lubricant composition in the ball

bearing tests. Important implications of the presence of ionic-type additives on the capacitance data interpretation have been underlined. If a comparison with a nonpolar base oil is not available, the noise seen in the capacitance data can be assumed to originate from the asperities contacts, while in fact it may also be a result of current leakage through the film due to a higher conductivity of the lubricant.

Similarly as in ball-on-flat experiments, for a certain bearing geometry and load conditions, nonpolar lubricants show the same trend of capacitance versus film thickness, if the effect of dielectric constant is considered. If the behaviour of the nonpolar base oil is established, it can be used as reference.

As the capacitance resolution, expressed as a change of capacitance for a certain film thickness change, strongly depends on the contact area, it is concluded that film thickness evaluation accuracy would always be improved if the load is increased. For the same reason the method should preferably be used in the thin film region.

The amount of experimental work, dealing with film thickness evaluation from capacitance in ball-on-flat setup, reported in the literature, is very limited. Also capacitance measurements in a modified bearing, which has only one steel ball and the rest made of ceramic material, have been reported first by the author.
The work presented underlines some of the applications of the method and shows a high potential as either a research tool to study various aspects of lubrication or to provide a better understanding of the behaviour of lubricants in EHD contacts.

9.2 Potential applications and recommendations for future work

- Due to its sensitivity to detect polar components in the lubricating film, the method can be used to study the effectiveness of surface-active species. Based on capacitance enhancement, it is possible to detect the presence of polar species adsorbing on the surfaces.
- Friction measurements carried out simultaneously with capacitance can provide complementary information about the behaviour of polar compounds, such as friction modifiers. This would eliminate the issue of carrying out film thickness measurements with different surfaces than those used for friction measurements, and therefore the interaction of the polar species would be the same.
- By performing experiments at different slide/roll ratios it is possible to study the alignment of molecules due to shear in the inlet region.
- The method is not limited to the materials specimens used in this study. It can also be applied to different conductive materials, therefore also surfaces made of e.g. copper alloys and aluminium can be studied.
- The modified ball bearing setup can be used to study the effect of different lubricants, including grease, however, a more accurate temperature measurement system is recommended. The alternative is carrying out the experiments in isothermal, rather than self-induced temperature conditions.
- By gradually increasing the number of steel balls and eventually replacing all ceramic balls, it is possible to perform tests in a very control manner. Variation of the sequence of steel balls in relation to ceramic balls (e.g. C-C-S-S-S-C-C, or C-S-C-S-C-S-C) allows studying different areas of the loaded zone simultaneously.
- The ball bearing experiments can also be carried out with a constant lubricant supply, where the most loaded point in the bearing is always immersed in an oil bath. This would ensure that the same amount of lubricant is always available around the contact, eliminating the uncertainty regarding the outside of contact calculation.

- The method is not limited to radially loaded bearings, it can also be used with rolling element bearings under axial load.
- Since the contact area strongly affects the measured capacitance, it is recommended to choose the biggest bearing that can be accommodated in the test rig used.

References

American Petroleum Institute (2012) *API 1509: Engine Oil Licensing and Certification System Appendix E – API base oil interchangeability guidelines for passenger car motor oils and diesel engine oils.*

Archard, J.F. and Kirk, M.T., (1961) Lubrication at Point Contacts. *Proceedings of the Royal Society of London. Series A. Mathematical and Physical Sciences*, 261(1307), p. 532–550.

Åström, H., Isaksson, O. and Höglund, E. (1991) Video recordings of an EHD point contact lubricated with grease. *Tribology International*, 24(3), p. 179–184.

Atkins, P. and de Paula, J. (2006) Atkins' physical chemistry. Oxford University Press.

Baly, H., Poll, G., Cann, P.M. and Lubrecht, A.A. (2006) Correlation between model test devices and full bearing tests under grease lubricated conditions. *IUTAM Symposium on Elastohydrodynamics and Micro-elastohydrodynamics*, p. 229–240.

Bantchev, G. and Biresaw, G. (2008) Elastohydrodynamic study of vegetable oil-polyalphaolefin blends. *Lubrication Science*, 20(4), p. 283–297.

Bantchev, G.B., Biresaw, G. and Cermak, S.C. (2012) Elastohydrodynamic study of blends of bio-based esters with polyalphaolefin in the low film thickness regime. *Journal of the American Oil Chemists' Society*, 89(6), p. 1091–1099.

Agilent Technologies. *Basics of Measuring the Dielectric Properties of Materials*. http://cp.literature.agilent.com/litweb/pdf/5989-2589EN.pdf (accessed 21.09.2014).

Bhushan, B. (2013) Introduction to tribology. John Wiley & Sons.

Bondi, A., and Penther, C.J. (1953) Some electrical properties of colloidal suspensions in oils. *The Journal of Physical Chemistry*, 57(1), p. 72–79.

Brow, R.K., Tallant, D.R., Myers, S.T. and Phifer, C.C. (1995) The short-range structure of zinc polyphosphate glass. *Journal of Non-Crystalline Solids*, 191, p. 45–55.

Cameron, A. (1966) The principles of lubrication. Longmans.

Cameron, A. and Gohar, R. (1966) Theoretical and Experimental studies of the Oil Film in Lubricated Point Contact, *Proceedings of the Royal Society of London*, A291, p. 520–536.

Cann, P.M. and Spikes, H.A. (1991) In Lubro Studies of Lubricants in EHD Contacts Using FTIR Absorption Spectroscopy. *Tribology Transactions,* 34(2), p. 248–256.

Cann, P.M., Williamson, B.P., Coy, R.C. and Spikes, H.A. (1992) The behaviour of greases in elastohydrodynamic contacts. *Journal of Physics D: Applied Physics*, *25*, p. A124–AI32.

Cann, P.M., Spikes, H.A., and Hutchinson, J. (1996) The Development of a Spacer Layer Imaging Method (SLIM) for Mapping Elastohydrodynamic Contacts, *Tribology Transactions*, 39(4), p. 915–921.

Cann, P.M. (1996) Starvation and Reflow in a Grease-Lubricated Elastohydrodynamic Contact. *Tribology Transactions*, 39(3), p. 698–704.

Cann, P.M. (1999) Starved Grease Lubrication of Rolling Contacts. *Tribology Transactions*, 42(4), p. 867–873.

Cann, P.M., Doner, J.P., Webster, M.N, and Wikstrom, V. (2001) Grease Degradation in Rolling Element Bearings. *Tribology Transactions*, 44(3) p. 399–404.

Cann, P.M., and Lubrecht, A.A. (2003) The effect of transient loading on contact replenishment with lubricating greases. *Tribology Series*, 43 p. 745–750.

Cann, P.M. (2007) Grease lubrication of rolling element bearings — role of the grease thickener. *Lubrication Science*, 19 p. 183–196.

Cann, P.M., Webster, M.N., Doner, J.P., Wikstrom, V. and Lugt P. (2007) Grease Degradation in R0F Bearing Tests. *Tribology Transactions*, 50(2) p. 187–197.

Cen, H., Lugt, P.M. and Morales-Espejel G. (2014) On the Film Thickness of Grease-Lubricated Contacts at Low Speeds. *Tribology Transactions*, 57(4) p. 668–678.

Chua, W.H. and Stachowiak, G.W. (2010) The Study of the Dynamic Thickness of Organic Boundary Films Under Metallic Sliding Contact. *Tribology Letters*, 39 p. 151–161.

Chiu, Y.P. (1974) An Analysis and Prediction of Lubricant Film Starvation in Rolling Contact Systems. *ASLE Transactions*, 17(1) p. 22–35.

Crook, A.W. (1958) The lubrication of rollers. *Philosophical Transactions of the Royal Society of London. Series A, Mathematical and Physical Sciences*, 250(981) p. 387–409.

Danforth, W.E. (1931) The Dielectric Constant Of Liquids Under High Pressure. *Physical Review*, 38(6) p. 1224–1235.

Davidson, D.W. and Cole, R.H. (1951) Dielectric Relaxation in Glycerol, Propylene Glycol, and n-Propanol. *The Journal of Chemical Physics*, 19(12) p. 1484–1490.

Dow Chemical Company. *OPTIM Synthetic Glycerine - Dielectric Constant*. http://www.dow.com/optim/optim-advantage/physical-properties/dielectric.htm (accessed January 2015).

Dowson, D. and Higginson, G.R. (1959) A numerical solution to the elasto-hydrodynamic problem. *Journal of Mechanical Engineering Science*, 1(1) p. 6–15.

Dwyer-Joyce, R.S., Drinkwater, B.W. and Donohoe, C.J. (2003) The measurement of lubricant-film thickness using ultrasound. *Proceedings of the Royal Society of London. Series A: Mathematical, Physical and Engineering Sciences*, 459(2032) p. 957-976.

Dyson, A., Naylor, H. and Wilson, A.R. (1965) The measurement of oil-film thickness in elastohydrodynamic contacts. *Proceedings of the Institution of Mechanical Engineers, Conference Proceedings*, 180(2) p. 119–134.

Dyson, A. and Wilson, A.R. (1965) Film Thicknesses in Elastohydrodynamic Lubrication by Silicone Fluids. *Proceedings of the Institution of Mechanical Engineers, Conference Proceedings*, 180(11) p. 97–112.

Dyson, A. and Wilson, A.R. (1969) Film thicknesses in elastohydrodynamic Lubrication of rollers by greases. *Proceedings of the Institution of Mechanical Engineers, Conference Proceedings*, 184(6) p. 1–11.

Foord, C.A., Hammann, W.C. and Cameron, A. (1968) Evaluation of Lubricants Using Optical Elastohydrodynamics. *ASLE Transactions*, 11(1) p. 31–43.

Foord, C.A., Wedeven, L.D., Westlake, F.J., Cameron, A. (1969) *Optical Elastohydrodynamics*. Proceedings of the Institution of Mechanical Engineers, 184(1) p. 487–505.

Forsman, H., Andersson, P. and Bäckström, G. (1986) Dielectric relaxation of glycerol and n-propyl alcohol at high pressure. *Journal of the Chemical Society, Faraday Transactions 2: Molecular and Chemical Physics*, 82(5) p. 857–868.

Fowell, M., Ioannides, S. and Kadiric, A. (2014) An Experimental Investigation into the Onset of Smearing Damage in Nonconformal Contacts with Application to Roller Bearings. *Tribology Transactions*, 57(3) p. 472–488.

Francon, M. (1966) Optical interferometry. Academic Press, New York.

Franke, E. and Poll, G. (1999) Service life and lubrication conditions of different grease types in high-speed rolling bearings. *Tribology Series*, 36 p. 601–609.

Fujita, H. and Spikes, H.A. (2004) The formation of zinc dithiophosphate antiwear films. *Proceedings of the Institution of Mechanical Engineers, Part J: Journal of Engineering Tribology*, 218(4) p. 265–277.

Furey, M.J. (1961) Metallic contact and friction between sliding surfaces. *ASLE Transactions*, 4(1) p. 1–11.

Galvin, G.D., Naylor, H. and Wilson, R. (1963) The Effect of Pressure and Temperature on Some Properties of Fluids of Importance in Elastohydrodynamic Lubrication. *Proceedings of the Institution of Mechanical Engineers, Conference Proceedings*, 178(14) p. 283–290.

Gatzen, M.M., Pape, F. and Poll, G.W.G. (2009) Physical properties of boundary layers in angular contact ball bearings lubricated with greases containing polymers. *Proceedings of the Institution of Mechanical Engineers, Part J: Journal of Engineering Tribology*, 223(3) p. 581–592.

Gatzen, M.M., Pape, F., Bruening, C., Gatzen, H.H., Arlinghaus, H.F. and Poll, G.W.G. (2010) Correlation between performance and boundary layers in high speed bearings lubricated with polymer-enhanced greases. *Tribology International*, 43(5) p. 981–989.

Georges, J.M., Martin, J.M., Mathia, T., Kapsa, P.H., Meille, G. and Montes, H. (1979) Mechanism of boundary lubrication with zinc dithiophosphate. *Wear*, 53(1) p. 9–34.

Gershuni, L., Larson, M.G. and Lugt, P.M. (2008) Lubricant Replenishment in Rolling Bearing Contacts. *Tribology Transactions*, 51(5) p. 643–651.

Gohar, R. and Cameron, A. (1963) Optical Measurement of Oil Film Thickness under Elasto-hydrodynamic Lubrication. *Nature*, 200 p. 458–459.

Gohar, R. and Cameron, A. (1967) The Mapping of Elastohydrodynamic Contacts. *ASLE Transactions*, 10(3) p. 215–225.

Greenall, A., Neville, A., Morina, A. and Sutton, M. (2012) Investigation of the interactions between a novel, organic anti-wear additive, ZDDP and overbased calcium sulphonate. *Tribology International*, 46(1) p. 52–61.

Guangteng, G. and Spikes, H. (1996) Fractionation of liquid lubricants at solid surfaces. *Wear*, 200(1) p. 336–345.

Guangteng, G. and Spikes, H.A. (1997) The control of friction by molecular fractionation of base fluid mixtures at metal surfaces. *Tribology transactions*, 40(3) p. 461–469.

Guangteng, G., Olver, A.V. and Spikes, H.A. (1999) Contact resistance measurements in mixed lubrication. *The Advancing Frontier of Engineering Tribology*," Wang, Q., Nethzel, J. and Sadeghi F. eds., STLE/ASME, p. 64–71.

Guangteng, G., Cann, P.M., Olver, A.V. and Spikes, H.A. (2000) An experimental study of film thickness between rough surfaces in EHD contacts. *Tribology International*, 33 p. 183–189.

Gunsel, S., Spikes, H.A. and Aderin, M. (1993) In-Situ Measurement of ZDDP Films in Concentrated Contacts. *Tribology Transactions*, 36(2) p. 276–282.

Guo, F. and Wong, P.L. (2002) A multi-beam intensity-based approach for lubricant film measurements in non-conformal contacts. *Proceedings of the Institution of Mechanical Engineers, Part J: Journal of Engineering Tribology*, 216(5) p. 281–291.

Gupta, P.K., Cheng, H.S., Zhu, D., Forster, N.H. and Shrand, J.B. (1992) Viscoelastic Effects in MIL-L-7808-Type Lubricant, Part 1: Analytical Formulation. *Tribology Transactions*, 35 p. 269–274.

Gustafsson, L., Höglund, E. and Marklund. O. (1994) Measuring Lubricant Film Thickness with Image Analysis. *Proceedings of the Institution of Mechanical Engineers, Part J: Journal of Engineering Tribology*, 208 p. 199–205.

Han, D.H. and Masuko, M. (1999) Comparison of Antiwear Additive Response Among Several Base Oils of Different Polarities. *Tribology Transactions*, 42(4) p. 902–906.

Hamrock, B.J. and Dowson, D. (1976) Isothermal elastohydrodynamic lubrication of point contacts: Part 1—Theoretical formulation. *Journal of Tribology*, 98(2) p. 223–228.

Hamrock, B.J. and Dowson, D. (1976) Isothermal elastohydrodynamic lubrication of point contacts: Part II—Ellipticity parameter results. *Journal of Tribology*, 98(3) p. 375–381.

Hamrock, B.J. and Dowson, D. (1977) Isothermal elastohydrodynamic lubrication of point contacts: Part III—Fully flooded results. *Journal of Tribology*, 99(2) p. 264–275.

Hamrock, B.J. and Dowson, D. (1977) Isothermal Elastohydrodynamic Lubrication of Point Contacts: Part IV—Starvation Results. *Journal of Tribology*, 99(1) p. 15–23.

Hamrock, B.J. and Anderson, W.J. (1983) Rolling-Element Bearings. *NASA report*, no 1105.

Hamrock, B.J., Jacobson, B.O. and Bergström, S.I. (1987) Measurement of the Density of Base Fluids at Pressures to 2.20 GPa. *ASLE Transactions*, 30(2) p. 196–202.

Hamrock, B.J., Schmid, S. and Jacobson B.O. (2004) Fundamentals of fluid film lubrication. Marcel Dekker (CRC press).

Hartl, M., Křupka, I. and Liška, M. (1997) Differential colorimetry: tool for evaluation of chromatic interference patterns. *Optical Engineering*, 36(9) p. 2384–2391.

Hartl, M., Křupka, I., Poliščuk, R. and Liška, M. (1999) An Automatic System for Real-Time Evaluation of EHD Film Thickness and Shape Based on the Colorimetric Interferometry. *Tribology Transactions*, 42(2) p. 303–309.

Hartl, M., Křupka, I., Poliščuk, R., Liška, M., Molimard, J., Querry, M. and Vergne P. (2001) Thin Film Colorimetric Interferometry, *Tribology Transactions*, 44(2) p. 270–276.

Harvey, T.J., Wood, R.J.K., Powrie, H.E.G. and Warrens, C. (2004) Charging Ability of Pure Hydrocarbons and Lubricating Oils. *Tribology Transactions*, 4(2) p. 263–271.

Heemskerk, R.S., Vermeiren, K.N. and Dolfsma, H. (1982) Measurement of Lubrication Condition in Rolling Element Bearings. *ASLE Trans*, 24(4) p. 519–527.

Herbst, C.A., Cook, R.L. and King, Jr H.E. (1993) High-pressure viscosity of glycerol measured by centrifugal-force viscometry. *Nature*, 361(11) p. 518–520.

Hertz, H. (1881) Uber die Beruhrung Fester Elastischer Korper (On the Contact of Elastic Solids). *J. Reine und Angewandte Mathematik*, 92 p. 156–171.

Höglund, E. and Larsson, R. (1997) Modelling Non-Steady EHL with Focus on Lubricant Density. *Tribology Series*, 32 p. 511–521.

Höglund, E. (1999) Influence of lubricant properties on elastohydrodynamic lubrication. *Wear*, 232 p. 176–184.

Hurley, S. and Cann, P.M.E. (2000) Infrared spectroscopic characterisation of grease lubricant films on metal surfaces. *NLGI Spokesman*, 64 p. 13–21.

International Organization for Standardization (1992) *ISO 3448:1992: Industrial liquid lubricants - ISO viscosity classification*.

Israelachvili, J.N. (2011) Intermolecular and surface forces: revised third edition. Academic Press.

Jacod, B., Publier, F., Cann, P.M.E. and Lubrecht, A.A. (1998) An Analysis of Track Replanishment Mechanisms in the Starved Regime. *Tribology Series*, 36, p. 483–492.

Johari, G.P. and Whalley, E. (1972) Dielectric Properties of Glycerol in the Range 0.1-10^5 Hz, 218-357 K, 0-53 kb. *Faraday Symposia of the Chemical Society*, 6 p. 23–41.

Johnston, G.J., Wayte, R.C. and Spikes H.A. (1991) The Measurements and Study of Very Thin Lubricant Films in Concentrated Contacts. *Tribology Transactions*, 34 p. 187–194.

Joshi, A., Marble, S. and Sadeghi, F. (2001) Bearing cage temperature measurement using radio telemetry. *Proceedings of the Institution of Mechanical Engineers, Part J: Journal of Engineering Tribology*, 215 p. 471–481.

Kirk, M.T. (1962) Hydrodynamic Lubrication of 'Perspex'. *Nature*, 194 p. 965–966.

Larsson, R., Larsson, P.O., Eriksson, E., Sjöberg, M. and Höglund, E. (2000) Lubricant properties for input to hydrodynamic and elastohydrodynamic lubrication analyses. *Proceedings of the Institution of Mechanical Engineers, Part J: Journal of Engineering Tribology*, 214 p. 17–27.

Larsson, P.O., Larsson, R., Jolkin, A. and Marklund, O. (2000) Pressure fluctuations as grease soaps pass through an EHL contact. *Tribology International*, 33 p. 211–216.

Leenders, P. and Houpert, L. (1987) Study of the lubricant film in rolling bearing; effects of roughness. *Tribology Series*, 11 p. 629–638.

Lord, J and, Larsson, R. (2008) Film-forming capability in rough surface EHL investigated using contact resistance. *Tribology International*, 41 p. 831–838.

Luo, J., Wen, S. and Huang, P. (1996) Thin film lubrication. Part I: study on transition between EHL and thin film lubrication using a relative intensity optical interference method. *Wear*, 194 p. 107–115.

Lugt, P.M., Severt, R.W.M, Fogelström, J. and Tripp, J.H. (2001) Influence of surface topography on friction, film breakdown and running-in in the mixed lubrication regime. *Proceedings of the Institution of Mechanical Engineers, Part J: Journal of Engineering Tribology*, 215 p. 519–553.

Lugt, P.M., Velickov, S. and Tripp, J.H. (2009) On the Chaotic Behavior of Grease Lubrication in Rolling Bearings. *Tribology Transactions*, 52(5) p. 581–590.

Lugt, P.M. (2009) A Review on Grease Lubrication in Rolling Bearings. *Tribology Transactions*, 52(4) p. 470–480.

Lugt, P.M. and Morales-Espejel, G.E. (2011) A review of elasto-hydrodynamic lubrication theory. *Tribology Transactions*, 54(3) p. 470–496.

Mang, T. and Wilfried, D. (eds.) (2007) Lubricants and Lubrication, John Wiley & Sons.

Masen, M.A., Venner, C.H., Lugt, P.M. and Tripp, J.H. (2002) Effects of Surface Micro-Geometry On the Lift-Off Speed of an EHL Contact. *Tribology Transactions*, 45(1) p. 21–30.

Mérieux, J-S., Hurley, S., Lubrecht, A.A. and Cann, P.M. (2000) Shear-degradation of grease and base oil availability in starved EHL lubrication. *Tribology Series*, 38 p. 581–588.

Metzik, M.S., Perevertaev, V.D. and Liopo, V.A. (1973) Timoshtchenko GT, Kiselev AB. New data on the structure and properties of thin water films on mica crystals. *Journal of Colloid and Interface Science*, 43 p. 662–669.

Morales-Espejel, G.E., Lugt, P.M., Pasaribu, H.R. and Cen, H. (2014) Film thickness in grease lubricated slow rotating rolling bearings. *Tribology International*, 74 p. 7–19.

Mortier, R.M., Fox, M.F. and Orszulik, S.T. (2010) Chemistry and Technology of Lubricants. Springer.

Nagata, Y., Kalogiannis, K. and Glovnea, R.P. (2012) Track Replenishment by Lateral Vibrations in Grease-Lubricated EHD Contacts. *Tribology Transactions.* 55(1) p. 91–98.

Natori, K., Otani, D. and Sano, N. (1998) Thickness dependence of the effective dielectric constant in a thin film capacitor. *Applied Physics Letters*, 73 p. 632–634.

Ohno, N. and Yamada, S. (2007) Effect of high-pressure rheology of lubricants upon entrapped oil film behaviour at halting elastohydrodynamic lubrication. *Proceedings of the Institution of Mechanical Engineers, Part J: Journal of Engineering Tribology*, 221(3) p. 279–285.

Paluch, M., Rzoska, S.J., Habdas, P. and Zioło J. (1996) Isothermal and high-pressure studies of dielectric relaxation in supercooled glycerol. *Journal of physics: Condensed matter*, 8 p. 10885–10890.

Pemberton, J. and Cameron, A. (1976) A mechanism of fluid replenishment in elastohydrodynamic contacts. *Wear*, 37(1) p. 185–190.

Poon, S.Y. (1972) Experimental Study of Grease in Elastohydrodynamic Lubrication. *Journal of Lubrication Technology Transations ASME*, 94(1) p. 27–34.

Ratoi, M., Anghel, V., Bovington, C. and Spikes, H.A. (2000) Mechanisms of oiliness additives. *Tribology international*, 33(3) p. 241–247.

Reynolds, O. (1886) On the Theory of Lubrication and its Application to Mr. Beauchamp Tower experiments including an experimental determination of the viscosity of olive oil. *Proceedings of the Royal Society of London*, 177 p. 157–234.

Roberts, A.D. and Tabor, D. (1971) The extrusion of liquids between highly elastic solids. *Proceedings of the Royal Society of London. A. Mathematical and Physical Sciences*, 325 p. 323–345.

Roelands, C.J.A. (1966) Correlation Aspects of the Viscosity-Temperature-Pressure Relationship of Lubricating Oils. Druk VRB. Groningen.

Rudnick, L.R. (ed.) (2006) Synthetics, mineral oils, and bio-based lubricants: chemistry and technology CRC Press.

Rudnick, L.R. (ed.) (2010) Lubricant additives: chemistry and applications, CRC Press.

SAE International (2005) *SAE J306: Automotive Gear Lubricant Viscosity Classification*.

SAE International (2013) *SAE J300: Engine Oil Viscosity Classification*.

Scaife, B.K.P. (1955) Isothermal Pressure Dependence of the Dielectric Properties of Eugenol, Glycerol and Water. *ournal of physics. B, Proceedings of the Physical Society*, 68:790–792.

Scaife, W.G.S. (1976) The effects of temperature and pressure on the complex dielectric permittivity of liquid eugenol and glycerol. *Journal of Physics D: Applied Physics*, 9 p. 1489.

Sengwa, R.J., Kaur, K. and Chaudhary, R. (2000) Dielectric properties of low molecular weight poly (ethylene glycol)s. *Polymer international*, 49(6) p. 599–608.

Segur, J.B. and Oberstar, H.E. (1951) Viscosity of glycerol and its aqueous solutions. *Industrial and Engineering Chemistry*, 43 p. 2117–2120.

Spikes, H.A. and Cann, P.M. (2001) The development and application of the spacer layer imaging method for measuring lubricant film thickness. *Proceedings of the Institution of Mechanical Engineers, Part J: Journal of Engineering Tribology*, 215 p. 261–277.

Spikes, H.A. (2006) Sixty years of EHL. *Lubrication Science*, 18(4) p. 265–291.

Stachowiak, G.W. and Batchelor, A.W. (2001) Engineering tribology. Butterworth-Heinemann.

Ståhl, J., Jacobson, B.O. (2003) Compressibility of Lubricants at High Pressures. *Tribology Transactions*, 46(4) p. 592–599.

Stengel, M. and Spaldin, N.A. (2006) Origin of the dielectric dead layer in nanoscale capacitors. *Nature*, 443 p. 679–682.

Svoboda, P., Kostal, D., Krupka, I. and Hartl, M. (2013) Experimental study of starved EHL contacts based on thickness of oil layer in the contact inlet. *Tribology International*, 67:140–145.

Taylor, L., Dratva, A. and Spikes, H.A. (2000) Friction and wear behaviour of zinc dialkyldithiophosphate additive. *Tribology Transactions*, 43 p. 469–479.

Teschke, O., Ceotto, G. and de Souza, E.F. (2001) Interfacial water dielectric-permittivity-profile measurements using atomic force microscopy. *Physical Review*, 64(1) p. 11605–11615.

Wedeven, L.D., Evans, D. and Cameron, A. (1971) Optical Analysis of Ball Bearing Starvation. *Journal of Tribology*, 93(3) p. 349–361.

Westlake, F.J. and Cameron, A. (1967) Fluid Film Interferometry in Lubrication Studies. *Nature*, 214 p. 633–634.

Wikström, V. and Höglund, E. (1996) Starting and Steady-State Friction Torque of Grease-Lubricated Rolling Element Bearings at Low Temperatures—Part I: A Parameter Study. *Tribology Transactions*, 39(3) p. 517–526.

Wikström, V. and Jacobson, B. (1997) Loss of lubricant from oil-lubricated near-starved spherical roller bearings. *Proceedings of the Institution of Mechanical Engineers, Part J: Journal of Engineering Tribology*, 211 p. 51–66.

Wilson, A.R. (1979) The relative thickness of grease and oil films in rolling bearings. *Proceedings of the Institution of Mechanical Engineers*, 193 p. 185–192.

Yamaguchi, E.S., Ryason, P.R., Yeh, S.W. and Hansen, T.P. (1998) Boundary Film Formation by ZnDTPs and Detergents Using ECR. *Tribology Transactions*, 41(2) p. 262–272.

Yamaguchi, E.S., Roby, S.H., Francisco, M.M., Ruelas, S.G. and Godfrey, D. (2002) Antiwear Film Formation by ZnDTP, Detergent, and Dispersant Components of Passenger Car Motor Oils. *Tribology Transactions*, 45(3) p. 425–429.

Appendix

I: Data for viscosity-pressure and density-pressure relationships

Table A.1: Coefficients for viscosity-pressure equations (Larsson et al., 2000)

Lubricant	S_0	G_0	C_Z	D_Z
Naphthenic mineral	1.60	5.13	-1.01	0.881
Paraffinic mineral	1.31	4.76	0.229	0.541
Naphthenic – paraffinic VG32	1.58	3.98	-0.014	0.727
Naphthenic – paraffinic VG68	1.68	4.49	0.010	0.692
Naphthenic – paraffinic	1.50	4.96	-0.443	0.711
PAO A	1.37	4.62	0.275	0.447
PAO B	1.25	4.57	-0.071	0.500
Polyglycol	1.06	4.39	-0.586	0.592

Table A.2: EOS coefficients and solidification pressure of fluids tested (Hamrock et al., 1987)

Lubricant	Pressure-density constants				Solidification pressure, GPa
	C_1, $(GPa)^{-2}$	C_2, $(GPa)^{-1}$	C_3, $(GPa)^{-1}$	C_4	
Naphthenic distillate	-0.271	0.430	0.0466	-0.135	0.706
Naphthenic raffinate	-0.151	0.302	0.0487	-0.106	0.839
Polyporpylene glycol	-0.121	0.297	0.0323	-0.145	1.092
Polyporpylene glycol	-0.0887	0.251	0.0395	-0.131	1.213
Ditridecyl adipate	-0.0531	0.202	0.0365	-0.129	1.561
Polyalphaolefin	-0.0444	0.190	0.0407	-0.126	1.682

Table A.3: Coefficients for curve-fitted density dependence of pressure (Ståhl and Jacobson, 2003)

Lubricant	Pressure-density constants			
	c_1	c_2, $(GPa)^{-1}$	c_3	c_4 $(GPa)^{-1}$
Mineral oil, η_{40C}=0.4 Ns/m^2	1.1842	0.0749	0.1808	1.5453
Traction fluid	1.1431	0.0614	0.1430	2.1121
Polyglycol VG460	1.1733	0.0635	0.1728	1.4335
Polyalphaolefin VG220	1.1886	0.0737	0.1833	1.5367
Mineral oil VG68	1.1913	0.0595	0.1882	1.4150

Table A.4: Constants for EOS at 20°C, based on Höglund and Larsson (1997)

Lubricant	p_1 (GPa)	p_2 (GPa)	Constants below p_1 (GPa)				Constants between p_1 and p_2 (GPa)			
			c_1	c_2	c_3	c_4	c_1	c_2	c_3	c_4
Naphthenic base oil	0.5	1.5	1.0	22.4	-	-1	-0.2	32.3	-	+1
Paraffinic base oil	1.0		1.7	19.7	-	-1				
Polyphenyl Ether 5P4E	1.8		1.1	49.1	-	-1				
PAO base oil	1.2		0.7	19.5	-	-1				
Santotrac traction fluid	0.45	1.9	0.9	20.6	-	-1	-16.6	90.7	1.1	+1
Naphthenic base oil + Li-12-OH	2.1		0.5	33.0	-	-1				
Polyglycol hydraulic fluid	1.2		0.3	27.1	-	-1				

Table A.5: Constants for refined Dowson and Higginson density-pressure relation (Larsson et al., 2000)

Lubricant	D_1 (GPa^{-1})	D_2 (GPa)$^{-1}$
Naphthenic mineral	0.64	2.89
PAO B	0.69	2.55
Naphthenic – paraffinic VG150	0.63	2.51
Polyglycol	0.67	2.68
Original constants	0.60	1.7

Table A.6: Atmospheric pressure parameters (Larsson et al., 2000)

Lubricant	ρ_{15} (kg/m^3)	$\rho'_T = -(\partial\rho/\partial T)_{p=0}$ (kg/m^3 °C)	ε_0 at 40°C (°C^{-1})
Naphthenic mineral	917	0.58	6.5×10^{-4}
Paraffinic mineral	884	0.58	6.6×10^{-4}
Naphthenic – paraffinic VG32	882	0.63	7.2×10^{-4}
Naphthenic – paraffinic VG68	887	0.59	6.9×10^{-4}
Naphthenic – paraffinic VG150	901	0.57	6.7×10^{-4}
PAO A	863	0.60	7.1×10^{-4}
PAO B	853	0.57	6.8×10^{-4}
Polyglycol	1000	0.75	7.6×10^{-4}

Table A.7: Measurements of dielectric constant and comparison with Clausius-Mosotti relation (Galvin et al., 1963)

Lubricant		Kinematic viscosity at 37.8°C	Dielectric constant at 20°C/100°C				C-M 345 MPa
			Atm. pressure	69 MPa	207 MPa	345 MPa	
A	High VI mineral oil (naphthenic and paraffinic)	175	2.29	2.34	2.41	2.42	2.52
			2.18	2.23	2.32	2.37	2.43
B	Medium VI mineral oil to OM 100 specification	83	2.33	2.28	2.44	2.46	2.57
			2.19	2.25	2.33	2.39	2.44
C	Medicinal white oil (naphthenic)	77	2.20	2.25	2.33	2.36	2.42
			2.08	2.13	2.20	2.27	2.34
D	High-viscosity, low VI mineral oil (aromatic and naphthenic)	180	2.58	2.63	2.54	2.53	2.87
			2.41	2.47	2.57	2.63	2.73
E	Low-viscosity, low VI mineral oil (aromatic and naphthenic)	22	2.49	2.54	2.62	2.62	2.76
			2.32	2.39	2.48	2.53	2.62
F	Low VI mineral oil + methacrylate polymer	220	2.57	2.63	2.60	2.53	2.85
			2.41	2.48	2.58	2.62	2.72
G	Ethylene oxide-propylene oxide	143	5.85	6.17	6.61	6.91	7.73
			4.74	5.09	5.62	6.01	6.27
H	Polydimethylsilicone fluid	130	2.77	2.91	3.08	3.20	3.32
			2.49	2.63	2.82	2.95	3.05
I	Castor oil	295	4.71	4.87	5.14	5.28	5.76
			3.89	4.06	4.30	4.48	4.80
J	Di(2-ethylhexyl) phthalate	30	5.35	5.49	5.74	5.93	6.74
			4.30	4.51	4.77	4.99	5.53

Table A.8: Dielectric constants of base oils and greases, based on Dyson and Wilson (1969)

Lubricant	Dielectric constant at 60°C		
	Atm. pressure	345 MPa	689 MPa[3]
O_1 (32.6 cSt at 37.8°C; 40 VI)	2.19	2.41[1]	2.46
O_2 (138.6 cSt at 37.8°C; 39 VI)	2.28	2.50[1]	2.57
O_3 (578.0 cSt at 37.8°C; -10 VI)	2.55	2.57[1]	2.70
O_4 (27.5 cSt at 37.8°C; 98 VI)	2.20	2.43[1]	2.48
G_1 (O_1; 9.8 % vol soap)	2.28	2.50[2]	2.55
G_2 (O_2; 10.0 % vol soap)	2.37	2.59[2]	2.66
G_3 (O_2; 5.6 % vol soap)	2.33	2.55[2]	2.62
G_4 (O_3; 10.4 % vol soap)	2.63	2.65[2]	2.77

[1] Direct measurement
[2] Calculated based on volume fraction
[3] Extrapolated

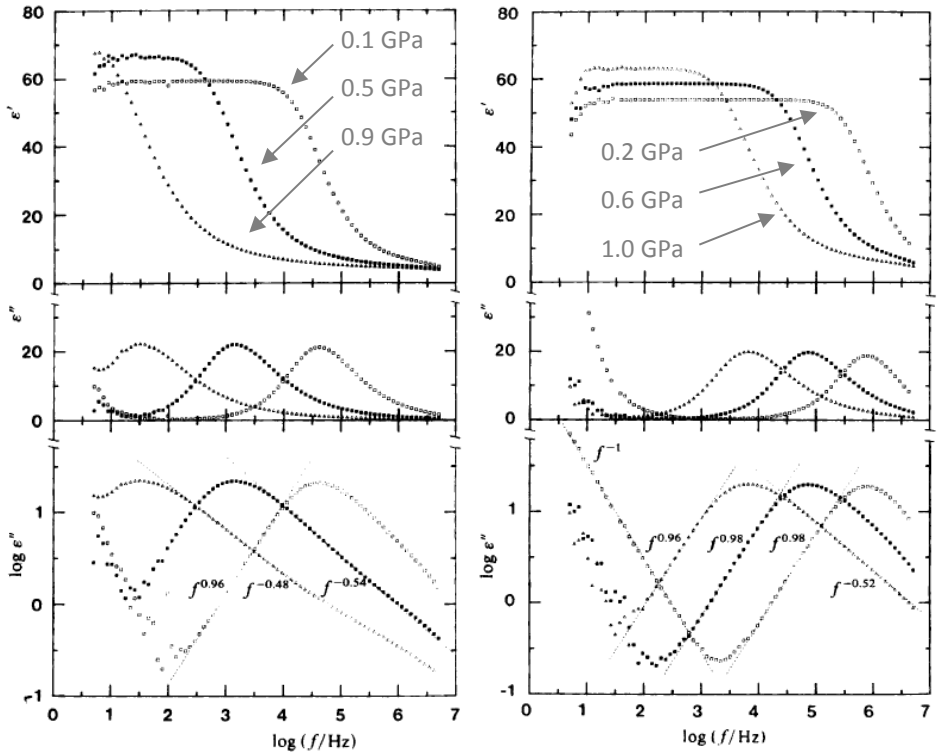

Figure A.1: Dielectric relaxation of glycerol at 243 K (left) and 258 K (right) for several pressures (Forsman et al., 1986)

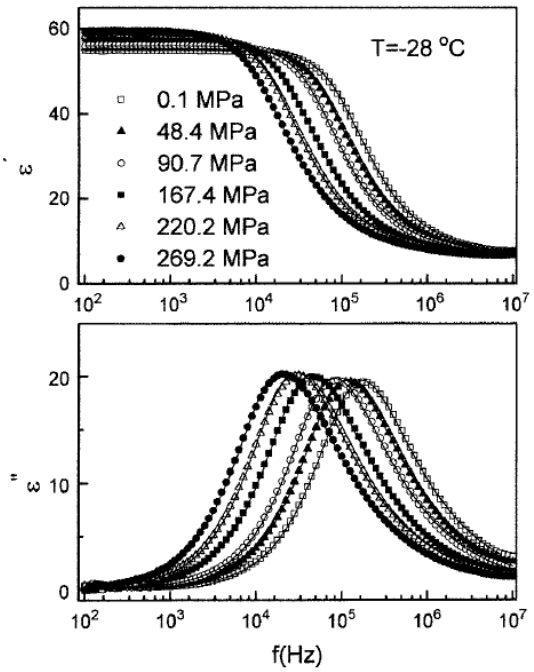

Figure A.2: Dielectric relaxation of glycerol at -28°C (Paluch et al., 1996)

II: Static load distribution

The distribution of the static load in radially loaded rolling bearings has been analysed by Hamrock and Anderson (1983) among others. They use Hertzian theory and consider the elastic deformation of the loaded balls to extract a relationship between the load at a given angular position and the geometry of the bearing and the elastic properties of the bearing material. The load at a given angle ψ is then given by:

$$F_\psi = K_j(\delta cos\psi - P_D/2)j \tag{A.1}$$

In this relationship K_j is the combined stiffness of the inner and outer ring contacts, δ is the normal approach between the two raceways, P_d is the diametral clearance of the bearing, and j is a constant which in this case takes the value 1.5. K_j in its turn is given by:

$$K_\psi = \frac{1}{\left\{\left[\frac{1}{(K_j)_o}\right]^{2/3} + \left[\frac{1}{(K_j)_i}\right]^{2/3}\right\}^{3/2}} \quad , \tag{A.2}$$

with

$$K_j = \pi k E' \sqrt{2\mathcal{E}R/9\mathcal{F}^3} \tag{A.3}$$

The elliptic integrals of first kind $\mathcal{F}$ and of the second kind $\mathcal{E}$ are functions of the curvature ratio R_y/R_x.

$$\mathcal{F} = \frac{\pi}{2} + \left(\frac{\pi}{2} - 1\right) ln\left(\frac{R_y}{R_x}\right) \tag{A.4}$$

$$\mathcal{E} = 1 + \left(\frac{\pi}{2} - 1\right)\left(\frac{R_y}{R_x}\right)^{-1} \tag{A.5}$$

Finally *E'* is the reduced elastic modulus. Looking back at relationships (A.2) to (A.5) it is seen that they depend on the geometry, and the elastic modulus of the balls and raceways, thus when all balls are made out of steel these relationships give identical parameters. In the arrangement of this study only one ball is made out of steel thus *E'*

is different for this ball from all the other, which are made out of silicon nitride. These are denoted by E'_s and E'_c for steel and ceramic ball respectively.

The numerical procedure for calculating the distribution of load is shown in the flow chart in Figure A.3. The steel ball is located at angular position ψ and the angle between two adjacent balls is denoted by θ.

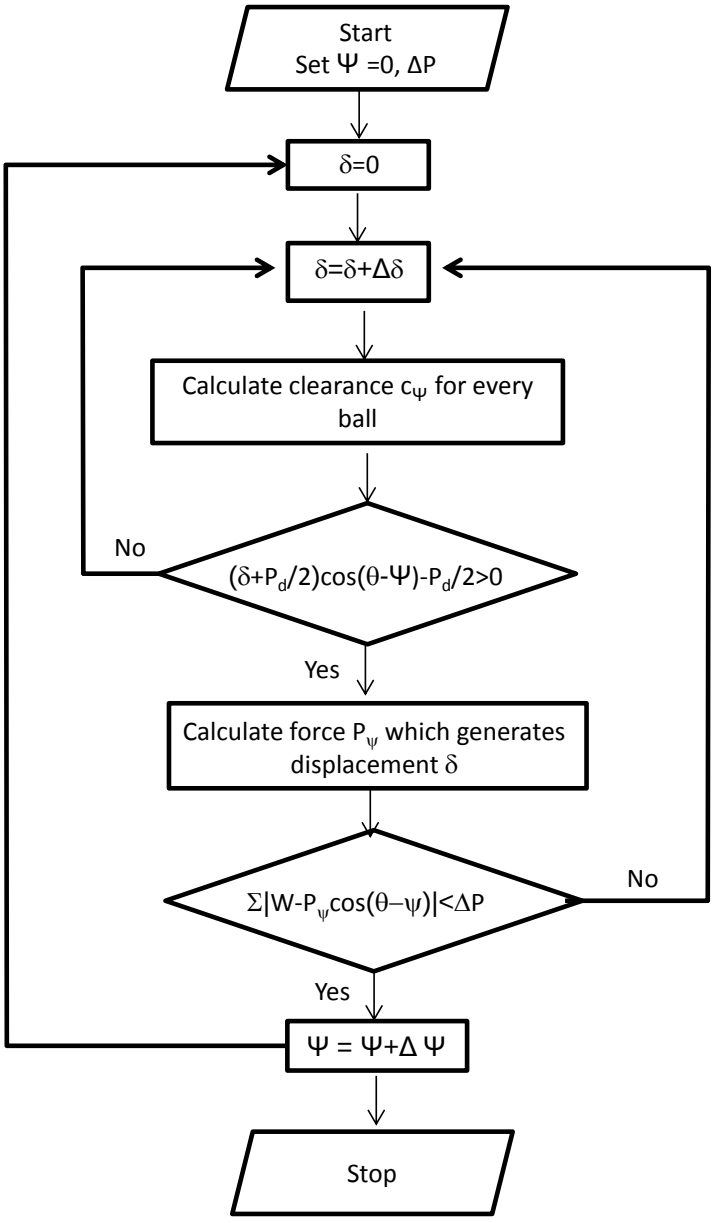

Figure A.3: Flow chart for the calculation of static force distribution